DEVELOPMENT OF AN ASSAY FOR FATTY ACYL-COAS USING LIQUID CHROMATOGRAPHY-ELECTROSPRAY IONIZATION-TANDEM MASS SPECTROMETRY AND ITS APPLICATION TO STABLE ISOTOPE-LABELING AND QUANTITATION OF SPHINGOLIPID METABOLISM

A Dissertation
Presented to
The Academic Faculty

by

Christopher A. Haynes

In Partial Fulfillment
of the Requirements for the Degree
Doctor of Philosophy in Biology

Georgia Institute of Technology

December, 2009

DEVELOPMENT OF AN ASSAY FOR FATTY ACYL-COAS USING LIQUID CHROMATOGRAPHY-ELECTROSPRAY IONIZATION-TANDEM MASS SPECTROMETRY AND ITS APPLICATION TO STABLE ISOTOPE-LABELING AND QUANTITATION OF SPHINGOLIPID METABOLISM

Approved by:

Prof. Alfred H. Merrill, Jr.
Schools of Biology and
Chemistry & Biochemistry
Georgia Institute of Technology

Prof. Nael McCarty
School of Biology
Georgia Institute of Technology

Prof. Jung Choi
School of Biology
Georgia Institute of Technology

Dr. M. Cameron Sullards
School of Chemistry & Biochemistry
Georgia Institute of Technology

Prof. Facundo Fernandez
School of Chemistry & Biochemistry
Georgia Institute of Technology

Date Approved: November 16, 2009

ACKNOWLEDGEMENTS

The assistance of the following persons in the Merrill lab was indispensable for the research described in this thesis: Elaine W. Wang, Samuel L. Kelly, Jia Wei, Kacee Sims, Ying Liu, Jessica Kollmeyer, and Hyejung Park.

The quantitation of sphingolipids during [U-^{13}C]-palmitate labeling experiments was done by Dr. Jeremy C. Allegood, with whom discussion of the data was invaluable during its interpretation.

Funding for the work described herein was provided by NIH glue grant U54-GM069338 to the Lipid MAPS Consortium.

The support of Frances Starling has been incalculable during all of this author's experiments and writing.

TABLE OF CONTENTS

LIST OF TABLES

LIST OF FIGURES

LIST OF ABBREVIATIONS

Sa (sphinganine)
So (sphingosine)
Sa-1-P (sphinganine-1-phosphate)
So-1-P (sphingosine-1-phosphate)
DHCer (dihydroceramide)
Cer (ceramide)
DHCMH (dihydroceramide monohexose)
CMH (ceramide monohexose)
GlcCer (glucosylceramide)
GalCer (galactosylceramide)
DHSM (dihydrosphingomyelin)
SM (sphingomyelin)
LC (liquid chromatography)
ESI (electrospray ionization)
MS (mass spectrometry)
MS/MS (tandem mass spectrometry)
LC-ESI-MS/MS (liquid chromatography-electrospray ionization-tandem mass spectrometry)
m/z (mass-to-charge ratio)
MRM (multiple reaction monitoring)
Q1;Q2;Q3 [quadrupole 1; quadrupole 2 (collision cell); quadrupole 3)
$[M + H]^+$ (singly protonated precursor ion)
$[M - H]^-$ (singly deprotonated precursor ion)
XIC (extracted ion chromatogram)
pmol (picomoles)
cps (counts per second)
LOD (limit of detection)
LOQ (limit of quantitation)
PBS (phosphate buffered saline)
FCS (fetal calf serum)
BSA (bovine serum albumin)
TTR (tracer / tracee ratio)
E_t (analyte enrichment at time = t)
E_p (plateau enrichment of the analyte at isotopic equilibrium)
k (fractional turn-over rate of analyte)
Q (analyte pool size)
R_a (rate of appearance)
Tlr4 (Toll-like receptor 4)

SUMMARY

Fatty acyl-Coenzyme As (Figure 1) are metabolites of lipid anabolism (1) and catabolism (2). A method was developed for their quantitation in extracts of cultured mammalian cells (3) using liquid chromatography-electrospray ionization-tandem mass spectrometry (LC-ESI-MS/MS). Palmitoyl-CoA (C16:0-CoA) is utilized for *de novo* sphingolipid biosynthesis catalyzed by serine palmitoyltransferase (SPT) (4-6), which condenses palmitoyl-CoA and serine to form 3-ketosphinganine. After reduction to form sphinganine (Sa), dihydroceramide synthase (CerS) can N-acylate the Sa using a second fatty acyl-CoA molecule, forming dihydroceramide (DHCer) (7-9). The CerS enzyme family utilizes different acyl chain lengths of fatty acyl-CoAs in an isoform-specific manner (7), resulting in DHCer with N-acyl chains ranging from C16 to C26 [and even longer (10)] in mammalian tissues. DHCer is *trans*-4,5-desaturated to yield ceramide (11, 12), which is further metabolized by the addition of moieties at the 1-O-position, forming sphingomyelin (SM) (13) and ceramide monohexose (CMH).

The rates of fatty acyl-CoA and sphingolipid biosynthesis were determined using stable isotope-labeling and LC-ESI-MS/MS analysis of the analyte isotopologues and isotopomers. Isotopic labeling of palmitoyl-CoA with [U-^{13}C]-palmitate in HEK293 and RAW264.7 cells was robust and rapid (~ 60% labeling of the metabolite pool in 3 hr). Isotopic labeling of sphingolipids indicated utilization of [M + 16]-palmitoyl-CoA by SPT and CerS isoforms in both cell types. Metabolic flux modeling was applied to the data for [U-^{13}C]-palmitate activation to [M + 16]-palmitoyl-CoA and its subsequent utilization in *de novo* sphingolipid biosynthesis, and this analysis indicated rapid turn-over rates for palmitoyl-CoA and ceramide in both cell types.

Palmitate treatment of cultured cells alters their metabolic status and gene expression, therefore labeling of palmitoyl-CoA by treatment with [1-^{13}C]-acetate was

employed. A distribution of mass-shifted palmitoyl-CoA species (isotopologues) is observed based on the number of incorporations of [1-^{13}C]-acetate during *de novo* biosynthesis, requiring computational analysis to derive two parameters: the isotopic enrichment of the precursor pool, and the fraction of palmitoyl-CoA that was biosynthesized during the experiment. Previous reports by others describe mass isotopomer distribution analysis (MIDA) (14) and isotopomer spectral analysis (ISA) (15) for this purpose, and both approaches indicated concurrent results.

In summary, the quantitation of fatty acyl-CoAs and their isotopic enrichment during stable isotope-labeling studies of lipid metabolism can provide data that significantly change the interpretation of analyte quantitation in these experiments, as demonstrated here for investigations of *de novo* sphingolipid biosynthesis.

CHAPTER 1

INTRODUCTION

1.1 Fatty acyl-CoAs and their metabolism

Fatty acyl-CoAs such as palmitoyl-CoA (Figure 1, *top panel*) are thioesters of fatty acids and Coenzyme A. They are intermediates in a wide array of metabolic processes, including the anabolism of more complex lipids, such as acylglycerols (16), glycerophospholipids (17), cholesteryl esters (18), and sphingolipids (19). The utilization of fatty acyl-CoAs during the *de novo* biosynthesis of sphingolipids is the central focus of this dissertation, however, a brief overview of fatty acyl-CoA metabolism (Figure 2) is warranted before proceeding to their participation in sphingolipid metabolism.

Fatty acyl-CoAs have been described as “activated” fatty acids in the sense that many of the cellular processes that consume acyl chains either for energy (e.g. carnitine palmitoyltransferase in mitochondria (20)) or for lipid biosynthesis (e.g. serine palmitoyltransferase in the endoplasmic reticulum (4, 21, 22)) require fatty acyl-CoAs as substrates and show little or no activity with free fatty acids as substrates. Thus, the generation and degradation of fatty acyl-CoAs are potential control points in lipid metabolism (23) that determine the availability of these substrates. A number of cellular processes are involved in determining the amounts of different fatty acyl-CoAs under a given set of conditions; these include the availability (24) and uptake (25, 26) of extracellular fatty acids, the synthesis of fatty acyl-CoAs (16, 27-36), their intracellular transport by carrier proteins (37, 38), their utilization by enzymes of lipid biosynthesis, their metabolism by elongases (39-45) and desaturases (46-48), their degradation by thioesterases (49-52), and their generation by intracellular lipid catabolism (53).

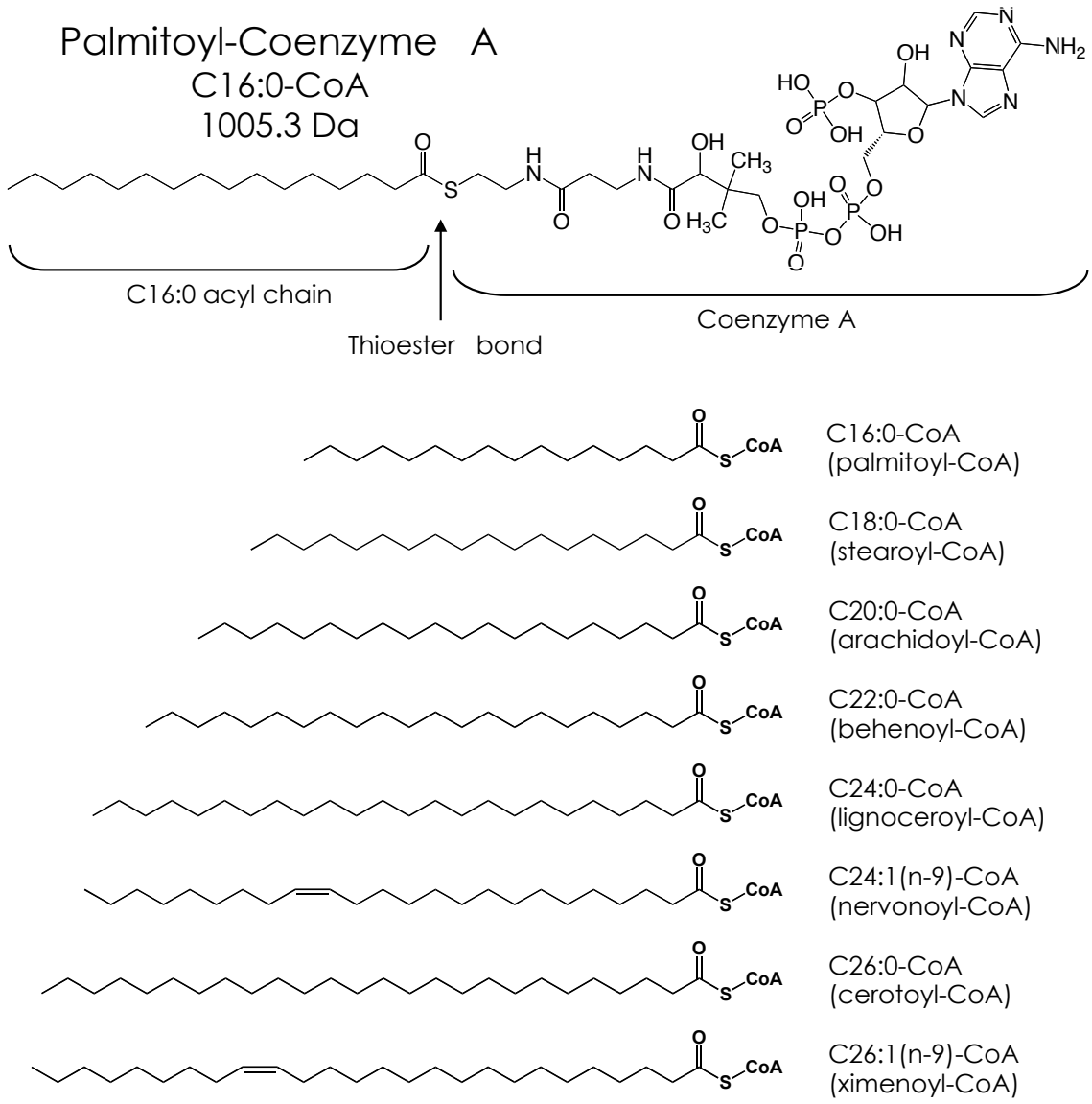

Figure 1. Palmitoyl-Coenzyme A with complete Coenzyme A structure (*upper panel*), and fatty acyl-CoAs utilized during *de novo* sphingolipid biosynthesis with abbreviated Coenzyme A structures (*lower panel*). In both panels, the Cx:y abbreviation denotes an acyl chain with x carbon atoms and y double bonds. The double bond nomenclature shown for nervonoyl- and ximenoyl-CoA specifies the first atom of the methylene bond counting from the omega (methyl) end of the acyl chain.

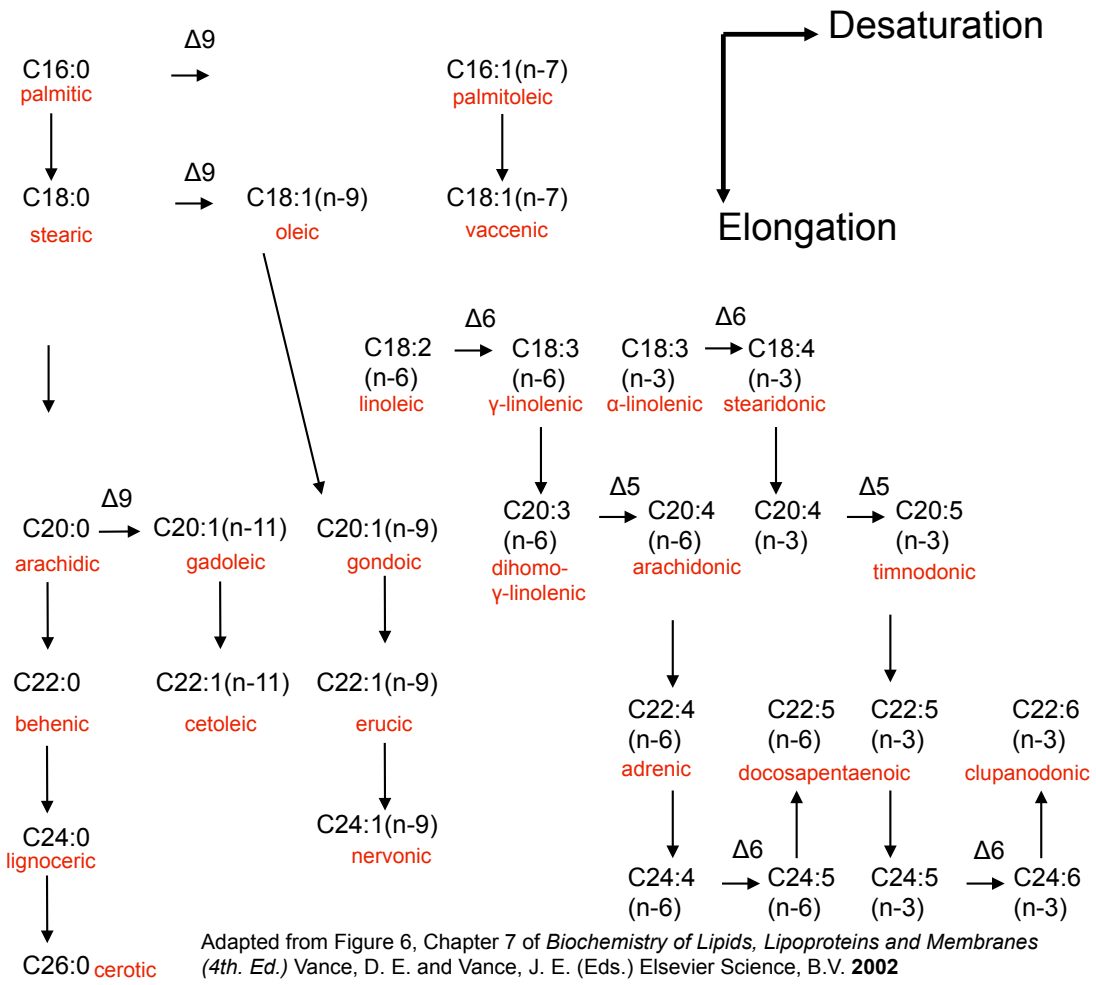

Figure 2. Fatty acyl-CoA acyl chain diversity generated by elongation, desaturation, and β-oxidation. The abbreviation Cx:y denotes an acyl chain with x carbon atoms and y double bonds. The common names in red font denote the fatty acid; fatty acyl-CoAs have the suffix –oyl rather than –ic. One example of a systematic name (docosapentaenoic) is also shown. The ΔN desaturase nomenclature indicates that the first carbon atom of the double bond is the Nth atom if numbering begins with the carbonyl carbon atom.

The wide variety of extracellular (dietary) and intracellular fatty acids together with the activities of synthetases, thioesterases, elongases and desaturases results in fatty acyl-CoAs with different chain lengths and numbers of double bonds (Figure 2). Despite this large number of fatty acyl-CoA molecular species, they appear to be selectively channeled into the biosynthesis of particular lipid classes (36) by mechanisms including enzyme specificity for a relatively narrow range of substrate fatty acyl-CoAs (54). For example, the *sn-2* acyl moiety of glycerophospholipids is frequently an acyl chain with 18 to 20 carbon atoms and 2 to 4 double bonds, based on the fatty acyl-CoA substrate specificity of 1-acyl-glycerol-3-phosphate O-acyltransferase (AGPAT) (55). The theme of lipid biosynthetic enzymes having relatively narrow substrate specificities for fatty acyl-CoAs will continue during the following overview of sphingolipid metabolism.

1.2 Sphingolipid metabolism

Sphingolipids are 1,3-hydroxy-2-amino alkanes or alkenes with substantial structural diversity. Sphingolipids are structural components of cellular membranes in all eukaryotes, and their variety of signal transduction roles is also established (56, 57). Selected sphingolipids and a portion of their *de novo* biosynthetic and turnover pathways are shown in Figure 3, from which it is clear that some molecular species are free sphingoid bases (non-acylated), other species are N-acylated sphingoid bases, and still other species are more complex N-acylated sphingoid bases with a polar moiety at the 1-position. Sphingoid bases shown in Figure 3 include sphinganine (Sa) and sphingosine (So), N-acyl species include dihydroceramide (DHCer) and ceramide (Cer), and 1-O-modified sphingolipids include ceramide-1-phosphate, glucosylceramide (GlcCer), and sphingomyelin (SM).

Although increasing molecular diversity results from a series of biosynthetic enzymatic reactions, it should not be overlooked that reversal of these reactions (catabolism or turnover) is a commonly encountered aspect of sphingolipid metabolism. Cells exert fine-tuned control over biosynthesis and catabolism, and opposing outcomes in cellular state may hang in the balance: So and sphingosine-1-phosphate (So-1-P) are interconverted by kinases and phosphatases (58); the non-phosphorylated sphingoid base is pro-apoptotic (59) but the phosphorylated sphingoid base is anti-apoptotic (60). Studies of sphingolipid biology require a high degree of specificity during the quantitation of multiple molecular species in a single sample because of the structural similarity and interconversion of sphingolipid species. Thus, the ability to analytically distinguish (resolve) these species is critical for the accurate determination of cellular sphingolipid quantities.

It is also important to emphasize that Figure 3 shows only a portion of sphingolipid metabolism, and numerous structural variations of sphingoid bases (61) and N-acyl sphingolipids have been described (61). The elaboration of carbohydrate-based 1-O-moieties, in particular, increases the number of sphingolipid structures into the thousands (www.sphingomap.org), indicating considerable room for further discoveries about sphingolipid structure, metabolism, and bioactivity.

1.3 Sphingolipid quantitation

Currently, among the numerous methodologies for the quantitation of multiple sphingolipids in small biological samples (which have been reviewed recently in (62) by this author) liquid chromatography-electrospray ionization tandem mass spectrometry (LC-ESI-MS/MS) analysis of cell extracts to which internal standards have been added is the most sensitive and specific. This approach is summarized below.

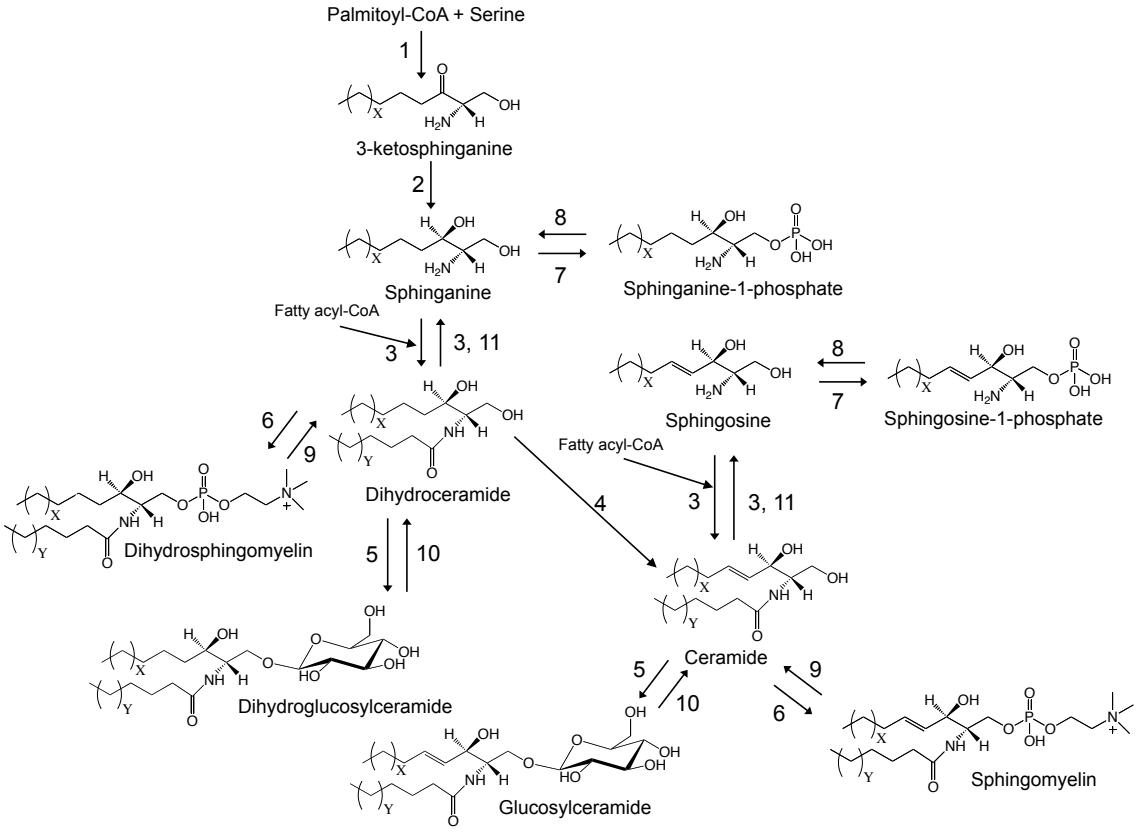

Figure 3. A portion of sphingolipid metabolism including *de novo* biosynthesis. The methylene subscript $-(CH_2)_x-$ is often 11 yielding a 1, 3-dihydroxy, 18 carbon alkyl chain with no sites of unsaturation (d18:0), but can range from 7 (d14:0) to greater than 15 (d22:0). The $-(CH_2)_y-$ of the fatty acyl chain typically ranges from 11 (16 carbons total) to greater than 25 (30 carbons total). Enzymes are serine palmitoyltransferase – 1, 3-ketosphinganine reductase – 2, (dihydro)ceramide synthase – 3, Δ4-dihydroceramide desaturase – 4, glucosylceramide synthase – 5, sphingomyelin synthase – 6, sphingosine/sphinganine kinase – 7, sphingosine-1-phosphate phosphatase – 8, sphingomyelinase – 9, ß-glucoceramidase – 10, and ceramidase – 11.

A typical experiment begins by culturing cells and treating them with, for example, stable isotope-labeled palmitate (63). Cells are collected after rinsing with phosphate-buffered saline (PBS) to remove medium and the lipids present in fetal calf serum (FCS), a common medium component. After the addition of appropriate internal standards ((64, 65), and see Experimental Procedures in Chapters 2-5) to the cell sample, organic solvents are added [typically 2:1 methanol / chloroform (v/v)] and sonication is used to disrupt cells and solubilize lipids. Further handling of the extract to purify sphingoid bases and N-acyl species has been reviewed recently (65).

The sample (see below) is injected onto a liquid chromatography (LC) column, and molecular species of sphingolipids are resolved (66) based on their relative affinities for the column's packing material (the stationary phase) and the solvents flowing through the column (the mobile phase) (67, 68). In addition to the resolution of analytes provided by LC, a second advantage is the washing away (non-retention on the column) of many cellular compounds that are not of interest and can have deleterious effects upon the detection of analytes.

The effluent from the LC column is connected to the electrospray ionization (ESI) source of a triple quadrupole tandem mass spectrometer (69). This ion source's central component is a hollow metal needle, which is held at a high positive or negative potential (70). At the exit tip of the needle, nebulizing gas produces highly charged solvent droplets containing analytes that are subsequently drawn towards the orifice of the mass spectrometer via both potential and atmospheric pressure differences. In the ESI source, these droplets become smaller by a combination of solvent evaporation (aided by the passage of high-temperature nitrogen through the electrospray stream) and the mutual repulsion of similar charges within and between droplets (acquired via passage through the high-potential electrospray needle). During the transition from atmospheric pressure

(in the ESI source) to vacuum (in the interface) the solvent is pumped away and the analytes are ionized in the gas phase (71).

Multiple reaction monitoring (MRM) is an MS/MS method used for quantitation (3, 65, 68, 72-77). MRM selects an ion with a particular mass-to-charge ratio (*m/z*) value (a precursor ion) using Q1, followed by collision-induced dissociation (78) of the precursor ion in Q2, and selection of a structure-specific *m/z* value (a fragment ion or product ion) with Q3. In practice, the instrument repeatedly monitors several precursor ion-product ion pairs, dwelling on each pair for 10 to 50 milliseconds. The entire list of MRM pairs can be monitored in less than 1 sec, allowing near-continuous monitoring for several analytes during LC elution time. Thus, as an analyte elutes from the LC column and is ionized in the ESI source, precursor ions selected with Q1 and product ions selected with Q3 via MRM result in a signal, or peak, on the extracted ion chromatogram (XIC). The integrated area of this peak is the basis for analyte quantitation.

LC-ESI-MS/MS of sphingolipids is sensitive and specific; analytes are identified by three criteria: LC elution time, precursor ion *m/z*, and structure-specific product ion *m/z*. In order to correct for sample-to-sample variability when quantitating an analyte by LC-ESI-MS/MS, a useful approach is the use of at least one internal standard molecular species. A stable isotope-labeled version of the analyte is desirable (see below), but in the absence of such a standard, analogs of the species of interest may be used, such as a sphingoid base with an odd number of carbon atoms (i.e., C_{17}) or a ceramide with an N-acyl chain length not observed in biological samples (i.e., C_{12}). A known quantity of this standard is added to the biological sample, the sample is extracted and analyzed, and the peak corresponding to the (internal) standard is used as a benchmark to determine the quantities represented by the peaks of the analytes. In this way, extraction inefficiency and sample-to-sample variation are corrected by the internal standard, assuming that its physical and chemical behavior in the extraction protocol is nearly

identical to that of the analyte. This is one reason that a stable-isotope labeled standard is desirable, another reason is that even small differences in molecular structure between the standard and the analyte can result in different ionization and / or fragmentation efficiencies between the standard and the analyte (3). These differences must be measured and, if they are significant, incorporated into the calculations that determine analyte quantity based on the standard's peak area. In both of the examples above, sphingoid bases and N-acyl sphingolipids, no such correction is necessary when using appropriate internal standards (65).

1.4 Stable isotope labeling of cultured mammalian cells

Because the catabolism (turnover) of sphingolipids has been shown to have a quantitatively significant contribution to the amounts of sphingolipids such as So (79) and Cer (80, 81), it is not always possible to distinguish the contributions of *de novo* biosynthesis and catabolism to the measured quantity of a particular sphingolipid. An important experimental approach for answering this question has been the treatment of cultured cells with radio-labeled precursors of sphingolipid metabolism, such as ^{3}H- or ^{14}C-labeled serine or palmitate (82, 83). An assumption of this technique is that these precursors are assimilated by the cells and metabolized in a manner identical to their unlabeled counterparts (an absence of "isotope effects"). In a well-implemented radio-labeling experiment the radioactivity of a purified metabolite and its quantity are measured, the specific activity of the metabolite (radioactivity per unit mass) is calculated, and this measurement provides direct information about the contribution of the labeled precursor to the biosynthesis of that metabolite during the time of the experiment.

A variation of this approach is to use stable isotope-labeled precursor (84) treatment of cultured cells, followed by quantitation of mass-shifted (and non-shifted)

metabolites using a (tandem) mass spectrometer (85-87). These mass-shifted molecules are isotopologues of the non-shifted (monoisotopic) molecules. By analogy to a radio-labeling experiment, the tracer-tracee ratio (TTR) or isotopic enrichment of an analyte can be calculated (shown in detail in Chapter 3 and (88)). Some advantages of using stable isotopes include avoiding the risk and regulations of radioisotope work, the ethical acceptance of stable isotope labeling during human experiments (89-91), and importantly, the availability of new dimensions of data (92). Specifically, MRM allows the molecular moieties labeled by the incorporation of stable isotope into analyte molecules to be determined, providing new details concerning their biosynthetic mechanisms, as demonstrated by the stable isotope labeling of palmitoyl-CoA and sphingolipids (Chapters 3-5).

1.5 Stable isotope labeling of fatty acyl-coenzyme A species and sphingolipids

Labeling with [U-^{13}C]-palmitate

The moiety common to fatty acyl-CoAs and sphingolipids is the acyl chain, therefore, treatment with a stable isotope-labeled fatty acid will label both types of lipids (93, 94), as well as other types of lipids (95, 96). The MS/MS analysis is greatly simplified if labeled molecules have mass shifts of more than 3 Da compared to unlabeled molecules (97), and [U-^{13}C]-palmitate, a C_{16} fatty acid in which every carbon atom is ^{13}C, was selected as the tracer during the first experiments (Figure 4). This tracer has a molecular mass (272 Da) that is 16 Da greater than that of

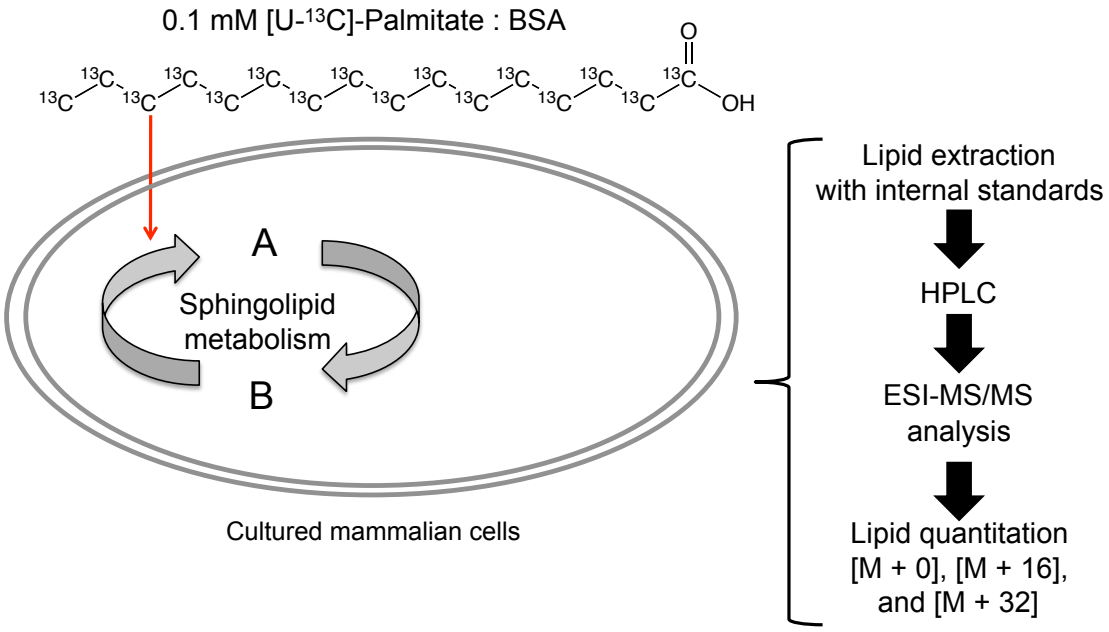

Figure 4. Labeling *de novo* biosynthesized sphingolipids with [U-^{13}C]-palmitate. Uptake of the stable isotope-labeled tracer by cultured cells and its incorporation into sphingolipids was quantitated by extracting lipids from samples of cells after different treatment times, and quantitating labeled and unlabeled lipids via LC-ESI-MS/MS as described in Chapters 2, 3, 4, and 5. Chemically identical molecular species of lipids were present as unlabeled [M + 0], singly-labeled [M + 16], and in certain cases, doubly-labeled [M + 32] isotopologues.

unlabeled palmitate (256 Da), and so labeled metabolites such as fatty acyl-CoAs and sphingolipids will have mass increases of 16 Da, or 32 Da if two labeled fatty acyl-CoA molecules were used to biosynthesize one sphingolipid molecule.

[U-^{13}C]-palmitate was added to the medium of HEK293 cells, and both labeled and unlabeled fatty acyl-CoAs and sphingolipids were quantitated by LC-ESI-MS/MS. The results of this analysis were compared with results for HEK293 cells stably over-expressing SPT (hereafter referred to as SPT1/2 cells), which have increased rates of *de novo* sphingolipid biosynthesis (Wei, et al., in preparation). The results indicated that SPT1/2 cells had significantly higher amounts of sphingolipids before [U-^{13}C]-palmitate treatment, and that the addition of the labeled palmitate caused a robust increase in [M + 16] and [M + 32] sphingolipids, which was several fold greater in SPT1/2 cells as detailed in Chapter 4.

The [U-^{13}C]-palmitate labeling experiments encompassed quantitation of palmitoyl-CoA, Sa, sphinganine-1-phosphate (Sa-1-P), So, and So-1-P using MRM pairs for the unlabeled [M + 0] and labeled [M + 16] isotopologues of each analyte. In addition, N-acyl sphingolipids were quantitated, including DHCer, Cer, dihydrosphingomyelin (DHSM), SM, ceramide monohexose (CMH), and dihydroceramide monohexose (DHCMH). These N-acyl sphingolipids have two acyl chains derived from fatty acyl-CoAs, and were therefore present as [M + 0] isotopologues (designated ^{12}C), [M + 32] isotopologues (designated dual labeled), and [M + 16] isotopologues. The latter were two isotopomers that could be discriminated by MS/MS fragmentation as being labeled on either the sphingoid base moiety (designated base labeled) or the N-acyl moiety (designated fatty acid labeled), with the exception of SM since positive ion mode MS/MS analysis of SM does not distinguish acyl chain labeling. However, the enzymatic

conversion of SM to ceramide-1-phosphate (Cer-1-P) by phospholipase D, followed by LC-ESI-MS/MS analysis of the Cer-1-P did distinguish fatty acid and base labeled isotopomers (Chapter 3).

Interpretation of dynamic [U-^{13}C]-palmitate labeling data to calculate the rate of appearance of unlabeled analytes

The dynamic collection of quantitative data from 0 to 6 hr for both labeled analytes (tracers) and unlabeled analytes (tracees) allowed the application of mathematical modeling (Figure 5) for the estimation of the rates of fatty acyl-CoA and sphingolipid biosynthesis. This previously described approach (88) uses quantitation of tracer and tracee to calculate the analyte isotopic enrichment (defined here as tracer / tracer + tracee), which is plotted vs. time in order to graphically visualize labeling of the analyte. Depending upon the analyte, the choice of tracer, the kinetics of the metabolic system under investigation, and the duration of the labeling experiment, a steady-state in the isotopic enrichment of a particular analyte may or may not be achieved. If so, the steady state is interpreted to be a condition where the rate of appearance (R_a) of tracer is equal to the rate of disappearance (R_d) of tracer from the metabolite pool, and knowledge of the pool size and its plateau isotopic enrichment can be used to back-calculate the R_a of tracee (unlabeled analyte).

Specifically, the labeling kinetics (of a single-pool metabolite with constant concentration during the experiment) are described by the following equation (88):

$$E_t = E_p\left(1 - e^{-kt}\right)$$

Eq. 1

E_t = analyte isotopic enrichment at time = t (in h)

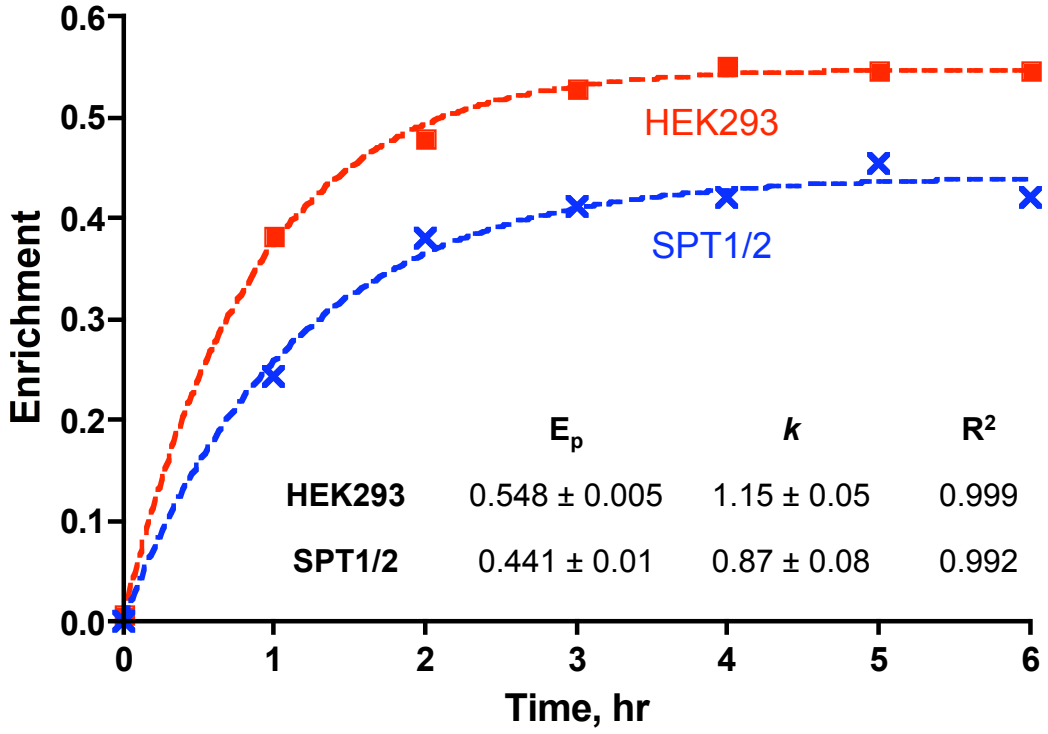

Figure 5. The isotopic enrichment of d18:1/C16:0 ceramide in HEK293 and SPT1/2 cells during 6 hr of treatment with 0.1 mM [U-^{13}C]-palmitate. Isotopic enrichment and curve-fitting were calculated as described in Experimental Procedures, Chapter 4. The plateau isotopic enrichment (E_p) and fractional turn-over rate per hr (*k*) estimated by the data, as well as goodness-of-fit (R^2) for each cell type is shown. Results are based on the mean of four Petri dishes for each cell type, and both *k* and E_p were significantly different ($p < 0.05$) by Student's t-test. The physiological interpretation of E_p for the analyte is the fraction of newly biosynthesized polymer (55% vs 44%), and of *k* is the turn-over rate per unit time (1.2 times per hr vs. 0.9 times per hr).

E_p = plateau isotopic enrichment of the analyte at steady-state

k = fractional turn-over rate of the analyte pool per unit time

By software-based curve-fitting of the observed isotopic enrichment data to Eq. 1 with concurrent estimation of E_p and *k*, the LC-ESI-MS/MS quantitation of the metabolite pool size (Q) allows the calculation of the R_a of (tracer + tracee). Finally, by calculating the R_a of tracer alone using E_p, this value can be subtracted from the R_a of (tracer + tracee), and the R_a of tracee determined. This value represents the rate of appearance of unlabeled analyte during the experiment, and in the work described here it is interpreted to represent the rate of *de novo* biosynthesis of the analyte.

The results of this analysis of fatty acyl-CoA and sphingolipid isotopic labeling are consistent with a high turn-over rate for palmitoyl-CoA, which is also supported by the coarse observation that it is rapidly (~ 3 h) and robustly (~ 60%) labeled in HEK293 cells using [U-^{13}C]-palmitate as the tracer. The fractional turn-over rate per unit time (*k*) of the palmitoyl-CoA pool in HEK293 and SPT1/2 cells was calculated to be approximately 0.7, or 70% turn-over of the palmitoyl-CoA pool in 1 h. In contrast to C16:0 Cer, there was not a significant difference in palmitoyl-CoA isotopic enrichment, *k*, or R_a when comparing HEK293 and SPT1/2 cells, supporting the hypothesis that increased sphingolipid *de novo* biosynthesis, rather than differences in the sphingolipid biosynthetic precursor palmitoyl-CoA, were the cause of increased quantities of labeled sphingolipids in SPT1/2 cells.

Labeling RAW264.7 cells with [1-^{13}C]-acetate: an alternative to the [U-^{13}C]-palmitate tracer

A second approach to the stable isotope-labeling of fatty acyl-CoAs and sphingolipids utilized [1-^{13}C]-acetate. The motivations for taking this approach were previously reported changes in lipid metabolism (98) and gene transcription (99) that

accompany treatment of cells with palmitate at concentrations similar to the one used in these experiments, and so an alternative metabolic route to the isotopic labeling of fatty acyl-CoAs and sphingolipids was desirable. One such route is *de novo* fatty acid biosynthesis (Figure 6), which can be probed by the treatment of cells with stable isotope-labeled acetate, such as [1-^{13}C]-acetate.

After uptake by cells, a metabolic fate of [1-^{13}C]-acetate is activation to acetyl-CoA, followed by conversion to malonyl-CoA via acetyl-CoA carboxylase (100-103), and finally incorporation into *de novo* biosynthesized palmitate via fatty acid synthase (FAS(103-106)). Since eight C_2 molecules are converted by FAS into a single C_{16} molecule, *de novo* palmitate (and therefore *de novo* palmitoyl-CoA) can be labeled with 0 to 8 ^{13}C atoms, depending upon the isotopic enrichment of the malonyl-CoA precursor pool. This biosynthetic action will change the abundances of palmitoyl-CoA isotopologues, and by using the multinomial distribution to describe the observed pattern, the isotopic enrichment of the malonyl-CoA precursor pool can be calculated. In addition, the fraction of the palmitoyl-CoA that was newly synthesized (and displays an altered mass isotopomer distribution) can be determined. Two approaches were taken for data analysis after the [1-^{13}C]-acetate treatment experiments: mass isotopomer distribution analysis (MIDA) as described by Hellerstein and Neese (14), and isotopomer spectral analysis (ISA) as described by Kelleher and Masterson (15). Both analyses calculated similar estimates of the isotopic enrichment of the precursor pool (~ 5-10%) and of the fraction of newly synthesized polymers (~60%).

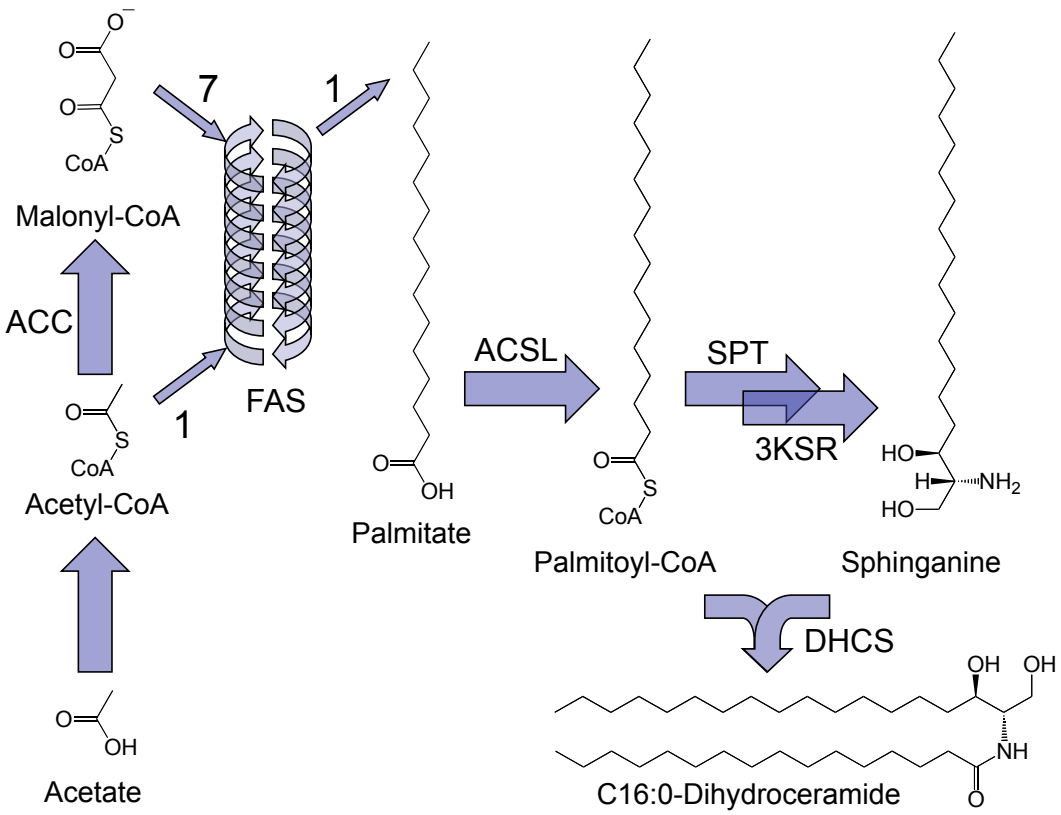

Figure 6. Labeling *de novo* biosynthesized sphingolipids with [1-^{13}C]-acetate. Enzyme abbreviations are acetyl-CoA carboxylase (ACC), fatty acid synthase (FAS), acyl-CoA synthetase (ACSL), serine palmitoyltransferase (SPT), 3-ketosphinganine reductase (3KSR), and (dihydro)ceramide synthase (DHCS).

1.6 Summary

The development of a method for quantitation of fatty acyl-CoAs by LC-ESI-MS/MS in small samples of biological material [Chapter 2 and (3)] supplements studies of the metabolism of complex lipids, such as sphingolipids. For example, a cultured cell paradigm in which increased quantities of sphingolipids were observed has been confirmed to be the results of increased *de novo* sphingolipid biosynthesis, rather than increased catabolism of pre-existing sphingolipids.

Specifically, the over-expression of serine palmitoyltransferase, the first enzyme of *de novo* sphingolipid biosynthesis, in HEK293 cells resulted in increased quantities of sphingolipids, and a greater accumulation of [M + 16] and [M + 32] sphingolipids after treatment with [U-^{13}C]-palmitate (Chapter 4). The ability to quantitate [M + 0] and [M + 16] palmitoyl-CoA showed that the isotopic enrichment of palmitoyl-CoA was not the source of observed differences in isotopically labeled sphingolipids.

Furthermore, the quantitation of the isotopic enrichment of palmitoyl-CoA allowed the total quantity of *de novo* biosynthesized sphingolipids to be estimated, if one assumes that a single, well-mixed pool of palmitoyl-CoA is available for SPT and CerS. Comparison of the observed quantity of unlabeled ceramide to the quantity that was calculated to have been *de novo* biosynthesized implied that ~ 50% of the observed unlabeled quantity could be accounted for by *de novo* biosynthesis in HEK293 and SPT1/2 cells (Chapters 3 and 4). Therefore, quantitation of the isotopic enrichment of palmitoyl-CoA provided data that significantly changed the interpretation of sphingolipid quantitation in these experiments.

The availability of data about isotopic labeling of sphingolipids (Chapter 3) suggested the application of previously described approaches for the analysis of metabolic labeling; one such approach (88) led to calculating enrichment for fatty acyl-CoAs and sphingolipids and the observation that some species clearly reached isotopic

equilibrium. Modeling this isotopic enrichment and measurement of metabolite quantities with LC-ESI-MS/MS allowed the estimation of the rate of appearance of unlabeled metabolite, which quantitated the increase in *de novo* sphingolipids (2 to 5-fold) caused by over-expression of SPT in HEK293 cells (Chapter 4).

Although metabolic labeling of *de novo* sphingolipid biosynthesis with [U-^{13}C]-palmitate was informative, an alternative to [U-^{13}C]-palmitate was also used: labeling of *de novo* biosynthesized palmitate via treatment of cultured cells with [1-^{13}C]-acetate (Chapter 5). Two previously described approaches based on multinomial distribution (14, 15) were taken for the analysis of the [1-^{13}C]-acetate labeling data; both approaches reached similar conclusions about the isotopic enrichment of the biosynthetic precursor acetate (6 to 10%) and the fraction of newly biosynthesized palmitoyl-CoA (~ 60%) after 6 hr of treating RAW264.7 cells with 1.0 mM [1-^{13}C]-acetate.

In summary, the quantitation of fatty acyl-CoAs, and particularly quantitation of their isotopic enrichment during stable isotope-labeling studies of lipid metabolism, can provide data that significantly change the interpretation of analyte quantitation in these experiments, as demonstrated here for investigations of *de novo* sphingolipid biosynthesis.

CHAPTER 2.

QUANTITATION OF FATTY ACYL-COENZYME A SPECIES IN MAMMALIAN CELL EXTRACTS BY LIQUID CHROMATOGRAPHY-ELECTROSPRAY IONIZATION-TANDEM MASS SPECTROMETRY (LC-ESI-MS/MS)[1]

2.1 Introduction

Fatty acyl-CoAs participate in energy metabolism, the biosynthesis and recycling of complex lipids, post-translational modification of proteins, regulation of gene expression, and other cellular processes (107). They are derived from *de novo* fatty acid biosynthesis and the recycling of preexisting fatty acids (73), and serve as intermediates of most fatty acid modification reactions, such as oxidation (108), elongation and desaturation (109). Hence, for both metabolic and regulatory studies, it would be useful to have an analytical method to quantitate a wide variety of these compounds.

Mass spectrometry (MS) and tandem mass spectrometry (MS/MS) have been shown to be particularly useful for analysis of fatty acyl-CoAs because they provide high levels of structural specificity and sensitivity (93, 110-115), especially when combined with liquid chromatography (LC) and electrospray ionization (ESI) (93, 110-113). Previously published methods have used negative ion mode MS (93) and MS/MS (111, 112), as well as positive ion mode MS/MS utilizing a precursor ion scan (110), but they have not been applied to a wide spectrum of fatty acyl-CoA molecular species, especially the very-long-chain fatty acyl-CoAs with alkyl chain lengths greater than 20 carbons.

[1] This chapter has been published; the authors are Haynes, C., Allegood, J., Sims, K., Wang, E., Sullards, M., and Merrill, A.

This chapter describes an LC-ESI-MS/MS protocol (3) that builds on some of the features of these methods for analysis of a wider profile of fatty acyl-CoAs than has heretofore been reported, i.e., with alkyl chain lengths varying from C14 (myristoyl-CoA) to C26 (cerotoyl-CoA), and is potentially applicable to species as short as C2 (acetyl-CoA) and free CoA-SH. Analysis of extracts from RAW264.7 cells (a mouse macrophage-like line) and MCF7 cells (a human breast carcinoma line) demonstrated the method's utility for profiling and quantitating multiple molecular species of fatty acyl-CoAs in relatively small samples, and revealed interesting differences in the fatty acyl-CoA profiles for these cell lines. The availability of this fairly simple and robust method should facilitate inclusion of this family of compounds in a wide range of studies, including more comprehensive analyses such as "lipidomics" and "metabolomics."

2.2 Experimental procedures

Reagents

Fatty acyl-CoAs (C14 to C26 and the odd chain-length internal standards C15:0-, C17:0-, C23:0-, and C25:0-CoA) were obtained as tri-ammonium salts from Avanti Polar Lipids (Alabaster, AL) and according to the manufacturer, analysis of the fatty acyl-CoAs by TLC, HPLC, mass spectrometry, NMR and other tests such as the Bartlett assay for phosphorus were consistent with the purity being >99%. CoASH (lithium salt monohydrate), acetyl- (C2:0-) (sodium salt), octanoyl- (C8:0-) (sodium salt) and lauroyl- (C12:0)-CoA (sodium salt) were from Sigma-Aldrich (St. Louis, MO) and were 95-99% pure. HPLC-grade CH_3OH (catalog number MX0475-1), CH_3CN (AX0145-1) and $CHCl_3$ (CX1058-1) were from EMD (Darmstadt, Germany). Triethylammonium acetate (TEAA) was from Fluka (Buchs, Switzerland), and triethylamine (TEA) was from Sigma-Aldrich (St. Louis, MO). The water (> 18 MΩ / cm) was purified by a Barnstead Diamond Nanopure system (Boston, MA).

Cell culture

MCF7 cells (HTB-22) and RAW264.7 cells (TIB-71) were obtained from the ATCC (Manassas, VA). RAW264.7 cells were grown in DMEM (Cellgro catalog number 10-013, that contains 4 mM L-glutamine, and 4.5 g/l glucose, Mediatech, Manassas, VA), and 10% heat-inactivated fetal calf serum (HyClone catalog number SH30071.03, Logan, UT). MCF7 cells were grown in MEM supplemented with 10% FBS (HyClone catalog number SV30071.03, Logan, UT), 2 mM L-glutamine, 0.1 mM non-essential amino acids, 1 mM sodium pyruvate, and 0.01 mg/ml bovine insulin. Media for both cell types included tissue-culture grade 1.5 g/l sodium bicarbonate (1.5 g/l), and 100 U/ml penicillin plus 0.1 mg/ml streptomycin (Gibco catalog number 15140-122, Invitrogen, Carlsbad, CA). Both cell types were cultured at 37°C, 95% relative humidity, and 5% CO_2. Dishes (60 mm, catalog number 430166, Corning Inc., Corning, NY) of RAW264.7 cells were seeded at 2 x 10^6 cells per dish and grown for approximately 30 h before harvesting for lipid analysis. Dishes (100 mm, catalog number 430293, Corning Inc., Corning, NY) of MCF7 cells were seeded at 2 x 10^6 cells/ml and grown for approximately 48 h. For the RAW264.7 cells, the cell culture conditions followed the standard protocol adopted by the Lipid MAPS Consortium (www.lipidmaps.org).

Cell extraction

Dishes of cells cultured as described above (typically 0.5 to 2 x 10^7 cells) were placed on ice, the medium was aspirated, and adherent cells were gently washed twice with 5 ml each of chilled PBS then once with 5 ml of chilled distilled water (which did not cause cell lysis as assayed by Trypan Blue exclusion, if added and removed rapidly). Using a rubber policeman, the cells were rapidly scraped into a corner of the tilted dish and mixed to a uniform suspension in the residual water (~0.3 ml) with a pipette from

which 50 μl was removed for cell quantitation by counting (or analysis of protein or DNA) and 200 μl for analysis of the fatty acyl-CoAs. This procedure avoids centrifugation of the cells after they have been removed from the Petri dish because a substantial percentage of RAW264.7 cells were broken during scraping; analysis of more robust cells can use centrifugation for the washes.

The aliquot for fatty acyl-CoA analysis was placed in a screw-cap tube (13 x 100 mm, catalog number 73750-13100, with a Teflon-lined cap, Kimble Chase, Vineland, NJ) on ice. To this was added 500 μl of CH_3OH containing 1 mM EDTA (added to the CH_3OH from a 0.5 M aqueous stock) and 10 μl of an internal standard mixture that contained 100 pmol each of C15:0-, C17:0-, C23:0- and C25:0-CoA which were prepared in $CH_3OH/CHCl_3$ (2:1, v/v) containing 30 mM TEAA. After a brief sonication (~0.5 min), 250 μl of $CHCl_3$ was added, followed by another brief sonication, and the single-phase extraction mixture was incubated for 30 min in a 50° C heating block. After cooling to room temperature, $CHCl_3$ and H_2O (250 μl each) were added with mixing by vortexing after each addition. After brief centrifugation (2000 rpm for 5 min at room temperature), the fatty acyl-CoAs were in the upper phase and interface and most of the other lipids (which would interfere with the subsequent reverse phase LC) were in the lower phase. The upper layer was removed with a Pasteur pipet and transferred into a screw-cap tube (13 x 100 mm, catalog number 73750-13100, with a Teflon-lined cap, Kimble Chase, Vineland, NJ), and the remainder (interface and lower layer) was re-extracted twice (each time with brief centrifugation to separate the two phases cleanly) with 0.5 μl each of synthetic upper phase ($H_2O:CH_3OH:CHCl_3$ (45:50:5, v/v/v), from which the upper phases were added to the same screw-cap tube as the first extract. To the pooled upper phases was added 180 μl of $CH_3OH:CH_3(CH_2)_2CH_2OH:CHCl_3$

(50:25:25, v/v/v), which was found to help keep the very-long-chain fatty acyl-CoAs in solution for at least 24 hr at room temperature and / or at least 3 days at -20°C.

Chromatographic conditions

The HPLC separations utilized a Shimadzu SCL-10A VP system controller, two LC-10AD VP pumps, a DGU-14A degassing unit, a Perkin-Elmer Series 200 autosampler, and a Phenomenex (Torrance, CA) Gemini C18 column (2 mm ID x 150 mm with 5 μm particles) and a 2 x 4 mm guard column with the same packing material. The column was maintained at 40° C using a MetaTherm column oven (MetaChem, Torrance, CA).

The flow rate was 200 μl per min in binary gradient mode with the following elution program: the column was equilibrated with mobile phase A (H_2O/CH_3CN, 85:15, v/v, containing 0.05% TEA), the sample was injected and mobile phase A was continued for 5 min, followed by a 14 min gradient to 50% mobile phase A and 50% B (H_2O/CH_3CN, 10:90, v/v, containing 0.05% TEA) during which the long- and very-long-chain fatty acyl-CoAs elute. Afterwards, the column was washed by a 1-min gradient to 100% B and a 5 min hold at 100% B, followed by re-equilibration of the column by a 1 min gradient to 100% A and a 5 min hold at 100% A before injection of the next sample.

Mass spectrometry of fatty acyl-CoAs

The analyses were conducted using an Applied Biosystems (Foster City, CA) 4000 QTrap triple quadrupole/linear ion trap mass spectrometer. Dry N_2 gas was used for nebulizing the column effluent (Gas 1), and for the desolvation gas (Gas 2), curtain and collision gases, with instrument settings of 35, 25, 15 (arbitrary units), and medium, respectively. The interface heater was on (100° C) and the Turbo V ESI source

temperature was 350° C. The ESI needle voltage was 5.5 kilovolts (kV) in positive ion mode and -4.5 kV in negative ion mode.

To establish the optimal parameters for MS and MS/MS, stocks of the fatty acyl-CoA standards (~ 0.5 mM each) were prepared in $CH_3OH/CHCl_3$ (2:1, v/v), then diluted before use to 1 μM with H_2O/CH_3CN (50:50, v/v) containing 30 mM TEAA. The compounds were infused at 10 μl/min to optimize desolvation potential (DP), collision energy (CE), and collision-activated dissociation (CAD) gas to yield maximum sensitivity for the singly protonated $(M + H)^+$ fatty acyl-CoA precursor ions in positive ion mode and for the singly deprotonated $(M – H)^-$ species in negative ion mode. A narrow (6 Da) width Q1 scan was used to determine the optimum DP for each standard.

The MS/MS parameters were determined by identifying the acyl-chain retaining product ions, which in positive ion mode resulted from loss of 507.0 Da from the $(M + H)^+$ precursor, as has been previously observed (110, 115) and optimizing CE, collision cell exit potential (CXP) and CAD gas values for each molecular species (Table I).
After the elution time for each fatty acyl-CoA of interest was determined using the LC conditions described in the preceding section, the compounds were dissolved in the corresponding proportions of mobile phase A and B for flow injection analysis (FIA) to re-optimize source-dependent parameters to values appropriate for the higher flow rate (200 μl/min) of the HPLC used in this study (Table I).

Quantitation of fatty acyl-CoAs in cultured cells

For each new biological sample, the fatty acyl-CoA species of a cell extract that was not spiked with internal standards were first profiled to determine the minimum number of precursor-product pairs that were needed for the multiple reaction monitoring (MRM) protocol. This was conducted using neutral loss (507.0 Da) scans during the

Table I. Mass Spectrometer Settings and Chromatographic Properties of Selected Fatty Acyl-CoAs

Acyl-CoA[a]	Q1 *m/z*	Q3 *m/z*	DP, CE, CXP[b] (eV)	LC Retention[c] (min)	Peak area per pmol[d] (cps x 10^5)
14:0	978.3	471.3	180, 50, 12.7	11.4	2.2
15:0	992.4	485.4	190, 50, 13.0	12.2	2.3
16:0	1006.4	499.4	180, 50, 13.3	12.7	2.5
17:0	1020.4	513.4	180, 53, 13.5	13.3	2.5
18:0	1034.4	527.4	190, 52, 14.3	14.1	2.9
αOH-18:0	1050.3	543.4	195, 55, 14.5	13.1	2.1
18:1	1032.4	525.4	185, 52, 13.9	13.1	2.1
18:2	1030.4	523.4	180, 52, 14.0	12.7	ND
18:3	1028.4	521.4	190, 50, 14.5	12.3	ND
20:0	1062.4	555.4	190, 52, 15.3	14.5	2.4
20:4	1054.4	547.4	180, 52, 15.0	12.3	1.8
22:0	1090.4	583.4	190, 53, 16.3	15.1	2.0
22:6	1078.4	571.4	190, 51, 16.0	12.3	1.1
23:0	1104.5	597.5	200, 55, 16.5	15.5	1.9
24:0	1118.5	611.5	210, 57, 17.0	15.9	1.3
24:1	1116.5	609.5	208, 57, 17.0	15.2	2.0
25:0	1132.5	625.5	218, 59, 17.5	16.2	1.1
26:0	1146.4	639.5	220, 58, 17.5	16.6	0.84

[a]Number of linear chain carbon atoms:number of double bonds; αOH denotes an α-hydroxy fatty acyl chain

[b]Desolvation potential (DP), collision energy (CE), and collison cell exit potential (CXP).

[c]During LC the ion source conditions were: temperature at 350°C, Gas 1 at 35 arbitrary units, Gas 2 at 25 arbitrary units, electrospray needle voltage at 5.5 kV.

[d]Slope of the linear regression of a calibration curve for each analyte (abcissa = pmol, ordinate = peak area (cps), y-intercept = 0); the slope has units of cps per pmol. All R-squared values were ≥ 0.999, except C26:0 (0.991).

HPLC elution with three periods having DP, CE, and CXP settings that were appropriate for analytes that eluted during those times: period 1 (0 to 11 min) scanned *m/z* values 750 to 980 which encompassed CoASH to C14:0-CoA; period 2 (11 to 15.1 min) scanned *m/z* values 980 to 1070, which encompassed C14:0-CoA to C20:0-CoA; and period 3 (15.1 to 18 min) scanned *m/z* values 1050 to 1150, which encompassed C20:0-CoA to C26:0-CoA. After identification of the analytes that were detectable (3 times signal to noise), the MRM program was built to include these, the internal standards, and sometimes additional analytes of potential interest.

The fatty acyl-CoAs were quantitated by LC-ESI-MS/MS in positive ion mode utilizing the MRM pairs shown in Table I, which correspond to $(M + H)^+$ precursor ions (selected with Q1), and the structure-specific product ion resulting from a neutral loss of 507.0 Da (selected with Q3). The amount of each analyte of interest was calculated as follows: 1) LC chromatogram peaks for internal standards and endogenous fatty acyl-CoAs were integrated using Analyst 1.4.2 software (Applied Biosystems, Foster City, CA) and peak areas were copied to spreadsheets, 2) for each endogenous analyte, a cognate internal standard was selected based upon either similarity of acyl chain length or similarity of LC elution time (whichever is most appropriate), and 3) the following equation was used to calculate pmol of analyte ($pmol_a$):

$$pmol_a = (A_a / A_{is}) \times (pmol_{is}) \times (M_{is} / M_a)$$

where A_a = analyte peak area, A_{is} = internal standard peak area, $pmol_{is}$ = spiked pmol of internal standard, M_{is} = slope of the linear regression of the internal standard's calibration curve, and M_a = slope of the linear regression of the analyte's calibration curve. If desired, the observed peak areas (representing monoisotopic ions) may be isotopically corrected; however, this is not usually necessary if the analyte and internal

standard are similar (i.e., the correction is less than 2% per methylene difference in the fatty acyl chain length).

The calibration curves for the fatty acyl-CoAs were prepared by serially diluting each compound and analysis by LC-ESI-MS/MS as described above. In addition, calibration curves were generated for select fatty acyl-CoAs by spiking six different quantities from 0.1 to 5 pmol of the internal standards (C15:0-, C17:0-, C23:0- and C25:0-CoA) into RAW264.7 cell extracts and analyzing by LC-ESI-MS/MS. The limit of detection (LOD) and the limit of quantitation (LOQ) were defined as 3 times signal to noise, and ten times signal to noise, respectively. Plotting quantities analyzed (abcissa) vs. observed peak areas (ordinate) was followed by linear regression (with y-intercept = 0) to calculate the slope of this regression line (Table I).

Validation of the extraction and LC-ESI-MS/MS conditions

To determine the efficiency with which fatty acyl-CoAs were recovered, the three upper phases from the cell extraction procedure (see above) were collected individually and the lower layer was extracted an additional fourth time, then each was analyzed separately by LC-ESI-MS/MS and compared to the peak areas for fatty acyl-CoAs not carried through these extraction procedures.

Statistical analysis

All data shown are the results of at least three analytical replicates (LC-ESI-MS/MS analyses) of at least three biological replicates (culture dishes) and are representative of at least two independent experiments (conducted on different days). Data are shown as means ± standard deviations; all statements of significant difference are based upon Student's t-test with $p \leq 0.05$.

2.3 Results

The goal of these experiments was to develop a quantitative LC-ESI-MS/MS analysis method for a wide range of fatty acyl-CoAs suitable for small samples, such as cultured mammalian cells. The strategy that was followed was to examine the ionization and fragmentation of purified fatty acyl-CoAs, to select candidate precursor ion-product ion pairs for multiple reaction monitoring (MRM) analysis, to determine LC conditions that separated a substantial number of species to allow unambiguous quantitation, and to identify internal standards and extraction conditions that are effective with biological samples, using two mammalian cell lines (RAW264.7 and MCF7) as prototypes.

Characterization of fatty acyl-CoAs by MS and MS/MS

The MS spectra of standard C16:0-CoA contain both $(M + H)^+$ ions and $(M + Na)^+$ adducts in positive ion mode (Figure 7A), and $(M – H)^-$ ions and $(M – 2H + Na)^-$ adducts in negative ion mode (Figure 7B) at the electrospray needle voltage yielding the most intense signal for singly (de)protonated precursor ions. The $(M - H)^-$ signal was approximately 7-fold more intense than the $(M + H)^+$ signal for identical sample, infusion, solvent, and ion source conditions, except the polarity of the electrospray needle, which was at the maximum voltage setting in both ionization modes.

The MS/MS spectra for collision-induced fragmentation of the $(M + H)^+$ molecular ions of C16:0-CoA (*m/z* 1006.4) yielded highly abundant product ions of *m/z* 499.4 (Figure 8, *upper*), which correspond to cleavage of the C-O bond of the 5'-ß-phosphate with charge retention on the acyl portion of the molecule. Less abundant product ions of *m/z* 428.4, 397.4, 261.1, 159.0, and 136.0 were also detected. Proposed fragmentations are shown (Figure 8, *upper*) which correspond to the *m/z* 428.4, 261.1 and 136.0 product ions. The *m/z* 397.4 product ion also retains the acyl chain (see below).

Collision-induced fragmentation of the $(M - H)^-$ molecular ions of C16:0-CoA (*m/z* 1004.4) yielded product ions of *m/z* 924.5, 657.4, 408.0, 328.1, and 159.0. The ion of *m/z* 657.4 corresponds to cleavage of the C-O bond of the 5'-α-phosphate, subsequent loss of water, and charge retention on the acyl portion of the molecule; the other product ions correspond to the proposed fragmentations shown (Figure 8, lower).

The MS/MS fragmentations of all of the fatty acyl-CoAs analyzed shared similarities in positive and negative ion modes, and a systematic nomenclature for these product ions is proposed in Figure 9. Positive ion mode MS/MS resulted in abundant product ions retaining the acyl moiety (Z ions; Figure 9*A* and 9*B*) as well as product ions derived from the coenzyme A moiety (A, B, and C ions; Figure 9*A* and 9*B*). At least one additional product ion resulting from a neutral loss of 609 Da retained the acyl moiety (*m/z* 383 and 523; Figure 9*A* and 9*B*, respectively). Similarly, negative ion mode MS/MS resulted in product ions retaining the acyl moiety (X ions; Figure 9*D* and 9*E*) as well as product ions derived from the coenzyme A moiety (A, B, and C ions; Figure 9*D* and 9*E*).

Many of these product ions have been noted in earlier publications. For example, positive ion mode ESI-MS/MS has been shown to yield Z, B, and C ions and product ions resulting from a neutral loss of 609 Da (110, 113), as well as A ions and *m/z* 261 and 159 products (110). Negative ion mode ESI-MS/MS has been shown to yield X, X-H_2O, X-HPO_3, C, and C-H_2O ions (111, 113) as well as B ions (113).

The results from the MS and MS/MS analyses were used to choose precursor (selected by Q1) and product (selected by Q3) ion pairs for multiple reaction monitoring (MRM). For maximum sensitivity and specificity, the product ion should be both abundant and structure-specific for the acyl moiety, and these criteria are met by the positive mode Z product ion (e.g., *m/z* 499.4 for C16:0-CoA, Figure 8, *upper*), which is easily optimized as the base peak of the tandem mass spectrum. In the negative ion

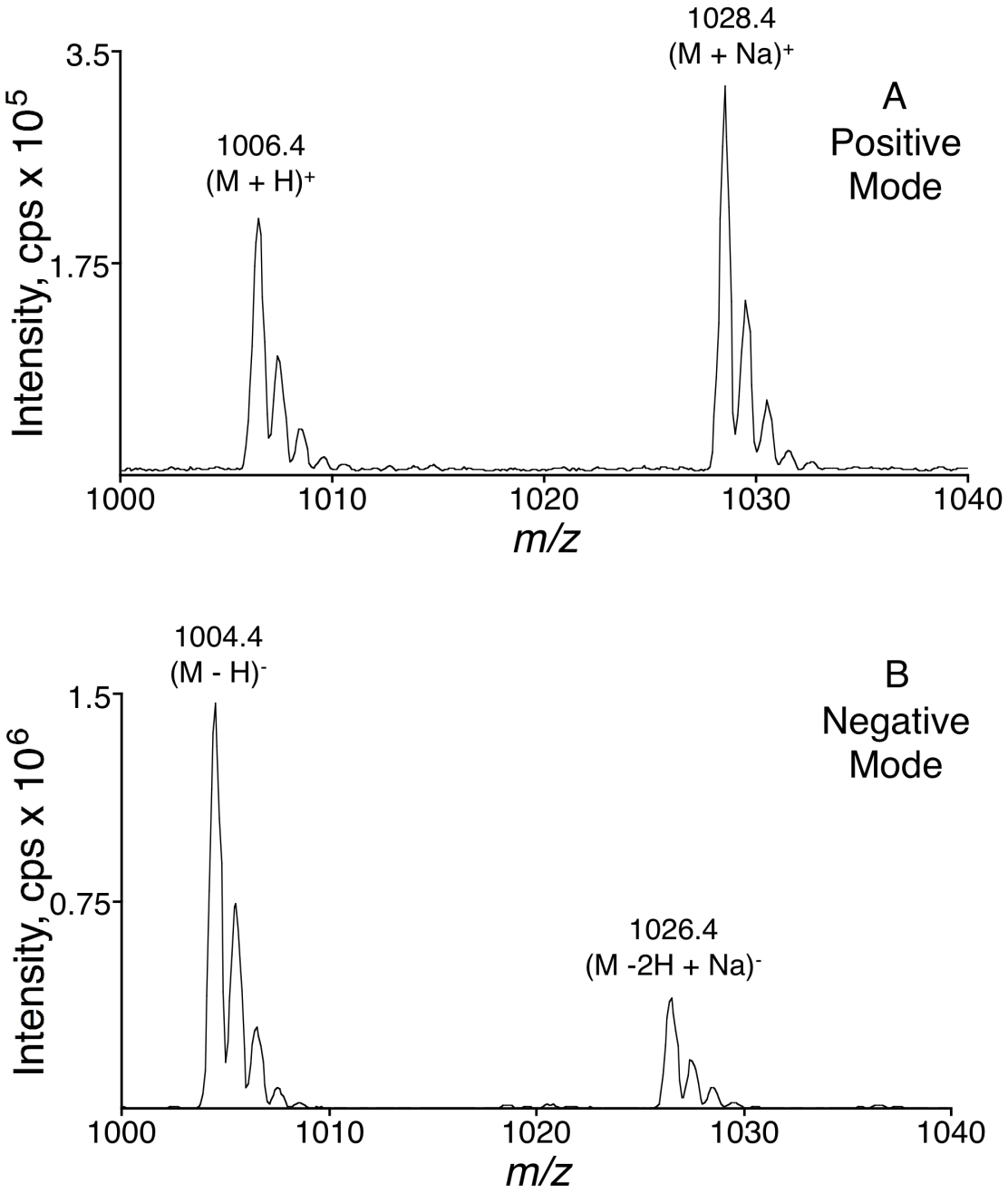

Figure 7. Mass spectra of C16:0-CoA in the high mass region using positive (A) and negative (B) ionization modes. Q1 scans using a triple quadrupole tandem mass spectrometer are shown. Labels above the peaks denote m/z values of the monoisotopic peaks and describe the (de)protonated or sodium adduct ions. Spectra (summation of 1 min scans) were collected during the infusion (10 μl / min) of C16:0-CoA at a concentration of 1 pmol / μl.

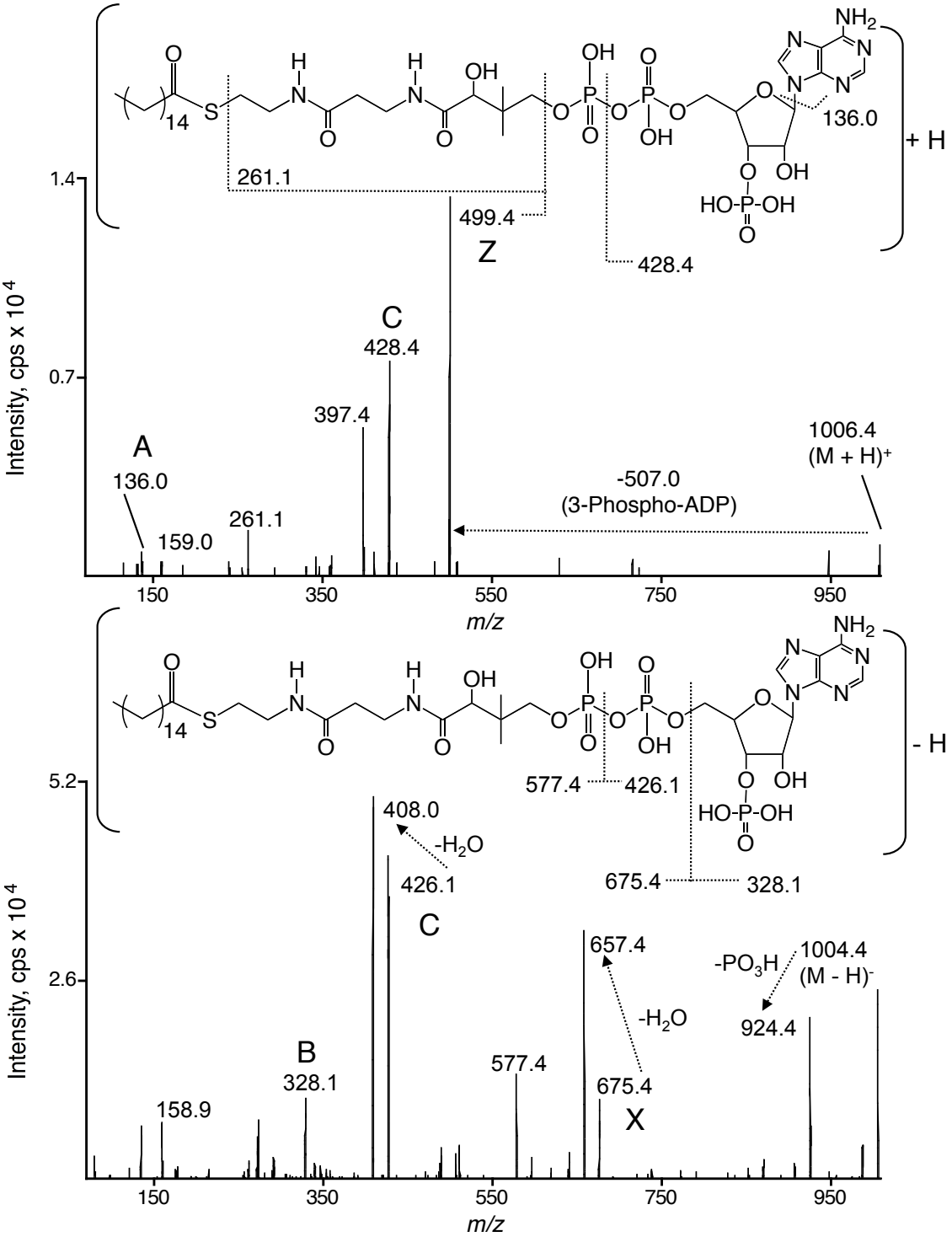

Figure 8. Tandem mass spectra of C16:0-CoA using positive (*upper panel*) and negative (*lower panel*) ionization modes.

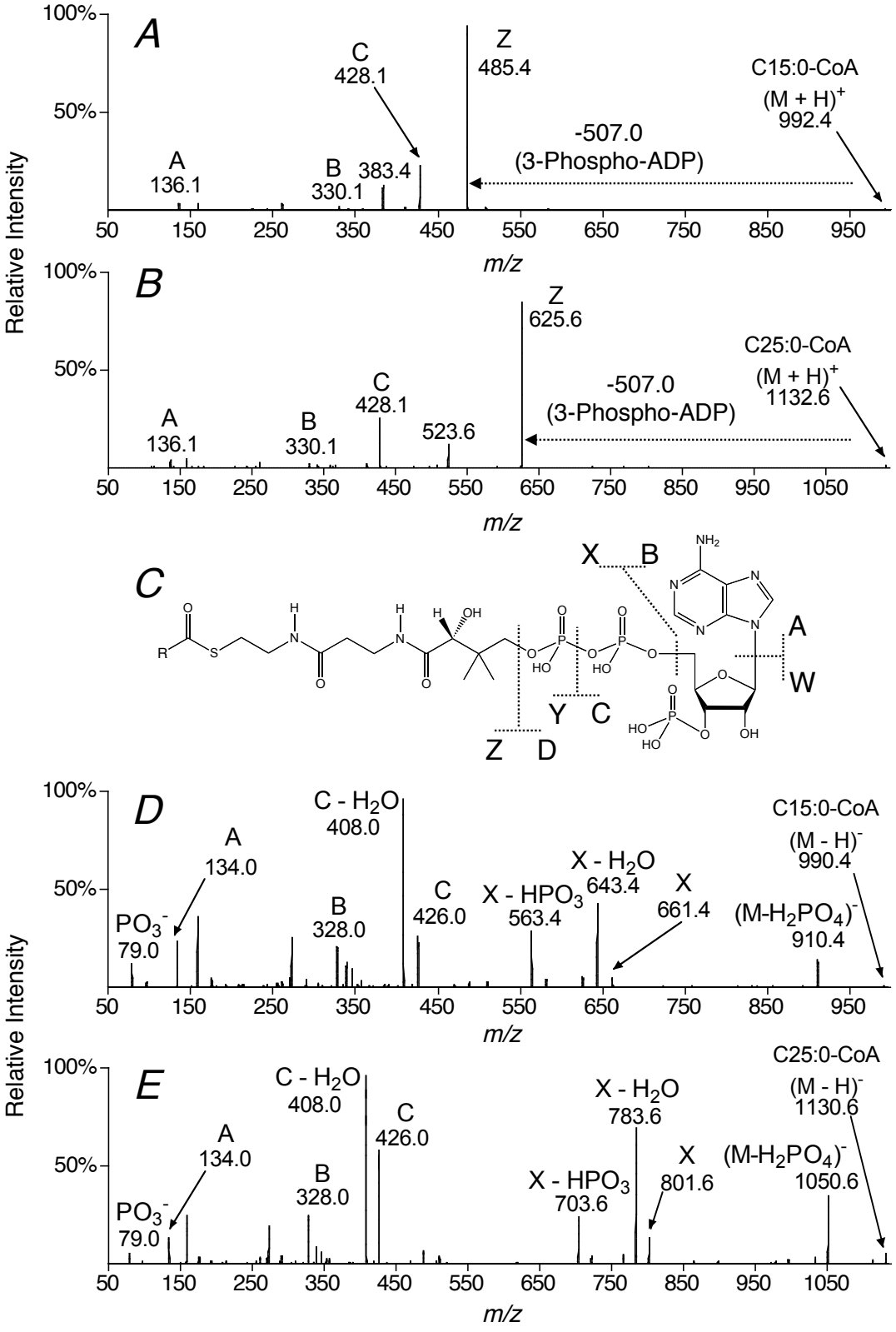

Figure 9. MS/MS spectra in positive ion mode (A, B) and negative ion mode (D, E) of C15:0-CoA (A, D) and C25:0-CoA (B, E). A proposed nomenclature for common fragmentations (C) is also shown.

mode, the X-H_2O product ion was more intense than the positive mode Z product ion under virtually identical infusion conditions (Figure 8), although neither of the product ions that retain the acyl chain (e.g., *m/z* 657.4 and *m/z* 577.4 for C16:0-CoA, Figure 8, *lower*) could be optimized as the base peak of the tandem mass spectrum.

Analysis of fatty acyl-CoAs by LC-ESI MS/MS

LC-ESI-MS/MS analysis of fatty acyl-CoAs utilized MRM pairs corresponding to singly (de)protonated precursor ions (selected by Q1), and the most abundant structure-specific product ion retaining the acyl chain (selected with Q3). For example, positive ion mode MRM analysis of C16:0-CoA utilized the MRM pair 1006.4 → 499.4 while negative ion mode MRM analysis utilized the pair 1004.4 → 657.4. The desolvation potentials, collision energies and collision cell exit potentials were optimized to yield maximum peak heights for the selected precursor and product ions in both polarities. Comparison of LC-ESI-MS/MS peak areas of C16:0-, C18:1- and C24:1-CoA using both negative and positive mode MRM revealed that the positive ion mode was approximately 3-fold more sensitive (Figure 10A), therefore, ionization, dissociation and separation conditions were optimized for maximum sensitivity and specificity for each individual acyl-CoA species in positive ion mode (Table I and Figure 10B).

The chromatographic conditions for Figure 10B (described in “Experimental Procedures”) were optimized for separation of saturated and monounsaturated fatty acyl-CoAs with chain lengths of C14 to C26 due to the interest of our laboratory in the precursors of sphingolipids. There is baseline resolution of acyl-CoAs with acyl chain differences of only one methylene unit and/or a single double bond (Figure 10B). The latter separation is advantageous because the (M + 2) isotopomer of monounsaturated

species match the MRM pair for the cognate saturated species, as seen in the small peak with the MRM pair for C18:0-CoA co-eluting with C18:1-CoA in Figure 10B as well as for the MRM pair for C24:0-CoA that co-elutes with C24:1-CoA. These chromatographic conditions also resolve many other species, including α-hydroxy-fatty acyl-CoAs (as shown for α-hydroxy-C18:0-CoA with a retention time 13.1 min *vs.* 14.1 min for the non-hydroxylated species, C18:0-CoA, Table I). Even when there is only partial chromatographic resolution for some of the fatty acyl-CoAs (such as C22:0- and C24:1-CoA, Figure 10B, and C20:4- and C22:6-CoA, not shown), the analytes are usually distinguishable by their characteristic MRM pairs. Shorter fatty acyl-CoAs elute earlier (for example, octanoyl-CoA, C8:0-CoA, elutes approximately 1 min after the void volume) and free CoASH elutes in the 5 min hold at 100% A after sample injection (data not shown). Therefore, this procedure might be usable for shorter chain species, including other categories of CoA-thioesters that can be distinguished by the MRM pairs and LC mobility.

For all of the fatty acyl-CoAs that were studied in depth by LC-ESI-MS/MS (i.e., species from C14 to C26), the limit of quantitation (LOQ) was on the order of 5 fmol, the linear range of quantitation was approximately 3 orders of magnitude (from the LOQ to at least 5 pmol) with $R^2 > 0.99$ from linear regression analysis (Figure 11A and Table I). Figure 11A shows the log-log relationship between the signal intensities for several representative fatty acyl-CoAs, from which the slopes and other results presented in Table I have been derived by linear regression analysis. In general, the covariance (SD divided by mean) for ten replicate injections of each standard was found to be <10% for 0.1 to 1 pmol of the analyte, ~15% for 10 to 50 fmol, and approximately 20% at the LOQ (5 fmol) (data not shown).

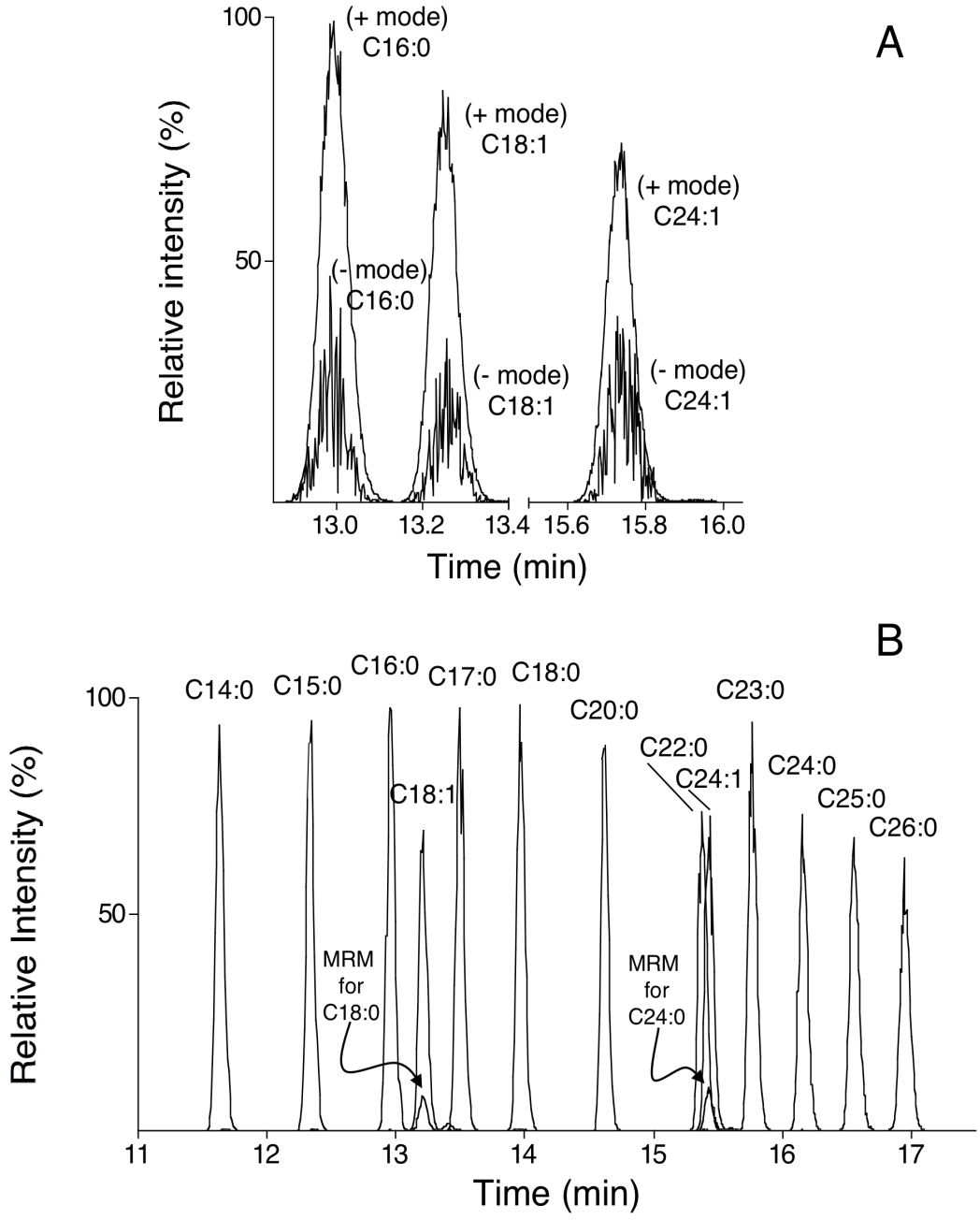

Figure 10. LC-ESI-MS/MS of palmitoyl-, oleoyl-, and nervonoyl-CoA in positive and negative modes (A) and a wider range of fatty acyl-CoAs in positive mode (B).

It is evident from Figures 10B and 10A that the relationship between peak area and pmol varies somewhat for different fatty acyl-CoAs, with a range of ~3 fold for the highest (C18:1-CoA) *vs.* the lowest (C26:0-CoA) studied here. This is not attributable solely to the increase in ^{13}C isotopomers with additional carbon atoms, nor, as best we have been able to ascertain, to differences in the concentrations of the fatty acyl-CoA standards. To ensure that the differences in ion yield were not due to hydrolysis of the fatty acyl-CoA standards, representative stocks (C18:0-, C18:1-, C24:0-, and C24:1-CoA) were analyzed for the amounts of free CoASH using this LC-ESI MS/MS method, and the mole % of free CoASH *versus* the fatty acyl-CoA was only 2 to 3%.

Thus, it appears that the signal intensities for the saturated species (solid circles, Figure 11B) are fairly constant for alkyl chain lengths of 14 to 20 carbons (with, perhaps, a slight peaking at C18), beyond which they decline. The simplicity of this relationship allows a reasonably accurate estimation of amounts of the saturated fatty acyl-CoAs using a limited number of internal standards (such as the C15:0-, C17:0-, C23:0- and C25:0-CoAs) as described under “Experimental Procedures”. Based on the similarity of the peak areas for C18:1- and C24:1-CoAs, it appears that alkyl chain length has less of an influence on monounsaturated fatty acyl-CoAs, however, it does appear that the number of double bonds affects signal intensity. Only one α-hydroxy-fatty acyl-CoA was available for comparison (α-hydroxy-C18:0-CoA), and its behavior was similar to oleoyl-CoA. Therefore, each analyte of interest should be examined to ascertain how it behaves under the LC-ESI-MS/MS conditions, and sufficient internal standards used for estimation of the quantities of the species as judged necessary based on the level of accuracy that is required by the investigation.

Analysis of fatty acyl-CoAs in cell extracts

Cell extracts were first examined by a neutral loss scan (507.0 Da) in positive ion mode because this fragmentation was common to all fatty acyl-CoA species including CoASH (e.g., Figure 9A and 9B, horizontal arrow) (110). Although this could be conducted by infusion of the extract, more analytes could be detected when LC was used to remove contaminants that suppress ionization, and to distinguish compounds that have overlapping MRM pairs, as discussed above. Accordingly, the chromatographic elution time was divided into three periods with distinct *m/z* scan, DP, CE, and CXP ranges as described under "Experimental Procedures." The results for an MCF7 cell extract analyzed by this procedure are shown in Figure 12. The ions eluting at or near the void volume (MS/MS of region B in Figure 12) are consistent with coenzyme A (*m/z* 768.4), propionyl-CoA (*m/z* 824.4) and the isomers succinyl-CoA and methylmalonyl-CoA (*m/z* 868.4). The abundant peaks eluting from 11 to 15 min (MS/MS of region C in Figure 12) were consistent with C14:0-CoA (*m/z* 978.4), C16:1-CoA (*m/z* 1004.4), C16:0-CoA (*m/z* 1006.4), C17:0-CoA (*m/z* 1020.4; internal standard), C18:1-CoA (*m/z* 1032.4), and C20:4-CoA (*m/z* 1054.4). A cluster of low abundance peaks eluting between 15 and 18 min (MS/MS of region D in Figure 12) were consistent with C24:1-CoA (*m/z* 1116.5), C24:0-CoA (*m/z* 1118.5), C25:0-CoA (*m/z* 1132.5; internal standard), C26:1-CoA (*m/z* 1144.5) and C26:0-CoA (*m/z* 1146.5). When the extracts were analyzed without the internal standard spikes, the odd chain-length fatty acyl-CoAs were ≤ 10 fmol per 10^7 cells, which allowed the use of these compounds as internal standards. Additionally, the removal of sodium ions from samples by reverse-phase HPLC is confirmed by the absence of a sodium adduct ion (predicted *m/z* 1042.4) of the abundant internal standard C17:0-CoA (Figure 12C).

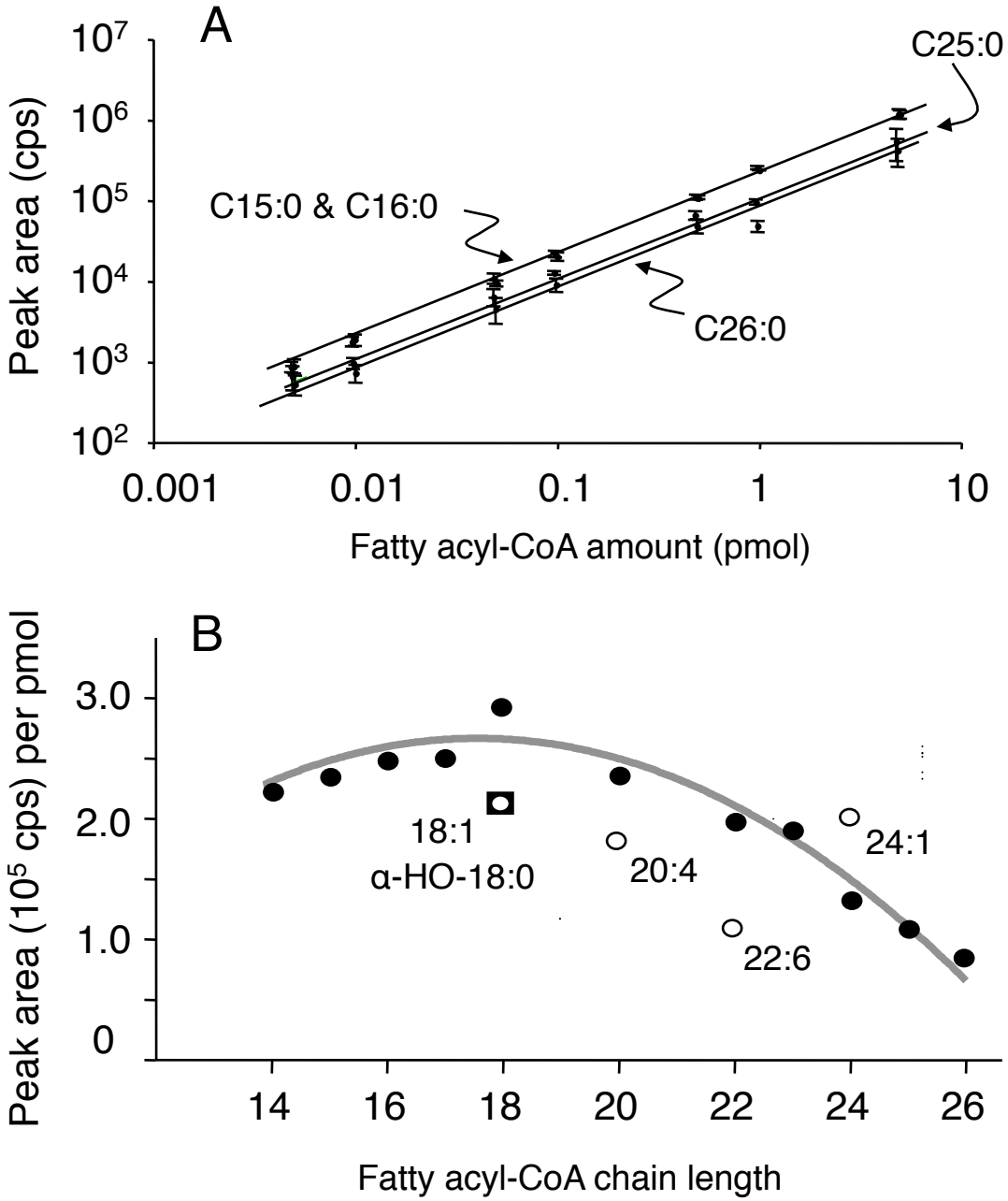

Figure 11. Relationships between peak area and fatty acyl-CoA amounts. A: Log-log plot of the means of peak areas ± SD (n = 4) for four representative analytes. B: Relationship between the slopes of the linear regression plots from Table I and the chain lengths of the fatty acyl-CoAs, with saturated species represented by closed circles, unsaturated species by open circles, and α-OH-C18:0-CoA by the closed square.

Subsequent LC-ESI-MS/MS analyses of cell extracts utilize the LC conditions described under “Experimental Procedures” and MRM pairs for the internal standards, the analytes identified for the biological sample of interest by neutral loss scan profiling (above), and any additional fatty acyl-CoA analytes of interest because they might be encountered during the course of the particular experiment. For the RAW264.7 and MCF7 cells, there were 19 MRM pairs, which could be accommodated using dwell and settling times of 40 msec and 5 msec, respectively. When the number of analytes exceeds the ability of the MRM program to scan them in the elution timeframe, it is possible to divide the chromatographic elution time into additional periods.

Analysis of multiple samples can be conducted using an auto-injector because the analytes are stable and remain in solution for at least 24 hr at room temperature and at least 3 days at -20 °C, which was verified by repeated injections of samples stored under these conditions and analysis by LC-ESI-MS/MS. However, this was only the case if the empirically derived conditions described under “Experimental Procedures” were followed—namely, the addition of an adequate amount of CH_3OH:$CH_3(CH_2)_2CH_2OH$:$CHCl_3$ (50:25:25, v/v/v) to the final extract to keep the very-long-chain fatty acyl-CoAs in solution during storage and analysis. Samples stored at -20 °C sometimes become cloudy, but a clear single phase can be restored by warming to room temperature and brief vortexing.

Depending on the nature of the biological sample, it may be necessary to replace the guard column somewhat frequently (after approximately 50 samples) if the backpressure increases from ca 700 psi to 900 or 1000 psi, which results in shifting retention times, peak splitting, etc. during the gradient. Clogging of needles and lines by the samples was uncommon. There was essentially no (i.e. ≤1%) carry-over of fatty acyl-

CoAs from either standards or samples, which was tested by inserting autoinjector vials that contain only the solvents at various intervals between vials containing standards or samples.

Quantitation of fatty acyl-CoAs in cell extracts

For quantitation of the fatty acyl-CoAs in extracts, the peak areas of the analytes of interest were compared to the peak areas of the internal standards, as described in "Experimental Procedures". To be reliable, this requires that the internal standard have the same recovery as the analyte under the extraction conditions used, and Figure 13A shows that this is the case. It is evident from the results that the odd chain-length spikes had recovery parameters similar to endogenous fatty acyl-CoAs of similar length and unsaturation. The necessity of the multiple extractions is also illustrated in Figure 13A because the recovery from each individual extraction differed among the species whereas the sum of the first three extractions (which are pooled when the method is followed as described in "Experimental Procedures") was > 90% for all internal standards and endogenous analytes. No significant difference between RAW264.7 and MCF7 cells was observed with respect to the percentage of total fatty acyl-CoAs recovered with each re-extraction. Similarly, the percentage of total of fatty acyl-CoAs recovered with each re-extraction did not significantly change if the number of cultured cells being extracted was between 5×10^6 and 2×10^7 (data not shown).

The linearity of the method was not compromised by the cell extract, as shown in Figure 13B where standard curves for two of the internal standards (C15:0- and C25:0-CoA) are compared for the standards alone versus spiked into a RAW264.7 cell extract ($R^2 \geq$

0.98). However, the signal intensities were reduced by ~50% in the biological extracts, which increased the LOQ to ~10 fmol.

Comparison of fatty acyl-CoAs in RAW264.7 and MCF7 cells

Quantitation of fatty acyl-CoAs in RAW264.7 and MCF7 cell extracts was conducted using the LC positive ion mode ESI MS/MS method described under "Experimental Procedures" and the MRM pairs that were selected on the basis of the results of the neutral loss scan. As can been seen from Figure 14, there are significant differences between the two cell lines with respect to the types and amounts of fatty acyl-CoAs. Very-long-chain fatty acyl-CoAs comprise a greater proportion of the total fatty acyl-CoAs' in MCF7 cells than in RAW264.7 cells (i.e., > 50% versus < 10%, respectively). Indeed, MCF7 cells contain approximately as much C24:0- and C26:0-CoAs as C16:0- and C18:0-CoAs, and essentially equal amounts of C26:1- and C18:1-CoAs. Oleoyl-CoA (C18:1-CoA) is one of the major fatty acyl-CoA species in both cell lines, as has been noted for many types of biological samples (20, 59, 62, 63), but we have been unable to find any previous reports of such high amounts of very-long-chain fatty acyl-CoAs in cells or tissues. Myristoyl-CoA (C14:0-CoA) was approximately 20% of the total fatty acyl-CoAs in RAW264.7 cells vs ~7% for MCF7 cells. Overall, MCF7 cells had much higher amounts of total fatty acyl-CoAs (80.4 $\pm$ 6.1 pmol per 10^6 cells) than RAW264.7 cells (12 $\pm$ 1.0 pmol per 10^6 cells) (N =3, P < 0.01).

For comparison, the quantities of very-long-chain fatty acids that have been reported for RAW264.7 cells (www.lipidmaps.org) and MCF7 cells (116), and the alkyl-chain length distribution of the ceramides from these cells, which were analyzed by published methods (74), are presented in Figure 15.

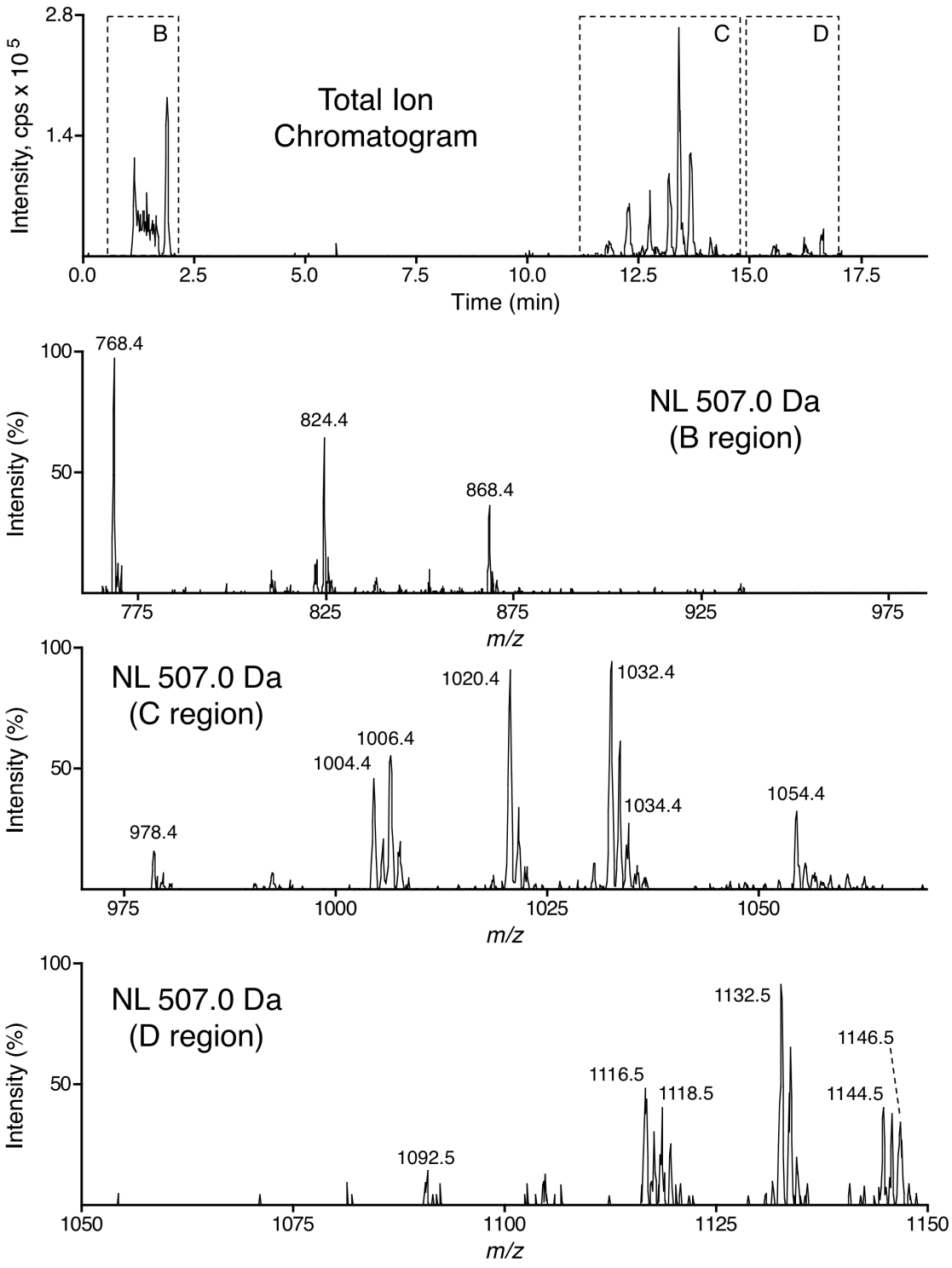

Figure 12. LC-ESI-MS/MS with neutral loss scanning (507.0 Da) of MCF7 cell extract. Dashed boxes labeled B to D on the total ion chromatogram indicate the time window from which the neutral loss scans in panels B-D were derived.

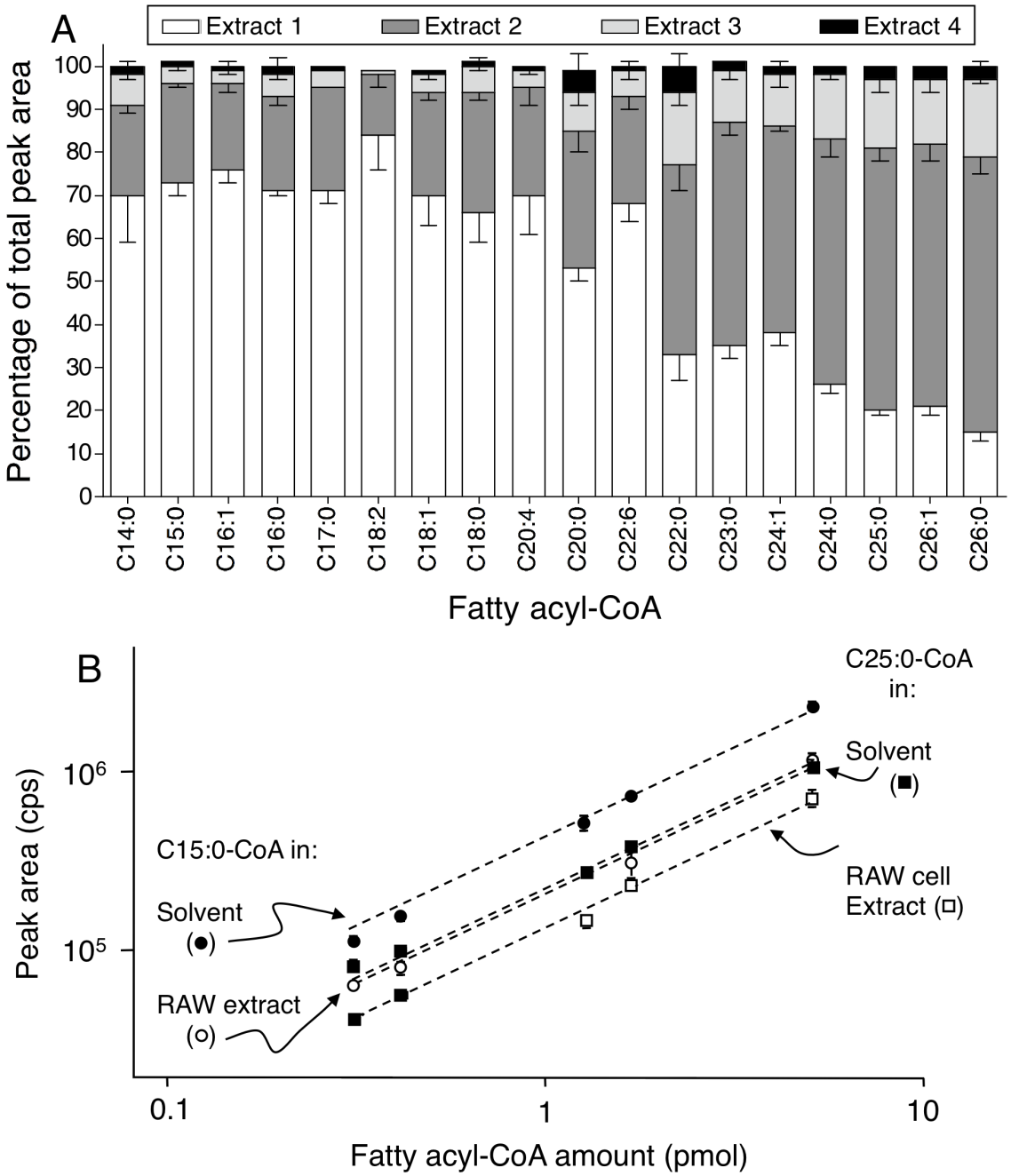

Figure 13. Recovery of fatty acyl-CoAs at each step of the extraction of MCF7 cells (A) and comparison of peak areas for analytes in solvent versus cell extracts (B). Results are means ± SD of analysis of three replicate Petri dishes. Circles are the C15:0-CoA and squares are the C25:0-CoA; closed symbols are analytes in methanol and open symbols are analytes in RAW264.7 cell extract.

2.4 Discussion

This chapter describes an LC-ESI-MS/MS method for the quantitation of a broad variety of fatty acyl-CoA molecular species, and its application to RAW264.7 and MCF7 cells. In many respects, it is similar to previous methods that have combined LC with ESI-MS and ESI-MS/MS for analysis of fatty acyl-CoAs, (93, 110-113), however, the extraction and LC conditions were optimized to allow quantitation of fatty acyl-CoAs from at least C14 to C26 using positive ion mode ESI-MS/MS and MRM parameters for structure-specific precursor-product ion pairs for the analytes of interest and commercially available odd chain-length fatty acyl-CoAs as internal standards. To the best of our knowledge, this is the first report of a method that is able to quantify intact fatty acyl-CoAs with saturated and monounsaturated alkyl chain lengths with >20 carbons, which include the very-long-chain fatty acids found in the ceramide backbones of sphingolipids (e.g., C24:0, C24:1, C26:0 and C26:1) (117).While it was somewhat surprising that LC-ESI-MS/MS (MRM) was more sensitive in the positive than negative mode despite the high pH of the LC eluant (Figure 10), perhaps this is due to removal of sodium ions by the LC separation which increased the proportion of the $(M + H)^+$ *versus* sodium adduct ions (Figure 7). Since the LC is conducted at high pH, it is possible to conduct the LC-ESI MS/MS analysis in negative ion mode, if necessitated by particular samples or instrumentation limitations; however, the *m/z* 79.0 product (phosphate) ion that is utilized in the negative ion mode has a greater potential for artifacts.

A major advantage of coupling HPLC to MS/MS is the resolution of isobaric analytes with different molecular structures, such as the naturally occurring (M + 2) isotopologue of C18:1-CoA, which can have the same precursor and product ion *m/z* values (1034.4 and 527.4, respectively) as those of C18:0-CoA. This resolution is a .

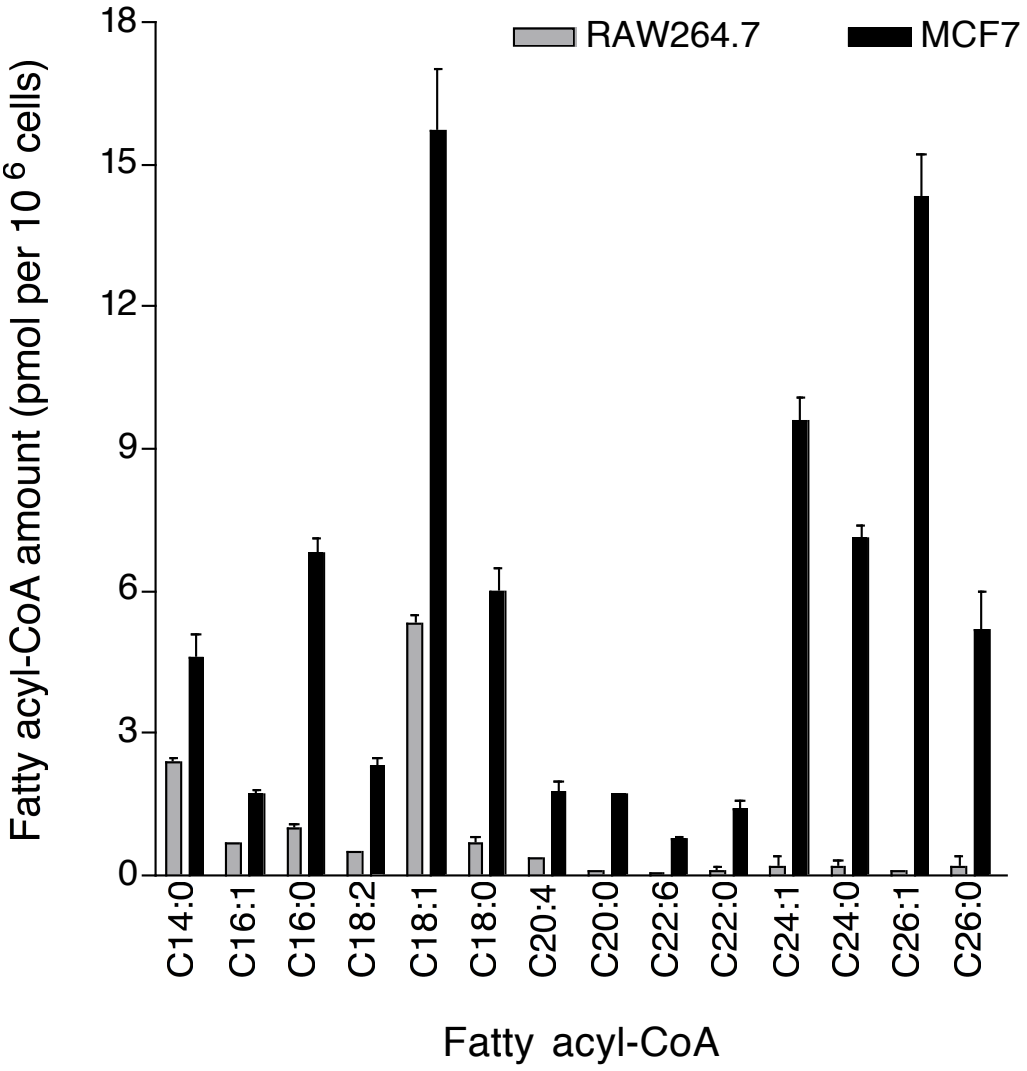

Figure 14. Quantitation of the fatty acyl-CoAs of RAW264.7 and MCF7 cells. The cells were extracted and analyzed as described in Experimental Procedures. Results are means ± SD of analysis of three replicate Petri dishes.

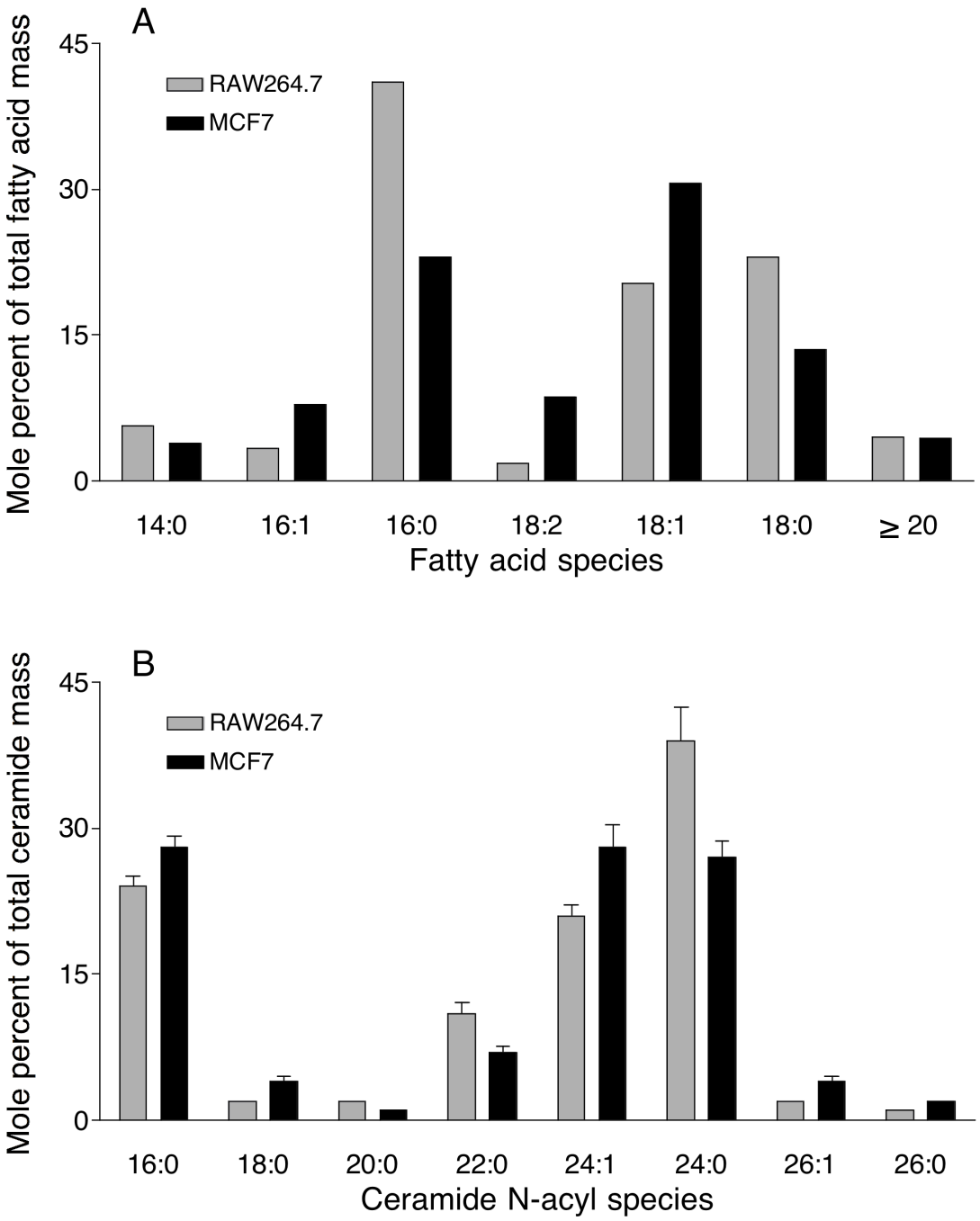

Figure 15. Fatty acid and ceramide compositions of RAW264.7 and MCF7 cells. The mole percentage of very long-chain fatty acids relative to other fatty acids was calculated from data for RAW264.7 cells from Lipid MAPS (www.lipidmaps.org) and for MCF7 cells from Welsh et al. The SD's of the latter data were not published.

feature of some (93, 110) but not all (111) previously published LC-ESI-MS/MS analyses of fatty acyl-CoAs.

The chain-length-determined differences in the recovery of fatty acyl-CoAs during repeated extraction (Figure 13) demonstrate the importance of using internal standards appropriate for the analytes of interest. This method could potentially be modified to include other molecular species of fatty acyl-CoAs after the validation of their recoveries with respect to these, or more appropriate, internal standards.

The fatty acyl-CoA composition of RAW264.7 and MCF7 cells displayed a diverse set of fatty acyl-CoA species, including those which may participate in the modification of proteins such as C14:0-CoA (12), and those that connect lipid biosynthesis with lipid signal transduction pathways such as C20:4-CoA (53). The most obvious difference in the fatty acyl-CoA compositions of RAW264.7 *versus* MCF7 cells is the proportion of the total fatty acyl-CoAs that have C20 and longer chain-lengths, which amount to over half of the total in MCF7 cells but are near the limit of quantitation in RAW264.7 cells. It is interesting that the quantities of very-long-chain fatty acyl-CoAs in these cells do not exactly match the amounts of free fatty acids that have been reported for them (Figure 15, *panel A*) nor the relative amounts of very-long-chain fatty acids that are found in a more complex sphingolipid, such as ceramide (Figure 15, *panel B*). Indeed, the proportions of ceramides with very-long-chain fatty acids are similar for RAW264.7 cells and MCF7 cells, despite the former having barely detectable very-long-chain fatty acyl-CoAs. Another difference was the 8-fold higher amounts of total fatty acyl-CoAs for MCF7 cells compared to RAW264.7 cells, which may reflect the often higher activity of fatty acid synthase in cancer cells, including this breast carcinoma cell line (118, 119).

Fatty acyl-CoA amounts have typically been estimated to be on the order of nanomoles per wet gram of tissue by previous studies of human muscle and adipose tissue (120), rabbit muscle (93) and rat tissues including liver (110-112, 121), brain (111, 121, 122), muscle (121), and kidney (121). Since a gram of tissue typically contains 10^8 to 10^9 cells (123), the amounts of fatty acyl-CoAs found in those studies are on the same order of magnitude (~10 pmol per 10^6 cells) as the fatty acyl-CoAs that have been obtained with RAW264.7 and MCF7 cells in this study.

Due to the sensitivity, breadth, and selectivity of this LC-ESI-MS/MS analysis, fatty acyl-CoAs can now be included in the list of compounds that can be analyzed in "lipidomics" studies of the roles of fatty acyl-CoAs in normal cell regulation and disease (107, 124-127). In addition, pharmacologic agents that affect the biosynthesis of fatty acyl-CoAs (i.e. triacsin C (34), sterculic acid (128), orlistat (129, 130), C75 (131), and cerulenin (132)), or that disrupt their utilization (i.e. inhibitors of mitochondrial oxidation (etomoxir) (133), glycerolipid biosynthesis (hypoglycin) (134), or sphingolipid biosynthesis (myriocin) (135)) can be re-investigated. In addition to being adaptable for analysis of fatty acyl-CoAs with acyl chains longer or shorter than those described here (and stable-isotope labeled fatty acids for kinetic studies) (93), the neutral loss (507.0 Da) scan should be able to detect and analyze CoA-thioesters with other compounds, such as bile acids (136) and certain xenobiotics (112).

CHAPTER 3.

SIMPLE: SPHINGOLIPID ISOTOPIC METABOLIC PRECURSOR LABELING EXPERIMENT USING [U-^{13}C]-PALMITATE TO ESTIMATE *DE NOVO* SPHINGOLIPID BIOSYNTHESIS[2]

3.1 Summary

Sphingolipid *de novo* biosynthesis is an important theme of this dissertation, with particular focus upon fatty acyl-CoA sphingolipid biosynthetic precursors. One approach that can be used to quantitate sphingolipids that are unambiguously the products of *de novo* biosynthesis is to treat cultured cells with [U-^{13}C]-palmitate. This stable isotope-labeled fatty acid is taken up by cells and converted to ^{13}C-labeled palmitoyl-CoA, which then contributes to *de novo* sphingolipid biosynthesis. Analysis of cellular lipid extracts by LC-ESI-MS/MS for fatty acyl-CoAs and sphingolipids, as described in Chapters 2 and 1, respectively, reveals the quantities of unlabeled and ^{13}C-labeled analytes.

The first cellular paradigm used to explore stable isotope-labeling of *de novo* sphingolipids with [U-^{13}C]-palmitate was HEK293 cells; in this study, the specific contributions of this author were the extraction and quantitation of fatty acyl-CoAs, analysis of their isotopic enrichment, and analysis of sphingolipid isotopic enrichments.

3.2 Introduction

Sphingolipids are integral to eukaryotic cellular membrane structures and are involved in many aspects of cell signaling (137-140). For example, the initial products of

[2] This chapter is in preparation for publication; the authors are Haynes, C., Allegood, J., Wang, E., Kelly, S., Sullards, M., and Merrill, A.

de novo sphingolipid biosynthesis (sphingoid bases and ceramides) are utilized as cell signals. Interest in both their structural roles and their biological activities has led to the development of methods to quantitate sphingolipids in many cell/tissue types, classically by thin-layer chromatography, gas chromatography, and high-performance liquid chromatography; more recently tandem mass spectrometric (MS/MS) detection (68, 75, 77, 141) has been used in conjunction with HPLC resolution to quantify sphingolipids. Quantitation of sphingolipids can provide considerable insight in numerous studies, however, some signaling mechanisms could be more fully elucidated by the ability to distinguish, for example, ceramide (Cer) derived from *de novo* biosynthesis and Cer derived from catabolism of pre-existing sphingomyelin (SM) (142-145).

Analysis of ^{13}C-labeled palmitate incorporation into sphingolipids by mass spectrometry (MS) has been explored previously (94, 146, 147); however, in the method described here labeling with uniformly-labeled [^{13}C]palmitate ([U-^{13}C]-palmitate) and sphingolipid quantitation by LC-ESI-MS/MS were used to distinguish pre-existing sphingolipids and *de novo* biosynthesized sphingolipids. One reason for selecting [U-^{13}C]-palmitate is its incorporation into the sphingolipid *de novo* biosynthetic pathway at two points: initially by serine palmitoyltransferase (SPT) (4, 148), which catalyzes the condensation of serine and palmitoyl-CoA to form 3-keto-sphinganine, and later by one of several (dihydro)ceramide synthase (CerS) isoforms (8, 76, 149), which N-acylate sphinganine / sphingosine using fatty acyl-CoAs.

Treatment of HEK293 cells with [U-^{13}C]-palmitate resulted in four kinds of N-acylated sphingolipid isotopologues [molecules with identical chemical structures and different isotopes at specific structural position(s)] and isotopomers [molecules with identical chemical structures and the same number of isotopic labels at different

structural position(s)] The isotopologues were either completely unlabeled, labeled on the sphingoid base or the N-acyl chain (isotopomers), or labeled on both the sphingoid base and N-acyl chain. The MS/MS analysis described here distinguishes both the number and the position of label incorporations; mass shifts in precursor and product ion pair *m/z* values by either 16 or 32 Da indicate whether the label is present in either the sphingoid base of N-acyl fatty acid or both. Interestingly, in HEK293 cells, ^{13}C-d18:1/^{13}C-16:0 Cer (but not SM) was the most abundant Cer isotopologue, suggesting a rapid turn-over rate for Cer (but not SM) in this cell line.

In addition, treatment of HEK293 cells with [U-^{13}C]-palmitate resulted in [M + 16] fatty acyl-CoAs, including 16:0-, 18:0-, 16:1- and 18:1-CoA, indicating the activation of [U-^{13}C]-palmitate to [M + 16] 16:0-CoA and its subsequent elongation (45) and desaturation (150). The utilization of these ^{13}C-labeled fatty acyl-CoAs during sphingolipid *de novo* biosynthesis was confirmed by the quantitation of d18:1/^{13}C-18:0 Cer, d18:1/^{13}C-24:0 Cer, and d18:1/^{13}C-24:1 Cer in this cell line. Importantly, treatment with 0.1 mM [U-^{13}C]-palmitate for 6 h resulted in ~ 60% isotopic enrichment of 16:0-CoA. Assuming that a single, well-mixed pool of 16:0-CoA is the biosynthetic precursor of d18:1/16:0 Cer, estimation of the rate of this sphingolipid's *de novo* biosynthesis using the criterion of ^{13}C-labeling results in a ~ 40% underestimate of this rate.

The utility of this sphingolipid isotope metabolic precursor labeling experiment (SIMPLE) method is demonstrated by the quantitation of sphingolipids in HEK293 cells treated with [U-^{13}C]-palmitate, and coupling SIMPLE with quantitation of the isotopic enrichment of biosynthetic precursor fatty acyl-CoAs provides corrections for sphingolipid biosynthetic rates that were inferred from ^{13}C-labeled sphingolipid quantities. Collectively, treatment of cultured cells with stable isotope-labeled precursors

followed by LC-ESI-MS/MS analysis as described here provides greater dynamic detail regarding sphingolipid anabolism than has been previously available.

3.3 Experimental procedures

Reagents

The internal standard cocktail (catalog number LM-6002) was provided by Avanti Polar Lipids (Alabaster, AL) in sealed ampoules and certified (64) to be > 95% pure and within 10% of the specified amount (250 μM); it was comprised of the 17-carbon chain length sphingoid base analogs: C17-sphingosine, (2S,3R,4E)-2-aminoheptadec-4-ene-1,3-diol (d17:1-So); C17-sphinganine, (2S,3R)-2-aminoheptadecane-1,3-diol (d17:0-Sa); C17-sphingosine 1-phosphate, heptadecasphing-4-enine-1-phosphate (d17:1-S1P); and C17-sphinganine 1-phosphate, heptadecasphinganine-1-phosphate (d17:0-Sa1P); and the C12-fatty acid analogs of the more complex sphingolipids C12-Cer, N-(dodecanoyl)-sphing-4-enine (d18:1/12:0-Cer); C12-Cer 1-phosphate, N-(dodecanoyl)-sphing-4-enine-1-phosphate (d18:1/12:0-Cer1P); C12-sphingomyelin, N-(dodecanoyl)-sphing-4-enine-1-phosphocholine (d18:1/12:0-SM); C12-glucosylceramide, N-(dodecanoyl)-1-β-glucosyl-sphing-4-eine (d18:1/12:0-GlcCer); and C12-lactosylceramide, N-(dodecanoyl)1-β-lactosyl-sphing-4-eine (d18:1/12:0-LacCer); as well as one very-long-chain Cer analog, C25-Cer, N-(pentacosanoyl)-sphing-4-enine (d18:1/25:0-Cer). [U-^{13}C]-palmitate (98%) was purchased from Cambridge Isotope (Andover, MA). Phospholipase D (*Streptomyces chromofuscus*) was purchased from Biomol (Plymouth Meeting, PA). Fumonisin B_1 (FB_1) was obtained from Matreya (Pleasant Gap, PA).

The HPLC grade solvents (acetonitrile, # EM-AX0145; chloroform, # EM-CX1050; hexane, # JT9304-33; and methanol, # EM-MX0475, as well as ACS grade

formic acid, # EM-FX0440-7), were obtained from VWR (West Chester, PA), and acetic acid (ACS grade, # A38C-212) was obtained from Fisher (Pittsburg, PA).

Cell culture

HEK293 cells were obtained from the American Type Culture Collection (Manassas, VA) (cat# CRL-1573). The cells were grown in 60-mm plastic culture dishes in DMEM supplemented with 10% FBS, 4 mM L-glutamine, 4.5 g/L glucose, 1.5 g/L sodium bicarbonate, 100 U/ml penicillin and 0.1 mg/ml streptomycin in ThermoForma Steri-cult CO_2 incubators with 5% CO_2 and 90% relative humidity at 37°C. In labeling experiments cells were incubated with 0.1 mM [U-^{13}C]-palmitate in a 1:1 molar complex with fatty acid-free bovine serum albumin. In experiments involving FB_1, an ethanol stock of FB_1 was added to the cell culture media for a final concentration of 50 μM.

Sphingolipid extraction from HEK293 cells

The harvesting of cells and sphingolipid extraction were performed as previously described (65). An aliquot of the reconstituted extracts of N-acyl sphingolipids was saved for phospholipase D treatment.

Phospholipase D treatment

1000 units of phospholipase D (PLaseD, from *Streptomyces chromofuscus*) were suspended in 0.1 ml of 3 mM decylglucopyranoside (Sigma, St. Louis, MO) and 100 mM Tris HCl (pH 8.0). An aliquot of the complex fraction was treated with PLaseD and incubated for 15 min at 37°C in a heating block. Samples were then dried under vacuum in a Savant AES2000 Automatic Environmental Speedvac and reconstituted in LC-ESI-

MS/MS mobile phase for analysis.

Liquid chromatography-electrospray ionization-tandem mass spectrometry of sphingolipids

The analysis of sphingolipids by liquid chromatography-electrospray ionization-tandem mass spectrometry (LC-ESI-MS/MS) was performed as previously described (65). Prior to selecting MRM pairs for each cell type, the variation in N-acyl chain length was determined, which allowed MRM transitions to correspond to the observed N-acyl species. This was accomplished by precursor ion scans (*m/z* 184.1) of the extracts containing N-acyl sphingolipids, which indicate the molecular species of sphingomyelin (SM) present in the extract. SM was selected because they are typically abundant and are indicative of both sphingosine (So) and sphinganine (Sa) species. For example, in HEK293 cells, the major SM molecular species are d18:1/16:0, d18:1/18:0, and d18:1/24:1.

Cell extraction and liquid chromatography-electrospray ionization-tandem mass spectrometry for fatty acyl-CoA quantitation

Fatty acyl-CoAs were extracted from HEK293 cells, and analyzed by LC-ESI-MS/MS as described previously (151).

Calculation of isotopic enrichment

The isotopic enrichment of fatty acyl-CoAs, sphingoid bases, and sphingoid base-1-phosphates was calculated as follows:

([M + 16] isotopologue, pmol) / ([M + 16] isotopologue, pmol + [M + 0] isotopologue, pmol)

3.4 Results

Tandem mass spectrometry

Sphingolipids undergo structure specific fragmentation during positive ion mode ESI-MS/MS that allows the analysis of large numbers of molecular species, including both abundant (i.e. SM and Cer) and non-abundant species (i.e. sphingoid base 1-phosphates (75). Free sphingoid bases, sphingoid base 1-phosphates, Cer, and ceramide monohexose (CMH) fragment by a mechanism that involves a dehydration or loss of the 1-position moiety, dehydration at the 3-position, and cleavage of the amide bond of the N-acyl chain (if present) to form a conjugated carbocation of *m/z* 264.4 for d18:1 species or 266.4 for d18:0 species (Figure 16). Utilization of [U-^{13}C]-palmitate by SPT and/or CerS during sphingolipid *de novo* biosynthesis gave rise to 4 sets of isotopologues and isotopomers for N-acylated sphingolipids designated unlabeled (e.g. ^{12}C-d18:1/^{12}C-16:0), base labeled (e.g. ^{13}C-d18:1/^{12}C-16:0), fatty acid labeled (e.g. ^{12}C-d18:1/^{13}C-16:0), and dual labeled (e.g. ^{13}C-d18:1/^{13}C-16:0, Figure 17). In conformity with IUPAC nomenclature, the unlabeled, singly-labeled, and dual-labeled species are isotopologues and the singly-labeled species (i.e., base-labeled and dual-labeled) are isotopomers of each other.

The SM phosphocholine moiety (184.1 *m/z*) is the most abundant product ion during positive mode ESI-MS/MS (Figure 16). Therefore, while the total number of carbon atoms and double bonds is determined for a given SM molecular species by its precursor *m/z*, the ^{13}C-labeling of the sphingoid base vs. fatty acid cannot be distinguished for [M + 16] precursor ions; however, treatment of SM with phospholipase D (PLaseD) generates ceramide-1-phosphate (Cer-1-P) that yields sphingoid base

product ions (see later).

Incorporation of [U-^{13}C]-palmitate into the fatty acyl-CoAs of HEK293 cells

Analysis of the fatty acyl-CoA profile in HEK293 cells treated with 0.1 mM [U-^{13}C]-palmitate revealed an isotopic enrichment (see Materials and Methods) of ~ 60% for 16:0-CoA at 6 h and that a portion of the ^{13}C-labeled 16:0-CoA had been elongated and / or desaturated. (Figure 18). The isotopic enrichment was rapid for 16:0-CoA (35% by 1 h), but elongated 18:0-CoA, and desaturated (16:1-CoA and 18:1-CoA) species showed a slower rate of enrichment. The isotopic enrichments of 16:0-CoA, 16:1-CoA, 18:0-CoA, and 18:1-CoA appeared to reach a steady-state between 3 and 6 h at 60%, 45%, 20%, and 8%, respectively.

It is possible that ^{13}C-labeled 16:0-CoA could be partially oxidized and then re-elongated to form 16:0- (or longer) CoA with fewer than 16 atoms of ^{13}C. To examine this possibility, the sphingolipid profile in extracts of HEK293 cells treated with 0.1 mM [U-^{13}C]-palmitate for 3 h was determined by precursor ion scans (*m/z* 184.1) of SM, allowing the determination of abundant sphingoid base and fatty acid combinations (Figure 19). Since precursor ion scans did not detect [M + 14] species (Figure 19), this oxidation and re-elongation was not observed under these conditions.

Incorporation of [U-^{13}C]-palmitate into the sphingolipids of HEK293 cells

To determine the sphingoid base and fatty acid combinations present in untreated HEK293 cells, extracts of HEK293 cells were analyzed using precursor ion scans (*m/z* 264.4 for d18:1 and *m/z* 266.4 for d18:0) to profile the corresponding molecular species of free sphingoid bases, Cer, and CMH. The N-acyl chain lengths of

Cer and CMH in HEK293 cells were 16:0, 18:0, 20:0, 22:0, 24:1, 24:0, 26:1, and 26:0 with both d18:1 and d18:0 sphingoid bases. After [U-^{13}C]-palmitate treatment of HEK293 cells, labeling of the sphingoid base was confirmed by the presence of [M + 16] precursor ions and [M + 16] product ions for Cer and CMH, and the elongation / desaturation of ^{13}C-labeled 16:0-CoA was confirmed by the quantitation of 18:0, 24:1, and 24:0 Cer and CMH with [M + 16] precursor ions and [M + 0] product ions (as well as by [M + 32] precursor ions and [M + 16] product ions).

To quantitate *de novo* sphingolipid biosynthesis, replicate dishes (N = 4) of HEK293 cells treated with [U-^{13}C]-palmitate were sampled at 1 h intervals for 6 h. A distribution of N-acyl chain lengths was observed for the unlabeled Cer (Figure 20, *upper panel*). The most abundant Cer, d18:1/16:0-Cer, decreased from 100 ± 20 to 50 ± 10 pmol/mg protein between 0 and 1 h, and stabilized between 3 and 6 h at 35 ± 5 pmol/mg protein. Other chain lengths of unlabeled Cer showed a similar pattern. For example, a decrease in d18:1/24:1-Cer was observed from 60 ± 10 to 40 ± 10 pmol/mg protein between 0 and 1 h, and then stabilization at 20 ± 5 pmol/mg protein between 3 and 6 h. Total unlabeled Cer decreased from 250 ± 70 to 110 ± 20 pmol/mg protein between 0 and 6 h. Minor species included d18:1/20:0, d18:1/26:1, and d18:1/26:0, each being present at < 3 pmol/mg protein. Unlabeled d18:1/16:0 and d18:1/24:0 Cer decreased by the largest percentage over 6 h: d18:1/24:1 Cer decreased by 67% and d18:1/16:0

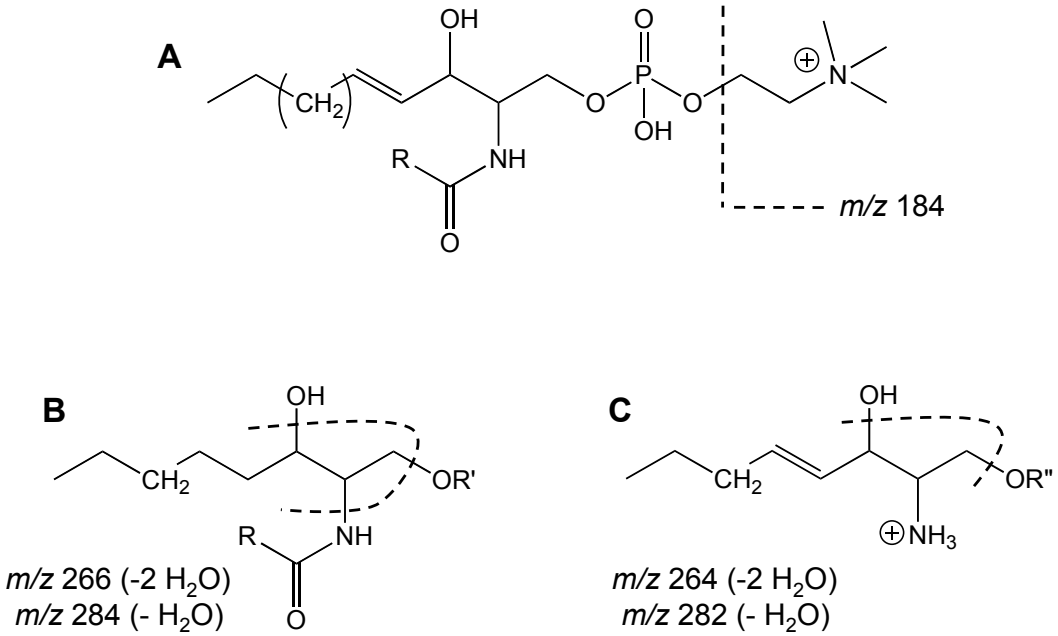

R = N-acyl chain, R' = glucose or galactose, R" = H or phosphate

Figure 16. Major routes of dissociation of sphingolipids in positive ion mode with orifice and ring voltages at 30 eV and 180 eV, respectively, (sphingoid bases) or 40 eV and 220 eV, respectively, (complex species). (A) Sphingomyelin fragments by loss of the phosphocholine moiety, which retains the charge. (B) Fragmentation of ceramides (R' = H) involves a double dehydration and loss of the N-acyl moiety. Analogous losses during fragmentation were observed for glucosylceramides (R = glucose) and Cer1P (R = PO_3). (C) Fragmentation of sphingoid bases and sphingoid base-1-phosphates involves a double dehydration (or single dehydration and phosphate loss) at the 1 and 3 positions.

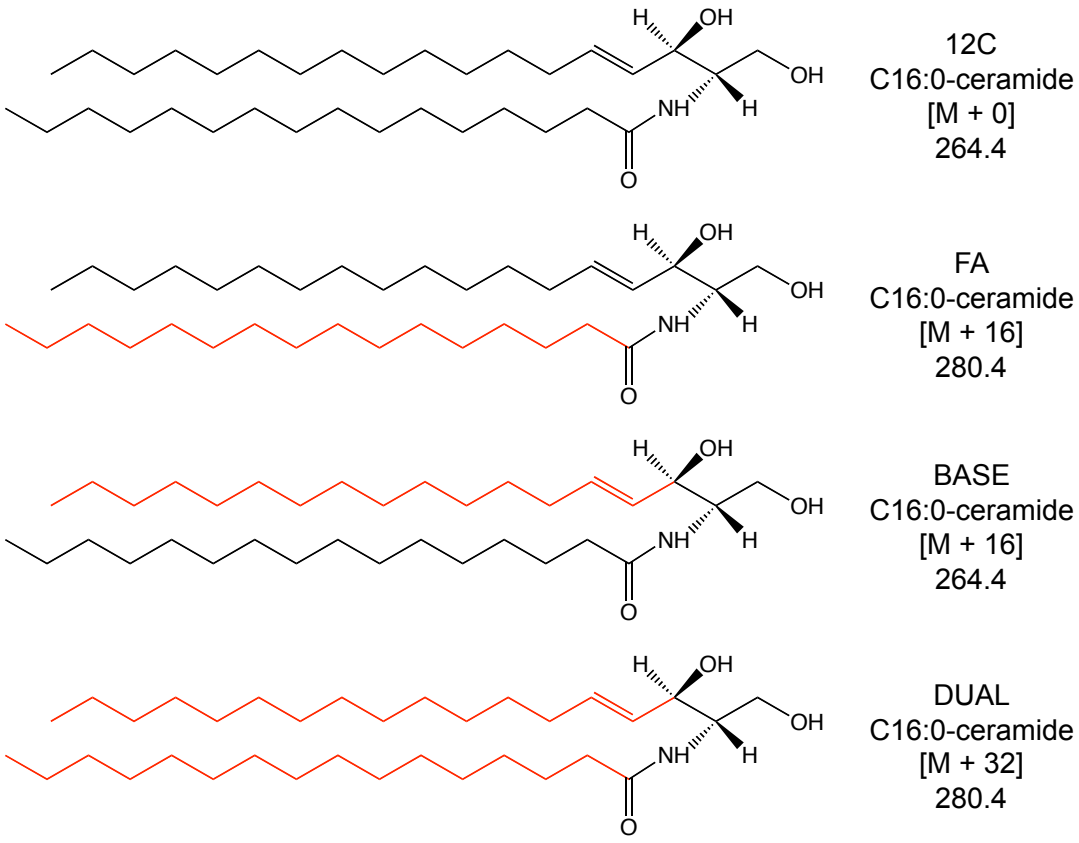

Figure 17. Isotopologues and isotopomers of d18:1 / C16:0 ceramide. The C16:0 abbreviation indicates an N-acyl chain with 16 carbon atoms and 0 double bonds. In these examples, 0, 1, or 2 acyl chains (*red structure*) of ceramide were derived from [U-^{13}C]-palmitate during *de novo* biosynthesis, and so the precursor ion *m/z* values are [M + 0], [M + 16], or [M + 32] Da. The MS/MS analysis distinguishes [M + 16] isotopomers into FA and BASE using the *m/z* value of the product ion (264.4 or 280.4). ^{12}C and DUAL designate [M + 0] and [M + 32] isotopologues, respectively.

decreased by 60%. This decrease in the quantity of unlabeled Cer may be attributable to the increasing quantity of ^{13}C-labeled Cer over 6 hr and cellular processes aiming for a homeostatic (constant) Cer concentration.

Alteration in the N-acyl chain length distribution over 6 h was observed in unlabeled Cer. The d18:1/16:0 Cer decreased from 39% of total unlabeled Cer to 33% by 6 h; likewise, d18:1/24:0 Cer declined from 24% to 17% by 6 h. The percent lost was almost compensated by an increase in d18:0/16:0 Cer, d18:1/18:0 Cer, and d18:1/22:0 Cer, which increased from 1% to 3%, 8% to 14%, and 7% to 9% respectively. The proportion of d18:1/24:1 Cer remained constant at 20% over 6 h (Figure 20, *lower*, and Figure 21). The d18:1/20:0, d18:1/26:1, and d18:1/26:0 species each comprised less than 2% of total Cer.

The quantities of unlabeled CMH (Figure 22, *upper panel*) and SM (Figure 24, *upper panel*) were greater than the amounts of unlabeled Cer; furthermore the chain-length distribution of CMH was predominantly 24:1 and 24:0 species in contrast to the predominance of 16:0 for SM and the approximate equivalence of 16:0, 24:1, and 24:0 for Cer. As was observed for Cer, the quantities of unlabeled CMH and SM decreased between 0 and 6 h although a slight (non-significant) increase in unlabeled CMH at 1 and 2 h was observed (Figure 22, *upper panel*).

[U-^{13}C]-palmitate was readily incorporated into the sphingolipids of HEK293 cells. Labeling of only the N-acyl chain was designated the fatty acid labeled isotopomer of Cer (Figure 20, *lower panel*), CMH (Figure 22, *lower panel*), and SM (Figure 24, *lower panel*). The quantity of ^{12}C-d18:1/^{13}C-16:0 Cer was 20 and 30 pmol/mg protein after 1 and 6 h, and the quantity of ^{12}C-d18:1/^{13}C-18:0 Cer was 5 pmol/mg protein between 1 and 6 hr. Fatty acid labeled ^{12}C-d18:0/^{13}C-16:0 Cer as well as ^{12}C-d18:1/^{13}C-20:0 and

^{12}C-d18:1/^{13}C-22:0 Cer quantities were 0.5 to 1 pmol/mg protein by 1 h and approximately doubled after 6 h. Fatty acid labeled ^{12}C-d18:1/^{13}C-26:1 and ^{12}C-d18:1/^{13}C-26:0 Cer were not above the limit of quantitation (~ 0.1 pmol/mg protein) during 6 h. These results indicate both the generation, elongation, and desaturation of ^{13}C-labeled 16:0-CoA, and the utilization of ^{13}C-labeled fatty acyl-CoAs by CerS in HEK293 cells.

The quantities of fatty acid labeled CMH (Figure 22, *lower panel*) and SM (Figure 24, *lower panel*) are small compared to the unlabeled species, and their chain length distributions tend to recapitulate the distribution of the unlabeled species rather that the chain length distribution of fatty acid labeled Cer. For example, fatty acid labeled CMH (Figure 22, *lower panel*) is predominantly 22:0 and 24:1 rather than predominantly 16:0 as was observed for fatty acid labeled Cer (Figure 20, *lower panel*).

N-acyl sphingolipids with ^{13}C labeling of both the fatty acid and sphingoid base moieties were designated dual labeled isotopologues, and interestingly they were quantitatively the predominant isotopologues of Cer (Figure 21, *upper panel*) but not of CMH (Figure 23, *upper panel*) or SM (Figure 25, *upper panel*) between 3 and 6 h. Furthermore, comparison of the quantities of 16:0 dual labeled Cer, CMH, and SM to the quantities of the other two 16:0 labeled species (fatty acid and base labeled) showed that the dual labeled isotopologue was the most abundant in every case. The ^{13}C-d18:1/^{13}C-16:0 Cer increased from an initial quantity of 25 ± 3 pmol/mg protein at 1 h to 50 ± 3 pmol/mg protein at 6 h. This increase represents a biosynthetic rate for ^{13}C-d18:1/^{13}C-16:0 Cer of 5 pmol/(mg protein*h) between 1 and 6 h. The ^{13}C-d18:1/^{13}C-18:0 Cer quantity at 1 h was 3 ± 1 pmol/mg protein, and was 5 ± 1 pmol/mg protein after 6 h. The ^{13}C-d18:1/^{13}C-22:0 Cer was 3 pmol/mg protein after 6 h, while ^{13}C-d18:1/^{13}C-20:0,

^{13}C-d18:1/^{13}C-24:1, and ^{13}C-d18:1/^{13}C-24:0 Cer were less than 3 pmol/mg protein at all times.

Incorporation of [U-^{13}C]-palmitate into only the sphingoid base of Cer (Figure 21, *lower panel*), CMH (Figure 23, *lower panel*), and SM (Figure 25, *lower panel*) was designated base labeled isotopomer, and during 6 h the quantities of these labeled sphingolipids were ~ 6 to 8 pmol/mg protein or less; however, a trend of increasing quantity can be observed. Unlike the other ^{13}C-labeled Cer species, the base labeled isotopomer was not predominantly 16:0, instead all N-acyl chain lengths except 26 were observed.

The total quantity of 16:0 Cer at 6 h was 40 pmol/mg protein (unlabeled) + 30 pmol/mg protein (fatty acid labeled) + 50 pmol/mg protein (dual labeled) + 4 pmol/mg protein (base labeled) = 124 pmol/mg protein. If one assumes that a single pool of palmitoyl-CoA (with ~ 60% isotopic enrichment) is available to both SPT and CerS, then both enzymes would utilize ^{13}C-labeled palmitoyl-CoA 60% of the time. Therefore, 60% of *de novo* biosynthesized Sa will be ^{13}C-labeled, and N-acylation of ^{13}C-labeled Sa by CerS using ^{13}C-labeled palmitoyl-CoA is again 60% likely, resulting in the prediction that 60% x 60% = 36% of the *de novo* 16:0 Cer will be dual labeled. By the same assumption, 60% x 40% = 24% of the *de novo* 16:0 Cer will be base labeled, 40% x 60% = 24% of the *de novo* 16:0 Cer will be fatty acid labeled, and 40% x 40% = 16% of the *de novo* 16:0 Cer will be unlabeled.

Given a total Cer quantity of 124 pmol/mg protein (the amount observed at 6 h), predicted *de novo* amounts are 20 pmol/mg protein (unlabeled), 30 pmol/mg protein (fatty acid labeled), 50 pmol/mg protein (dual labeled), and 30 pmol/mg protein (base

labeled). These predictions are similar to the observed quantities of dual labeled and fatty acid labeled 16:0 Cer.

The observed unlabeled 16:0 Cer amount (40 pmol/mg protein) was greater than the predicted *de novo* amount (20 pmol/mg protein), which could result from catabolism of, for example, unlabeled SM to yield Cer. The observed base labeled amount (4 pmol/mg protein) was lower than the predicted *de novo* amount (30 pmol/mg protein), and the absence of detectable (> 0.1 pmol/mg protein) ^{13}C-labeled Sa-1-P at any time (data not shown) indicated that accumulation of ^{13}C-labeled Sa-1-P did not explain the "missing" ^{13}C-labeled Sa. This difference between fatty acid labeled and base labeled amounts was also observed for 16:0 CMH and 16:0 SM, for which there were 3-fold and 10-fold, respectively, more fatty acid labeled isotopomers.

In summary, Figures 20 through 25 show the quantities of N-acyl sphingosine-based species of HEK293 cells cultured for 0 to 6 h in media containing 0.1 mM [U-^{13}C]-palmitate. Base and fatty acid labeled SM were distinguished using PLaseD treatment (see above). The product of SPT, 3-keto-sphinganine, as well as sphinganine were presumably quickly metabolized because their quantities were consistently at or below the limit of detection (~ 0.1 pmol/mg protein). Likewise the incorporation of label into dihydroceramide (DHCer) was observed, but DHCer was also presumably quickly desaturated to Cer, as evidenced by substantial quantities of labeled sphingosine-based species (Figures 20 and 21). A similar pattern was observed for dihydroceramide monohexose (DHCMH, Figures 22 and 23) and dihydrosphingomyelin (DHSM, Figures 24 and 25).

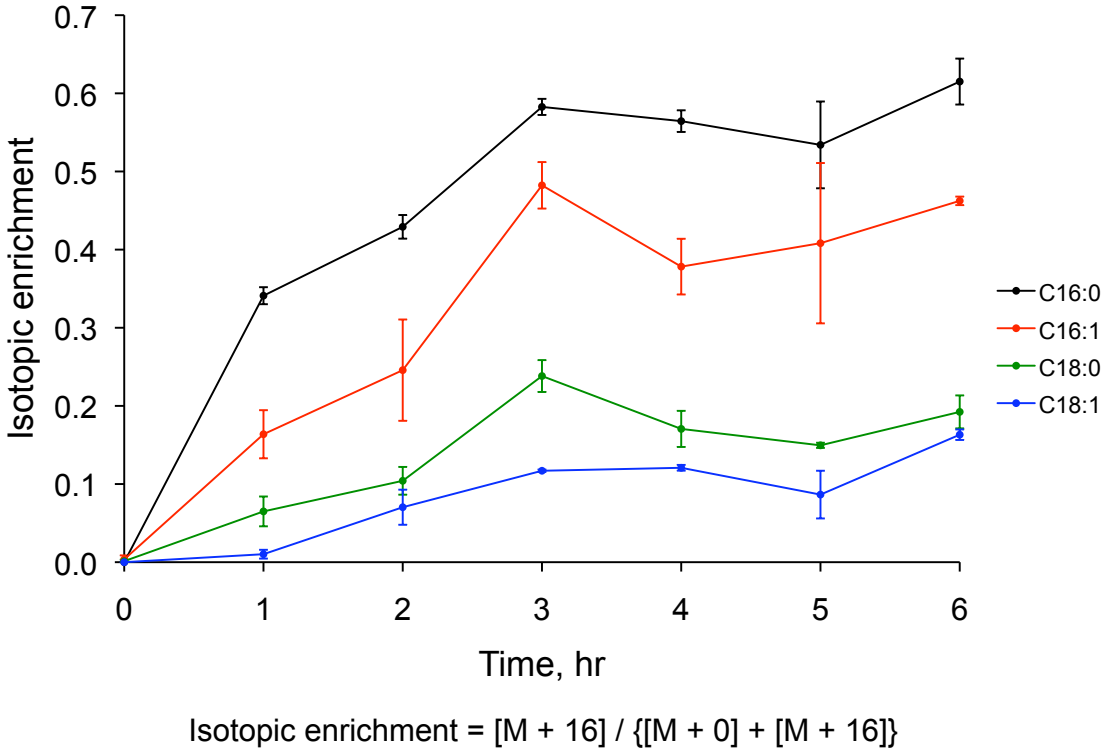

Figure 18. Isotopic enrichment of palmitoyl-, palmioleoyl-, stearoyl-, and oleoyl-CoA in HEK293 cells after treatment with 0.1 mM [U-^{13}C]-palmitate for 0 to 6 hr. The mean and range of duplicate Petri dishes is shown.

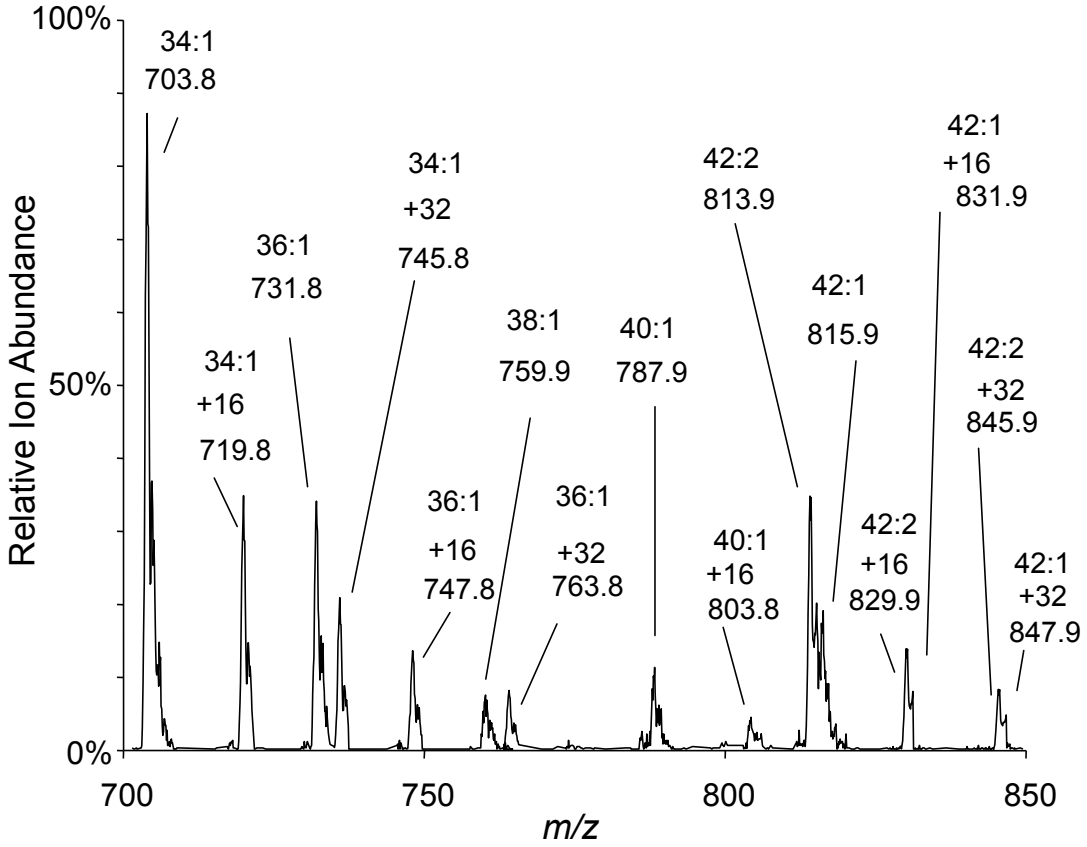

Figure 19. Positive mode precursor ion scan (184.1 Da) of extracts of HEK293 cells treated with 0.1 mM [U^{13}C]-palmitate. The abundant sphingomyelin product ion (*m/z* 184.1) was used to survey molecular species present in the sample. Incorporation of one label (+16) or two labels (+32) are designated. Signal is representative of continuous syringe infusion of approximately 1x10^6 cells (1/10 total infused).

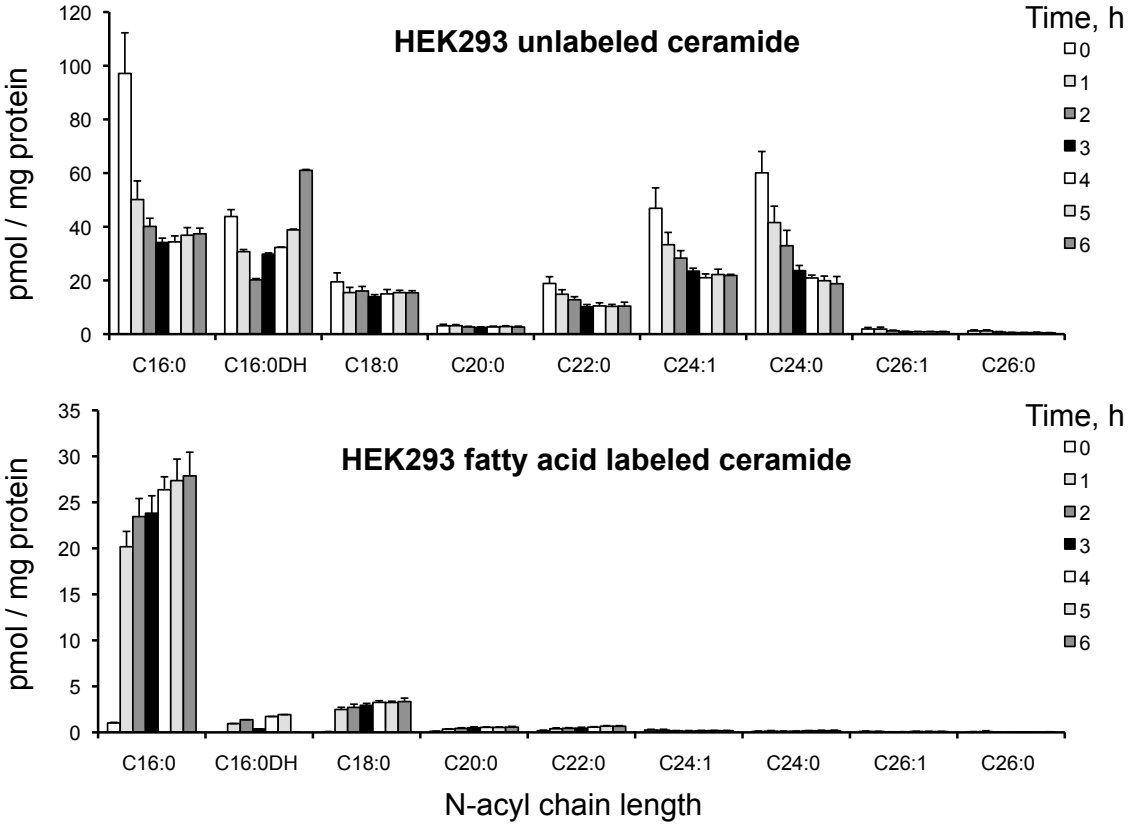

Figure 20. Unlabeled (^{12}C) and fatty acid labeled (FA) ceramide from extracts of HEK293 cells treated with 0.1 mM [U-^{13}C]-palmitate for 0 - 6 h. Cells were grown in culture for the indicated duration, and then collected. Lipids were extracted and analyzed as described in Experimental Procedures. Protein was determined by Lowery assay. Results are the mean ± SD with N = 4, except C16:0 DHCer for which not all SD values were available.

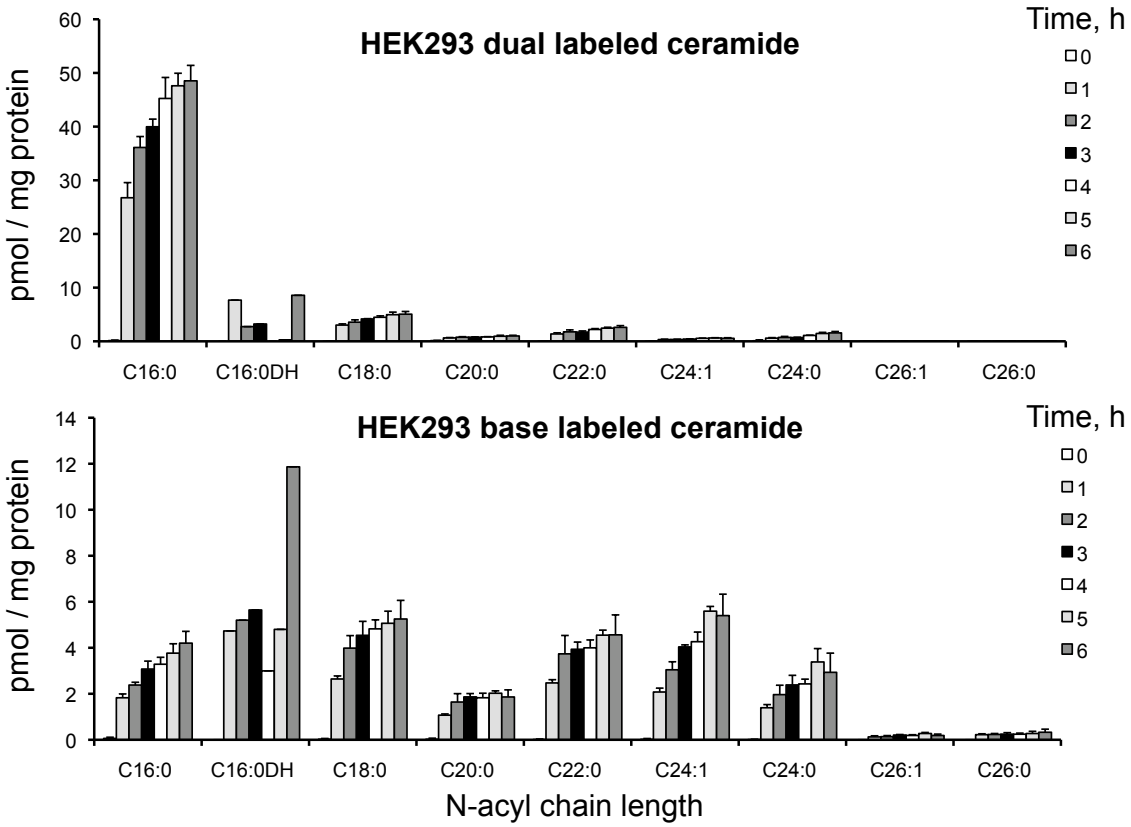

Figure 21. Dual (DUAL) and base labeled (BASE) ceramide from extracts of HEK293 cells treated with 0.1 mM [U-^{13}C]-palmitate for 0 - 6 h. Cells were grown in culture for the indicated duration, and then collected. Lipids were extracted and analyzed as described in Experimental Procedures. Protein was determined by Lowery assay. Results are the mean ± SD with N = 4, except C16:0 DHCer for which not all SD values were available.

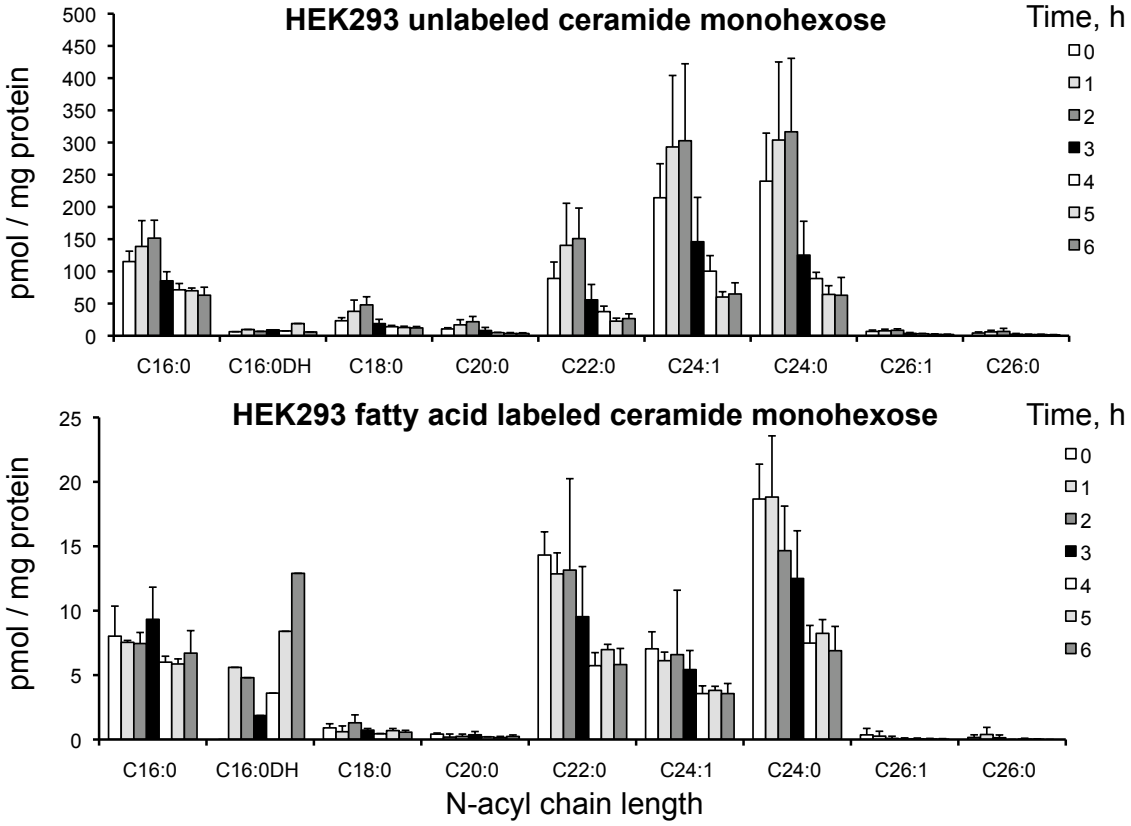

Figure 22. Unlabeled (^{12}C) and fatty acid labeled (FA) ceramide monohexose from extracts of HEK293 cells treated with 0.1 mM [U-^{13}C]-palmitate for 0 - 6 h. Cells were grown in culture for the indicated duration, and then collected. Lipids were extracted and analyzed as described in Experimental Procedures. Protein was determined by Lowery assay. Results are the mean ± SD with N = 4, except C16:0 DHCer for which not all SD values were available.

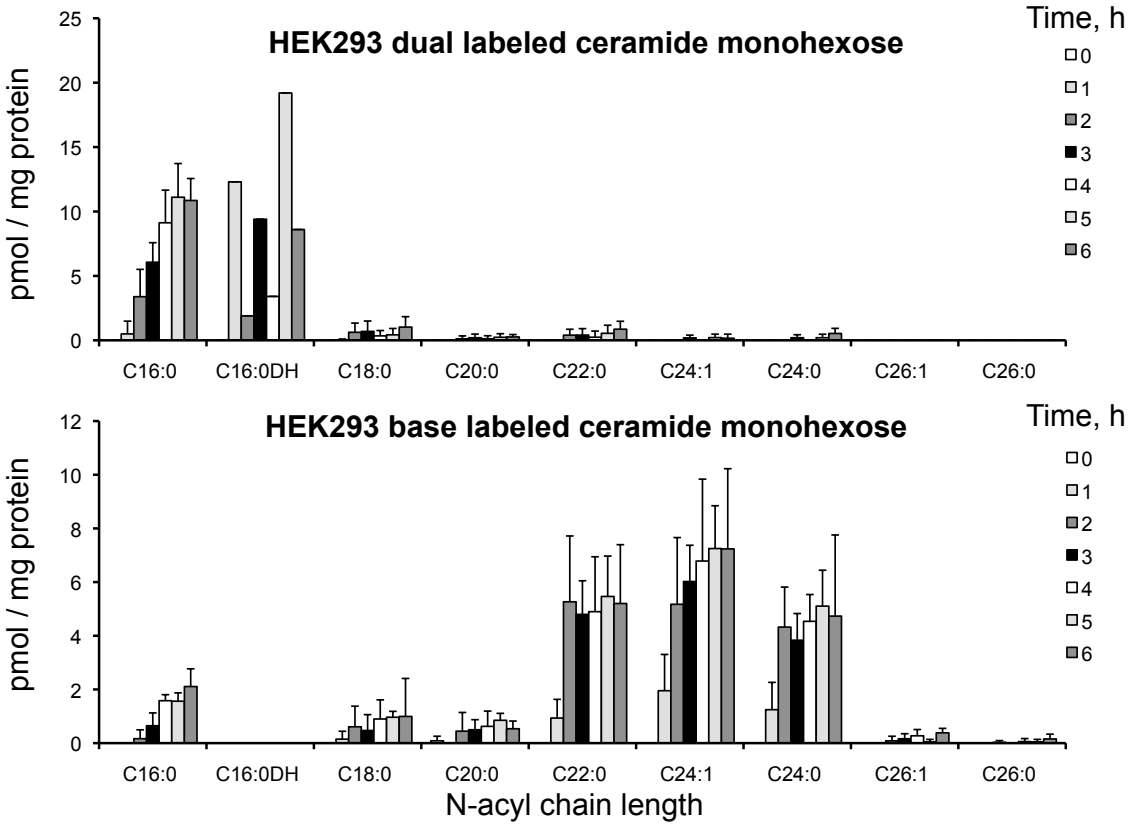

Figure 23. Dual (DUAL) and base labeled (BASE) ceramide monohexose from extracts of HEK293 cells treated with 0.1 mM [U-^{13}C]-palmitate for 0 - 6 h. Cells were grown in culture for the indicated duration, and then collected. Lipids were extracted and analyzed as described in Experimental Procedures. Protein was determined by Lowery assay. Results are the mean ± SD with N = 4, except C16:0 DHCer for which not all SD values were available.

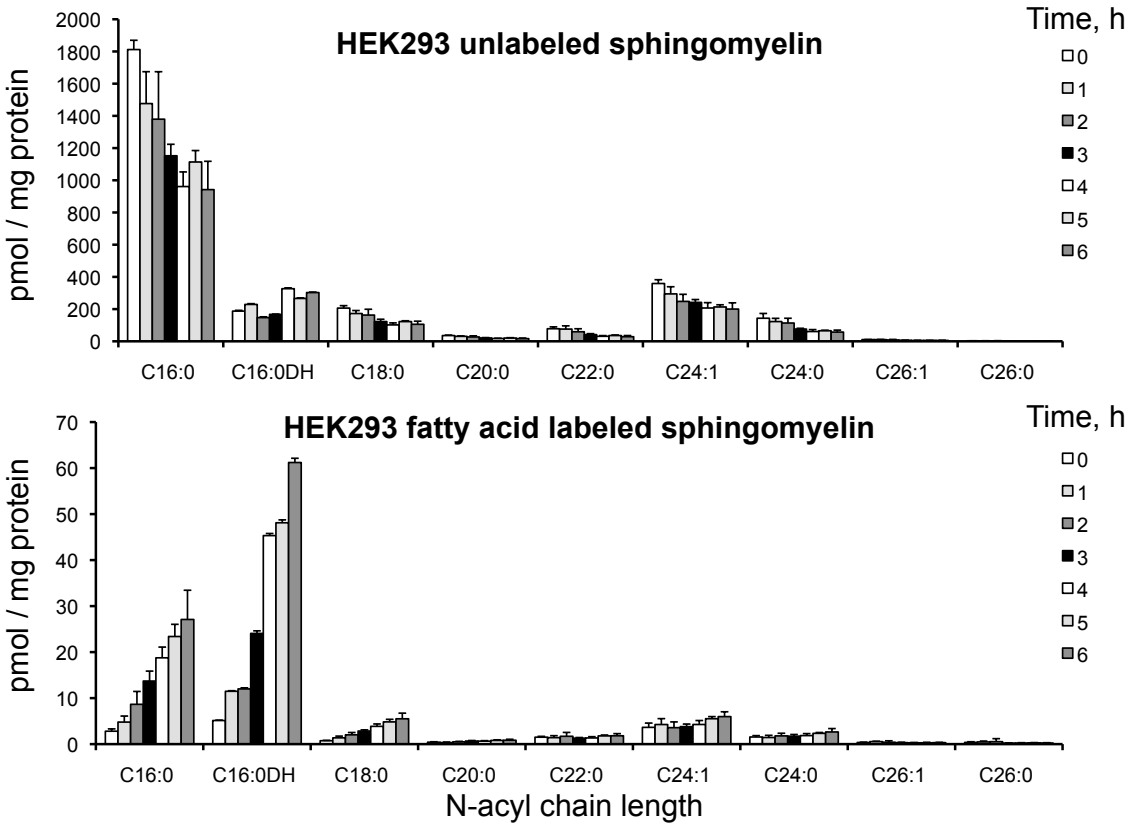

Figure 24. Unlabeled (^{12}C) and fatty acid labeled (FA) sphingomyelin from extracts of HEK293 cells treated with 0.1 mM [U-^{13}C]-palmitate for 0 - 6 h. Cells were grown in culture for the indicated duration, and then collected. Lipids were extracted and analyzed as described in Experimental Procedures. Protein was determined by Lowery assay. Results are the mean ± SD with N = 4, except C16:0 DHCer for which not all SD values were available.

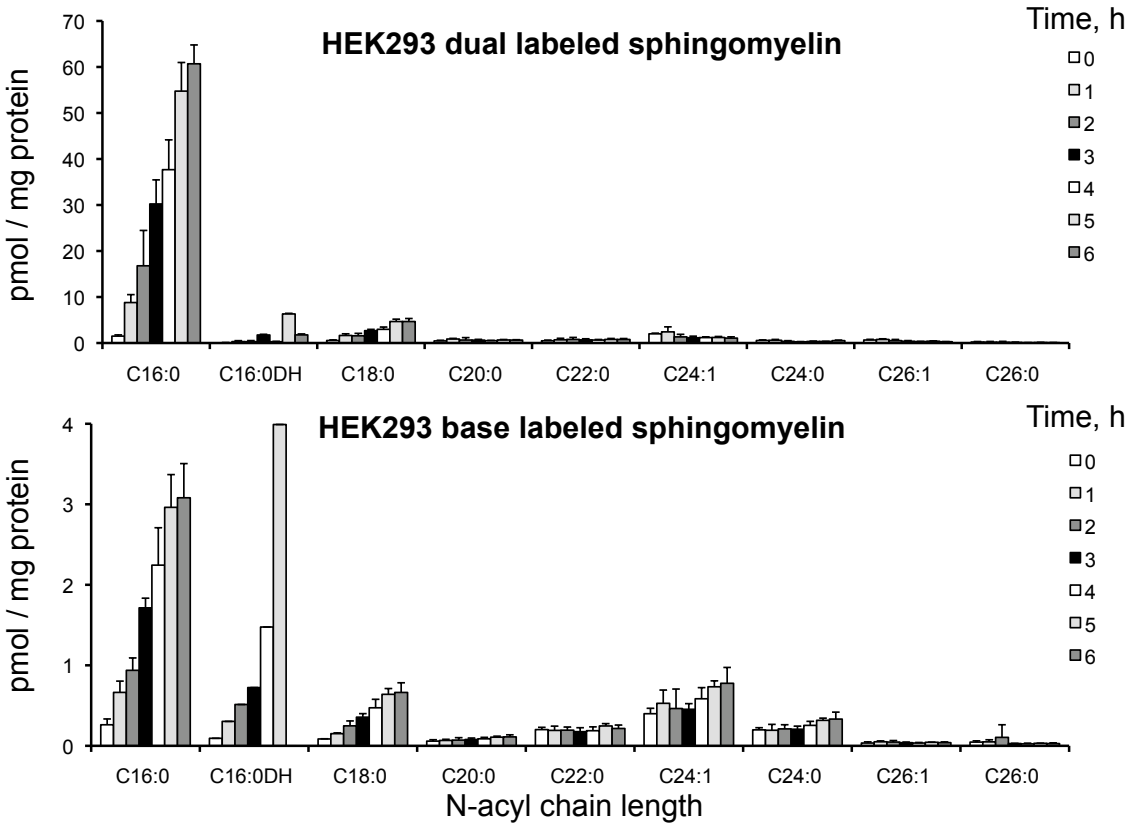

Figure 25. Dual (DUAL) and base labeled (BASE) sphingomyelin from extracts of HEK293 cells treated with 0.1 mM [U-^{13}C]-palmitate for 0 - 6 h. Cells were grown in culture for the indicated duration, and then collected. Lipids were extracted and analyzed as described in Experimental Procedures. Protein was determined by Lowery assay. Results are the mean ± SD with N = 4, except C16:0 DHCer for which not all SD values were available.

Differential rates of [U-^{13}C]-palmitate incorporation into N-acyl sphingolipids were observed when comparing Cer, CMH and SM. While only 35% of the total Cer was unlabeled at 3 h, unlabeled CMH and SM were 85% and 96%, respectively, of their total quantities at 3 h. SM comprised the quantitative majority of the N-acyl sphingolipids; however, label incorporation into SM at 3 h was low (3%).

Phospholipase D treatment

Positive ion mode ESI-MS/MS analysis of SM did not yield abundant product ions indicative of sphingoid base vs. N-acyl labeling for [M + 16] precursor ions, therefore phospholipase D (PLaseD) treatment was used to convert SM to Cer-1-P, which fragments in a manner similar to Cer and provides quantitation of base labeled vs. fatty acid labeled SM isotopomeric derivatives. Before PLaseD treatment, the Cer-1-P isotopomers were quantitated to ascertain the pre-existing amount that should be subtracted from the SM-derived Cer-1-P quantity after PLaseD treatment. Total Cer-1-P quantities in 1 x 10^6 HEK293 cells were consistently less than 50 pmol (the sum of all N-acyl chain lengths).

To distinguish base labeled vs. fatty acid labeled SM in HEK293 cells by the PLaseD conversion of SM to Cer-1-P, cells were grown for 3 h in media containing 0.1 mM [U-^{13}C]-palmitate (Figure 26). Before PLaseD treatment, the quantity of Cer-1-P was 5 ± 2 pmol/mg protein for both fatty acid and base labeled isotopomers, and total [M + 16] SM was 690 ± 20 pmol/mg protein. After treatment with PLaseD, 70 ± 10 pmol/mg protein of ^{13}C-d18:1/^{12}C-(fatty acid) Cer-1-P was observed and 560 ± 20 pmol/mg protein of ^{12}C-d18:1/^{13}C-(fatty acid) Cer-1-P for a sum of 630 ± 20 pmol/mg protein, which represents a 91% recovery of the original SM. The N-acyl chain length distribution of SM was also preserved with ^{13}C-d18:1/^{12}C-16:0, ^{13}C-d18:1/^{12}C-24:1, ^{12}C-d18:1/^{13}C-16:0 and ^{12}C-d18:1/^{13}C-24:1 Cer-1-P being the most abundant chain lengths. These results

reveal that there was ~ 8-fold greater ^{13}C-labeling of the fatty acid moiety compared to the sphingoid base moiety in the singly labeled SM in HEK293 cells.

Correction based on isotopic labeling of the fatty acyl-CoAs of HEK293 cells

Analysis of the fatty acyl-CoA profile in HEK293 cells treated with 0.1 mM [U-^{13}C]-palmitate revealed that the 16:0-CoA was ~ 60% ^{13}C-16:0-CoA between 3 and 6 h. A portion of the ^{13}C-16:0-CoA was elongated and / or desaturated (Figure 18), with 18:0-CoA isotopic enrichment being 25% at 6 h, while 16:1-CoA and 18:1-CoA isotopic enrichments were 40% and 10%, respectively, at 6 h.

Thus, considering this time (3 to 6 h) during which isotopic equilibrium for 16:0-CoA ^{13}C-labeling appears to have been established, and assuming that 16:0-CoA is a single, well-mixed precursor pool, the simplest prediction would be that in addition to the incorporation of ^{13}C-16:0-CoA into *de novo* biosynthesized 16:0 Cer (~ 60%), there will also be incorporation of unlabeled precursor (^{12}C-16:0-CoA) into *de novo* biosynthesized 16:0 Cer (~ 40%). Between 3 and 6 h of HEK293 cell treatment with [U-^{13}C]-palmitate, the average hourly quantity of 16:0-Cer with unambiguously *de novo* sphingoid bases was ~ [(45 ± 4) + (4 ± 0.5)] = 49 ± 4 pmol/ mg protein [dual labeled (^{13}C-d18:1/^{13}C-16:0) + base labeled (^{13}C-d18:1/^{12}C-16:0)]. Based on the estimated isotopic enrichment of 16:0-CoA of 60% during this period (Figure 18), and a total *de novo* 16:0-Cer = *x*, then 49 pmol/mg protein = 0.6*x*, and *x* = 49 pmol/mg protein/0.6, or *x* = 82 pmol/mg protein. Thus, the quantity of *de novo* biosynthesized C16:0-Cer with a ^{12}C sphingoid base was ~ 82 - 49 = 33 pmol/mg protein. This value is similar to the average hourly quantity of unlabeled 16:0-Cer (36 ± 2 pmol) and to the average hourly quantity of fatty acid

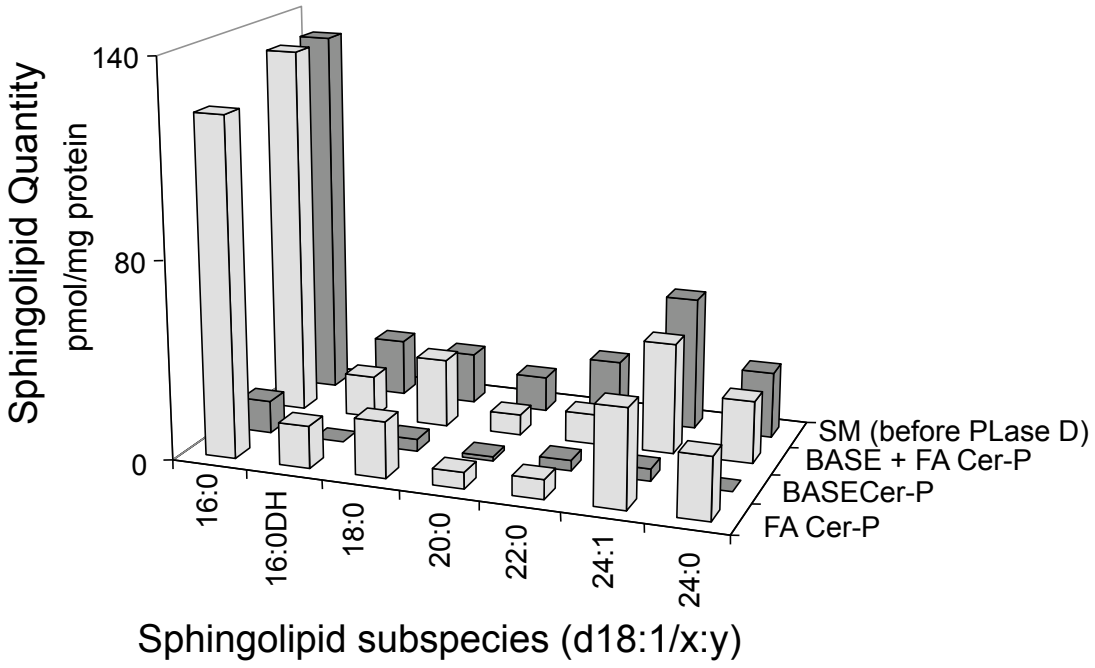

Figure 26. Determination of the label position in singly labeled sphingomyelins using PLaseD treatment. 1000 units of PLaseD were suspended in 0.1 ml of 3 mM decylglucopyranoside and 100 mM Tris (pH 8.0). The reserved complex sphingolipid aliquot was treated with PLaseD and incubated for 15 min in a heating block at 37°C. Samples were then dried in a Speed-Vac and reconstituted in mobile phase for LC-ESI-MS/MS analysis as described in Experimental Procedures.

labeled 16:0 Cer (26 ± 2 pmol) between 3 and 6 h, suggesting that a significant proportion of the observed quantities of these isotopologues could have been derived from *de novo* biosynthesis utilizing ^{12}C-16:0-CoA. Thus, taking together the isotopic enrichment of the 16:0-CoA pool and the quantities of 16:0 Cer isotopologues and isotopomers in HEK293 cells leads to the hypothesis that the majority of 16:0 Cer was derived from *de novo* biosynthesis under the conditions described here.

The average hourly amount of unambiguously *de novo* biosynthesized 16:0 CMH between 3 and 6 h was 11 ± 2 pmol/mg protein [dual labeled (^{13}C-d18:1/^{13}C-16:0) + base labeled (^{13}C-d18:1/^{12}C-16:0)]. Based on the estimated isotopic enrichment of 16:0-CoA of 60% during this period, a prediction of the average hourly amount of *de novo* ^{12}C-C16:0 CMH would be (see above) ~ 7 pmol/mg protein. This is a small quantity compared to the average hourly amount of ^{12}C-d18:1/^{12}C-16:0 CMH (72 ± 9 pmol/mg protein), and is similar to the average hourly amount of ^{12}C-d18:1/^{13}C-16:0 CMH (7 ± 2 pmol/mg protein) between 3 and 6 h. Thus, taking together the isotopic enrichment of the 16:0-CoA pool and the quantities of CMH isotopologues and isotopomers in HEK293 cells leads to the hypothesis that a modest portion of unlabeled 16:0 CMH was derived from *de novo* biosynthesis under the conditions described here.

The average hourly amount of unambiguously *de novo* biosynthesized 16:0 SM between 3 and 6 h was 49 ± 14 pmol/mg protein [dual (^{13}C-d18:1/^{13}C-C16:0) + base (^{13}C-d18:1/^{12}C-C16:0)]. Based on the estimated isotopic enrichment of 16:0-CoA of 60% during this period, a prediction of the average hourly amount of *de novo* ^{12}C-C16:0 SM would be (see above) 33 pmol/mg protein. This is a minute quantity compared to the average hourly amount of ^{12}C-d18:1/^{12}C-C16:0 SM (1040 ± 110 pmol/mg protein), and is similar to the average hourly amount of ^{12}C-d18:1/^{13}C-C16:0 SM (21 ± 6 pmol/mg protein) between 3 and 6 h. Thus, taking together the isotopic enrichment of the C16:0-

CoA pool and the quantities of SM isotopologues and isotopomers in HEK293 cells leads to the hypothesis that only a small fraction of unlabeled 16:0 SM was derived from *de novo* biosynthesis under the conditions described here.

Treatment of HEK293 cells with fumonisin B_1

Fumonisin B_1 (FB_1) is an inhibitor of CerS (73, 152, 153), and exposure of HEK293 cells to FB_1 for 24 and 48 h caused decreases in the quantities of unlabeled and ^{13}C-labeled Cer. The unlabeled Cer quantity at 24 h was 46 ± 2 pmol/mg protein in control cells and 27 ± 1 pmol/mg protein in FB_1 treated cells. An even larger difference was observed for ^{13}C-labeled Cer after 24 h. The quantity of base labeled ^{13}C-d18:1/^{12}C-(fatty acid) Cer was 13 ± 1 pmol/mg protein in control cells, but in FB_1 treated cells was only 3 ± 1 pmol/mg protein. The quantity of dual labeled ^{13}C-d18:1/^{13}C-(fatty acid) Cer was 36 ± 1 pmol/mg protein in control cells, but was only 4 ± 1 pmol/mg protein in FB_1 treated cells. Thus, an 86% reduction in the quantity of unambiguously *de novo* biosynthesized Cer (base labeled + dual labeled) was observed.

Changes in sphingoid base quantities were also informative regarding the responses to FB_1 treatment (Figure 27). In control cells ^{13}C-Sa and ^{13}C-Sa-1-P were below the limits of quantitation (~ 0.1 pmol/mg protein); however, they were the most abundant sphingoid bases in FB_1 treated cells, having quantities of 79 ± 12 pmol/mg protein and 450 ± 67 pmol/mg protein, respectively. Unlabeled Sa and Sa-1-P were observed to be 17 ± 4 pmol/mg protein and 88 ± 12 pmol/mg protein respectively in FB_1 treated cells, which yields a 0.18 Sa/Sa-1-P ratio and a 0.19 ^{13}C-Sa/^{13}C-Sa-1-P ratio. These results indicate that FB_1 inhibition of CerS resulted in the accumulation of a considerable quantity of *de novo* biosynthesized Sa and Sa-1-P, as well as significant

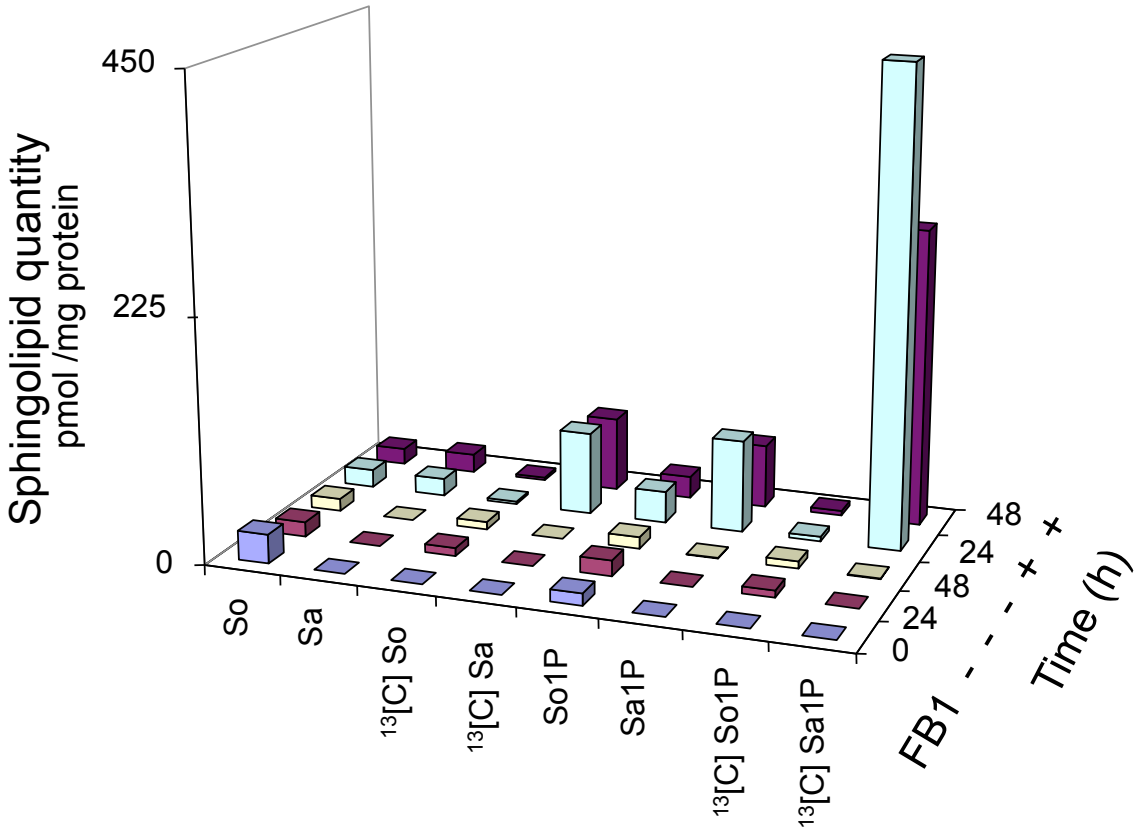

Figure 27. Sphingoid bases from HEK293 cells treated with 0.1 mM [U-^{13}C]-palmitate ± 50 μM FB_1 for the indicated times.

decreases in the quantity of *de novo* biosynthesized Cer. Collectively, these results show the utility of SIMPLE for determination of the metabolic reaction (CerS) that is inhibited (86%) by a pharmacological agent (FB_1) during sphingolipid biosynthesis.

3.5 Discussion

Described here is a sensitive and selective LC-ESI-MS/MS method utilizing [U-^{13}C]-palmitate tracer for the quantitation of *de novo* biosynthesized sphingolipids. Utilizing an isotopic precursor to measure sphingolipid biosynthesis has been previously examined, but the SIMPLE method presented here has several distinct advantages over these previous reports (94, 146). First, HPLC resolution of sphingolipid classes (Cer, CMH, and SM) in extracts of cellular lipids is faster and more selective than solid-phase extraction. Second, the multiple reaction monitoring (MRM) mode of tandem mass spectrometry utilized here provides sensitivity superior to the *m/z* scanning MS utilized previously. Third, the collision-induced dissociation (CID) fragmentation of sphingolipid precursor ions generated by relatively gentle electrospray ionization reveals the presence of three labeled isotopologues and isotopomers of N-acyl sphingolipids that were, in the previous reports, superimposed into two isotopic enrichment patterns (for palmitate and sphingosine) by the trimethylsilyl derivatization of Cer required before gas chromatography-electron impact-MS (GC-EI-MS).

Fatty acid β-oxidation of the [U-^{13}C]-palmitate coupled with re-elongation could produce non-uniformly labeled [^{13}C]-palmitate, and lead to the misinterpretation of data, as previously stated (146). To address this issue, precursor scans for *m/z* 184.1 (Figure 4) and *m/z* 264.4 in [U-^{13}C]-palmitate treated HEK293 cell extracts were performed, and did not show significant quantities of labeled N-acyl sphingolipids containing less than 16 amu shifts due to the activity of this putative palmitate metabolism. This conclusion was

based upon the sphingolipid fragmentations during positive ion mode ESI-MS/MS shown in Figure 16.

During positive ion mode ESI-MS/MS, Cer and CMH fragment to produce the same conjugated carbocation as the sphingoid bases. SM species fragment differently and largely retain the charge on their phosphocholine moiety after dissociation; therefore, almost no charge remains on Cer moiety fragments to determine the sphingoid base vs. N-acyl labeling if the SM is singly-labeled. To determine the label position in the singly-labeled SM, extracts of HEK293 cells cultured with [U-^{13}C]-palmitate were treated with PLaseD to convert the SM to Cer-1-P. The resulting Cer-1-P fragmented during positive ion mode ESI-MS/MS in a manner similar to Cer. The results indicated that Cer-1-P derived from SM had a ratio of ~ 8:1 for [^{12}C]-d18:1/[^{13}C]-(fatty acid) : [^{13}C]-d18:1/[^{12}C]-(fatty acid), revealing that the contribution of pre-existing sphingoid bases to SM biosynthesis in HEK293 cells is ~ 8-fold greater than the contribution of *de novo* sphingoid bases under these experimental conditions.

The immediate product of SPT is 3-ketosphinganine; however, [^{13}C]-3-ketosphinganine was below the limit of detection (~ 0.1 pmol/mg protein) in HEK293 cells. The quantity of [^{12}C]-3-ketosphinganine in HEK293 cells is also consistently low (less than 5% of the signal from Sa). This implies that 3-ketosphinganine is rapidly reduced to Sa and does not accumulate under these experimental conditions.

It has been previously shown that when cells are treated with FB_1, production of Cer is blocked and Sa accumulates (154-157). The [U-^{13}C]-palmitate tracer experiments described here independently confirm this conclusion by showing decreases in the quantity of [^{13}C]-N-acyl sphingolipids, and provide additional details regarding the fate of labeled Sa demonstrated by the accumulation of [^{13}C]-labeled Sa-1-P.

Chain length-specific differences were observed in the relative quantities of the isotopologues and isotopomers of N-acyl sphingolipids in HEK293 cells. For example,

the quantity of [^{13}C]-d18:1/[^{13}C]-16:0 Cer was equal to or greater than the quantity of any other isotopomer between 2 and 6 h, including the quantity of presumably pre-existing [^{12}C]-d18:1/[^{12}C]-16:0, while in contrast the quantity of [^{13}C]-d18:1/[^{13}C]-18:0 (and longer) Cer was equal to or less than the quantities of either the [^{12}C]-d18:1/[^{12}C] or [^{13}C]-d18:1/[^{12}C] isotopomers from 0 to 6 h. The [^{12}C]-d18:1/[^{13}C]-(fatty acid) isotopomer was of the lowest relative quantity for all chain lengths except C16:0, for which it was the second-lowest abundance isotopomer (the [^{13}C]-d18:1/[^{12}C]-16:0 Cer was the least abundant).

The relative abundances of isotopomers for CMH and SM largely recapitulated the chain length-dependent variations described above for Cer with certain exceptions. First, the quantities of CMH and particularly SM [^{12}C]-d18:1/[^{12}C]-(fatty acid) species were greater than the quantities of any labeled isotopomer for all chain lengths between 0 and 6 h, in contrast to the robust isotopic enrichment of Cer, especially 16:0 Cer. As observed for Cer, the [^{13}C]-d18:1/[^{13}C]-16:0 species of CMH and SM was the most abundant labeled 16:0 isotopologue, while for chain lengths longer than 16:0 the [^{13}C]-d18:1/[^{12}C]-(fatty acid) was typically the most abundant labeled isotopomer. The results for CMH preclude definitive statements about [^{12}C]-d18:1/[^{13}C]-(fatty acid) isotopomers due to the apparent presence of these isotopomers at 0 hr; this observation is explained by the previously described presence of α-hydroxy fatty acid moieties on CMH (158).

Quantitation of unlabeled and ^{13}C-labeled fatty acyl-CoAs provides a correction factor for the estimates of sphingolipid biosynthesis, if one assumes a single, well-mixed precursor pool of fatty acyl-CoAs. Between 3 and 6 hr this correction for palmitoyl-CoA is ~ 40%, and is even higher for elongated ^{13}C-labeled fatty acyl-CoAs, such as stearoyl-CoA (Figure 18). This suggests that at least some of the unlabeled N-acyl sphingolipids could have been generated by *de novo* biosynthesis utilizing unlabeled fatty acyl-CoA substrates, with the remainder of the unlabeled sphingolipids likely being derived from

catabolism of more complex species. Thus, measurement of the fatty acyl-CoA biosynthetic precursor pools for sphingolipids allows the estimation of *de novo* biosynthetic and turnover contributions.

Overall, these results are both consistent with previous knowledge about sphingolipid *de novo* biosynthesis and suggestive of new hypotheses regarding this complicated metabolic process. The rapid and robust isotopic labeling of 16:0 Cer indicates that *de novo* biosynthesis accounts for the majority of this metabolite pool under these experimental conditions, while the slow and minimal labeling of SM indicates a minor contribution of *de novo* biosynthesis to this metabolite pool under these conditions. These results, as well as the ^{13}C-labeling of 16:0 CMH being intermediate between those of 16:0 Cer and 16:0 SM, are consistent with the step-wise biosynthesis of sphingolipids, beginning with sphinganine and ceramide in the endoplasmic reticulum (ER), followed by CMH in the ER and *cis*-Golgi (159), and then SM in the *trans*-Golgi and plasma membrane. The decrease in isotopic labeling as the N-acyl chain length increases for Cer, CMH, and SM is also consistent with the requirement for elongation of the ^{13}C-labeled palmitoyl-CoA in the ER before its utilization as substrate by CerS isoforms.

[U-^{13}C]-palmitate treatment in conjunction with LC-ESI-MS/MS analysis yields highly informative data regarding the quantities of sphingolipid isotopomers. It is also important to note that pharmacological impairment of sphingolipid biosynthetic pathways can be detected, as demonstrated by FB_1 treatment resulting in a ~85% decrease of ^{13}C-labeled Cer amount, and in [^{13}C]-Sa accumulating up to amounts 5-fold greater than either [^{13}C]-So or [^{13}C]-So-1-P in control cells. Thus, a hypothesis generated by these experiments is a substantial contribution of *de novo* biosynthesis to the C16:0 Cer metabolite pool. In brief, the sphingolipid isotopic metabolic precursor labeling experiment (SIMPLE) allows a deeper exploration of biosynthetic rates and

pharmacological modulators within the sphingolipid metabolic pathway than has been previously available.

CHAPTER 4

METABOLOMIC ANALYSIS OF THE CONSEQUENCES OF ELEVATION OF SERINE PALMITOYLTRANSFERASE ACTIVITY BY STABLE OVEREXPRESSION OF *SPTLC1* AND *SPTLC2* IN HEK293 CELLS: A USEFUL APPROACH TO TEST CURRENT DOGMA AND RAISE NEW HYPOTHESES[3]

4.1 Summary

Sphingolipids and fatty acyl-CoAs can be labeled with stable isotopes by treatment of cultured cells with [U-^{13}C]-palmitate, as described in Chapter 3. A cellular paradigm for increased *de novo* biosynthesis of sphingolipids is the over-expression of serine palmitoyltransferase (SPT) in HEK293 cells, which results in greater quantities of sphingolipids in SPT1/2 cells both with and without [U-^{13}C]-palmitate treatment, compared to HEK293 cells.

One approach for a more sophisticated analysis of the isotopic enrichment data involved calculating the dynamic (time-dependent) isotopic enrichment of fatty acyl-CoAs and sphingolipids, and using this information to estimate metabolic parameters of a particular analyte pool (i.e. palmitoyl-CoA) such as its isotopic enrichment at labeling steady-state, and its fractional turn-over rate per unit time. Using these estimated parameters and the analyte pool size (determined by LC-ESI-MS/MS quantitation) the rate of appearance of unlabeled analyte was determined, which is synonymous with the forward rate of *de novo* biosynthesis for that analyte. In this study, the specific contributions of this author were the extraction and quantitation of fatty acyl-CoAs,

[3] This chapter is in preparation for publication; the authors are Wei, J., Allegood, J., Wang, E., Kelly, S., Haynes, C., Park, H., Carton, J., Uhlinger, D., Sullards, M., and Merrill, A.

analysis of their dynamic isotopic enrichment, and analysis of sphingolipid dynamic isotopic enrichments.

4.2 Introduction

Sphingolipids are an incredibly diverse family of compounds that are found in eukaryotes and some prokaryotes and viruses (74) where they have structural functions as well as participating in cell recognition and cell signaling (160, 161). Sphingolipids are elaborations of a category of lipid backbones called “sphingoid bases” or “long-chain bases,” of which the three most commonly encountered in mammalian sphingolipids are sphingosine (So), sphinganine (Sa, dihydrosphingosine) and phytosphingosine (4-hydroxydihydrosphingosine) (61).

Sphingoid base biosynthesis is catalyzed by serine palmitoyltransferase (SPT), a family of pyridoxal 5’-phosphate-dependent enzymes that condense serine and palmitoyl-CoA to make the “traditional” sphingoid bases (sphinganine, sphingosine, etc.) (4-6), and they also accommodate alanine to make 1-deoxysphinganine and glycine to make 1-desoxymethylsphinganine (73). So far, at least three isoforms (SPT1, SPT2 and SPT3, and their corresponding genes, *SPTLC1*, *SPTLC2* and *SPTLC3*) have been identified in humans (162-164). Both *SPTLC1* and *SPTLC2* are expressed widely in mouse and human tissues (21, 163), while the *SPTLC3* is expressed in certain tissues and is absent in HEK293 cells (164). The minimal requirement for SPT activity is a heterodimer of SPT1 with SPT2 and/or SPT3 (4, 164, 165), and in at least some cases, other associated proteins may be involved (166, 167).

SPT is generally regarded to be rate-limiting for *de novo* sphingolipid biosynthesis (168, 169), and changes in activity have been correlated with up-regulation of this pathway by agents such as endotoxin (170), retinoic acid (171), 4-HPR (172), etoposide (173) and UV light (174-176) etc. However, there have been no studies of

how elevation of SPT activity alone, by transient or stable transfection with cDNA for *SPTLC1* and *SPTLC2*, affects this pathway and, possibly, compromises cell survival since downstream metabolites such as sphingoid bases and ceramides are growth inhibitory and cytotoxic (160, 177). Mouse and Chinese hamster *SPTLC1* and *SPTLC2* genes have been over-expressed in HEK293 cells (163) and CHO cells (22), respectively, but the effects on flux through the pathway and the sphingolipid profile have not been reported.

Therefore, to explore this fundamental question of sphingolipid biosynthesis, a HEK293 cell line was generated that stably over-expresses SPT1 and SPT2 proteins, it was confirmed that this elevates SPT activity, and the effects of the higher sphingoid base biosynthesis on production of the downstream species was evaluated using liquid-chromatography-electrospray ionization-tandem mass spectrometry (LC-ESI-MS/MS), which also allowed the monitoring of sphingoid base *de novo* biosynthesis using [U-^{13}C]-palmitate as a stable isotope-labeled precursor. The studies confirmed some aspects of the current dogma about SPT and sphingolipid biosynthesis (i.e., SPT over-expression not only increased the rate of sphingolipid biosynthesis but also increased the amounts of sphingolipids in the cells), and also illustrated how downstream steps can become rate-limiting, and raised several interesting new questions and hypotheses.

4.3 Experimental procedures

Materials

The HEK293 cells were obtained from the American Type Culture Collection (Manassas, VA). All tissue culture plastic ware was obtained from Corning (Corning, NY). Fetal bovine serum was supplied by Hyclone (Logan, Utah). Anti-BiP antibody was from StressGen, Inc. (Victoria, BC, Canada). The secondary antibodies were Alexa Fluor-conjugated goat anti-rabbit and anti-mouse obtained from Molecular Probes, Inc.

(Eugene, OR). The affinity purified polyclonal rabbit anti-human primary antibodies raised against SPT1 peptides have been previously described (21). C6-NBD-SM and C6-NBD-Cer are from Avanti Polar Lipids (Alabaster, AL). Protease inhibitor cocktail was obtained from Roche (Indianapolis, IN).

The internal standard cocktail (catalog number LM-6002) was provided by Avanti Polar Lipids (Alabaster, AL) in sealed ampoules and certified (64) to be > 95% pure and within 10% of the specified amount (250 μM); it was comprised of the 17-carbon chain length sphingoid base analogs: C17-sphingosine, (2S,3R,4E)-2-aminoheptadec-4-ene-1,3-diol (d17:1-So); C17-sphinganine, (2S,3R)-2-aminoheptadecane-1,3-diol (d17:0-Sa); C17-sphingosine 1-phosphate, heptadecasphing-4-enine-1-phosphate (d17:1-S1P); and C17-sphinganine 1-phosphate, heptadecasphinganine-1-phosphate (d17:0-Sa1P); and the C12-fatty acid analogs of the more complex sphingolipids C12-Cer, N-(dodecanoyl)-sphing-4-enine (d18:1/C12:0-Cer); C12-Cer 1-phosphate, N-(dodecanoyl)-sphing-4-enine-1-phosphate (d18:1/C12:0-Cer1P); C12-sphingomyelin, N-(dodecanoyl)-sphing-4-enine-1-phosphocholine (d18:1/C12:0-SM); C12-glucosylceramide, N-(dodecanoyl)-1-β-glucosyl-sphing-4-eine (d18:1/C12:0-GlcCer); and C12-lactosylceramide, N-(dodecanoyl)1-β-lactosyl-sphing-4-eine (d18:1/C12:0-LacCer); as well as one very-long-chain Cer analog, C25-Cer, N-(pentacosanoyl)-sphing-4-enine (d18:1/C25:0-Cer). [U-^{13}C]-palmitate (98%) was purchased from Cambridge Isotope (Andover, MA).

The HPLC grade solvents (acetonitrile, # EM-AX0145; chloroform, # EM-CX1050; hexane, # JT9304-33; and methanol, # EM-MX0475, as well as formic acid (ACS grade, # EM-FX0440-7), were obtained from VWR (West Chester, PA), and acetic acid (ACS grade, # A38C-212) was obtained from Fisher (Pittsburg, PA).

Cell culture

HEK293 cells and SPT1/2 cells were grown in DMEM / F12 medium (1:1) (Gibco BRL, MD**)** supplemented with 10% fetal bovine serum (FBS), penicillin (100 U / ml) and streptomycin (100 μg /ml) at 37 °C in a humidified 5 % CO_2 atmosphere.

Generation of SPT1 and SPT2 over-expressing cell lines

SPTLC1 and *SPTLC2* were cloned from human monocytes. Briefly, total RNA from cells treated for 4 hr with 1 mM dexamethasone was isolated using the RNeasy RNA isolation kit (Qiagen, Valencia, CA). The SPT gene-specific RNA was reverse transcribed and PCR amplified using Superscript One-Step RT-PCR System (Invitrogen, Carlsbad, CA). The following oligos were used as amplification primers: *SPTLC1* 5'-CCGGAATTCATGGCGACCGCCACGGAGCAG, *SPTLC1* 3'-CCGGAATTCGACTCTGCCTAGAGCAGGAC, *SPTLC2* 5'-CCGCTCGAGATGCGGCCGGAGCCCGGAGGCTG, *SPTLC2* 3'-CTAGTCTAGAGGCTCAGTCTTCTGTTTGTTC. The SPT1 gene was cloned into pcDNA3.1NEO and SPT2 was cloned into pcDNA3.1ZEO. The expression plasmids were transfected separately or co-transfected into HEK293 cells using Superfect (Qiagen, Valencia, CA) according to the manufacture's directions. 50 mg of plasmid DNA were mixed with 30 ml of the Superfect reagent in 500 ml serum-free media (DMEM, 2 mM L-glutamine) and incubated at room temperature for 15 minutes. The liposomes were added to 5 ml of serum-containing media (DMEM, 10% FBS, 2 mM L-glutamine, 10 Units/ml penicillin, 10 ug/ml streptomycin) and incubated on $5X10^6$ HEK293 cells for 2 hours at 37^{o}C, 5% CO_2. The cells were washed and the serum-containing media was replaced. 400 mg/ml geneticin or 200 mg/ml zeocin were added to the culture media 48 hours after transfection to select for cells stably expressing SPT1 or SPT2, repsectively. The co-transfection was selected in media containing both geneticin and zeocin. The media was changed every 4 days. After 2 weeks, surviving

colonies were selected and grown in individual wells of a 6-well plate. 3 colonies for each transfection, *SPTLC1*, *SPTLC2*, *SPTLC1/SPTLC2*, pcDNA 3.1 NEO vector control and pcDNA3.1Zeo vector control, were selected and checked by RT-PCR for the transfected gene transcript and by Western blot for recombinant protein expression. The highest expressing cell line for each gene transfection and vector controls were selected for further study.

Western blotting

50 μg of microsomal membrane protein were loaded on a 10 % SDS-PAGE gel (BIO RAD, Hercules, CA). For Western blotting, the gel was transferred to nitrocellulose membrane using Tris-glycine buffer with 20 % methanol, as the transfer medium, for 1 hour at 100 V (constant), in a transfer unit (BIO RAD, Hercules, CA). After blocking overnight at 4 ^{o}C with 5% milk/TBST (Tris buffered saline with 0.05 % Tween 20) the membrane was incubated with rabbit anti-SPT1 serum diluted in 5% milk/TBST for 2 hours and then with a AP-conjugated secondary antibody and its substrate using a ECF western blotting kit (GE Healthcare, Piscataway, NJ).

SPT activity assay

SPT activity was assayed as previously described (178). Data of specific activity for SPT represent results from 2 or more assays conducted under the same conditions. Values are presented as mean ± SD of all acquired values.

Immunofluorescence confocal microscopy

Cells were cultured on glass cover-slips (VWR, Inc., West Chester, PA) in a 24-well plate and fixed with 4 % formaldehyde in PBS at room temperature for 15 min. Fixed cells were permeabilized with 0.1 % Triton X-100 for 5 min, blocked in 10 % fetal

bovine serum in PBS (serum-PBS) for 30 min and then subjected to indirect immunofluorescence staining. Cells were incubated for 1 h at room temperature, with rabbit anti-SPT1 or rabbit anti-SPT2 primary antibody and mouse anti-Bip antibody, then washed 3 times with PBS-serum for 5 min each, and incubated for 1 h at room temperature with Alexa Fluor 488 anti-rabbit or Alexa Fluor 568 anti-mouse secondary antibody. Stained cells were rinsed in PBS and mounted in Fluoromount G (Southern Biotechnology Associates, Inc., Birmingham, AL) before observing under a Zeiss LSM 510 inverted laser scanning confocal microscope (Heidelberg, Germany).

[U-^{13}C]-Palmitate isotopic labeling

Uniformly labeled [^{13}C]-palmitate was mixed with fatty acid-free bovine serum albumin (BSA) at 1:1 molar ratio to make a 1 mM solution which was further diluted to a final concentration of 0.1 mM with complete cell culture medium just before use and filter sterilized. Twenty-four hours before the experiment cells were seeded in 100 mm Petri dishes in complete growth medium. Just before treatment, medium was removed from the Petri dish and [U-^{13}C]-palmitate/BSA medium mixture was applied to the cells for a certain period of time.

Liquid chromatography-electrospray ionization-tandem mass spectrometry of sphingolipids

The method has been described previously (68, 74). All data were collected using a Perkin Elmer Series 200 MicroPump system coupled to a PE Sciex API 3000 triple quadrupole mass spectrometer equipped with a Turbo Ion-Spray source. Free sphingoid bases and the Cer-1-P were separated by reverse phase HPLC using a binary solvent system and a Supelco 2.1 mm i.d. x 5 cm Discovery C18 column and a flow rate of 1 ml/min. Mobile phase A consisted of $CH_3OH/H_2O/HCOOH$ (58:41:1) (v/v/v) with 5

mM ammonium formate. Mobile phase B consisted of CH_3OH/HCOOH (99:1) (v/v) with 5 mM ammonium formate. Before every run, the column was equilibrated for 0.4 min with 60:40 (A/B) prior to injection. After sample injection (50 μL by a Perkin Elmer Series 200 autosampler), the column was eluted with 60:40 A/B for 0.5 min, followed by a 1.8 min linear gradient to 100% B, which was held for 5.3 min and followed by a 0.5 min re-equilibration with 60:40 A/B before the next run.

The complex sphingolipids (ceramides, monohexosylceramides, and sphingomyelins) were separated by normal phase HPLC using a binary solvent system and a Supelco 2.1 mm i.d. x 5 cm LC-NH_2 column at a flow rate of 1.5 ml/min. Mobile phase A consisted of $CH_3CN/CH_3OH/CH_3COOH$ (97:2:1) (v/v/v) with 5 mM ammonium acetate. Mobile phase B consisted of $CH_3OH/H_2O/CH_3(CH_2)_3OH/CH_3COOH$ (64:15:20:1) (v/v/v/v) with 5 mM ammonium acetate. Before every run the column was equilibrated for 0.5 min at 98:2 A/B prior to injection. After sample injection, the column was eluted with 98:2 A/B for 1.1 min, followed by a 0.2 min linear gradient to 82% A, which was held for 0.4 min, and then followed by a 0.8 min linear gradient to 100% B. The column was then re-equilibrated at 98:2 A/B for 0.5 min.

In the API 3000 triple quadrupole mass spectrometer, dry ultra high-purity N_2 was used as the nebulizing gas at a flow rate of 6 liters/min. The ionspray needle was held at 5500 V, and the orifice and ring voltages were kept low (30-40 V and 180-220 V, respectively) to prevent collisional decomposition of molecular ions prior to entry into the first quadrupole, and the N_2 Turbo Ion Spray gas temperature was 500 °C. N_2 was used to collisionally induce dissociations in Q2, which was offset from Q1 by 30-40 V. Q3 was then set to pass molecularly distinctive product ions. A multiple reaction monitoring (MRM) method was created by setting Q1 and Q3 to pass the precursor and product ions of the most abundant sphingolipid molecular species. For example, for Cer, these transitions occur at *m/z* 538.7/264.4, 566.5/264.4, 594.6/264.4, 622.7/ 264.4,

648.7/264.4, 650.7/264.4, which correspond to Cer with a d18:1 sphingoid base and 16:0, 18:0, 20:0, 22:0, 24:1, and 24:0 N-acyl chain, respectively. The dwell time was 25 ms for each transition. Quantitation was achieved by spiking the samples prior to extraction with the synthetic internal standards.

Prior to selecting MRM pairs for each cell type, the variation in fatty-acyl chain length was determined, which allowed MRM transitions to be tailored for the major N-acyl species. This was usually accomplished by precursor ion scans of *m/z* 184.4, the structure specific fragmentation indicative of SM. SM were chosen because they are typically abundant and are indicative of both sphingosine (So) and sphinganine (Sa) based species. For example, in HEK293 cells, the major SM are 16:0, 18:0, and 24:1.

Cell extraction and liquid chromatography-electrospray ionization-tandem mass spectrometry of fatty acyl-CoA species

Fatty acyl-CoAs were extracted from HEK293 cells and quantitated by LC-ESI-MS/MS as described previously (3).

Quantitation of sphingolipid isotopologues and isotopomers by LC-ESI-MS/MS

Sphingolipids [sphingoid bases and (dihydro)N-acyl species] were extracted from samples of cultured cells and quantitated by LC-ESI-MS/MS essentially as described previously (74) . To quantitate sphingoid bases labeled with [U-^{13}C]-palmitate, additional multiple reaction monitoring (MRM) pairs corresponding to [M + 16] precursor ions and [M + 16] product ions were used. To quantitate N-acyl (dihydro)sphingolipids labeled with a single [U-^{13}C]-palmitate moiety, MRM pairs corresponding to [M + 16] precursor ions and both [M + 0] and [M + 16] product ions were used, providing discrimination of labeling on the N-acyl and sphingoid base moieties, respectively. These [M + 16] isotopomers are designated FA and BASE. To quantitate N-acyl (dihydro)sphingolipids

labeled with two [U-^{13}C]-palmitate moieties, MRM pairs corresponding to [M + 32] precursor ions and [M + 16] product ions were used; the [M + 32] isotopologue was designated DUAL. Unlabeled [M + 0] sphingolipids were designated ^{12}C. The MRM extracted ion chromatogram peak areas of all four sphingolipid isotopologues and isotopomers were integrated (Analyst 1.4), converted to picomoles using the peak areas of the internal standards, and normalized to the mg of protein in the extracted sample.

Calculation of N-acyl sphingolipid isotopic enrichment

The presence of ^{13}C labeled N-acyl sphingolipids (tracer; DUAL, BASE, and FA species) together with unlabeled sphingolipids (tracee; ^{12}C isotopologue) allows the calculation of the isotopic enrichment (tracer / tracer + tracee) of a particular molecular species, such as C16:0 Cer. The approach taken was to quantitate ^{12}C, BASE, DUAL, and FA isotopologues and isotopomers (pmol per mg protein) and to calculate the enrichment of a particular N-acyl chain length as the number of labeled acyl chains divided by the total number of acyl chains:

$$(1 \times \text{BASE})+(2 \times \text{DUAL})+(1 \times \text{FA}) \,/\, (2 \times 12\text{C})+(2 \times \text{BASE})+(2 \times \text{DUAL})+(2 \times \text{FA})$$

Calculation of the rate of appearance of tracee using enrichments and measured N-acyl sphingolipid quantities

One method for the quantitation of metabolic flux is calculation of the rate of appearance of tracee (R_a) using measurements of the isotopic enrichment of metabolites over time (88). This approach was applied to N-acyl sphingolipids by plotting enrichment (see above) vs. time, and showed that (in both cell types) some sphingolipids, such as C16:0-Cer, achieved isotopic equilibrium (a plateau in enrichment) during the 6 hr [U-^{13}C]-palmitate treatment while others, such as C24:0- and C24:1-Cer, did not (Figure

39). Curve-fitting (Prism 4.0) was performed upon the enrichment plot data using the following formula (88):

$$E_t = E_p\left(1 - e^{-kt}\right)$$

in which E_t is the enrichment at time t, E_p is the plateau enrichment at isotopic equilibrium, and *k* is the metabolite pool's fractional turn-over rate per unit time.

Using the estimations of E_p and *k* together with the measured quantities of ^{12}C sphingolipids (Q; tracee pool size), the following equation (88) was used to calculate the rate of appearance (R_a) of tracee (unlabeled N-acyl sphingolipid):

$$R_a \text{ (tracee)} = k\ Q$$

Thin layer chromatography

TLC was performed as described previously (179). Neutral GSLs and acidic GSLs were dissolved in chloroform/methanol (2:1, v/v) separately and applied to silica gel-coated plates with glass backing (Merck, Darmstadt, Germany). The neutral GSL plate was developed with a solvent system of chloroform/methanol/water (65:35:8, v/v/v) and detected with orcinol reagent. The acidic GSLs plate was developed with a solvent system of chloroform/methanol/0.2% $CaCl_2$ (55:45:10, v/v/v) and detected with resorcinol reagent.

In vitro sphingomyelinase activity assay

The methods for nSMase assay and aSMase assay have been thoroughly described before (180) and the modified part is described below. Cells were collected in

the lysis buffer as described (180) plus protease inhibitor cocktail (Roche, Indianapolis, IN). For this experiment, instead of using radiolabeled SM as a substrate, fluorescent NBD-labeled SM (C6-NBD-SM) was used at 2 nmol per 100 μl reaction. Each reaction was performed in triplicate and stopped by adding 1.4 ml of HPLC solvent that was composed of 90% methanol and 10% aqueous phase (5 mM K_2HPO_4). The sample was centrifuged at 2500 rpm for 8 min and 1.2 ml of the supernatant was transferred to a glass HPLC sample tube. C6-NBD-SM and C6-NBD-Cer were diluted separately or together in the HPLC solvent as a standard. For each analysis 100 μl of sample was injected onto the HPLC column and the isocratic flow rate of the solvent was 2 ml / min. BCA protein assay (Pierce, Rockford, IL) was used to determine the protein concentrations.

In situ sphingomyelinase activity assay

NBD-C6-SM was dissolved in ethanol to make a 5 mM solution. Fatty acid free BSA was dissolved in PBS to make a 2 mM stock solution. The two solutions were mixed at 1:1 molar ratio and sonicated. Then the NBD-C6-SM/BSA complex was diluted to 5 μM working solution in complete cell culture medium and filter sterilized. Twenty-four hr before the experiment cells were seeded in 60 mm dishes in complete growth medium. The old medium was replaced with the medium containing NBD-C6-SM/BSA and the cells were incubated for 7 hr before they were collected for analysis.

4.4 Results

Sphingolipid de novo synthesis pathway

The *de novo* synthesis of sphingolipids begins with the condensation of serine and palmitoyl-CoA by SPT to form 3-keto-Sa which is reduced to Sa. This Sa may be acylated by a family of (dihydro)ceramide synthases (CerS) using different fatty acyl-

CoAs to form the corresponding DHCer subspecies (Figure 28). In mammals, six genes that encode CerS have been cloned (7, 9, 181, 182). Individual ceramide synthase isoforms show substrate preference for specific fatty acyl-CoA chain lengths, thus generating (dihydro)ceramides with distinct acyl chain lengths. For example, CerS1 shows a significant preference for stearoyl-CoA, whereas CerS5 and CerS6 preferentially catalyze the acylation of Sa with myristoyl- and palmitoyl-CoAs (8, 9). The DHCer are reduced to Cer by dihydroceramide reductase (DES) and both DHCer and Cer are converted to complex sphingolipids (SM, DHSM, CMH, DHCMH) by adding different moieties to the 1-hydroxyl oxygen atom.

Generation of a functional HEK293/SPTLC1/SPTLC2 stable cell line

Since SPT is the first enzyme of sphingolipid *de novo* biosynthesis it would be interesting to know the impact of increasing SPT activity on the pathway. To explore this issue a SPT over-expression cell model was constructed. The *SPTLC1* and *SPTLC2* cDNAs were cloned from human monocytes and inserted into pcDNA3.1NEO and pcDNA3.1ZEO separately. The expression plasmids were transfected separately or co-transfected into HEK293 cells. Antibiotic selection was used to generate cells stably expressing *SPTLC1* or *SPTLC2* or *SPTLC1/SPTLC2*. For convenience we call these transformants SPT1, SPT2 and SPT1/2 cells. Using quantitative real-time PCR analysis significant elevations of *SPTLC1* and/or *SPTLC2* mRNA were detected in these cell lines (data not shown). When microsomal fractions were isolated and resolved by SDS-PAGE followed by Western blotting using anti-SPT1 or anti-SPT2 antibodies, the protein

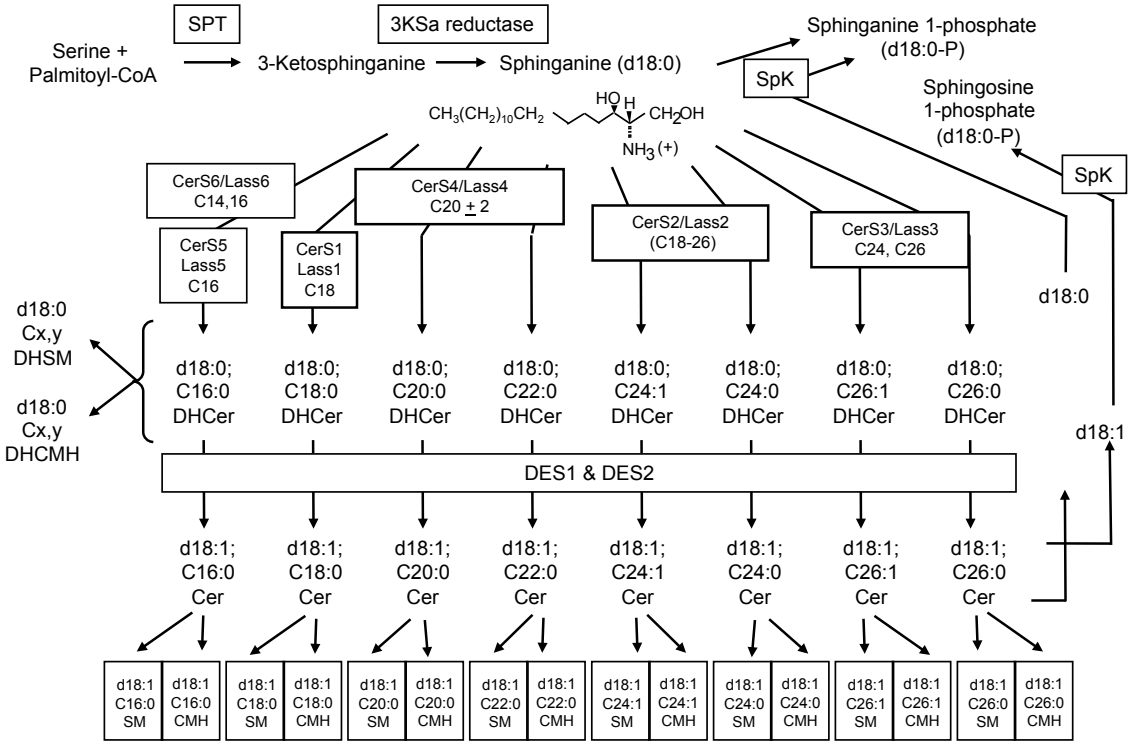

Figure 28. Diagram of the sphingolipid *de novo* biosynthesis pathway. d18:0 denotes sphingoid bases with an 18-carbon chain and 0 double bonds. C16:0 denotes an N-acyl chain with 16 carbons and 0 double bonds.

amounts of SPT1 and/or SPT2 increased significantly in the stable transfected cells compared with either wild type or empty vector-transfected HEK293 cells (Figure 29A).

The above results showed that over-expression of SPT1 and SPT2 was successful and then the next question was whether the over-expressed proteins were functional. Previous studies showed that SPT activity was mainly detected in the microsomal fraction (183). Microsome fractions were isolated from the same set of cells as those used for Western blotting for *in vitro* SPT enzyme activity assay. There was no significant change of SPT activity in SPT1 stably transfected cells while a 3.5-fold SPT activity increase was observed in SPT2 stably transfected cells, which is consistent with the previous finding that SPT2 is the catalytically active subunit of the SPT enzyme (163) (Figure 29A, *bar graph*). Co-expression of *SPTLC1* and *SPTLC2* caused SPT activity to increase 5-fold suggesting a cooperative effect between the two subunits (22) (Figure 29A, bar graph). The high SPT activity made the SPT1/2 stable cells a useful model in studying sphingolipid *de novo* synthesis and this cell model was used for our further studies. The sub-cellular localizations of the over-expressed SPT1 and SPT2 in SPT1/2 cells were examined using an anti-SPT1 or anti-SPT2 antibody. The fluorescence staining of SPT1 or SPT2 co-localizes with the staining of BiP protein, an endoplasmic reticulum (ER) marker (Figure 29B). This result is consistent with the previous finding that SPT activity is enriched in the microsomal fraction (169, 183) and that overexpressed Chinese hamster SPT1 localized in ER (22).

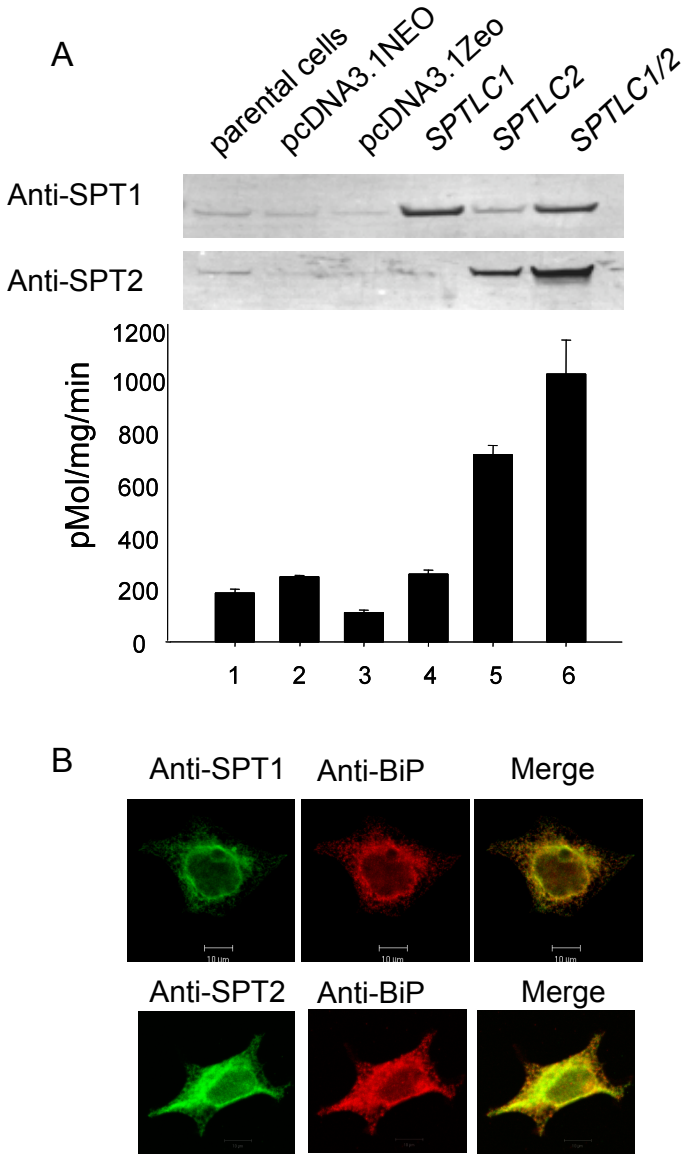

Figure 29. Characterization of *SPTLC* transfected cell lines. (A) Protein analysis and *in vitro* enzyme activity assay. 50 μg of microsomal membrane protein from untransfected HEK293 cells (Lane 1), cells tranfected with vector controls (pcDNA3.1NEO, lane 2 and pcDNA3.1ZEO lane 3), *SPTLC1* transfected cells (Lane 4), *SPTLC2* tranfected cells (Lane 5), or cells co-transfected with *SPTLC1* and *SPTLC2* (lane 6) was applied for Western blotting (upper two panels) and SPT enzyme activity assay (lower bar graph). The nitrocellulose membrane was probed with either anti-SPT1 antibodies (upper panel) or anti-SPT2 antibodies (lower panel). The enzyme activity assay data represent the mean of three independent experiments. (B) Co-localization of SPT1 or SPT2 with Bip, an ER marker protein. SPT1/2 cells grown on glass coverslips were immunostained with rabbit anti-SPT1 antibody or rabbit anti-SPT2 antibody and mouse anti-Bip antibody followed by AlexaFluor 488 (green) anti-rabbit and AlexaFluor 568 (red) anti-mouse secondary antibody. Bar: 10 μm.

An in situ SPT activity assay was developed using stable isotope-labeling and LC-ESI-MS/MS

To explore changes in the *de novo* biosynthesis of sphingolipids an *in situ* assay using stable isotope labeling was developed. Uniformly [^{13}C]-labeled palmitate was used as a tracer to follow the synthesis of sphingolipids. After conversion to [^{13}C]-labeled palmitoyl CoA it can be condensed with serine by SPT to form sphingoid bases (3-ketoSa and Sa), and [^{13}C]-labeled fatty acyl-CoA can also be incorporated at the N-acyl position by CerS to form DHCer. Using MS/MS the sphingoid base labeling and N-acyl labeling can be distinguished. If an N-acyl sphingolipid molecule is labeled only on the sphingoid base moiety it was designated BASE. If it is labeled only on the N-acyl moiety it was designated FA. If it is labeled on both the sphingoid base and N-acyl moieties it was designated DUAL. Unlabeled N-acyl sphingolipids were designated ^{12}C. Only the DUAL and BASE isotopologues are considered to have originated by *de novo* biosynthesis because labeling of the sphingoid base unambiguously indicates that they were biosynthesized from serine and [^{13}C]-labeled palmitoyl-CoA by SPT. The FA isotopomer may not represent *de novo* biosynthesis because the unlabeled sphingoid base may have come from catabolism of pre-existing N-acyl sphingolipids. The details of this assay are described in the Experimental Procedures section.

The dynamics of de novo synthesis of sphingoid bases in SPT1/2 cells versus HEK293 cells

Both SPT1/2 cells and HEK293 cells were treated with [U-^{13}C]-palmitate and collected every hour for 6 hours. Then lipids were extracted from the cell pellets, resolved by a reverse phase C18 column and analyzed by LC-ESI-MS/MS. The first intermediate of the sphingolipid *de novo* biosynthesis pathway is 3-ketosphinganine produced by SPT but in HEK293 cells [^{13}C]-Sa was below the detection limit (~ 0.1

pmol/mg protein) and the amount of [^{12}C]-Sa was constant (~ 10 pmol/mg protein) for the first 6 h after [U-^{13}C]-palmitate treatment (Figure 30A, upper left). This observation suggests that the endogenous Sa (~ 10 pmol/mg protein) is derived from catabolism of pre-existing N-acyl sphingolipids and since the downstream products of the *de novo* biosynthesis pathway in HEK293 cells were [^{13}C]-labeled (Figure 32), the absence of [^{13}C]-labeling of Sa indicates that the *de novo* biosynthesized Sa was quickly converted to DHCer. Both [^{13}C]-labeled and unlabeled [^{12}C]-Sa rapidly accumulated in SPT1/2 cells, reached a maximum (and similar) quantity after 2 h of [U-^{13}C]-palmitate treatment, and then decreased and stabilized in quantity (Figure 30A, upper left). The above observation suggests that SPT enzyme activity significantly increased in SPT1/2 cells and the elevated Sa quantity exceeded the capacity of CerS in those cells.

To determine whether the SPT substrate pool of palmitoyl-CoA was the same in HEK293 cells and SPT1/2 cells the quantities of labeled and unlabeled palmitoyl-CoA ([^{13}C]-Pal-CoA and [^{12}C]-Pal-CoA, respectively) were measured. Both cell types were treated with either 0.1 mM [U-^{13}C]-palmitate / BSA complex or with BSA alone (control) for 2 h and then collected for lipid extraction. The lipid samples were analyzed by LC-ESI-MS/MS as described previously. As shown in Figure 31B, in both types of cells, [U-^{13}C]-palmitate treatment did not affect the endogenous pool of [^{12}C]-Pal-CoA (black bar vs. white bar, $p > 0.1$) and the quantity of [^{13}C]-Pal-CoA was about 3-fold that of [^{12}C]-Pal CoA after 2 h of treatment. Without [U-^{13}C]-palmitate treatment, the quantity of [^{12}C]-Pal-CoA was higher in HEK293 cells than in SPT1/2 cells; with [U-^{13}C]-palmitate treatment, the quantities of both [^{12}C]-Pal-CoA and [^{13}C]-Pal-CoA were slightly but significantly higher in HEK293 cells than in SPT1/2 cells. This observation suggests that the amount of palmitoyl-CoA substrate for SPT (and the isotopic enrichment of this pool) was not the origin of the greater quantities of sphingolipids in SPT1/2 cells compared to HEK293 cells. The higher amount of [^{13}C]-Sa in SPT1/2 cells as observed above indicates higher

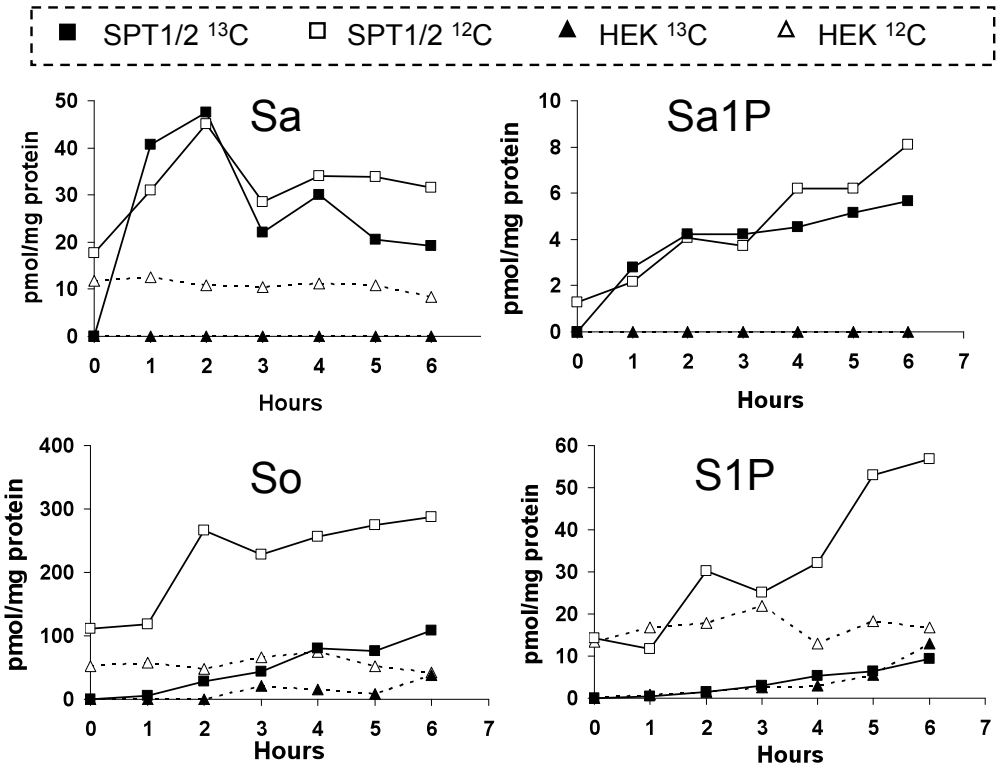

Figure 30. The dynamic changes of sphingoid bases in HEK293 cells and SPT1/2 cells after [U-^{13}C]-palmitate treatment. Lipids were extracted from replicate dishes (N = 4) of HEK293 cells and SPT1/2 cells treated with 0.1 mM [U-^{13}C]-palmitate for different periods of time (0 to 6 hr) followed by analysis of sphingoid bases by LC-ESI-MS/MS. Both labeled ([^{13}C]) and unlabeled ([^{12}C]) sphinganine (Sa, *upper left*), sphinganine-1-phosphate (Sa-1-P, *upper right*), sphingosine (So, *lower left*) and sphingosine-1-phosphate (So-1-P, *lower right*) were measured.

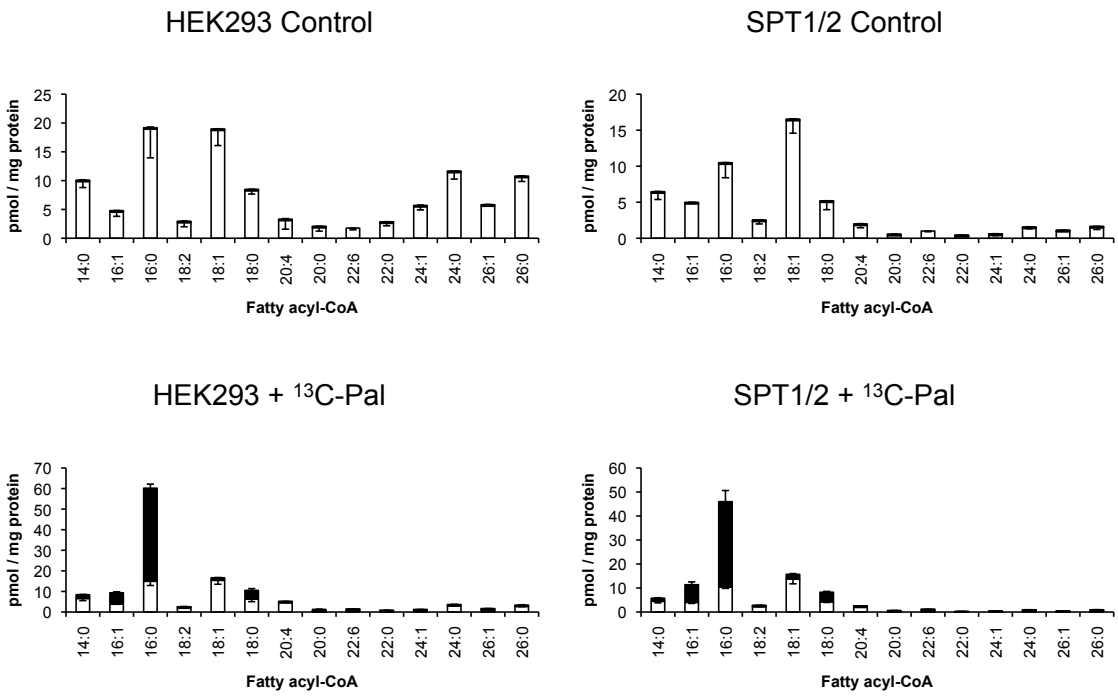

Figure 31. Quantitation of fatty acyl-CoAs in HEK293 and SPT1/2 cells. HEK293 cells and SPT1/2 cells were treated *(lower panels*) or not (*upper panels*) with 0.1 mM [U-^{13}C]-palmitate for 2 h. Lipid were extracted from the cells and analyzed by LC-ESI-MS/MS as described in Experimental Procedures. Both labeled (*black bars*) and unlabeled fatty acyl-CoAs (*white bars*) were quantitated. The mean and SD of four replicate Petri dishes is shown.

SPT activity. The lower amount of Pal-CoA in SPT1/2 cells is possibly caused by more vigorous consumption of this substrate by elevated SPT activity in SPT1/2 cells.

Sa can be converted to either DHCer by CerS or to Sa-1-P by sphingosine kinase. The quantity of [^{13}C]-Sa-1-P significantly increased over 6 h in SPT1/2 cells but was not detectable in HEK293 cells (Figure 30A, *upper right*). Another sphingoid base is So which in HEK293 cells was more abundant than Sa (50 pmol / mg protein vs. 10 pmol / mg protein). In HEK293 cells, no increase in [^{12}C]-So quantity was observed after [U-^{13}C]-palmitate treatment and [^{13}C]-So increased after 2 h of treatment (Figure 30A, *bottom left*). In SPT1/2 cells, during the 6 h of [U-^{13}C]-palmitate treatment, the quantity of [^{12}C]-So increased from 112 to 288 pmol / mg protein, consistently higher than the quantity of [^{13}C]-So, which increased from 0 to 109 pmol/ mg protein. Furthermore, there was no increase of either labeled or unlabeled So in SPT1/2 cells during the first hour of [U-^{13}C]-palmitate treatment. These observations are consistent with the fact that So is derived exclusively from the catabolism of CMH, SM or Cer and, unlike Sa, cannot be directly generated by *de novo* biosynthesis (184). A similar observation was made for the phosphorylated metabolite So-1-P (Figure 30A, *bottom right*). Thus, unlike [^{13}C]-Sa and [^{13}C]-Sa1P, [^{13}C]-So and [^{13}C]-S1P are affected much less by the over-expression of SPT and do not fully recapitulate the consequent increase in *de novo* biosynthesis.

The dynamics of de novo biosynthesis of complex sphingolipids in SPT1/2 cells versus HEK293 cells

To quantify *de novo* synthesized N-acyl sphingolipids, the sum of DUAL and BASE labeled isotopologues was used, which represents unambiguous *de novo* biosynthesis. The first N-acyl sphingolipid in the *de novo* biosynthesis pathway is DHCer, which is formed by the N-acylation of Sa by CerS. The quantity of [^{13}C]-DHCer in SPT1/2 cells rapidly increased to 600 pmol / mg protein during the first 2 h of [U-^{13}C]-

palmitate treatment, reached a maximum between 2 to 4 h, and then decreased to 415 pmol / mg protein (Figure 32A) at 6 h. In contrast, in HEK293 cells the quantity of [^{13}C]-DHCer increased slowly to 15 pmol / mg protein after 2 h of [U-^{13}C]-palmitate treatment and to 114 pmol / mg protein after 6 h (Figure 32A). Therefore, 2 h after treatment, the quantity of [^{13}C]-DHCer in SPT1/2 cells was 40-fold that of HEK293 cells. DHCer can be reduced to Cer or converted to 1-O-modified sphingolipids such as DHCMH and DHSM. Both DHCMH and DHSM quantities were significantly increased over 6 h in a similar pattern in SPT1/2 cells while the increase in HEK293 cells was much smaller (Figures 32B and 32C). The *de novo* biosynthesis of Cer showed a pattern similar to that of DHCer in HEK293 cells and SPT1/2 cells (Figure 32D). An increase in the quantity of [^{13}C]-CMH over 6 h was observed in both cell lines after [U-^{13}C]-palmitate treatment, but was more rapid in SPT1/2 cells (Figure 32E). SM originating from *de novo* biosynthesis also accumulated over 6 h in both cell lines, however, unlike other sphingolipids its quantity was lower in the SPT1/2 cells than that in HEK293 cells (Figure 32F).

In HEK293 cells, the quantities of *de novo* biosynthesized unsaturated sphingolipids are higher than the quantities of their corresponding dihydro-species, while the opposite was true in SPT1/2 cells if the DUAL and BASE isotopologues of DHCer and Cer (after 3 h of treatment) are added and compared in the two types of cells (Figure 32G). Together with the presence of [^{13}C]-Sa in SPT1/2 cells but not HEK293 cells (Figure 30) this result suggests that over-expression of SPT in SPT1/2 cells increases the flux of downstream molecules which exceed the capacities of downstream enzymes. For example, the [^{13}C]-Sa quantity exceeded the capacity of CerS and the [^{13}C]-DHCer quantity exceeded the capacity of DES.

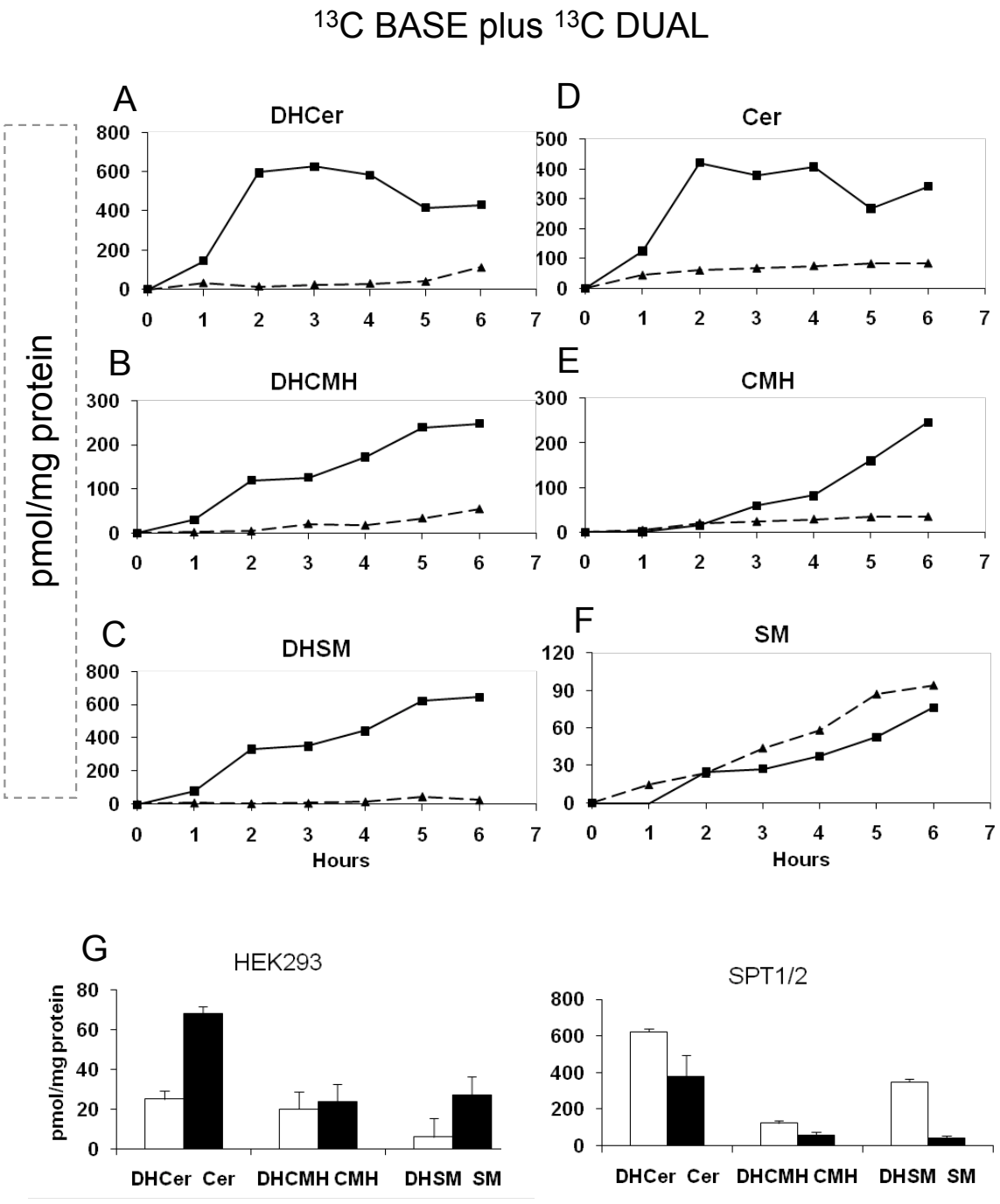

Figure 32. The dynamic changes of *de novo* synthesis of complex sphingolipids in HEK293 cells and SPT1/2 cells after [U-^{13}C]-palmitate treatment. HEK293 cells and SPT1/2 cells (N = 4 dishes) were treated with 0.1 mM [U-^{13}C]-palmitate for 0 to 6 h. Sphingolipid extractions from those cells were analyzed by LC-ESI-MS/MS for DHCer (A), DHCMH (B), DHSM (C), Cer (D), CMH (E) and SM (F). At each time the quantity shown for each complex sphingolipid is a sum of the total [^{13}C] dual labeled subspecies and the total [^{13}C] base labeled subspecies. (G) *De novo* biosynthesized dihydro-sphingolipids and their desaturated species are compared in HEK293 cells (left panel) and SPT1/2 cells (right panel).

The distribution of de novo synthesized sphingolipids with varying acyl-chain lengths in SPT1/2 cells versus HEK293 cells

Most sphingolipids are built upon So or Sa sphingoid bases and can have various lengths of fatty acyl-chains. Acyl chains designated C16:0, C18:0, C20:0, C22:0, C24:0, C24:1, C26:0 and C26:1 were observed to be the most common ones in HEK293 and SPT1/2 cells. These different subspecies of N-acyl sphingolipids are generated by acylation of Sa or So by different CerS isoforms which prefer certain chain lengths of fatty acyl-CoA substrates (7, 9, 181, 182). For example, CerS1 prefers stearoyl-CoA (C18:0-CoA) and CerS5/6 prefers palmitoyl-CoA (C16:0-CoA) (Figure 28). To compare the sphingolipid subspecies with varying N-acyl chain lengths the sum of DUAL and BASE isotopologue quantities was used. The majority of [^{13}C]-labeled subspecies of each N-acyl sphingolipid were increased in SPT1/2 cells, however, the quantity of [^{13}C]-SM decreased compared to HEK293 cells (Figure 33).

Among all the unambiguously *de novo* subspecies of DHCer, Cer, DHSM and SM, those with a C16:0 N-acyl chain (derived from palmitoyl-CoA) are the most abundant in both HEK293 cells and SPT1/2 cells (Figure 33). The subspecies distribution of unambiguously *de novo* DHCMH and CMH is different from that of other N-acyl sphingolipids and the C16:0 species is not the dominant species in either cell line (Figure 33, *middle panels*). Among all the sphingolipid subspecies (except those of SM) the fold increase of molecules with C18:0 acyl chains is the highest in SPT1/2 cells (Figure 33). For example, C18:0 DHCer, Cer and CMH quantities in SPT1/2 cells are 47-fold, 11-fold and 8-fold greater, respectively, than those species in HEK293 cells; C18:0 DHCMH and DHSM were below the detection limit in HEK293 cells but became quite abundant in SPT1/2 cells.

^{13}C BASE plus ^{13}C DUAL

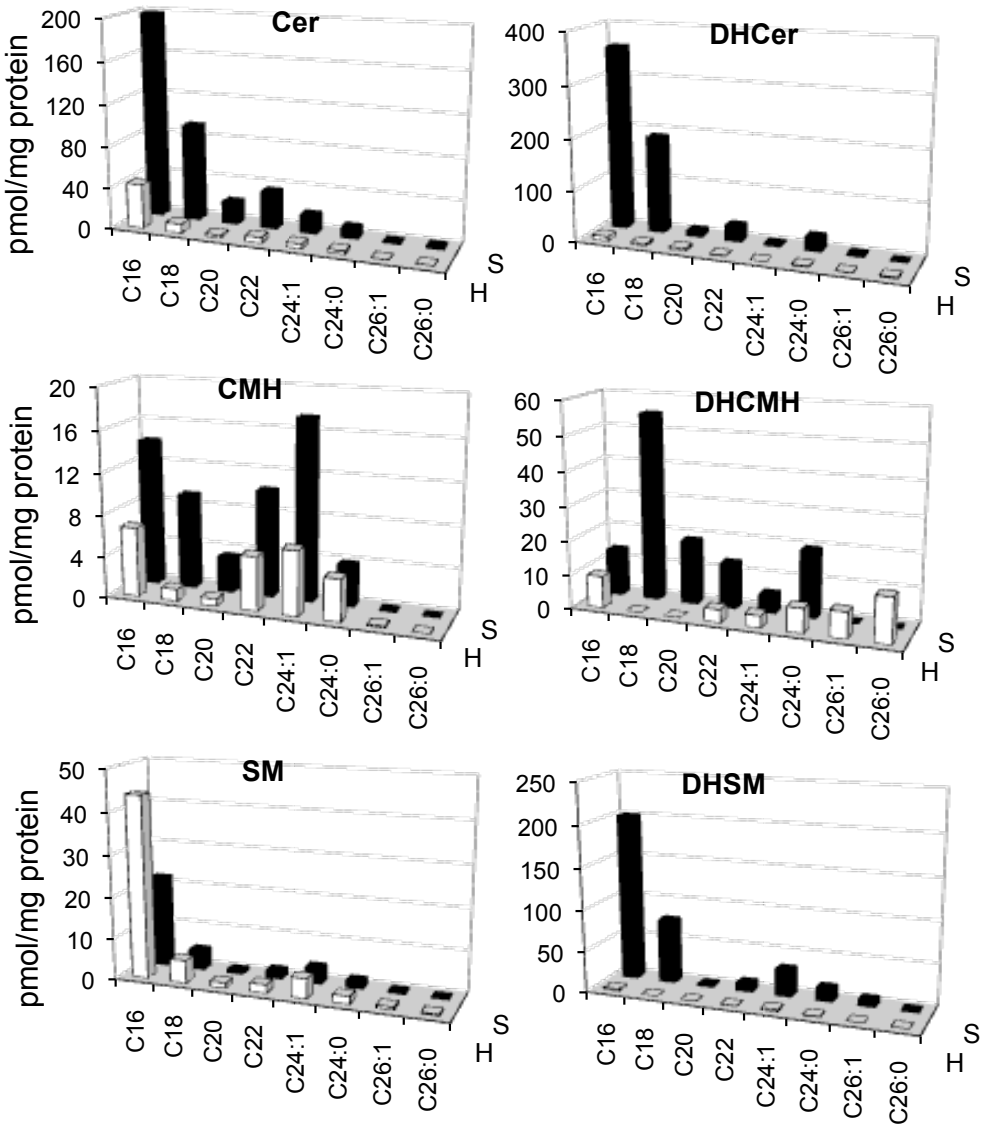

Figure 33. Comparison of sphingolipids with different N-acyl chains in HEK293 cells and SPT1/2 cells. Sphingolipids were extracted from HEK293 cells (*white bars*) and SPT1/2 cells (*black bars*) treated with 0.1 mM [U-^{13}C]-Pal for 3 h and analyzed by LC-ESI-MS/MS. The value shown is the sum of [^{13}C] dual labeled and [^{13}C] base labeled molecules, which represents unambiguous *de novo* biosynthesis. The x-axis is the N-acyl chain length. Data are shown as means (N = 4) of replicate Petri dishes.

When the proportionate change of each Cer subspecies was compared in HEK293 and SPT1/2 cells, the biggest difference was seen for C18:0 Cer (Figure 34). Using the sum of DUAL and BASE isotopologue quantities to represent unambiguously *de novo* biosynthesized sphingolipids, the proportion of C18 Cer was 13% in HEK293 cells and 24% in SPT1/2 cells (Figure 34A). To exclude the possibility of an effect arising from substrate pool difference, C18:0-CoA was quantitated by LC-ESI-MS/MS. As previously observed for C16:0-CoA, the quantity of [^{12}C]-18:0-CoA was greater in HEK293 cells in the absence of [U-^{13}C]-palmitate treatment, and the quantities of [^{13}C]-C18:0-CoA and [^{12}C]-C18:0-CoA were greater in HEK293 cells with [U-^{13}C]-palmitate treatment (Figure 31), showing that differences in the stearoyl-CoA pool are not the origin of increased C18:0 N-acyl sphingolipids in SPT1/2 cells. Furthermore, when the [^{12}C]-Cer subspecies were measured without adding [U-^{13}C]-palmitate, the proportion of C18 Cer still had the highest increase, from 8% in HEK293 cells to 18% in SPT1/2 cells (Figure 34B).

These results suggest that elevation of sphingolipid subspecies quantities is not a simple recapitulation of SPT over-expression, and they also confirm that [U-^{13}C]-palmitate treatment *per se* is not causing the increase in C18:0 Cer proportion. The disproportionate increase in C18 Cer might indicate a connection between SPT and ceramide synthase 1 (CerS1). Consistent with this hypothesis, CerS1 mRNA was found to be elevated in SPT1/2 cells by quantitative PCR analysis (Y. Liu, personal communication) suggesting that elevation of SPT activity may affect the gene expression of downstream enzymes.

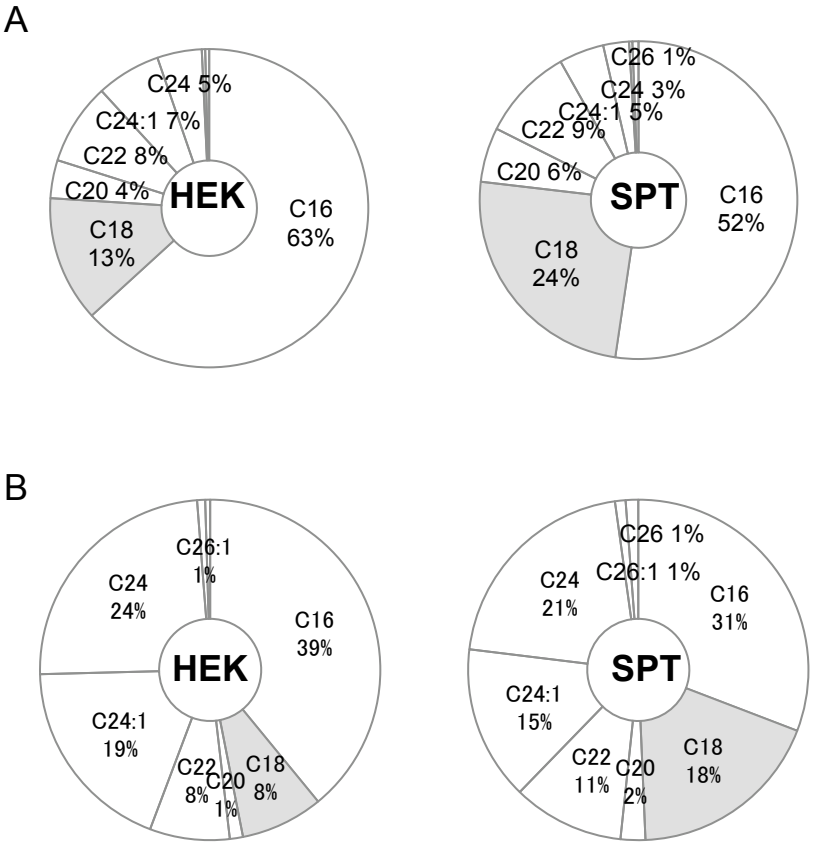

Figure 34. Distribution of ceramide subspecies with various N-acyl chain lengths. (A) The proportion of DUAL and BASE Cer isotopologues was determined in HEK293 cells (*left*) and SPT1/2 cells (*right*) after 3 h of [U-^{13}C]-palmitate labeling. (B) The proportions of ^{12}C Cer isotopologues were determined in HEK293 cells (*left*) and SPT1/2 cells (*right*) without adding [U-^{13}C]-palmitate.

Sphingolipid differences between SPT1/2 cells vs. HEK293 cells without [U-^{13}C]-palmitate treatment

The above data showed increased *de novo* biosynthesis of sphingolipids in SPT1/2 cells versus HEK293 cells with [U-^{13}C]-palmitate treatment. To explore the effect of SPT over-expression in the steady state, HEK293 and SPT1/2 cells without any [U-^{13}C]-palmitate treatment were analyzed (Figures 34B and 35). Quantitation of all the unlabeled sphingolipids species and comparison of HEK293 and SPT1/2 cells showed that a significant increase was seen in Cer (4.5-fold), DHCer (3.7-fold) and DHCMH (1.8-fold), no change was seen in CMH and a decrease was seen in SM (1.9-fold) and DHSM (1.6-fold). Compared with the data for *de novo* biosynthesized sphingolipids (Figures 32 and 33), the elevation of sphingolipid quantities in the steady state of SPT1/2 cells was lower, but showed similar trends including lower quantities of DHSM compared to HEK293 cells.

To examine more complex glycosphingolipids (GSL) in the two cell lines thin layer chromatography (TLC) was used. TLC of neutral GSL showed significant increases in the quantities of CMH, LacCer and Gb_3 in SPT1/2 cells (Figure 36, *left panel*). Elevation of quantities of acidic GSL, such as GM_3, GM_2, and GM_1, were also observed for SPT1/2 cells by TLC (Figure 36, *right panel*). These results show that over-expression of SPT increases not only the immediate products of *de novo* sphingolipid biosynthesis, but also more distant metabolites along the pathway.

The proportions of N-acyl sphingolipids were compared in HEK293 cells and SPT1/2 cells. From the most abundant to the least abundant species for HEK293 cells they are SM (65%), CMH (17%), DHSM (8%), Cer (6%), DHCer (3%) and DHCMH (1%) while the abundances for SPT1/2 cells are SM (34%), Cer (28%), CMH (20%), DHCer (11%), DHSM (5%), DHCMH (2%). The proportion of Cer and DHCer dramatically

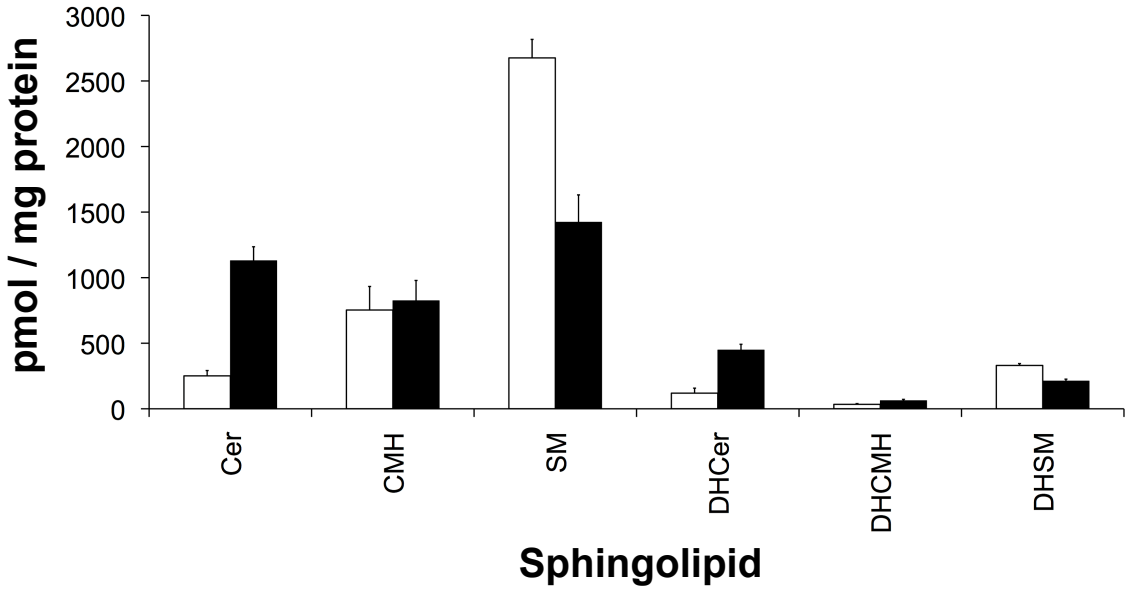

Figure 35. Comparison of sphingolipid totals in HEK293 cells and SPT1/2 cell extracts without [^{13}C]-palmitate treatment. The total quantity of each N-acyl sphingolipid was determined by LC-ESI-MS/MS analysis in replicate dishes (N = 4) of HEK293 cells (*white bars*) and SPT1/2 cells (*black bars*) without [U-^{13}C]-palmitate treatment.

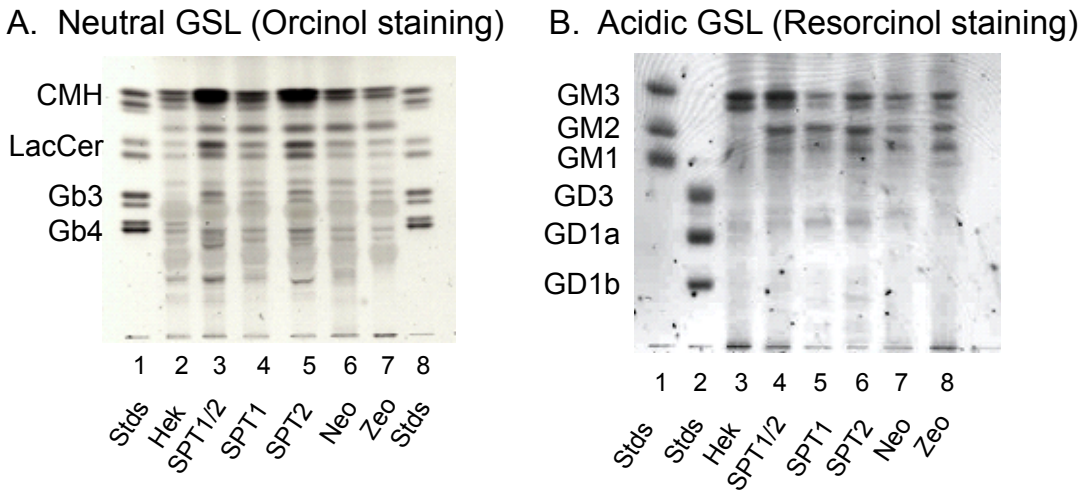

Figure 36. Comparison of glycosphingolipids (GSL) in HEK293 and SPT1/2 cells by TLC. Samples from HEK293 cells and SPT1/2 cells were applied to two TLC plates. (A) Neutral GSL visualized by Orcinol staining. Lanes 1 and 8 are standards and from lanes 2 to lane 7 are HEK293 cells, SPT1/2 cells, SPT1 cells, SPT2 cells, cells stably transfected with empty vectors NEO or ZEO, respectively. (B) Acidic GSL visualized by Resorcinol staining. Lane 1 and 2 are standards and from 3 to 8 are in the same order as in (A), above.

increased in SPT1/2 cells while that of SM decreased. Therefore, elevation of SPT activity not only increased the absolute quantities of sphingolipids (Figure 32) but also changed the relative proportions of the sphingolipid classes.

Comparison of the rate of appearance of ceramide in HEK293 and SPT1/2 cells

To determine whether SPT over-expression increased the rate of appearance (R_a) of N-acyl sphingolipids, a previously described approach (88) that uses quantitation of stable isotope labeled metabolites and mathematical modeling to estimate R_a for tracee molecules (e.g. ^{12}C C16:0-Cer) was used. This was applied to Cer in [U-^{13}C]-palmitate treated HEK293 and SPT1/2 cells by 1) measuring the quantities of ^{12}C, BASE, DUAL and FA isotopologues and isotopomers of Cer, 2) calculating the enrichment of each N-acyl species at 1 hr intervals from 0 to 6 hr, 3) plotting enrichment vs. time for each Cer N-acyl species, 4) using curve-fitting to estimate the plateau isotopic enrichment (E_p) and fractional turn-over rate (*k*) of each analyte (Figure 37), and, 5) using the estimates of E_p, *k*, and the measured quantities of ^{12}C Cer (Q, tracee quantity) to calculate the rate of appearance (R_a) of ^{12}C Cer in pmol / mg protein * hr.

Values of R_a, *k*, and E_p for Cer in HEK293 and SPT1/2 cells are shown in Table II. For example, C16:0-Cer E_p was 0.548 ± 0.005 in HEK293 cells and 0.441 ± 0.01 in SPT1/2 cells; C16:0-Cer *k* was 1.15 ± 0.05 in HEK293 cells and 0.87 ± 0.08 in SPT1/2 cells (mean and SEM, N = 4). The physiological interpretation of E_p is that the C16:0-Cer enrichment at isotopic equilibrium is 54.8% and 44.1% in HEK293 and SPT1/2 cells, while the value of *k* implies that the C16:0-Cer pool is completely turned over 1.15 and 0.87 times per hour in HEK293 and SPT1/2 cells, respectively. The C16:0-Cer E_p ($p < 0.0001$) and *k* ($p < 0.03$) values were significantly different between the two cell types, as well as the C26:0-Cer E_p ($p < 0.01$) values and the C18:0-, C22:0-, and C26:0-Cer *k* ($p < 0.005$, 0.0008, and 0.02) values.

Table II. Estimated values of tracee rate of appearance (R_a), fractional turn-over rate (*k*), and plateau isotopic enrichment (E_p) for ceramide in HEK293 cells (HEK) and SPT1/2 cells (SPT). The units of R_a are pmol per mg protein * hr, ceramide N-acyl chain lengths are designated x:y, where x = number of carbon atoms and y = number of double bonds, the correlation coefficient (R^2) is shown for curve fits, and estimation of a value for $E_p > 1$ is designated NA. Significant ($p < 0.05$) differences in E_p and *k* are designated *, and tracee (^{12}C) quantities at 0 hr (Q) were used to calculate R_a from *k*. Data are derived from 4 replicate Petri dishes of each cell type.

		16:0	18:0	20:0	22:0	24:1	24:0	26:1	26:0
R_a	**HEK**	111.6	24.1	4.0	12.3	13.9	4.0	0.6	0.6
R_a	**SPT**	303.2	110.0	15.6	21.2	39.9	NA	3.0	1.4
k	**HEK**	1.15 *	1.24 *	1.30	0.652 *	0.296	0.066	0.296	0.479 *
k	**SPT**	0.874 *	0.528 *	0.590	0.178 *	0.241	NA	0.267	0.106 *
E_p	**HEK**	0.548 *	0.314	0.355	0.287	0.151	0.423	0.219	0.251 *
E_p	**SPT**	0.441 *	0.321	0.345	0.421	0.125	NA	0.140	0.381 *
R^2	**HEK**	0.999	0.989	0.952	0.995	0.988	0.987	0.842	0.951
R^2	**SPT**	0.992	0.992	0.988	0.982	0.994	NA	0.949	0.994

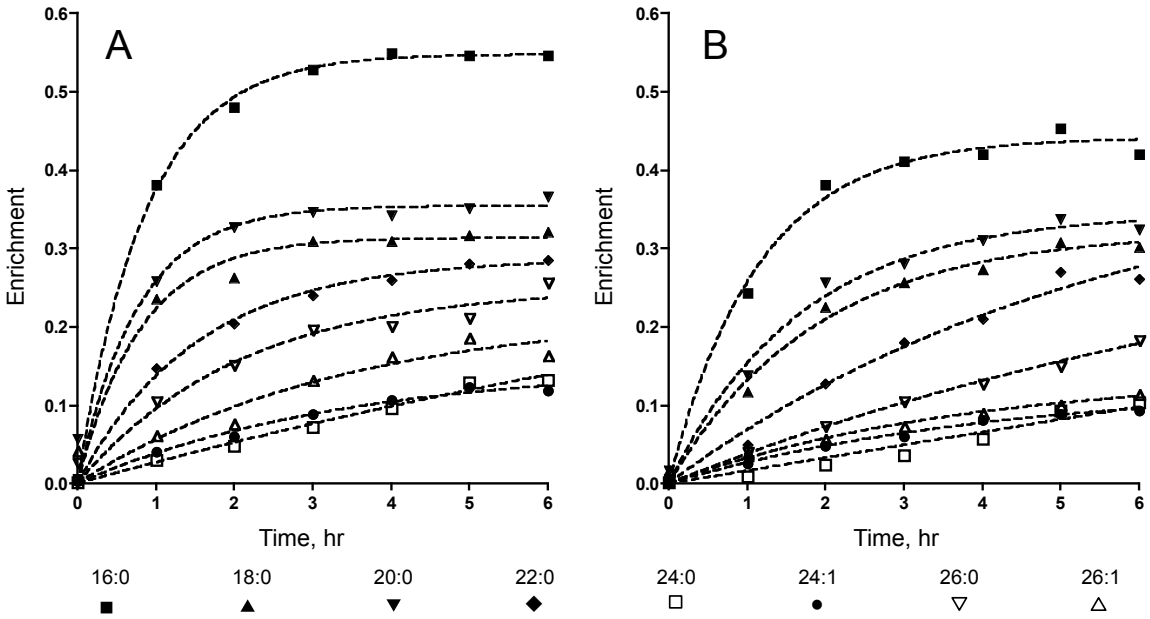

Figure 37. Isotopic enrichment of ceramide in HEK293 (A) and SPT1/2 cells (B). The isotopic enrichment of each ceramide N-acyl chain length was calculated using data for the unlabeled, fatty acid labeled, dual labeled, and base labeled isotopologues and isotopomers as the number of labeled acyl chains divided by the total number of acyl chains. This was plotted vs. time, and the data was curve-fit using Prism 4.0. This estimated the plateau isotopic enrichment (E_p) and the fractional turn-over rate of the pool (*k*) of each ceramide species. The physiological interpretation of E_p is the plateau isotopic enrichment of the analyte, and of *k* is the fractional turn-over rate per hr of the ceramide pool. Data are shown as the mean of replicate Petri dishes (N = 4).

To calculate whether SPT over-expression increased the rate of appearance of tracee (R_a), Cer *k* values were multiplied by the ^{12}C isotopologue Cer quantities at 0 hr. For example, C16:0-Cer R_a was 112 and 303 pmol / mg protein hr in HEK293 and SPT1/2 cells, respectively, an increase of 2.7-fold associated with SPT stable over-expression. The fold increase of R_a values in SPT1/2 cells for other chain lengths of Cer (where R^2 during curve-fitting was > 0.9) was similar to C16:0-Cer [i.e. C22:0-Cer (1.7-fold), C24:1-Cer (2.9-fold), and C26:0-Cer (2.5-fold)]. However, some increases of R_a values in SPT1/2 cells were higher [i.e. C18:0-Cer (4.6-fold) and C20:0-Cer (3.9-fold)], consistent with the increased proportion of C18:0-Cer and the induction of CerS1 mRNA transcription in the SPT1/2 cell line.

Comparison of the rate of appearance and de novo biosynthesis of non-ceramide N-acyl sphingolipids in HEK293 and SPT1/2 cells

Using the above approach to estimate the rate of appearance of d18:1 N-acyl sphingolipids other than Cer (e.g. SM, CMH) either resulted in values of $E_p > 1$ (isotopic enrichment of > 100%, which is not possible), or low values (< 0.90) of R^2. Neither of these Cer metabolites appeared to reach isotopic equilibrium in 6 hr in either cell type. Regarding dihydrosphingolipids, in HEK293 cells only C24:0-DHCer resulted in satisfactory modeling ($R^2 > 0.9$, $E_p < 1$), whereas in SPT1/2 cells all DHSM, many DHCer, and half of the DHCMH molecular species resulted in satisfactory modeling. The R_a of C24:0-DHCer was 1.4 pmol per mg protein hr in HEK293 cells and 11 pmol per mg protein hr in SPT1/2 cells, which is a 7.9-fold increase.

Identification of novel sphingolipid species in SPT1/2 cells

SPT prefers serine as its substrate, however, sphingoid bases generated from alanine and glycine were also recently identified in mammalian cells (73) and they are

quite abundant in cells treated with fumonisin B_1, a (dihydro)ceramide synthase inhibitor (73). Condensation of alanine and palmitoyl-CoA by SPT generates 1-deoxysphinganine (1-deoxy-Sa) and its N-acylated form is 1-deoxy dihydroceramide (1-deoxy-DHCer). Condensation of glycine and palmitoyl-CoA produces 1-desoxymethyl sphinganine (1-desoxyMe-Sa) and its N-acylated form is 1-desoxyMe-DHCer. After incubating the cells with [U-^{13}C]-palmitate for 36 h both 1-deoxy-Sa and 1-desoxyMe-Sa were dramatically elevated in SPT1/2 cells compared with HEK293 cells (Figure 38). Among the [^{13}C]-labeled sphingoid bases 1-deoxy-Sa was lower than So but significantly higher than other species, while in HEK293 cells, 1-deoxy-Sa was at the same level as all other sphingoid bases except for So (Figure 40). Both the BASE and DUAL isotopologue quantities showed that 1-deoxy-DHCer and 1-desoxyMe-DHCer were significantly increased in SPT1/2 cells compared with HEK293 cells (Figure 40B). It was remarkable that the amount of 1-deoxy-DHCer was comparable to that of Cer in SPT1/2 cells. Unlike Cer for which the C16 acyl-chain was the most abundant subspecies, the C18 subspecies was the most abundant for 1-deoxy-DHCer and 1-desoxyMe-DHCer.

Analysis of the decrease of SM in SPT1/2 cells

An interesting observation regarding SPT1/2 cells is that unlike other sphingolipids species the amount of SM decreases. Is this because sphingomyelinase activity is higher in SPT1/2 cells? To address this question, the activities of both acidic and neutral SMase (aSMase and nSMase, respectively) were measured *in vitro* for HEK293 and SPT1/2 cells. Fluorescent NBD-labeled SM was used as a substrate and after reaction the samples were analyzed by HPLC. As shown in Figure 39, the aSMase activity is slightly but significantly higher in SPT1/2 cells than in HEK293 cells, whereas activity of nSMase in SPT1/2 cells is about 50% of that in HEK293 cells (Figure 39). The *in vitro* assay suggests that SM degradation might be faster in HEK293 cells.

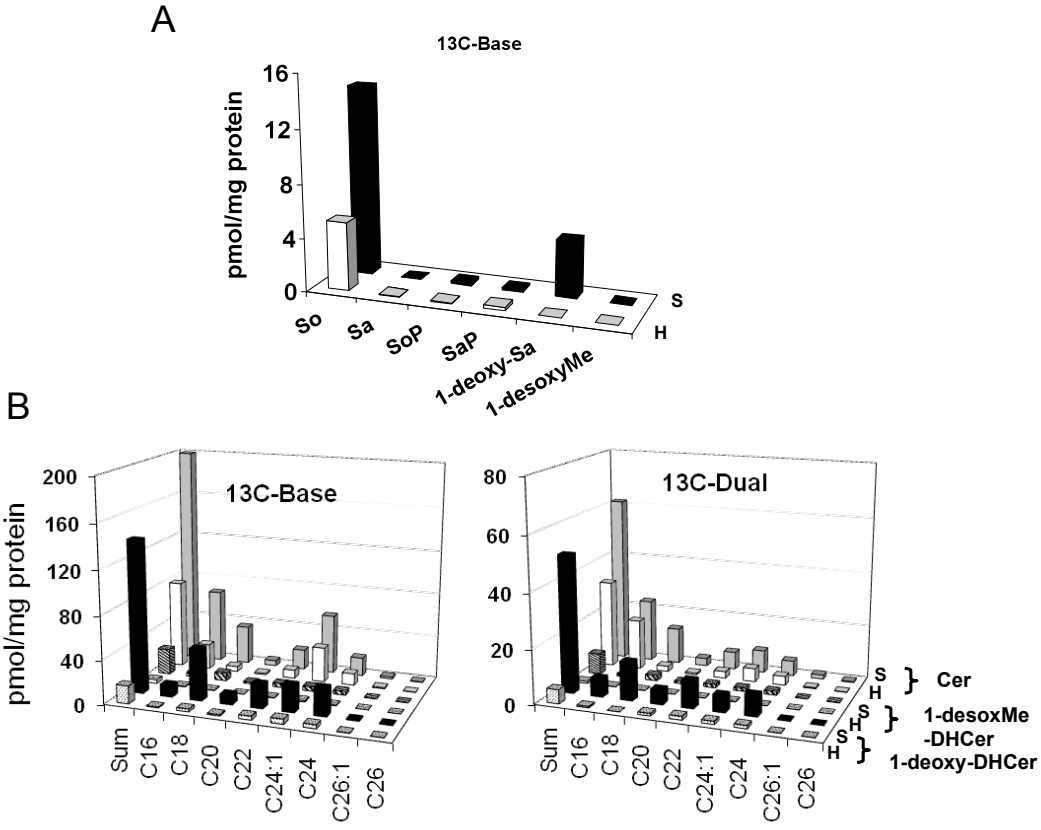

Figure 38. Quantitation of novel sphingolipid species after [U-^{13}C]-palmitate labeling. (A) [^{13}C]-labeled sphingoid bases were measured in replicate dishes (N = 3) of HEK293 cells (H, white bars) and SPT1/2 cells (S, black bars). (B) Quantitation of N-acylated forms of the novel sphingoid bases. 1-deoxy-DHCer and 1-desoxMe-DHCer with different N-acyl chain lengths were measured in HEK293 cells and SPT1/2 cells and compared with Cer. From the left to the right are the sum of all subspecies, C16, C18, C20, C22, C24:1, C24, C26:1, C26. The left panel is [^{13}C]-base labeling and the right panel is [^{13}C]-dual labeling.

SM degradation was also measured *in situ* by incubating HEK293 cells and SPT1/2 cells with C6-NBD-SM for 7 hours and then the cells were collected and extracted in methanol at 37° C for one hour. After centrifugation, the supernatant was analyzed by HPLC and NBD fluorescence was measured, and normalized by protein amount, from which the percentage of SM signal over total NBD signal was calculated. The remaining SM was 8% in HEK293 cells and 15% in SPT1/2 cells after 7 hours of NBD-SM treatment, which suggests that SM degradation is faster in HEK293 cells than in SPT1/2 cells, and accounts for the decrease in SM. The most likely explanation is that DHSM is produced instead (Figures 32C and 33).

The composition of CMH in HEK293 cells and SPT1/2 cells

Ceramide monohexose (CMH) is a collective term for glucosylceramide (GlcCer) and galactosylceramide (GalCer). The former is synthesized in the Golgi and the latter in the ER. GlcCer and GalCer were quantitated in HEK293 and SPT1/2 cells via a specialized HPLC-ESI-MS/MS method designed to resolve these isobaric analytes (74). As shown in Figure 40, HEK293 and SPT1/2 cells synthesize GlcCer ranging in N-acyl chain lengths from C16 to C26 and varying in saturation (C24:0 – C24:1, C26:0 – C26:1). In HEK293 cells, the amount of C16 GlcCer is 100 ± 20 pmol/mg of protein, which is not significantly different from the C24:1 quantity (70 ± 20 pmol/mg of protein), or the C24:0 quantity (70 ± 20 pmol/mg of protein) (Figure 40, *upper left*). However in SPT1/2 cells, the amount of C16:0 GlcCer is 250 ± 50 pmol/mg of protein, which is more than twice the quantity of C24:0 and of C24:1 (Figure 40, *lower left*). In HEK293 cells, the amount of C16:0 GlcCer is 100 ± 20 pmol/mg of protein, which is more than 5 times higher than the amount of C18:0 GlcCer, 15 ± 3 pmol/mg of protein (Figure 40, *upper left*); in contrast for SPT1/2 cells, C16:0 and C18:0 differ by only 50%, 250 ± 50 pmol/mg

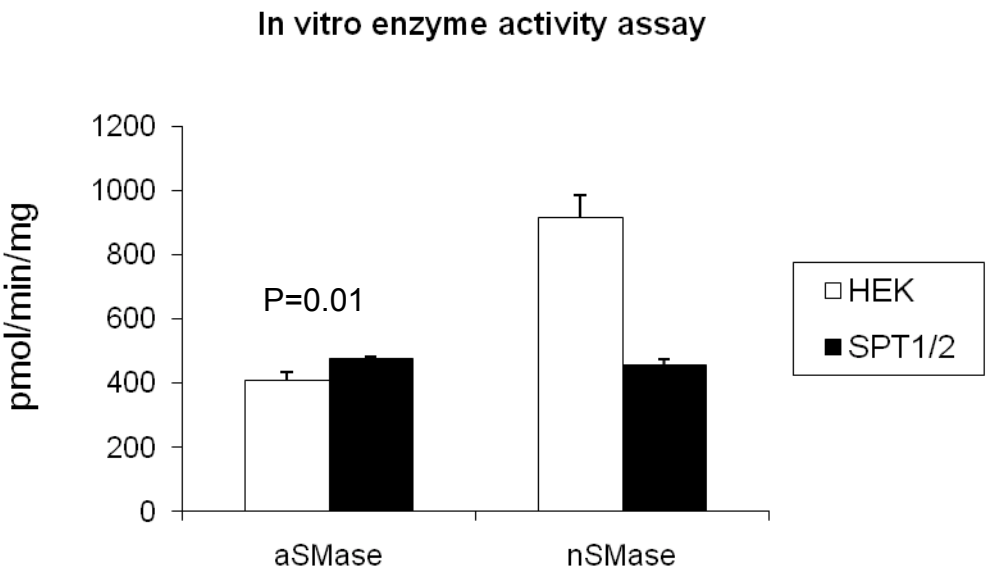

Figure 39. Comparison of neutral and acidic sphingomyelinase activities in HEK293 cells and SPT1/2 cells. Enzyme activities of acidic sphingomyelinase (aSMase) and neutral sphingomyelinase (nSMase) were measured *in vitro* using a C6-NBD-SM substrate and HPLC analysis as described in Experimental Procedures. The data shown represent the mean of two independent experiments.

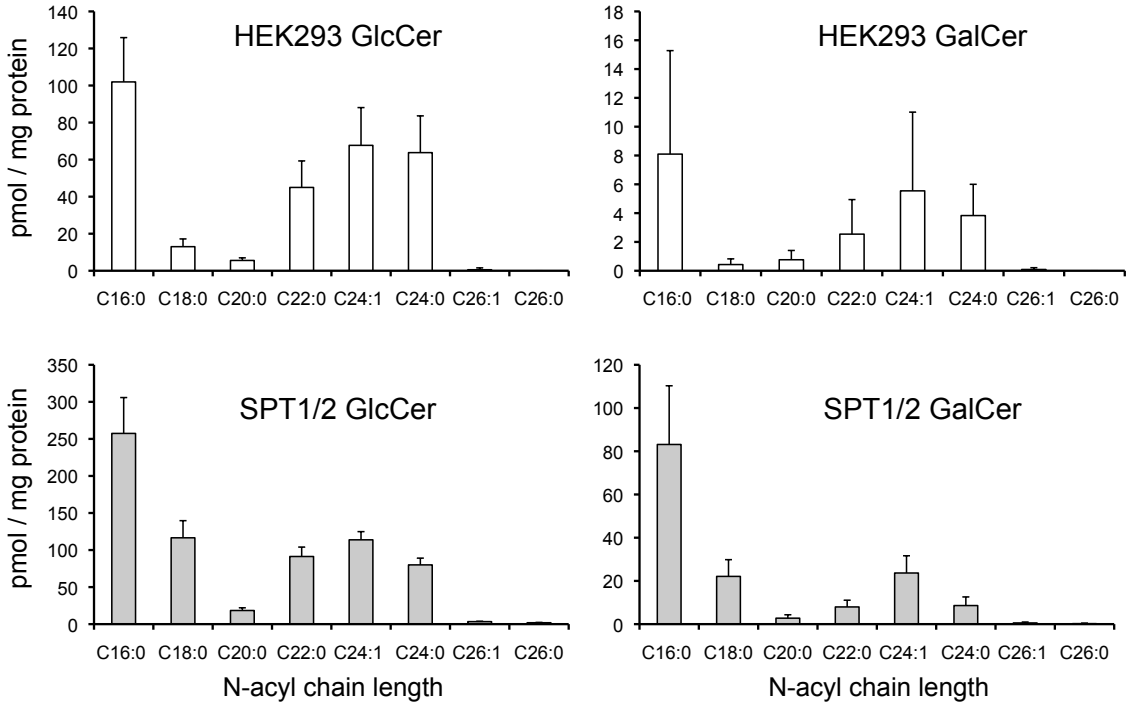

Figure 40. Comparison of ceramide monohexose quantities in HEK293 (*upper panels*) and SPT1/2 (*lower panels*) cells. The quantities of glucosylceramide (GlcCer, *left panels*) and galactosylceramide (GalCer, *right panels*) of varying N-acyl chain lengths (16, 18, etc) were determined by LC-ESI MS/MS analysis as described in Experimental Procedures. Data are the mean ± SD of triplicate Petri dishes.

of protein and 120 ± 20 pmol/mg of protein (Figure 40, *lower left*). Thus it can be seen that SPT1/2 cells not only have an increase in total GlcCer quantity, but also a significant change in the distribution of chain lengths.

GalCer was 3 to 10-fold elevated in quantity in SPT1/2 cells compared to HEK293 cells (Figure 40, *right panels*). The most abundant N-acyl chain lengths of GalCer in SPT1/2 cells are C16:0, C18:0, and C24:1, while they were C16:0, C24:0, and C24:1 in HEK293 cells.

4.5 Discussion

Sphingolipid biosynthesis is one of the most complex metabolic processes of mammalian cells, involving hundreds of enzymes, multiple pathways for intra- and extra-cellular trafficking and transport, and dozens (at least) of associated biological functions that are regulated by the types and amounts of sphingolipids that are present. Previously over-expression of SPT has been demonstrated in mammalian cells (22, 163), however, its molecular impact on the *de novo* biosynthesis pathway has not been fully investigated. To study the impact of SPT on the sphingolipid *de novo* biosynthesis pathway, a biological model that has elevated SPT activity and an analysis method that can quantify various sphingolipids are required. Furthermore, stable isotope labeling is needed for differentiating sphingolipid *de novo* synthesis and turnover pathways. We generated a cell line stably expressing SPT1 and SPT2 and with 5-fold higher SPT activity than its parental cell line. The [U-^{13}C]-palmitate stable isotope labeling of cultured cells followed by LC-ESI-MS/MS analysis allowed the quantitation of *de novo* biosynthesis of sphingolipids. The downstream metabolites were measured at each step along the pathway. Not only the total amount of each sphingolipid molecule but also each subspecies with different fatty acyl chain lengths were quantitated. The results revealed the molecular consequences of increasing SPT activity: while the majority of

the downstream metabolite quantities increased, unexpectedly the quantity of SM decreased; sphingolipid subspecies with various fatty acyl chain lengths increased disproportionally and C18 subspecies showed the greatest increase.

In the past, studies have focused on So, Cer and their derivatives which were potent bioactive lipids involved in cell growth, death, senescence, adhesion, migration, inflammation, angiogenesis and intracellular trafficking (160, 185, 186). Recently, Sa, dihydro-sphingolipids and their derivatives, which are typically of low quantity in cells, have been found to be bioactive (187-189). *De novo* synthesized Sa and dihydro-sphingolipids have been found to play a role in 4HPR induced cancer cell apoptosis (187). *De novo* generated Sa and DHCer were increased in tumor cells by celecoxib, a COX-2 specific inhibitor, and were suggested to contribute to the anti-proliferative effects of celecoxib (189). L-*threo*-Sa, a synthetic stereoisomer, induces autophagy in solid tumor cells (188). So far few studies have analyzed those species, furthermore, traditional TLC cannot differentiate dihydro-species from the cogent desaturated species, which might have masked the effect of dihydro-species in some studies.

Some novel *de novo* synthesized sphingolipids, such as 1-deoxy-Sa and its acylated form, were found to be quite abundant in [U-^{13}C]-palmitate treated SPT1/2 cells. This suggests that the sphingolipid *de novo* biosynthesis pathway may be more complicated than is currently appreciated. New molecular species could be generated under certain circumstances and some previous sphingolipid studies using various stress stimuli might need to be carefully re-interpreted. Recently it was reported that 1-deoxy-Sa (spisulosine) isolated from the Arctic surf clam *(Spisula polynyma)* induced prostate tumor cell death by increasing the *de novo* synthesis of Cer (190). If mammalian SPT can generate 1-deoxy-Sa under certain circumstances it would be interesting to know what are the targets of the novel compound.

The *de novo* biosynthesis of all other sphingolipids increased in SPT1/2 cells while that of SM decreased. This is apparently not caused by elevated degradation of SM (Figure 38) but rather by an impairment of SM biosynthesis, i.e. the accumulation of DHSM (which uses the same SM synthase) in SPT1/2 cells (Figures 32C and 33), since the ratio of DHCer to Cer is much higher (3:2) in SPT1/2 cells than in HEK293 cells (1:4). It is likely that DHCer competes with Cer for the synthesis of SM.

In addition, the data showed that the quantities of not only GlcCer but also GalCer increased in SPT1/2 cells. Since the amount of GalCer was 3 to 8-fold lower in HEK293 cells the ratio of GalCer / GlcCer is higher in SPT1/2 cells than it is in HEK293 cells (Figure 40). It is known that GalCer is synthesized in the lumen of the ER (159) and GlcCer in the Golgi (191). The increased quantity of Cer in the ER compartment of SPT1/2 cells may provide more substrate for GalCer synthase, which resides in the same compartment, while the production of GlcCer could be limited by the ER to Golgi transportation of Cer. Thus any promoters of sphingolipid *de novo* biosynthesis, such as agents that can up-regulate SPT and CerS, may cause the same effect. Whether this effect plays a role in the biological consequences of those stimuli needs to be further characterized.

It was interesting that SPT1/2 cells did not show any cytotoxicity despite the remarkable accumulation of various sphingolipid molecules (e.g. Cer) that have been reported to have these effects. Furthermore, no toxicity was observed in SPT1/2 cells even after 36 hours of [U-^{13}C]-palmitate treatment. The mechanism(s) by which the SPT1/2 cells are able to tolerate these large quantities of sphingolipids is presently unknown and the subject of future investigation.

CHAPTER 5

STABLE ISOTOPE LABELING OF FATTY ACYL-COAS VIA *DE NOVO* FATTY ACID BIOSYNTHESIS USING [1-^{13}C]-ACETATE TREATMENT OF RAW264.7 CELLS[4]

5.1 Summary

Fatty acyl-CoAs are intermediates in the metabolism of many lipids. In cultured mammalian cells, two sources of the palmitoyl moiety of palmitoyl-CoA include palmitate from *de novo* fatty acid biosynthesis (via fatty acid synthase [FAS] activity) and palmitate from the extracellular medium (via fatty acid uptake and acyl-CoA synthetase [ACSL] activity). The separate contributions of extracellular palmitate and *de novo* fatty acid biosynthesis to the palmitoyl-CoA pool were quantitated in RAW264.7 mouse macrophage-like cells by treatment with [U-^{13}C]-palmitate and [1-^{13}C]-acetate, respectively, followed by liquid chromatography-electrospray ionization-tandem mass spectrometric analysis of palmitoyl-CoA. Exogenous [U-^{13}C]-palmitate (0.1 mM) labeled ~ 60% of the palmitoyl-CoA after 6 hr, and [1-^{13}C]-acetate (0.1 mM) labeling indicated by mass isotopomer distribution analysis (MIDA) and isotopomer spectral analysis (ISA) that ~ 60% of palmitoyl-CoA was newly biosynthesized after 6 hr. The similar labeling of palmitoyl-CoA by these different biosynthetic inputs indicates a rapid turn-over rate for palmitoyl-CoA from both *de novo* fatty acid biosynthesis and uptake of exogenous fatty acid in RAW264.7 cells with and without Kdo_2-Lipid A treatment. In this chapter, the specific contribution of the author was all work shown, except the culturing and treatment of cells.

[4] This chapter is in preparation for publication; the authors are Haynes, C., Wang, E., Kelly, S., Sullards, M., and Merrill, A.

5.2 Introduction

Fatty acyl-CoAs are intermediates in the metabolism of many lipids. In cultured mammalian cells, two sources of the palmitoyl moiety of palmitoyl-CoA include palmitate from *de novo* fatty acid biosynthesis (via fatty acid synthase [FAS] activity (119)) and palmitate from the extracellular medium (via fatty acid uptake (192) and acyl-CoA synthetase [ACSL] activity (28, 35)). The *de novo* biosynthesis of C_{16} palmitate by FAS uses one C_2 unit from acetyl-CoA and seven C_2 units from malonyl-CoA (8 $C_2 \rightarrow C_{16}$); acetyl-CoA is converted to malonyl-CoA by acetyl-CoA carboxylase (ACC). Thus, all 16 of the carbon atoms of *de novo* biosynthesized palmitate are derived from acetyl-CoA, and treatment of cultured cells with [1-^{13}C]-acetate can add 0 to 8 atoms of ^{13}C to each newly biosynthesized palmitate molecule. Extracellular palmitate, in contrast, is present as a component of the serum required to grow most mammalian cell lines, and represents *in vivo* bloodstream fatty acids that are derived from adipose and dietary sources. Several mechanisms of fatty acid uptake by cultured cells have been demonstrated (25, 26, 192). Intracellular palmitate may be bound to carrier proteins such as fatty acid binding protein (37) or activated to palmitoyl-CoA by fatty acyl-CoA synthetases (27, 29-32). Thus, treatment of cultured cells with [U-^{13}C]-palmitate can add 0 or 16 atoms of ^{13}C to each newly biosynthesized palmitoyl-CoA molecule.

Treatment of cultured cells with stable isotope-labeled substrates of these two metabolic pathways (i.e. acetate and palmitate) followed by fatty acyl-CoA extraction and palmitoyl-CoA quantitation by liquid chromatography-electrospray ionization-tandem mass spectrometry (LC-ESI-MS/MS) (3) is a powerful technique that can distinguish the contributions of *de novo* palmitate biosynthesis and extracellular palmitate to palmitoyl-CoA. A triple quadrupole tandem mass spectrometer was used in multiple reaction monitoring (MRM) mode, with precursor and product ion pairs corresponding to mass isotopologues of palmitoyl-CoA with labeled palmitoyl moieties. In this way, [M + 0]

unlabeled and [M + 16] [U-^{13}C]-palmitate labeled palmitoyl-CoA were easily distinguished, as well as [M + 1] through [M + 4] palmitoyl-CoA isotopologues labeled by [1-^{13}C]-acetate.

To determine the contribution of extracellular palmitate to cellular palmitoyl-CoA, RAW264.7 mouse macrophage-like cells were treated with 0.1 mM [U-^{13}C]-palmitate (in a 1:1 molar complex with fatty-acid free albumin) for times ranging from 0.5 to 24 hr. Quantitation of [M + 0] (unlabeled) and [M + 16] (labeled) palmitoyl-CoA isotopomers indicated rapid and robust utilization of the [U-^{13}C]-palmitate (presumably via ACSL); more than 50% of the total palmitoyl-CoA was [M + 16] within 3 hr.

Treatment of cultured cells with palmitate has been reported to cause changes in their metabolism (98, 193) and gene transcription (99, 194). In order to avoid these unintended consequences of palmitate treatment, and to explore the quantitative contribution of *de novo* fatty acid biosynthesis to palmitoyl-CoA, an alternative method for stable isotope-labeling of fatty acyl-CoAs was employed. RAW264.7 cells were treated with 0, 0.1, or 1.0 mM [1-^{13}C]-acetate for 6, 12, and 24 hr. In this experimental approach, the stable isotope-labeled acetate is taken up by cells, activated to form labeled acetyl-CoA, carboxylated to form labeled malonyl-CoA, and then fatty acid synthase (FAS) polymerizes one acetyl-CoA and seven malonyl-CoA molecules into one palmitate molecule.

A particular isotopic enrichment of acetate in the biosynthetic precursor pool for FAS generates a unique “fingerprint”, or mass isotopologue distribution (MID), in the structure-specific product ion of newly biosynthesized palmitoyl-CoA. A second factor to consider is that mixing of pre-existing and newly biosynthesized palmitoyl-CoA will cause the MID observed by LC-ESI-MS/MS to be the sum of an unlabeled and a labeled distribution. Two approaches can be used for the analysis of MID’s to estimate the isotopic enrichment of the biosynthetic precursor pool, and the fraction of newly

biosynthesized molecules; mass isotopomer distribution analysis (MIDA), as described by Hellerstein and Neese (14), and isotopomer spectral analysis (ISA), as described by Kelleher and Masterson (15).

To determine the quantitative contribution of *de novo* palmitate biosynthesis to palmitoyl-CoA, RAW264.7 mouse macrophage-like cells were treated with 0, 0.1, and 1.0 mM [1-^{13}C]-acetate for 6, 12, and 24 hr. Quantitation of [M + 0] through [M + 4] palmitoyl-CoA followed by both MIDA and ISA analysis indicated robust utilization of this metabolic precursor after 6 hr; 60% of the total palmitoyl-CoA was determined to have been newly biosynthesized after treatment with both concentrations of [1-^{13}C]-acetate. In addition, the higher concentration of labeled acetate increased the isotopic enrichment of the FAS precursor pool from ~ 4% to ~ 6%.

The similar extent of palmitoyl-CoA labeling (~ 60%) by both 0.1 mM [U-^{13}C]-palmitate and 0.1 mM [1-^{13}C]-acetate indicates a rapid turn-over rate for cellular palmitoyl-CoA, and also suggests future investigations. For example, the relative contributions of extracellular palmitate and *de novo* fatty acid biosynthesis to palmitoyl-CoA could be determined if both palmitate and acetate were simultaneously present in cell media.

5.3 Experimental procedures

Materials

Fatty acyl-CoA standards with purity ≥ 99% were provided by Avanti Polar Lipids, Inc. (Alabaster, AL). Methanol and chloroform (EMD, Darmstadt, Germany) were HPLC grade. Triethylamine was from Sigma-Aldrich (St. Louis, MO). Both [U-^{13}C]-palmitate and [1-^{13}C]-acetate with purity ≥ 98% were from Cambridge Isotope Laboratories (Cambridge, MA).

Cell culture and treatment with stable isotope-labeled substrates

RAW264.7 mouse macrophages were cultured in DMEM + 10% FCS at 37°C, 95% relative humidity and 5% CO_2. Media included 0.1 mM [U-^{13}C]-palmitate: fatty-acid free BSA (in a 1:1 molar ratio) or [1-^{13}C]-acetate (0, 0.1, and 1 mM) as indicated. Cells were collected after 0.5, 1, 2, 4, 8, 12, and 24 hr ([U-^{13}C]-palmitate experiment) or after 6, 12, and 24 hr (1.0 mM [1-^{13}C]-acetate experiment).

Extraction of fatty acyl-CoAs

For the experiment with 1.0 mM [1-^{13}C]-acetate at 12 and 24 hr, fatty acyl-CoAs were extracted and analyzed as previously described (151).

For all other experiments, RAW264.7 cells were rinsed twice with ~ 5 ml each of 4°C PBS in their culture dishes, scraped up in ~ 2 ml of 4°C PBS using a rubber policeman, centrifuged in a bench-top unit at a low speed, and the PBS was aspirated. Methanol containing 1 mM EDTA (0.5 ml) and internal standards (10 μl of a 2:1 methanol/chloroform (v/v) solution containing a total of 100 pmol each pentadecanoyl-CoA [C15:0-CoA] and pentacosanoyl-CoA [C25:0-CoA]) were added to the cell pellet, followed by 3 water-bath sonications for 15 sec each. Chloroform (0.25 ml) was added to each pellet followed by 1 water-bath sonication for 15 sec. After heating for 30 min at 50°C in a dry block, chloroform (0.25 ml) was added and the mixture vortexed for 30 sec. Water was added and the mixture vortexed for 30 sec. Centrifugation at 2500 rpm for 5 min separated the mixture into upper (aqueous) and lower (organic) layers with a protein disc interface. The upper layer (~550 μL) was removed with a Pasteur pipet, and analyzed by HPLC-ESI-MS/MS.

Quantitation of fatty acyl-CoAs by LC-ESI-MS/MS

Resolution of fatty acyl-CoA species used a modification of the reverse-phase chromatographic method of Sun (93), et al. and multiple reaction monitoring (MRM) MS/MS detection. Briefly, solvent A was 85:15 water / acetonitrile (v/v) containing 0.05% triethylamine (TEA), and solvent B was 10:90 water / acetonitrile (v/v) containing 0.05% TEA. The flow rate was 200 μL per min and the column was a Waters XTerra MS C18 2.1 x 30 mm (2.5 μm particles) with a 2.1 x 10 mm guard. The pump program of Sun et al. was changed for this (smaller) column to retain the same number of column volumes at each step of the (shorter) program.

Each palmitoyl-CoA MRM pair consisted of a $(M + H)^+$ precursor ion and a product ion generated by a 507.0 Da neutral loss, a fragmentation of fatty acyl-CoAs which has been previously reported[4]. Each palmitoyl-CoA isotopomer had its own MRM pair; for example, the [M + 0] isotopomer MRM pair was *m/z* 1006.4 → 499.4, the [M + 1] MRM pair was *m/z* 1007.4 → 500.4, etc. Quantitation was achieved by comparison of palmitoyl-CoA isotopomer peak areas to the peak area for the pentacosanoyl-CoA (C15:0-CoA) internal standard (100 pmol) added at the beginning of cellular extraction.

Calculation of palmitoyl-CoA isotopic enrichment after [U-^{13}C]-palmitate treatment

The isotopic enrichment of the palmitoyl-CoA was calculated as follows:

$$\left[M+16\right] \div \left\{\left[M+0\right]+\left[M+16\right]\right\}$$

Eq. 2

Where [M + 16] and [M + 0] indicate the extracted ion chromatogram peak areas for the MRM pairs 1022.4 → 515.4 and 1006.4 → 499.4, respectively.

Mass isotopomer distribution analysis (MIDA) of [1-^{13}C]-acetate labeling

Table III. **Table of p-values for the palmitoyl-CoA product ion.**

Isotopologue	[M + 0]	[M + 1]	[M + 2]	[M + 3]	[M + 4]	[M + 5]
Exact *m/z*	499.357	500.357	501.357	502.357	503.357	504.357
p = 0.000	0.6893	0.2222	0.0709	0.0149	0.0024	0.0003
0.001	0.6838	0.2259	0.0721	0.0154	0.0025	0.0003
0.002	0.6783	0.2296	0.0733	0.0158	0.0026	0.0003
0.003	0.6729	0.2333	0.0745	0.0162	0.0027	0.0004
0.004	0.6675	0.2368	0.0757	0.0167	0.0028	0.0004
0.005	0.6622	0.2403	0.0770	0.0172	0.0029	0.0004
0.006	0.6569	0.2438	0.0782	0.0176	0.0030	0.0004
0.007	0.6516	0.2472	0.0795	0.0181	0.0031	0.0004
0.008	0.6464	0.2505	0.0808	0.0186	0.0032	0.0004
0.009	0.6412	0.2538	0.0821	0.0190	0.0033	0.0005
0.01	0.6360	0.2570	0.0835	0.0195	0.0034	0.0005

For each [M + n] isotopologue, n refers to the mass shift relative to the monoisotopic product ion.

Table IV. **Table of molar fractions for the palmitoyl-CoA product ion.**

Molar fraction	[M + 0] / $\sum_{x=0}^{3}[M+x]$	[M + 1] / $\sum_{x=0}^{3}[M+x]$	[M + 2] / $\sum_{x=0}^{3}[M+x]$	[M + 3] / $\sum_{x=0}^{3}[M+x]$
p = 0.000	0.6912	0.2228	0.0711	0.0150
0.001	0.6857	0.2266	0.0723	0.0154
0.002	0.6804	0.2303	0.0735	0.0158
0.003	0.6750	0.2340	0.0747	0.0163
0.004	0.6697	0.2376	0.0760	0.0168
0.005	0.6644	0.2412	0.0772	0.0172
0.006	0.6592	0.2446	0.0785	0.0177
0.007	0.6540	0.2481	0.0798	0.0182
0.008	0.6488	0.2514	0.0811	0.0186
0.009	0.6437	0.2547	0.0824	0.0191
0.01	0.6386	0.2580	0.0838	0.0196

Each molar fraction is the quotient of a particular isotopologue and the sum of all measured isotopologues.

Table V. Table of molar excesses for the palmitoyl-CoA product ion.

Excess isotopologue	E[M + 1]	E[M + 2]	E[M + 3]
p = 0.000	0.0000	0.0000	0.0000
0.001	0.0038	0.0012	0.0004
0.002	0.0075	0.0024	0.0009
0.003	0.0112	0.0036	0.0013
0.004	0.0148	0.0049	0.0018
0.005	0.0184	0.0061	0.0023
0.006	0.0219	0.0074	0.0027
0.007	0.0253	0.0087	0.0032
0.008	0.0287	0.0100	0.0037
0.009	0.0320	0.0114	0.0042
0.01	0.0352	0.0127	0.0046

Each E[M + n] is the change in the abundance of the nth isotopologue as p increases.

Table VI. Table of ratios of molar excesses for the palmitoyl-CoA product ion.

Ratio of excess isotopologue	E[M + 1] / $\sum_{x=1}^{3} E[M+x]$	E[M + 2] / $\sum_{x=1}^{3} E[M+x]$	E[M + 3] / $\sum_{x=1}^{3} E[M+x]$
p = 0.001	0.6999	0.2190	0.0811
0.002	0.6966	0.2215	0.0819
0.003	0.6933	0.2241	0.0826
0.004	0.6899	0.2266	0.0834
0.005	0.6866	0.2292	0.0842
0.006	0.6833	0.2317	0.0851
0.007	0.6800	0.2341	0.0859
0.008	0.6767	0.2366	0.0867
0.009	0.6734	0.2391	0.0875
0.01	0.6701	0.2415	0.0884

Each ratio of excess is a quotient of the excess for that isotopologue divided by the sum of all measured excesses.

The analytical workflow of MIDA (14) is summarized below. First, the molecular formula of the palmitoyl-CoA product ion ($C_{37}H_{66}N_7O_{17}P_3S$) was used to calculate (software courtesy of Dr. Richard Neese) a table of p-values (Table III). This software used information about the natural isotopic abundances of different elements and the input molecular formula to calculate the abundances of palmitoyl-CoA product ion isotopologues, beginning with [M + 0] and ending with isotopologues having a fractional abundance of less than 1 x 10^{-8} (only [M + 0] through [M + 5] are shown in Table III). The first row of p-values is the MID of the palmitoyl-CoA product ion when p = 0; this is the un-enriched or "natural" MID of the product ion. Subsequent rows show the palmitoyl-CoA product ion MID with increasing values of p, up to a user-specified value of p (only p up to 0.01, or 1%, is shown in Table III). It should be emphasized that any given row of p-values indicates the MID that would be observed if 100% of the palmitoyl-CoA was newly biosynthesized.

Mass isotopomer distribution analysis (MIDA) of [1-^{13}C]-acetate labeling

The analytical workflow of MIDA (14) is summarized below. First, the molecular formula of the palmitoyl-CoA product ion ($C_{37}H_{66}N_7O_{17}P_3S$) was used to calculate (software courtesy of Dr. Richard Neese) a table of p-values (Table III). This software uses information about the natural isotopic abundances of different elements and the input molecular formula to calculate the abundances of palmitoyl-CoA product ion isotopologues, beginning with [M + 0] and ending with isotopologues having a fractional abundance of less than 1 x 10^{-8} (only [M + 0] through [M + 5] are shown in Table III). The first row of p-values is the MID of the palmitoyl-CoA product ion when p = 0; this is the un-enriched or "natural" MID of the product ion. Subsequent rows show the palmitoyl-CoA product ion MID with increasing values of p, up to a user-specified value of p (only p up to 0.01, or 1%, is shown in Table III). It should be emphasized that any given row of

p-values indicates the MID that would be observed if 100% of the palmitoyl-CoA measured by LC-ESI-MS/MS had been newly biosynthesized during the treatment time from a biosynthetic precursor pool of acetyl-CoA with stable isotope enrichment p.

Second, Table III was used to generate a table of molar fractions (Table IV). Each entry in Table IV is a fraction:

$$[M+x] \div \{[M+0]+[M+1]+[M+2]+[M+3]\}$$

Eq. 3

which relates the abundance of isotopologue [M + x] to the sum of the abundances of the first four isotopologues . This is essentially a normalization operation that converts the comprehensive isotopologue frequencies (p-values) into frequencies that reflect the limited ability of the LC-ESI-MS/MS analysis to quantitate every possible labeled isotopologue; in the experiments described here the [M + 3] isotopologue was the highest labeled mass that was above the limit of quantitation on the instrument used. Thus, each row in the table of molar fractions (Table IV) represents the normalized abundances of the MID at a given value of p and a given experimental sensitivity.

Third, Table IV was used to generate a table of molar excesses (Table V). The first row (where p = 0) of the table of molar fractions (Table IV) is subtracted from each subsequent row to calculate the excesses of each labeled isotopologue at different values of p. Thus, each row in the table of molar excesses represents the changing frequency of isotopologues as a function of p (again assuming that 100% of the palmitoyl-CoA had been biosynthesized during the 6 hr of treatment with [1-^{13}C]-acetate). In MIDA nomenclature these molar excess values are A_x*, the asymptotic value that is approached by each isotopomer at a given value of p as the fraction of newly biosynthesized palmitoyl-CoA approaches 100%.

Fourth, Table V was used to generate the table of ratios of molar excesses (Table VI). Each value in Table VI is a fraction:

$$E[M+x] \div \{E[M+0] + E[M+1] + E[M+2] + E[M+3]\}$$

Eq. 4

that represents the normalized excess [M + x] isotopologue as a function of p. This is the key calculation of MIDA. Ratios of molar excesses are used because they are independent of the fraction of newly synthesized palmitoyl-CoA; in other words ratios of molar excesses are not influenced by a mixture of pre-existing and newly-biosynthesized polymers (palmitoyl-CoA in this case). The mathematical proof of this independence has been previously described by Hellerstein and Neese (14).

Fifth, Table VI was used to generate a plot of ratios of molar excesses vs. p for [M + 1] through [M + 3] (Figure 41). This plot shows theoretical relationships between ratios of molar excesses and p, and so the actual values of p during these experiments were easily estimated by calculating the observed ratios of molar excesses for the [M + 1] through [M + 3] isotopologues and using the linear regressions shown in Figure 41 to calculate p.

Sixth, the table of molar excesses (Table V) was used to generate a plot of molar excesses (A_x*) vs. p for the [M + 1] through [M + 3] isotopologues (Figure 42). On this plot, each curve represents the asymptotic (maximum) molar excess for that isotopologue as a function of p. Using the actual values of p estimated as shown in Figure 1 for [M + 1] through [M + 3], the linear regressions shown in Figure 42 were used to calculate the A_x*-value of that isotopologue if 100% of the palmitoyl-CoA had been newly biosynthesized. Finally, the observed molar excesses of [M + 1] through [M + 3] were divided by the cogent derived A_x*-value, resulting in estimates of the fraction of newly biosynthesized palmitoyl-CoA.

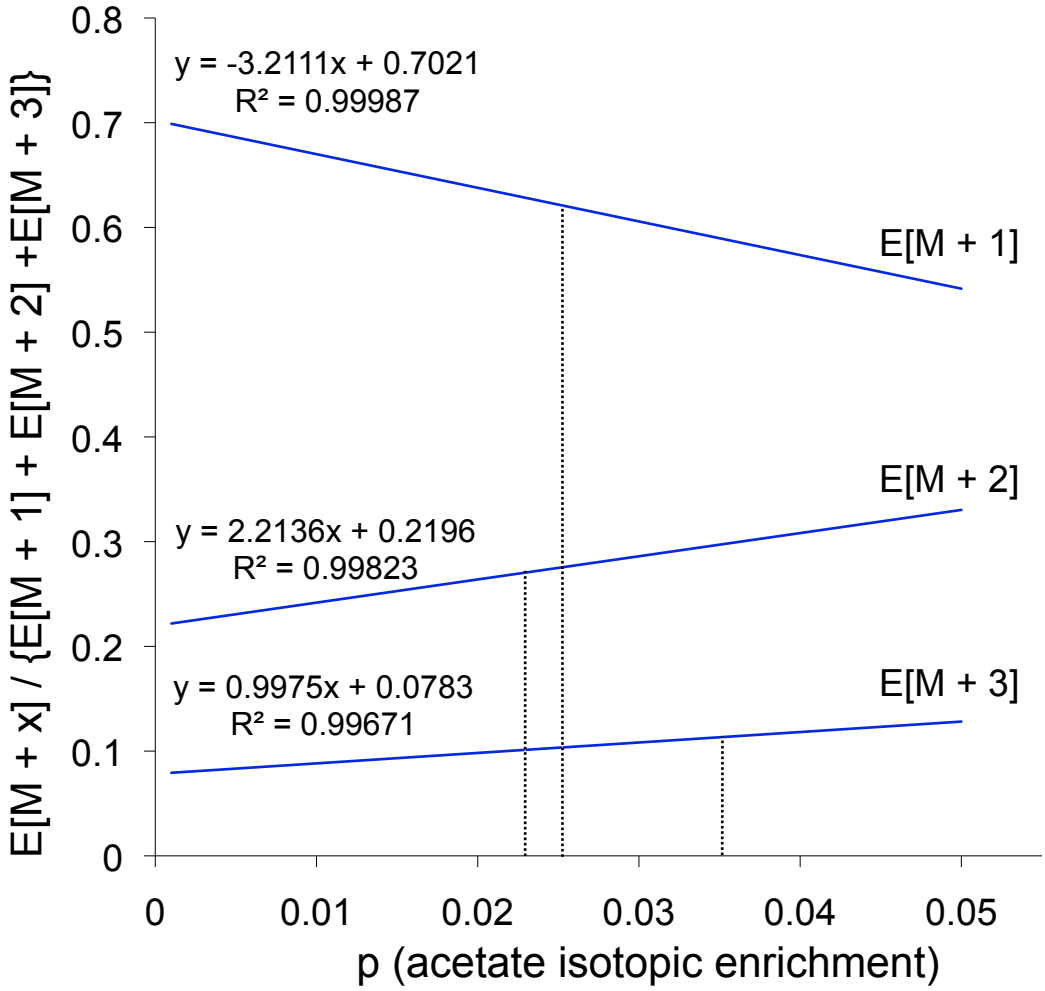

Figure 41. Plots of calculated ratios of molar excess vs. acetate isotopic enrichment for the [M + 1] through [M + 3] isotopologues of the palmitoyl-CoA product ion. The independence of ratios of molar excesses from the fraction of newly biosynthesized palmitoyl-CoA allows the estimation of p. For example, after treatment of RAW264.7 cells with 0.1 mM [1-^{13}C]-acetate for 6 hr, the observed ratios for [M + 1] through [M + 3] were 0.625, 0.265, and 0.114, respectively. These lead to estimates of p having been 0.025, 0.021, and 0.036, respectively, or 0.027 ± 0.008.

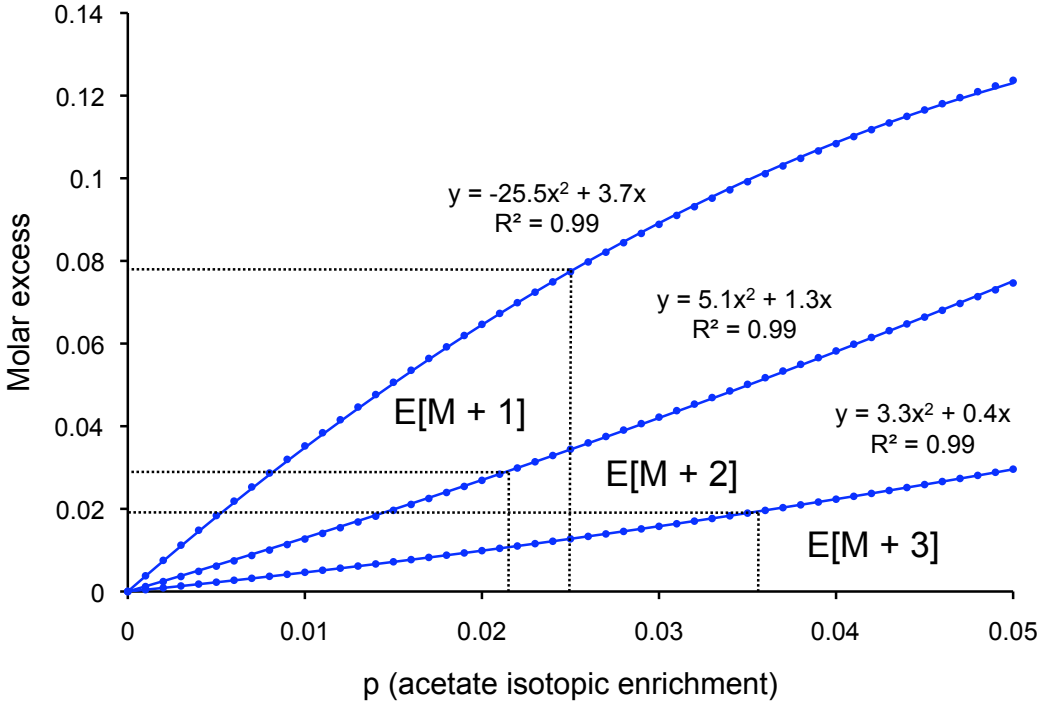

Figure 42. Calculated molar excesses of palmitoyl-CoA product ion isotopologues [M + 1] through [M + 3]. The estimates of p obtained from the [M + 1] through [M + 3] isotopologues in Figure 41 were substituted into the polynomial trendlines shown here to obtain the molar excess values representing 100% newly biosynthesized palmitoyl-CoA. Observed molar excesses were divided by these asymptotic values to estimate the fraction of newly biosynthesized palmitoyl-CoA. For example, after treating RAW264.7 cells with 0.1 mM [1-^{13}C]-acetate for 6 hr, the estimated p-values for [M + 1] through [M + 3] were 0.025, 0.021, and 0.036, respectively, resulting in estimated molar excesses (asymptotes) of 0.078, 0.028, and 0.019, respectively. The observed molar excesses for the [M + 1] through [M + 3] isotopologues were 0.044, 0.019, and 0.008, respectively, resulting in an estimate of 0.55 ± 0.13, or ~ 55% newly biosynthesized palmitoyl-CoA.

Isotopomer spectral analysis (ISA) of [1-^{13}C]-acetate labeling

The analytical work-flow of ISA (15) is summarized below. The central concept of ISA is to model the biosynthetic reaction of interest as the mixing of labeled and unlabeled monomers to form labeled polymers, which in turn mix with unlabeled (pre-exisitng) polymers, Figure 43. The key parameters of ISA are the precursor dilution factor, D, and the time-dependent proportion of newly biosynthesized polymer, g(t). In the model shown in Figure 43, D is the contribution of labeled monomer from the compartment *tracer A* to *mix A* and (1 - D) is the contribution of unlabeled monomer from the compartment *natural A* to *mix A*. Note that both labeled and natural monomers are associated with unique MID's in this modeling approach, making ISA flexible in terms of accounting for the natural occurrence of stable isotopes in *natural A*, isotopic impurity of the labeled tracer in *tracer A*, the use of multiple stable isotope-labeled substrates in one experiment (*tracer A*, *tracer B*), etc.

In the ISA model, *mix A* is not accessible to the experimenter, and represents the true *in situ* biosynthetic precursor pool for the polymerization reaction, which was *de novo* fatty acid biosynthesis in this case. Activity of FAS converted eight acetate-derived two-carbon units into one C_{16} palmitate molecule in the compartment *synthesis B*, which was activated to palmitoyl-CoA by acyl-CoA synthetases. The newly biosynthesized (and isotopically labeled) palmitoyl-CoA mixed with pre-existing (and unlabeled) palmitoyl-CoA in the compartment *sampled B*, which was quantitated with LC-ESI-MS/MS. By measuring the MID of palmitoyl-CoA in *sampled B*, the parameters D and g(t) were determined, as detailed below.

First, the MID's of acetate in the compartments *natural A* and *tracer A* were specified: in the experiment described here *natural A* contained acetate isotopologues

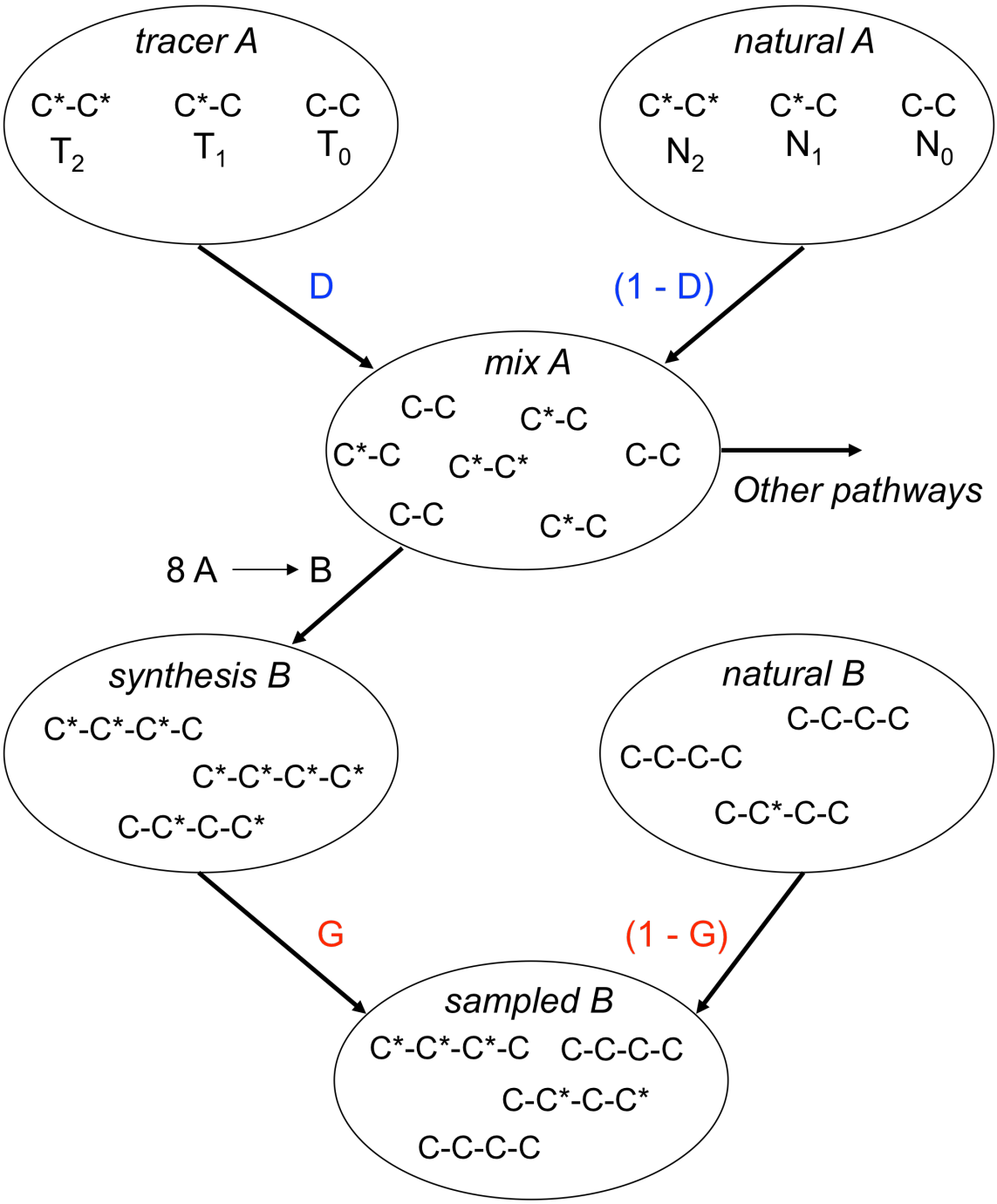

Figure 43. Model of biosynthesis used for isotopomer spectral analysis (ISA). The mass isotopologue distributions (MID's) of acetate in *natural A* and *tracer A* were specified at the beginning of the experiment, and *sampled B* represents palmitoyl-CoA analyzed by LC-ESI-MS/MS. The fractional contribution of *tracer A* to *mix A* is D, and the fractional contribution of *synthesis B* to *sampled B* is G.

with N_0 = 0.989, N_1 = 0.011, and N_2 = 0.0001, while *tracer A* contained [1-^{13}C]-acetate isotopologues with T_0 = 0.01, T_1 = 0.98, and T_2 = 0.01.Assignment of these values accounted for both the natural abundance of ^{13}C and the manufacturer's stated 98% purity of the [1-^{13}C]-acetate tracer.

Second, the mixing of *natural A* and *tracer A* in the compartment *mix A* was modeled using the parameter D (fractional flux from *tracer A* to *mix A*):

$$X_0 = DT_0 + (1 - D)N_0$$

Eq. 5

$$X_1 = DT_1 + (1 - D)N_1$$

Eq. 6

$$X_2 = DT_2 + (1 - D)N_2$$

Eq. 7

Equations 5-7 describe the abundance of *mix A* compartment isotopologues (X_0, X_1, and X_2) as functions of the sums of the flux (D) of tracer isotopologues (T_0, T_1, and T_2) and the flux (1 – D) of natural isotopologues (N_0, N_1, and N_2).

Third, equations based on multinomial probability were written describing the abundance of every palmitate isotopologue that accounted for 1) the combinations and permutations of X_0, X_1, and X_2 as *mix A* is converted to *synthesis B* by FAS, 2) the combinations and permutations of N_0, N_1, and N_2 in the pre-existing palmitate, and 3) the fractional flux contribution of *mix B* to *sampled B*, which was g(t):

$$\sum_{i=0}^{16} P_i = g(t)(X_0 + X_1 + X_2)^8 + [1 - g(t)](N_0 + N_1 + N_2)^8$$

Eq. 8

where P_i is the palmitate isotopologue from 1 to 16, and other symbols are as defined above.

Because the tracer and natural acetate isotopologue abundances were defined at the beginning of the experiment, X_i was expressed in terms of T_i and N_i (Eq. 5-7), and Eq. 8 was re-written so that all of its isotopologue terms were known values:

$$\sum_{i=0}^{16} P_i = g(t)\left[D(T_0 + T_1 + T_2) + (1 - D)(N_0 + N_1 + N_2)\right]^8 + \left[1 - g(t)\right](N_0 + N_1 + N_2)^8$$

Eq. 9

Equation 9 is a multinomial expression for the sum of all possible ways of generating all sixteen isotopologues of completely unlabeled to completely labeled palmitate. By expanding the exponential terms on the right-hand side of Eq. 9 into a polynomial expression (which, incidentally, has 6435 terms) and grouping the terms by their isotopologue molecular weight, sixteen equations resulted describing the combinations and permutations of N_i and T_i that formed the sixteen isotopologues of palmitate. Importantly, these equations were linear with respect to g(t), and hence were easily solved for that parameter.

Fourth, the values initially assigned to N_i and T_i were substituted into these sixteen equations, and each was re-arranged so that g(t) was alone on the left-hand side. After substituting the observed value for the abundance of isotopologue P_i into the cogent equation, the only remaining variable was D. For the [M + 0] to [M + 3] isotopologues , a plot was made of the solutions to each equation, with D on the x-axis and g(t) on the y-axis, by varying D from 0 to 1, solving for g(t), and plotting the value of g(t). This plot graphically showed the only values of D and g(t) that would have resulted in the observed abundance of P_i, given the known values of N_i and T_i. Lastly, the solution curves for the [M + 0] to [M + 3] isotopologues were overlaid on a single plot, and the convergence of the solution curves indicated the values of D and g(t) that were consistent with all of the observed isotopologue abundances.

The application of ISA to data for [1-^{13}C]-acetate labeling of palmitoyl-CoA in RAW264.7 cells required implementation of the above steps using Mathematica (Wolfram Software) by this author. The general strategy was: 1) to begin with Eq. 9 which is specific to the formation of palmitate from acetate, 2) expand the right-hand side, 3) create a list of the terms in this expanded polynomial, 4) evaluate each term to determine which of the sixteen isotopologues it represented based on the superscript (stoichiometry) and subscript (isotopomer) of each N_i and T_i component, 5) sort the terms into sixteen lists (equations) based on which of the sixteen palmitate isotopologues each represented, 6) substitute into each equation the values of N_i and T_i assigned at the beginning of the experiment, 7) solve each of the sixteen equations for g(t), 8) substitute the observed isotopologue abundances into the cogent equations for the four most abundant isotopologues , 9) vary D from 0 to 1 and plot the resulting g(t) for each of the four equations, and 10) overlay the four isotopologue solution curves on a single plot.

5.4 Results

Labeling of fatty acyl-CoAs by [U-^{13}C]-palmitate treatment

To determine the isotopic enrichment of palmitoyl-CoA in RAW264.7 cells either with (Figure 44, *red lines*) or without (Figure 44, *black lines*) 100 ng/ml Kdo_2-Lipid A, cells were cultured as described in Experimental Procedures with 0.1 mM [U-^{13}C]-palmitate:BSA (in a 1:1 molar ratio) in the medium. After extracting fatty acyl-CoAs from the cells, palmitoyl-CoA, both [M + 0] (*m/z* 1006.4; (Figure 44, *upper left*) and [M + 16] (*m/z* 1022.4; (Figure 44, *upper right*) was quantitated.

The results show that the quantity of [M + 0] palmitoyl-CoA initially decreased for the first 2 hr, then increased between 4 and 24 hr, and there was a slight (but not significant) increase in the quantity of unlabeled palmitoyl-CoA associated with Kdo_2-

Lipid A treatment. The quantity of [M + 16] palmitoyl-CoA increased between 0.5 and 24 hr, and there was a significantly higher amount of labeled palmitoyl-CoA at 24 hr with Kdo_2-Lipid A treatment. Isotopic enrichment of palmitoyl-CoA reached ~ 0.6, or 60%, either with or without Kdo_2-Lipid A treatment by 6 hr, and was constant between 6 and 24 hr (Figure 44, *lower panel*). These observations indicate rapid and robust isotopic labeling of cellular palmitoyl-CoA by extracellular [U-^{13}C]-palmitate, presumably via acyl-CoA synthetase activity, and also indicate achievement of isotopic equilibrium (Figure 44, *lower panel*) during labeling with extracellular [U-^{13}C]-palmitate.

To determine whether the labeled palmitoyl-CoA was metabolized by elongases and desaturases, control RAW264.7 cell extracts were analyzed for C16:1- and C18:0-CoA. Both analytes were measured as unlabeled and [M + 16] species, and the quantities (Figure 45, *upper panels*) and isotopic enrichment (Figure 45, *lower panels*) are shown. Both of these fatty acyl-CoAs appeared to reach isotopic equilibrium, but at a lower isotopic enrichment than precursor palmitoyl-CoA. These results indicate desaturation and elongation of the labeled palmitoyl-CoA in this cell type.

Labeling of palmitoyl-CoA by [1-^{13}C]-acetate treatment

To measure the contribution of *de novo* palmitate biosynthesis to palmitoyl-CoA quantitites, RAW264.7 cells were treated with 0, 0.1, and 1.0 mM [1-^{13}C]-acetate for 6 hr, and with 0 and1.0 mM [1-^{13}C]-acetate for 12 and 24 hr. After extraction of fatty acyl-CoAs, palmitoyl-CoA isotopologues from [M + 0] to [M + 4] were quantitated using LC-ESI-MS/MS. This provided a mass isotopologue distribution (MID) for the palmitoyl-CoA product ion (Figure 46), which was analyzed by mass isotopomer distribution analysis and isotopomer spectral analysis, as described below.

MIDA of palmitoyl-CoA labeling by [1-^{13}C]-acetate treatment

MIDA begins with the generation of a table of p-values specific to the molecule being analyzed (Table III). In MIDA nomenclature, p is the isotopic enrichment of the biosynthetic precursor pool for the polymerization reaction of interest. In the experiments described here, p = the isotopic enrichment of malonyl-CoA in the biosynthetic precursor pool for FAS, and when p = 0 there is no isotopic labeling.

The calculated MIDs of the palmitoyl-CoA product ion are shown in Figure 46, *white bars*, and in Figure 47. The *central panel* of Figure 47 shows that a vertical line at any given value of p indicates the unique MID at that p-value. For example, if p = 0 (Figure 47, *upper right*), the "natural" MID of the palmitoyl-CoA product ion is predicted; the [M + 1], [M + 2], etc. isotopologues result from the natural abundance of isotopes such as ^{13}C, ^{18}O and ^{2}H. It should be noted that comparing the calculated MID at p = 0 (Figure 46, *blue bars*) to the observed MID in unlabeled RAW264.7 cells (Figure 46, *white bars*) resulted in low (< 6%) error, indicating the accuracy of both the software prediction and the LC-ESI-MS/MS quantitation.

If one assumes that p = 0.05 (Figure 47, *lower left)* or p = 0.10 (Figure 47, *lower right*), it is obvious that the MID shifts toward labeled molecules, creating a unique "fingerprint" of the palmitoyl-CoA product ion isotopic enrichment for a given isotopic enrichment of the acetyl-CoA biosynthetic precursor. The observed MIDs of the palmitoyl-CoA product ion after 6 hr of treatment with 0.1 mM [1-^{13}C]-acetate (Figure 46, *grey bars*) and 1.0 mM [1-^{13}C]-acetate (Figure 46, *black bars*) showed the expected dose-dependent shift towards labeled molecules. It must be emphasized that these predicted MIDs represent a sample that is 100% the product of *de novo* fatty acid biosynthesis.

After generating tables of molar fractions (Table IV), molar excesses (Table V) and ratios of molar excesses (Table VI) as detailed in Experimental Procedures, a plot was generated of ratios of molar excesses vs. p for the [M + 1] through [M + 3]

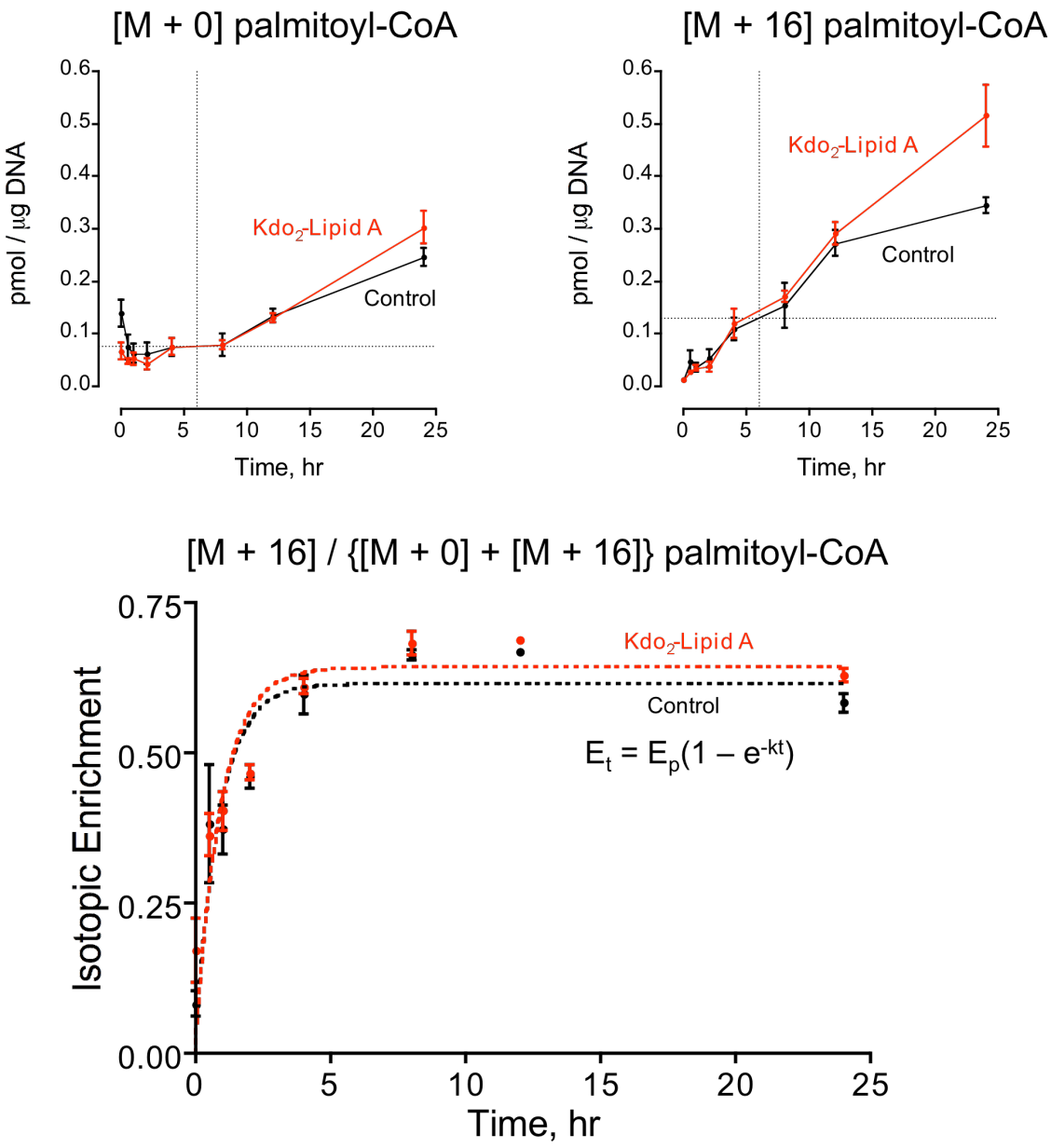

Figure 44. Quantities (*upper panels*) and isotopic enrichment (*lower panel*) of palmitoyl-CoA in RAW264.7 cells treated with 0.1 mM [U-^{13}C]-palmitate. In both panels *red lines* indicate Kdo_2-Lipid A treatment and *black lines* indicate control cells. Dashed lines in the *upper panels* indicate achievement of isotopic enrichment equilibrium (at~ 60%) after 6 hr. The quantities of [M + 16] palmitoyl-CoA at 24 hr were significantly different between control and Kdo_2-Lipid A treated cells ($p < 0.05$ by Student's t-test). Isotopic enrichment was calculated as described in Experimental Procedures; all data are the mean and SEM of triplicate Petri dishes.

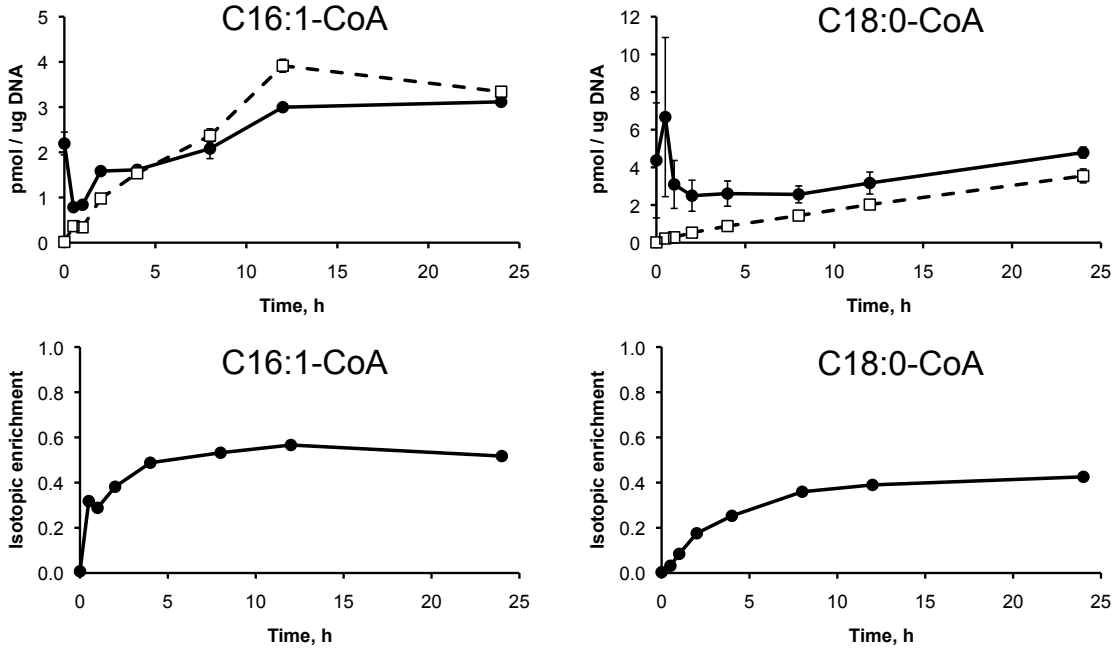

Figure 45. Quantities and isotopic enrichments of C16:1- and C18:0-CoA in RAW264.7 cells treated with 0.1 mM [U-^{13}C]-palmitate. The *upper panels* show the quantity of unlabeled (*solid lines*) and labeled (*dashed lines*) fatty acyl-CoA. The *lower panels* show isotopic enrichment, calculated as labeled / (unlabeled + labeled). Results are the mean and range of duplicate Petri dishes.

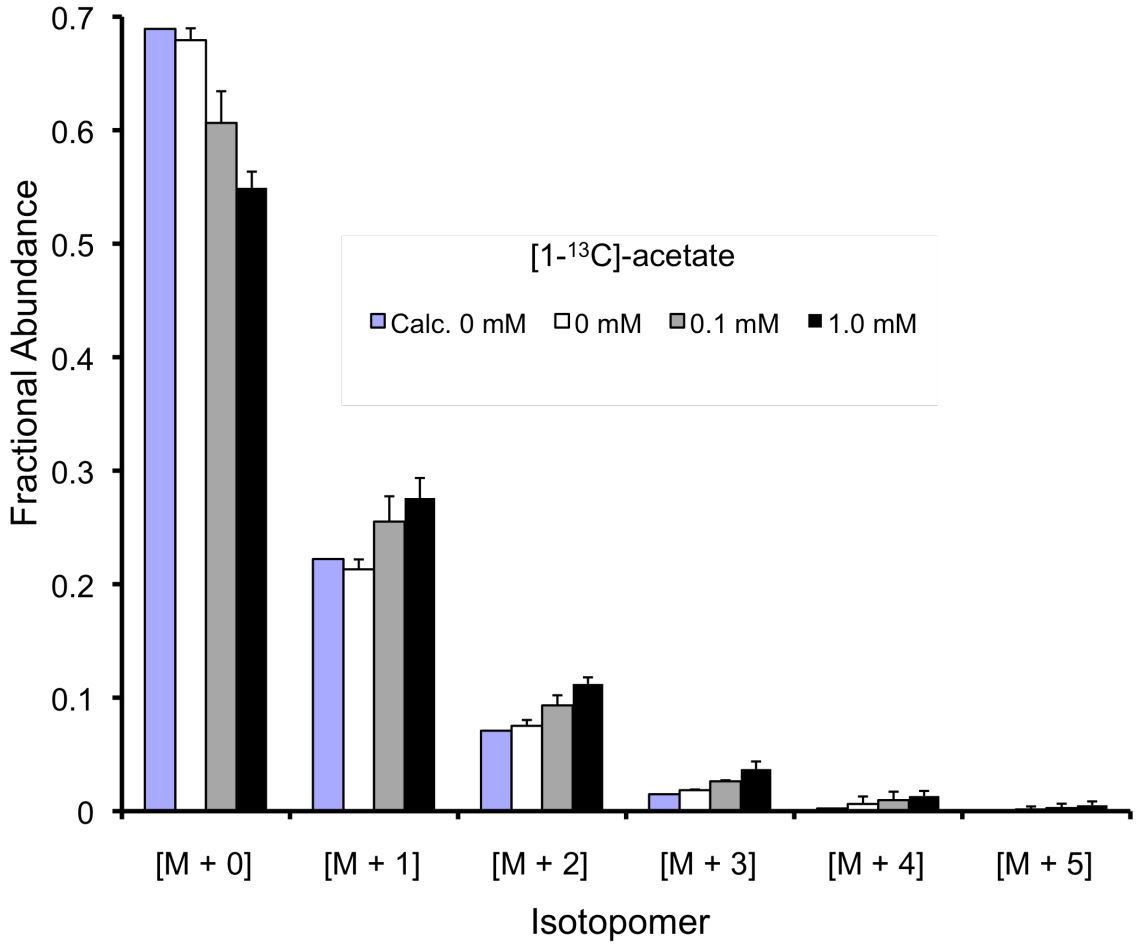

Figure 46. Mass isotopologue distributions (MID's) of the palmitoyl-CoA product ion. The MID calculated for the unenriched product ion (*blue*) had less than 6% error compared to the observed MID with 0 mM [1-^{13}C]-acetate (*white*). Treatment with 0.1 mM [1-^{13}C]-acetate (*grey*) and 1.0 mM [1-^{13}C]-acetate (*black*) showed the expected dose-dependent shift towards labeled isotopologues. Data shown are the mean ± SD of four replicate Petri dishes.

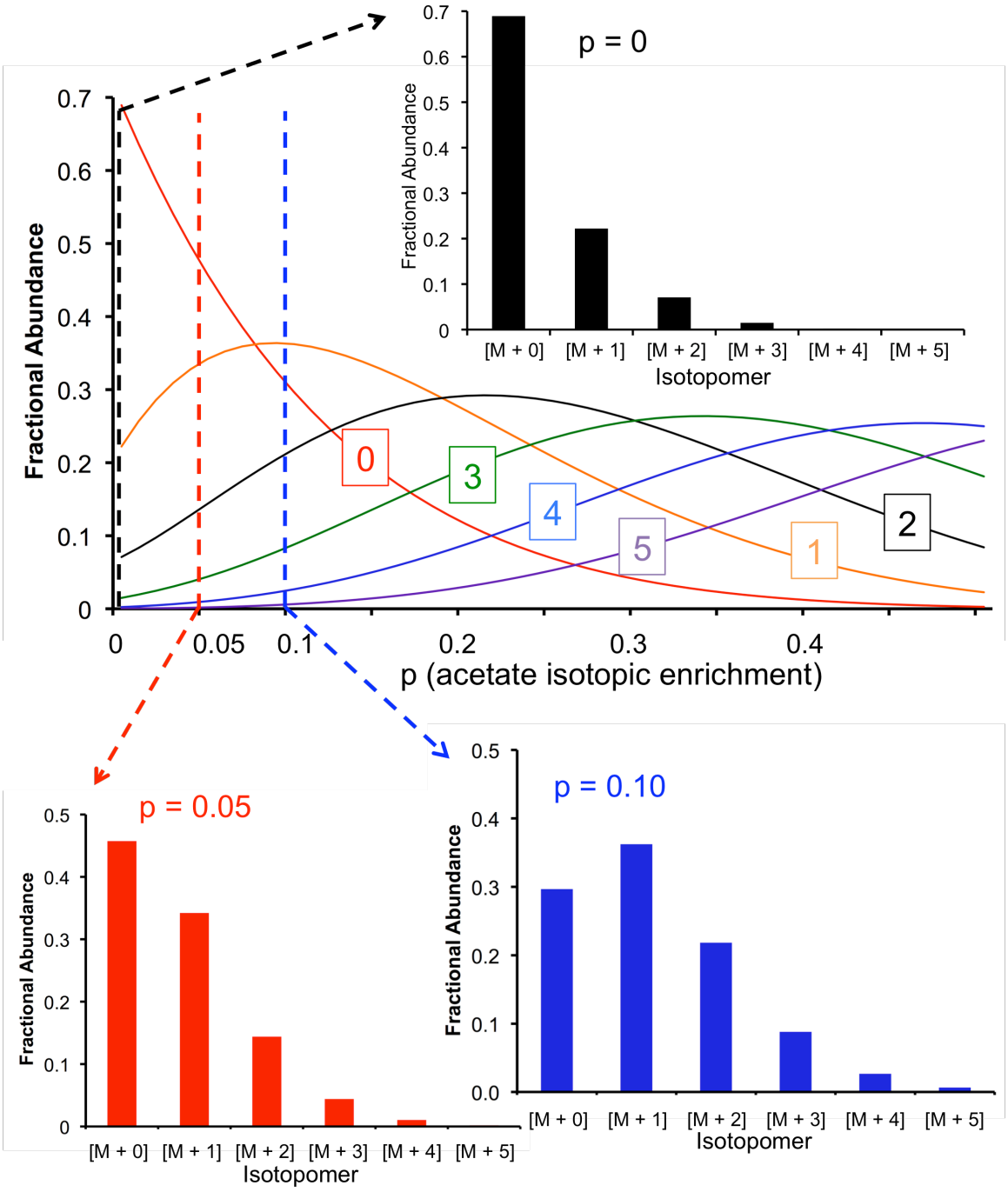

Figure 47. Calculated mass isotopologue distributions (MIDs) for the palmitoyl-CoA product ion. The central panel shows predicted fractional abundances of [M + 0] through [M + 5] (*boxed numbers*) with vertical lines at p = 0, 0.05, and 0.10. The MIDs at p = 0 (*upper right*), p = 0.05 (*lower left*), and p = 0.10 (*lower right*) are shown.

isotopologues (Figure 41). After treatment of RAW264.7 cells with 0.1 mM [1-^{13}C]-acetate for 6 hr, the observed ratios of molar excesses for [M + 1] through [M + 3] isotopologues of the palmitoyl-CoA product ion (0.62, 0.27, and 0.11, respectively) were used in conjunction with this plot to estimate a p-value of 0.027 ± 0.008, or ~ 2.7% isotopic enrichment of the acetyl-CoA pool that was the biosynthetic precursor for palmitoyl-CoA.

This estimate of p was used in conjunction with a plot of molar excesses vs. p (Figure 42) to determine the asymptotic molar excess approached by the [M + 1] through [M + 3] isotopologues as the fraction of newly biosynthesized palmitoyl-CoA approached 100%. The observed molar excesses of [M + 1] through [M + 3] isotopologues were divided by these asymptotic values, resulting in an estimated fraction of 0.55 ± 0.13, meaning ~ 55% of the palmitoyl-CoA pool had been biosynthesized after 6 hr of RAW264.7 cell treatment with 0.1 mM [1-^{13}C]-acetate.

Treatment of RAW264.7 cells with 1.0 mM [1-^{13}C]-acetate (a ten-fold higher concentration than in the above experiment) for 6 hr resulted in an estimated p-value of 0.056 ± 0.02, or ~ 5.6% enrichment (two-fold higher than was calculated for 0.1 mM [1-^{13}C]-acetate treatment) and an estimate of 0.55 ± 0.13, or ~ 52% newly biosynthesized palmitoyl-CoA (not significantly different from the result for 0.1 mM [1-^{13}C]-acetate treatment). This outcome indicates that the higher concentration of [1-^{13}C]-acetate labeled the biosynthetic precursor pool to a greater extent, but did not affect the rate of biosynthesis of palmitoyl-CoA by FAS.

In addition to palmitoyl-CoA, the experiment with 1.0 mM [1-^{13}C]-acetate treatment quantitated isotopologues of myristoyl-, palmitoleoyl-, stearoyl-, and oleoyl-CoA after 12 and 24 h of treatment. Interestingly, the calculated value of p was non-identical (and significantly different) when comparing these fatty acyl-CoAs, suggesting

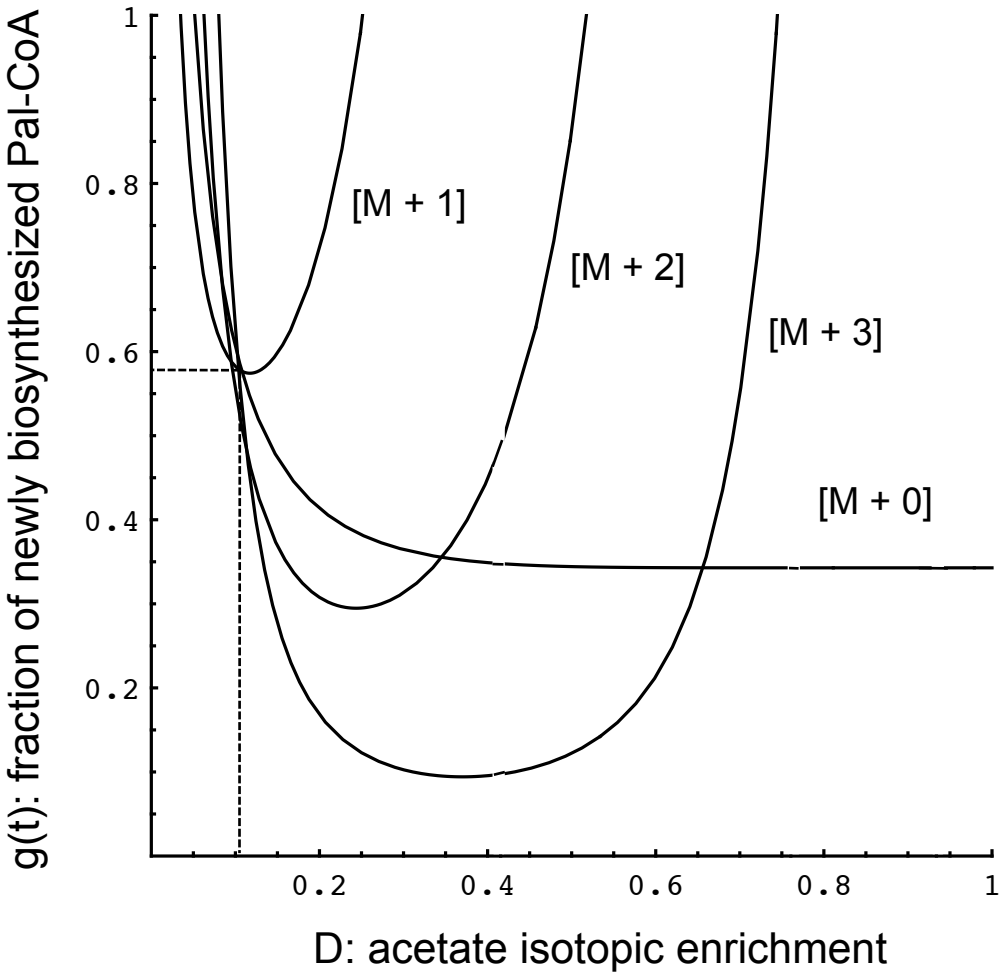

Figure 48. Graphical output of Mathematica program for the estimation of D and g(t) during palmitoyl-CoA biosynthesis. Isotopomer spectral analysis (ISA) was used as described in Experimental Procedures to estimate the parameters D and g(t) for RAW264.7 cells treated with 1.0 mM [1-^{13}C]-acetate for 6 hr. Observed isotopologue abundances for [M + 0] through [M + 3] were used.

that they are biosynthesized and / or elongated using distinct pools of malonyl-CoA derived from acetyl-CoA. Furthermore, the fraction of newly biosynthesized polymers was also non-identical when comparing these species, and treatment with Kdo_2-Lipid A caused (in some cases) significant changes in p, in f, and in quantity. These results are summarized in Table VII.

ISA of palmitoyl-CoA labeling by [1-^{13}C]-acetate treatment

ISA of palmitoyl-CoA labeling after 6 hr of treating RAW264.7 cells with 1 mM [1-^{13}C]-acetate using the [M + 0] through [M + 3] isotopologues indicated that D = 0.1 and g(6 hr) = 0.6 (Figure 48), meaning there was a 10% fractional flux of *tracer A* to *mix A* and that 60% of the palmitoyl-CoA in *sampled B* was derived from *synthesis B*. Compared to the MIDA analysis, for which p = 0.056 ± 0.02 and the fraction of newly biosynthesized palmitoyl-CoA was 0.55 ± 0.13, both methods of calculating isotopic enrichment reached the same conclusion regarding the fraction of newly biosynthesized palmitoyl-CoA (~ 60%) and similar estimates of the contribution of the labeled acetate to the biosynthetic precursor pool for FAS (6% vs. 10%). Thus, both ways of calculating the contribution of *de novo* palmitate biosynthesis to the palmitoyl-CoA pool indicated that despite the moderate concentration of [1-^{13}C]-acetate tracer in the medium (1 mM) and the modest labeling of the acetyl-CoA biosynthetic precursor pool for FAS (6 to 10%), the palmitoyl-CoA pool was rapidly (6 hr) and robustly (~ 60%) labeled by the *de novo* biosynthesized palmitate.

Table VII. Calculated values of p and f, and quantitation for fatty acyl-CoAs after 12 and 24 h ± Kdo2-Lipid A (KLA) treatment in the presence of 1.0 mM [1-^{13}C]-acetate.

Fatty acyl-CoA	Treatment, time	p (acetate enrichment, %)	f (fraction of new polymers, %)	Q (pmol / ug DNA)
C14:0		(4)	(4)	(3)
	Control, 12 h	7.1 ± 1.9	40 ± 5	0.9 ± 0.1
	KLA, 12 h	8.5 ± 1.4	38 ± 5	0.8 ± 0.1
	Control, 24 h	6.0 ± 0.5 *	54 ± 4 *	1 ± 0.1
	KLA, 24 h	13 ± 2.6 *	31 ± 8 *	1 ± 0.2
C16:0		(5)	(5)	(3)
	Control, 12 h	4.5 ± 0.3 *	73 ± 7 *	1.3 ± 0.1 *
	KLA, 12 h	6.0 ± 0.8 *	42 ± 3 *	1.6 ± 0.1 *
	Control, 24 h	5.0 ± 0.5	62 ± 8	1.3 ± 0.1
	KLA, 24 h	4.7 ± 0.1	64 ± 6	1.5 ± 0.2
C18:0		(5)	(5)	(3)
	Control, 12 h	6.5 ± 1	49 ± 9	0.4 ± 0.1 *
	KLA, 12 h	6.3 ± 1	39 ± 7	0.6 ± 0.1 *
	Control, 24 h	5.2 ± 1	48 ± 2	0.6 ± 0.1 •
	KLA, 24 h	6.2 ± 1	48 ± 7	0.9 ± 0.1 •
C16:1		(4)	(3)	(3)
	Control, 12 h	10 ± 2.4	35 ± 8	1.0 ± 0.14 *
	KLA, 12 h	7.1 ± 1.4	30 ± 2	0.4 ± 0.02 *
	Control, 24 h	10 ± 1.8	36 ± 8	0.9 ± 0.03 •
	KLA, 24 h	6.9 ± 2.5	35 ± 6	0.3 ± 0.01 •
C18:1		(5)	(4,5)	(3)
	Control, 12 h	5.1 ± 0.2 *	49 ± 5 *	1.5 ± 0.18 *
	KLA, 12 h	3.3 ± 0.2 *	65 ± 6 *	0.9 ± 0.04 *
	Control, 24 h	5.9 ± 1.1 •	50 ± 13	3.2 ± 0.16 •
	KLA, 24 h	13 ± 2.8 •	25 ± 4	0.9 ± 0.05 •

The number in parenthesis above each column shows the number of isotopologues used to calculate the results; the symbols * and • denote a significant difference ($p < 0.05$ by Student's t-test) for adjacent rows' entries.

5.5 Discussion

The goal of this study was to use treatment with stable isotope-labeled precursors ([U-^{13}C]-palmitate and [1-^{13}C]-acetate) to compare the utilization of extracellular palmitate (192) and *de novo* fatty acid biosynthesis (195), respectively, for the production of palmitoyl-CoA in RAW264.7 mouse macrophage-like cells. Treatment of this cell type with Kdo_2-Lipid A has been shown to cause extensive changes in the transcription of genes encoding enzymes of lipid metabolism, including fatty acyl-CoA metabolism (www.lipidmaps.org); therefore stable isotope labeling of fatty acyl-CoAs was also measured in the presence of Kdo_2-Lipid A in some experiments.

Extracellular 0.1 mM [U-^{13}C]-palmitate labeled ~60% of the palmitoyl-CoA pool between 4 and 24 hr in control cells, and treatment with Kdo_2-Lipid A increased the quantities of both unlabeled and labeled palmitoyl-CoA (Figure 44, *upper panels*), so that there was no significant difference in palmitoyl-CoA isotopic enrichment ± Kdo_2-Lipid A (Figure 44, *lower panel*). The [U-^{13}C]-palmitate treatment also resulted in the labeling of palmitoyl-CoA metabolites, including desaturated palmitoleoyl-CoA and elongated stearoyl-CoA, and these fatty acyl-CoAs reached isotopic equilibrium at enrichments (50% and 40%, respectively) lower than that of palmitoyl-CoA (60%; Figures 44 and 45). This is consistent with an additional metabolic step (elongation (196) or desaturation (197)) causing a reduction in the amount of tracer (labeled palmitoyl-CoA) entering the pool of unlabeled palmitoleoyl- and stearoyl-CoA.

Treatment with 0.1 m [1-^{13}C]-acetate followed by MIDA analysis (198-202) showed that ~ 60% of the palmitoyl-CoA pool was newly biosynthesized after 6 h, as well as ~ 3% labeling of the precursor malonyl-CoA pool. Treatment with a higher concentration of [1-^{13}C]-acetate (1 mM) again indicated that ~ 60% of the palmitoyl-CoA pool was newly biosynthesized (via analyses with MIDA and ISA (86, 87, 198, 203-206)), and indicated an increased labeling (MIDA, 6%; ISA, 10%) of the malonyl-CoA precursor

pool. These results indicate that *de novo* palmitate biosynthesis labels palmitoyl-CoA to a similar extent (~ 60%) as extracellular palmitate labels palmitoyl-CoA, and that higher concentrations of acetate tracer increase the isotopic enrichment of the acetate precursor pool, but do not change the fraction of newly biosynthesized palmitoyl-CoA. This is in agreement with the results of palmitate labeling in NIH3T3-L1 cells using [1,2-^{13}C]-acetate, which showed a similar increase in precursor enrichment but not the fraction of new polymers with increasing concentrations of tracer (87).

In the presence of Kdo_2-Lipid A, the isotopic enrichment of the acetate precursor pool for palmitoyl-CoA after 12 h significantly ($p < 0.05$) increased from 4.5 ± 0.3% to 6.0 ± 0.8%, while the fraction of newly biosynthesized palmitoyl-CoA significantly decreased from 73 ± 7% to 42 ± 3%. Taken together with the significant increase in palmitoyl-CoA quantity after 12 h caused by Kdo_2-Lipid A (1.6 ± 0.1 pmol/μg DNA vs. 1.3 ± 0.1 pmol/μg DNA), these results indicate that a smaller amount of new palmitoyl-CoA (42% vs. 73%) is more isotopically enriched (6% vs. 4.5%) with Kdo_2-Lipid A treatment, and that the contribution of unlabeled palmitoyl-CoA from (for example) extracellular or catabolic sources is not large enough (1.6 vs. 1.3 pmol/μg DNA, a 23% increase) to explain the smaller amount of new palmitoyl-CoA. A lower rate of *de novo* palmitate biosynthesis would be consistent with these observations, and Kdo_2-Lipid A does cause a 60-70% reduction in the transcription of fatty acid synthase in RAW264.7 cells (www.lipidmaps.org).

The acetate isotopic enrichments, fractions of newly biosynthesized analyte, and quantities of select fatty acyl-CoAs are shown in Table VII, and some of these results are also in agreement with previously observed changes in gene expression in RAW264.7 cells caused by Kdo_2-Lipid A treatment. For example, the quantity of monounsaturated fatty acyl-CoAs (i.e. C16:1- and C18:1-CoA) decreased significantly ($p < 0.05$) in the

presence of Kdo_2-Lipid A after 12 and 24 h of treatment, consistent with a ~ 50% reduction in the transcription of stearoyl-CoA desaturase (www.lipidmaps.org).

In contrast to palmitoyl-CoA, Kdo_2-Lipid A treatment resulted in oleoyl-CoA significantly ($p < 0.05$) decreasing in acetate precursor enrichment (5.1 ± 0.2% vs. 3.3 ± 0.2%) and significantly increasing in the fraction of newly biosynthesized analyte (49 ± 5% vs. 65 ± 6%) compared to control cells. Taken together with the aforementioned significant decrease in the quantity of oleoyl-CoA (1.5 ± 0.2 vs. 0.9 ± 0.04 pmol/μg DNA), after 12 h, these results suggest that newly biosynthesized oleoyl-CoA is becoming a larger proportion of the metabolite pool as its total quantity diminishes.

The results of 1.0 mM [1-^{13}C]-acetate labeling also showed that a substantial amount of myristoyl-CoA (12, 207, 208) was newly biosynthesized after 12 h (40 ± 5%). Compared to the small amount of myristoyl-CoA labeling observed with [U-^{13}C]-palmitate treatment (~ 5%, data not shown), this result is consistent with *de novo* fatty acid biosynthesis producing myristate as well as palmitate, which has been demonstrated *in vitro* (104) for recombinant human fatty acid synthase. In addition, after 24 h of Kdo_2-Lipid A treatment, the myristoyl-CoA showed significantly higher acetate precursor enrichment (13 ± 3% vs. 6 ± 5%) and a significantly lower fraction of newly biosynthesized analyte (31 ± 8% vs. 54 ± 4%), which is consistent with increased labeling of the polymerized myristate, and a reduction in the biosynthesis of myristate, such as the aforementioned 60-70% reduction in fatty acid synthase transcription caused by Kdo_2-Lipid A treatment of RAW264.7 cells (www.lipidmaps.org).

In summary, both extracellular fatty acids and *de novo* fatty acid biosynthesis rapidly (~ 6 h) and robustly (~ 60%) contributed to the intracellular palmitoyl-CoA pool of RAW264.7 cells, as shown by treatment with the stable isotope tracers [U-^{13}C]-palmitate and [1-^{13}C]-acetate. In addition, the elongation and desaturation of palmitoyl-CoA was

observed after treatment with both tracers, as indicated by mass-shifted C16:1 and C18:0-CoA. Several of the changes in gene expression caused by Kdo_2-Lipid A treatment (www.lipidmaps.org), such as decreased transcription of stearoyl-CoA desaturase (47, 48, 150, 209-212) and fatty acid synthase, were reflected by the changes in fatty acyl-CoA quantites and/or isotopic enrichment. The labeling of myristoyl-CoA with [1-^{13}C]-acetate confirms previous findings (104) about the biosynthesis of this species, and is an example of the power of stable isotope labeling experiments to quantitate metabolic activities in cultured mammalian cells with unprecedented sensitivity and specificity.

CONCLUDING STATEMENT

The development of a method for quantitation of unlabeled and stable isotope-labeled fatty acyl-CoAs by LC-ESI-MS/MS in small samples of biological material [Chapter 2 and (3)] provides important information about the metabolism of complex lipids, such as sphingolipids. For example, a cultured cell paradigm in which basal (Chapter 3) and increased (Chapter 4) quantities of sphingolipids were observed has been confirmed to be the results of increased *de novo* sphingolipid biosynthesis, rather than increased catabolism of pre-existing sphingolipids.

Specifically, the over-expression of SPT, the first enzyme of *de novo* sphingolipid biosynthesis, in HEK293 cells resulted in increased quantities of sphingolipids, and a greater accumulation of [M + 16] and [M + 32] sphingolipids after treatment with [U-^{13}C]-palmitate (Chapter 4). In addition, the induction of SPT mRNA expression in RAW264.7 cells by Kdo_2-Lipid A treatment resulted in increased quantities of sphingolipids, and a greater accumulation of [M + 16] and [M + 32] sphingolipids after treatment with [U-^{13}C]-palmitate (Chapter 4). The ability to quantitate [M + 0] and [M + 16] palmitoyl-CoA showed that in both paradigms the isotopic enrichment of palmitoyl-CoA was not the source of observed differences in isotopically labeled sphingolipids.

Furthermore, the quantitation of the isotopic enrichment of palmitoyl-CoA allowed the true quantity of *de novo* biosynthesized sphingolipids to be estimated, if one assumes that a single, well-mixed pool of palmitoyl-CoA is available for serine palmitoyltransferase. Comparison of the observed quantity of unlabeled ceramide to the quantity that was calculated to have been *de novo* biosynthesized implied that all of the observed unlabeled quantity could be accounted for by *de novo* biosynthesis in HEK293, SPT1/2, and control RAW264.7 cells, but not in Kdo_2-Lipid A-treated RAW264.7 cells (Chapters 3 and 4). Therefore, quantitation of the isotopic enrichment of palmitoyl-CoA

provided data that significantly changed the interpretation of sphingolipid quantitation in these experiments.

The wealth of data for isotopic labeling of sphingolipids (Chapter 3) suggested the application of previously described approaches for the analysis of metabolic labeling, one such approach (88) led to calculating enrichment for fatty acyl-CoAs and sphingolipids and the observation that some species clearly reached isotopic equilibrium. Modeling this isotopic enrichment and measurement of metabolite quantities with LC-ESI-MS/MS allowed the estimation of the rate of appearance of unlabeled metabolite, which quantitated the increase in *de novo* sphingolipid caused by over-expression of serine palmitoyltransferase in HEK293 cells (Chapter 4).

Although informative, an alternative to metabolic labeling of *de novo* sphingolipid biosynthesis with [U-^{13}C]-palmitate was also used: labeling of *de novo* biosynthesized palmitate via treatment of cultured cells with [1-^{13}C]-acetate (Chapter 5). Two previously described mathematical approaches based on multinomial distribution (14, 15) were taken for the analysis of the [1-^{13}C]-acetate labeling data; both approaches reached similar conclusions about the isotopic enrichment of the biosynthetic precursor acetate (6 to 10%) and the fraction of newly biosynthesized palmitoyl-CoA (~ 60%) after 6 hr of treating RAW264.7 cells with 1.0 mM [1-^{13}C]-acetate.

In summary, the quantitation of fatty acyl-CoAs, and particularly quantitation of their isotopic enrichment during stable isotope-labeling studies of lipid metabolism, can provide data that significantly change the interpretation of analyte quantitation, as demonstrated here for investigations of *de novo* sphingolipid biosynthesis.

REFERENCES

1. Choy, P. C., M. Skrzypczak, D. Lee, and F. T. Jay. 1997. Acyl-GPC and alkenyl/alkyl-GPC:acyl-CoA acyltransferases. *Biochim Biophys Acta* **1348**: 124-133.

2. Kerner, J., and C. Hoppel. 2000. Fatty acid import into mitochondria. *Biochim Biophys Acta* **1486**: 1-17.

3. Haynes, C. A., J. C. Allegood, K. Sims, E. W. Wang, M. C. Sullards, and A. H. Merrill Jr. 2008. Quantitation of fatty acyl-coenzyme As in mammalian cells by liquid chromatography-electrospray ionization tandem mass spectrometry. *The Journal of Lipid Research* **49**: 1113.

4. Hanada, K. 2003. Serine palmitoyltransferase, a key enzyme of sphingolipid metabolism. *Biochim Biophys Acta* **1632**: 16-30.

5. Wei, J., Tokumbo, Y., Liepelt, M., Momin, A., Wang, E., Hanada, K., Merrill, A.H. . 2006. Serine Palmitoyltransferase. *In* Sphingolipid Biology. Y. Hirabayashi, Igarashi, Y., Merrill, A.H., editor. Springer, Tokyo. 25~47.

6. Hornemann, T., Y. Wei, and A. von Eckardstein. 2007. Is the mammalian serine palmitoyltransferase a high-molecular-mass complex? *Biochem J* **405**: 157-164.

7. Riebeling, C., J. C. Allegood, E. Wang, A. H. Merrill, Jr., and A. H. Futerman. 2003. Two mammalian longevity assurance gene (LAG1) family members, trh1 and trh4, regulate dihydroceramide synthesis using different fatty acyl-CoA donors. *J Biol Chem* **278**: 43452-43459.

8. Lahiri, S., and A. H. Futerman. 2005. LASS5 is a bona fide dihydroceramide synthase that selectively utilizes palmitoyl-CoA as acyl donor. *J Biol Chem* **280**: 33735-33738.

9. Mizutani, Y., A. Kihara, and Y. Igarashi. 2005. Mammalian Lass6 and its related family members regulate synthesis of specific ceramides. *Biochem J* **390**: 263-271.

10. Farwanah, H., J. Wohlrab, R. H. Neubert, and K. Raith. 2005. Profiling of human stratum corneum ceramides by means of normal phase LC/APCI-MS. *Anal Bioanal Chem* **383**: 632-637.

11. Ternes, P., S. Franke, U. Zahringer, P. Sperling, and E. Heinz. 2002. Identification and characterization of a sphingolipid delta 4-desaturase family. *J Biol Chem* **277**: 25512-25518.

12. Beauchamp, E., D. Goenaga, J. Le Bloc'h, D. Catheline, P. Legrand, and V. Rioux. 2007. Myristic acid increases the activity of dihydroceramide Delta4-desaturase 1 through its N-terminal myristoylation. *Biochimie*.

13. Tafesse, F. 2006. The Multigenic Sphingomyelin Synthase Family. *Journal of Biological Chemistry* **281**: 29421-29425.

14. Hellerstein, M. K., and R. A. Neese. 1992. Mass isotopomer distribution analysis: a technique for measuring biosynthesis and turnover of polymers. *Am J Physiol* **263**: E988-1001.

15. Kelleher, J. K., and T. M. Masterson. 1992. Model equations for condensation biosynthesis using stable isotopes and radioisotopes. *Am J Physiol* **262**: E118-125.

16. Askari, B., J. E. Kanter, A. M. Sherrid, D. L. Golej, A. T. Bender, J. Liu, W. A. Hsueh, J. A. Beavo, R. A. Coleman, and K. E. Bornfeldt. 2007. Rosiglitazone inhibits acyl-CoA synthetase activity and fatty acid partitioning to diacylglycerol and triacylglycerol via a peroxisome proliferator-activated receptor-gamma-independent mechanism in human arterial smooth muscle cells and macrophages. *Diabetes* **56**: 1143-1152.

17. Yang, Y., J. Cao, and Y. Shi. 2004. Identification and characterization of a gene encoding human LPGAT1, an endoplasmic reticulum-associated lysophosphatidylglycerol acyltransferase. *J Biol Chem* **279**: 55866-55874.

18. Chao, H., M. Zhou, A. McIntosh, F. Schroeder, and A. B. Kier. 2003. ACBP and cholesterol differentially alter fatty acyl CoA utilization by microsomal ACAT. *J Lipid Res* **44**: 72-83.

19. Merrill, A. H., Jr., and R. D. Williams. 1984. Utilization of different fatty acyl-CoA thioesters by serine palmitoyltransferase from rat brain. *J Lipid Res* **25**: 185-188.

20. Louet, J. F., G. Hayhurst, F. J. Gonzalez, J. Girard, and J. F. Decaux. 2002. The coactivator PGC-1 is involved in the regulation of the liver carnitine palmitoyltransferase I gene expression by cAMP in combination with HNF4 alpha and cAMP-response element-binding protein (CREB). *J Biol Chem* **277**: 37991-38000.

21. Batheja, A. D., D. J. Uhlinger, J. M. Carton, G. Ho, and M. R. D'Andrea. 2003. Characterization of serine palmitoyltransferase in normal human tissues. *J Histochem Cytochem* **51**: 687-696.

22. Yasuda, S., M. Nishijima, and K. Hanada. 2003. Localization, topology, and function of the LCB1 subunit of serine palmitoyltransferase in mammalian cells. *J Biol Chem* **278**: 4176-4183.

23. Durgan, D. J., J. K. Smith, M. A. Hotze, O. Egbejimi, K. D. Cuthbert, V. G. Zaha, J. R. Dyck, E. D. Abel, and M. E. Young. 2006. Distinct transcriptional regulation of long-chain acyl-CoA synthetase isoforms and cytosolic thioesterase 1 in the rodent heart by fatty acids and insulin. *Am J Physiol Heart Circ Physiol* **290**: H2480-2497.

24. Vasandani, C., A. I. Kafrouni, A. Caronna, Y. Bashmakov, M. Gotthardt, J. D. Horton, and D. K. Spady. 2002. Upregulation of hepatic LDL transport by n-3 fatty acids in LDL receptor knockout mice. *J Lipid Res* **43**: 772-784.

25. Jia, Z., Z. Pei, D. Maiguel, C. J. Toomer, and P. A. Watkins. 2007. The fatty acid transport protein (FATP) family: very long chain acyl-CoA synthetases or solute carriers? *J Mol Neurosci* **33**: 25-31.

26. Pohl, J., A. Ring, R. Ehehalt, T. Herrmann, and W. Stremmel. 2004. New concepts of cellular fatty acid uptake: role of fatty acid transport proteins and of caveolae. *Proc Nutr Soc* **63**: 259-262.

27. Watkins, P. A. 2007. Very long-chain acyl-CoA synthetases. *J Biol Chem*.

28. Mashek, D. G., M. A. McKenzie, C. G. Van Horn, and R. A. Coleman. 2006. Rat long chain acyl-CoA synthetase 5 increases fatty acid uptake and partitioning to cellular triacylglycerol in McArdle-RH7777 cells. *J Biol Chem* **281**: 945-950.

29. Li, L. O., D. G. Mashek, J. An, S. D. Doughman, C. B. Newgard, and R. A. Coleman. 2006. Overexpression of rat long chain acyl-coa synthetase 1 alters fatty acid metabolism in rat primary hepatocytes. *J Biol Chem* **281**: 37246-37255.

30. Mashek, D. G., L. O. Li, and R. A. Coleman. 2006. Rat long-chain acyl-CoA synthetase mRNA, protein, and activity vary in tissue distribution and in response to diet. *J Lipid Res* **47**: 2004-2010.

31. Achouri, Y., B. D. Hegarty, D. Allanic, D. Becard, I. Hainault, P. Ferre, and F. Foufelle. 2005. Long chain fatty acyl-CoA synthetase 5 expression is induced by insulin

and glucose: involvement of sterol regulatory element-binding protein-1c. *Biochimie* **87**: 1149-1155.

32. Marszalek, J. R., C. Kitidis, C. C. Dirusso, and H. F. Lodish. 2005. Long-chain acyl-CoA synthetase 6 preferentially promotes DHA metabolism. *J Biol Chem* **280**: 10817-10826.

33. Pei, Z., Z. Jia, and P. A. Watkins. 2005. The second member of the human and murine "bubblegum" family is a testis- and brainstem-specific acyl-CoA synthetase. *J Biol Chem*.

34. Vessey, D. A., M. Kelley, and R. S. Warren. 2004. Characterization of triacsin C inhibition of short-, medium-, and long-chain fatty acid: CoA ligases of human liver. *J Biochem Mol Toxicol* **18**: 100-106.

35. Mashek, D. G., K. E. Bornfeldt, R. A. Coleman, J. Berger, D. A. Bernlohr, P. Black, C. C. DiRusso, S. A. Farber, W. Guo, N. Hashimoto, V. Khodiyar, F. A. Kuypers, L. J. Maltais, D. W. Nebert, A. Renieri, J. E. Schaffer, A. Stahl, P. A. Watkins, V. Vasiliou, and T. T. Yamamoto. 2004. Revised nomenclature for the mammalian long-chain acyl-CoA synthetase gene family. *J Lipid Res* **45**: 1958-1961.

36. Coleman, R. A., T. M. Lewin, C. G. Van Horn, and M. R. Gonzalez-Baro. 2002. Do long-chain acyl-CoA synthetases regulate fatty acid entry into synthetic versus degradative pathways? *J Nutr* **132**: 2123-2126.

37. Maeda, K., H. Cao, K. Kono, C. Z. Gorgun, M. Furuhashi, K. T. Uysal, Q. Cao, G. Atsumi, H. Malone, B. Krishnan, Y. Minokoshi, B. B. Kahn, R. A. Parker, and G. S. Hotamisligil. 2005. Adipocyte/macrophage fatty acid binding proteins control integrated metabolic responses in obesity and diabetes. *Cell Metab* **1**: 107-119.

38. Erol, E., L. S. Kumar, G. W. Cline, G. I. Shulman, D. P. Kelly, and B. Binas. 2004. Liver fatty acid binding protein is required for high rates of hepatic fatty acid oxidation but not for the action of PPARalpha in fasting mice. *Faseb J* **18**: 347-349.

39. Toyama, T., N. Kudo, A. Mitsumoto, and Y. Kawashima. 2005. Regulation of palmitoyl-CoA chain elongation by clofibric acid in the liver of Zucker fa/fa rats. *Lipids* **40**: 463-470.

40. Wang, Y., D. Botolin, B. Christian, J. Busik, J. Xu, and D. B. Jump. 2005. Tissue-specific, nutritional, and developmental regulation of rat fatty acid elongases. *J Lipid Res* **46**: 706-715.

41. Lagali, P. S., J. Liu, R. Ambasudhan, L. E. Kakuk, S. L. Bernstein, G. M. Seigel, P. W. Wong, and R. Ayyagari. 2003. Evolutionarily conserved ELOVL4 gene expression in the vertebrate retina. *Invest Ophthalmol Vis Sci* **44**: 2841-2850.

42. Moon, Y. A., and J. D. Horton. 2003. Identification of two mammalian reductases involved in the two-carbon fatty acyl elongation cascade. *J Biol Chem* **278**: 7335-7343.

43. Inagaki, K., T. Aki, Y. Fukuda, S. Kawamoto, S. Shigeta, K. Ono, and O. Suzuki. 2002. Identification and expression of a rat fatty acid elongase involved in the biosynthesis of C18 fatty acids. *Biosci Biotechnol Biochem* **66**: 613-621.

44. Leonard, A. E., B. Kelder, E. G. Bobik, L. T. Chuang, C. J. Lewis, J. J. Kopchick, P. Mukerji, and Y. S. Huang. 2002. Identification and expression of mammalian long-chain PUFA elongation enzymes. *Lipids* **37**: 733-740.

45. Matsuzaka, T., H. Shimano, N. Yahagi, T. Yoshikawa, M. Amemiya-Kudo, A. H. Hasty, H. Okazaki, Y. Tamura, Y. Iizuka, K. Ohashi, J. Osuga, A. Takahashi, S. Yato, H. Sone, S. Ishibashi, and N. Yamada. 2002. Cloning and characterization of a mammalian fatty acyl-CoA elongase as a lipogenic enzyme regulated by SREBPs. *J Lipid Res* **43**: 911-920.

46. Rodriguez-Cruz, M., A. R. Tovar, B. Palacios-Gonzalez, M. Del Prado, and N. Torres. 2006. Synthesis of long-chain polyunsaturated fatty acids in lactating mammary gland: role of Delta5 and Delta6 desaturases, SREBP-1, PPARalpha, and PGC-1. *J Lipid Res* **47**: 553-560.

47. Man, W. C., M. Miyazaki, K. Chu, and J. M. Ntambi. 2006. Membrane topology of mouse stearoyl-CoA desaturase 1. *J Biol Chem* **281**: 1251-1260.

48. Wang, J., L. Yu, R. E. Schmidt, C. Su, X. Huang, K. Gould, and G. Cao. 2005. Characterization of HSCD5, a novel human stearoyl-CoA desaturase unique to primates. *Biochem Biophys Res Commun* **332**: 735-742.

49. Mandel, C. R., B. Tweel, and L. Tong. 2009. Crystal structure of human mitochondrial acyl-CoA thioesterase (ACOT2). *Biochem Biophys Res Commun* **385**: 630-633.

50. Zhao, H., B. M. Martin, M. Bisoffi, and D. Dunaway-Mariano. 2009. The Akt C-terminal modulator protein is an acyl-CoA thioesterase of the Hotdog-Fold family. *Biochemistry* **48**: 5507-5509.

51. Wei, J., H. W. Kang, and D. E. Cohen. 2009. Thioesterase superfamily member 2 (Them2)/acyl-CoA thioesterase 13 (Acot13): a homotetrameric hotdog fold thioesterase with selectivity for long-chain fatty acyl-CoAs. *Biochem J* **421**: 311-322.

52. Carper, M. J., S. Zhang, J. Turk, and S. Ramanadham. 2008. Skeletal muscle group VIA phospholipase A2 (iPLA2beta): expression and role in fatty acid oxidation. *Biochemistry* **47**: 12241-12249.

53. Sakuma, S., K. Usa, and Y. Fujimoto. 2006. The regulation of formation of prostaglandins and arachidonoyl-CoA from arachidonic acid in rabbit kidney medulla microsomes by linoleic acid hydroperoxide. *Prostaglandins Other Lipid Mediat* **79**: 271-277.

54. Yuki, K., H. Shindou, D. Hishikawa, and T. Shimizu. 2009. Characterization of mouse lysophosphatidic acid acyltransferase 3: an enzyme with dual functions in the testis. *J Lipid Res* **50**: 860-869.

55. Shindou, H., D. Hishikawa, T. Harayama, K. Yuki, and T. Shimizu. 2009. Recent progress on acyl CoA: lysophospholipid acyltransferase research. *J Lipid Res* **50 Suppl**: S46-51.

56. Buccoliero, R., and A. H. Futerman. 2003. The roles of ceramide and complex sphingolipids in neuronal cell function. *Pharmacol Res* **47**: 409-419.

57. Spiegel, S., and A. H. Merrill, Jr. 1996. Sphingolipid metabolism and cell growth regulation. *Faseb J* **10**: 1388-1397.

58. Le Stunff, H., I. Galve-Roperh, C. Peterson, S. Milstien, and S. Spiegel. 2002. Sphingosine-1-phosphate phosphohydrolase in regulation of sphingolipid metabolism and apoptosis. *J Cell Biol* **158**: 1039-1049.

59. Hung, W. C., H. C. Chang, and L. Y. Chuang. 1999. Activation of caspase-3-like proteases in apoptosis induced by sphingosine and other long-chain bases in Hep3B hepatoma cells. *Biochem J* **338 (Pt 1)**: 161-166.

60. Osawa, Y., Y. Banno, M. Nagaki, D. A. Brenner, T. Naiki, Y. Nozawa, S. Nakashima, and H. Moriwaki. 2001. TNF-alpha-induced sphingosine 1-phosphate inhibits apoptosis through a phosphatidylinositol 3-kinase/Akt pathway in human hepatocytes. *J Immunol* **167**: 173-180.

61. Pruett, S. T., A. Bushnev, K. Hagedorn, M. Adiga, C. A. Haynes, M. C. Sullards, D. C. Liotta, and A. H. Merrill, Jr. 2008. Biodiversity of sphingoid bases ("sphingosines") and related amino alcohols. *J Lipid Res* **49**: 1621-1639.

62. Haynes, C. A., J. C. Allegood, H. Park, and M. C. Sullards. 2009. Sphingolipidomics: methods for the comprehensive analysis of sphingolipids. *J Chromatogr B Analyt Technol Biomed Life Sci* **877**: 2696-2708.

63. Tserng, K. Y., and R. Griffin. 2004. Studies of lipid turnover in cells with stable isotope and gas chromatograph-mass spectrometry. *Analytical biochemistry* **325**: 344-353.

64. Moore, J. D., W. V. Caufield, and W. A. Shaw. 2007. Quantitation and standardization of lipid internal standards for mass spectroscopy. *Methods Enzymol* **432**: 351-367.

65. Shaner, R. L., J. C. Allegood, H. Park, E. Wang, S. Kelly, C. A. Haynes, M. C. Sullards, and A. H. Merrill, Jr. 2009. Quantitative analysis of sphingolipids for lipidomics using triple quadrupole and quadrupole linear ion trap mass spectrometers. *J Lipid Res* **50**: 1692-1707.

66. Isaac, G., D. Bylund, J. E. Mansson, K. E. Markides, and J. Bergquist. 2003. Analysis of phosphatidylcholine and sphingomyelin molecular species from brain extracts using capillary liquid chromatography electrospray ionization mass spectrometry. *J Neurosci Methods* **128**: 111-119.

67. Fyrst, H., D. R. Herr, G. L. Harris, and J. D. Saba. 2004. Characterization of free endogenous C14 and C16 sphingoid bases from Drosophila melanogaster. *J Lipid Res* **45**: 54-62.

68. Sullards, M. C., and A. H. Merrill, Jr. 2001. Analysis of sphingosine 1-phosphate, ceramides, and other bioactive sphingolipids by high-performance liquid chromatography-tandem mass spectrometry. *Sci STKE* **2001**: PL1.

69. Tsui, Z. C., Q. R. Chen, M. J. Thomas, M. Samuel, and Z. Cui. 2005. A method for profiling gangliosides in animal tissues using electrospray ionization-tandem mass spectrometry. *Anal Biochem* **341**: 251-258.

70. Taguchi, R., J. Hayakawa, Y. Takeuchi, and M. Ishida. 2000. Two-dimensional analysis of phospholipids by capillary liquid chromatography/electrospray ionization mass spectrometry. *J Mass Spectrom* **35**: 953-966.

71. Sullards, M. C., and J. A. Reiter. 2000. Primary and secondary locations of charge sites in angiotensin II (M + 2H)2+ ions formed by electrospray ionization. *J Am Soc Mass Spectrom* **11**: 40-53.

72. Boscaro, F., G. Pieraccini, G. la Marca, G. Bartolucci, C. Luceri, F. Luceri, and G. Moneti. 2002. Rapid quantitation of globotriaosylceramide in human plasma and urine: a potential application for monitoring enzyme replacement therapy in Anderson-Fabry disease. *Rapid Commun Mass Spectrom* **16**: 1507-1514.

73. Zitomer, N. C., T. Mitchell, K. A. Voss, G. S. Bondy, S. T. Pruett, E. C. Garnier-Amblard, L. S. Liebeskind, H. Park, E. Wang, M. C. Sullards, A. H. Merrill, Jr., and R. T. Riley. 2009. Ceramide synthase inhibition by fumonisin B1 causes accumulation of 1-deoxysphinganine: a novel category of bioactive 1-deoxysphingoid bases and 1-deoxydihydroceramides biosynthesized by mammalian cell lines and animals. *J Biol Chem* **284**: 4786-4795.

74. Sullards, M. C., J. C. Allegood, S. Kelly, E. Wang, C. A. Haynes, H. Park, Y. Chen, and A. H. Merrill. 2007. Structure-specific, quantitative methods for analysis of sphingolipids by liquid chromatography-tandem mass spectrometry: "inside-out" sphingolipidomics. *Methods in enzymology* **432**: 83-115.

75. Merrill, A. H., Jr., M. C. Sullards, J. C. Allegood, S. Kelly, and E. Wang. 2005. Sphingolipidomics: high-throughput, structure-specific, and quantitative analysis of sphingolipids by liquid chromatography tandem mass spectrometry. *Methods* **36**: 207-224.

76. Menaldino, D. S., A. Bushnev, A. Sun, D. C. Liotta, H. Symolon, K. Desai, D. L. Dillehay, Q. Peng, E. Wang, J. Allegood, S. Trotman-Pruett, M. C. Sullards, and A. H. Merrill, Jr. 2003. Sphingoid bases and de novo ceramide synthesis: enzymes involved, pharmacology and mechanisms of action. *Pharmacol Res* **47**: 373-381.

77. Sullards, M. C., E. Wang, Q. Peng, and A. H. Merrill, Jr. 2003. Metabolomic profiling of sphingolipids in human glioma cell lines by liquid chromatography tandem mass spectrometry. *Cell Mol Biol (Noisy-le-grand)* **49**: 789-797.

78. Metelmann, W., J. Peter-Katalinic, and J. Muthing. 2001. Gangliosides from human granulocytes: a nano-ESI QTOF mass spectrometry fucosylation study of low abundance species in complex mixtures. *J Am Soc Mass Spectrom* **12**: 964-973.

79. Tani, M., T. Sano, M. Ito, and Y. Igarashi. 2005. Mechanisms of sphingosine and sphingosine 1-phosphate generation in human platelets. *J Lipid Res* **46**: 2458-2467.

80. Prinetti, A., D. Millimaggi, S. D'Ascenzo, M. Clarkson, A. Bettiga, V. Chigorno, S. Sonnino, A. Pavan, and V. Dolo. 2006. Lack of ceramide generation and altered sphingolipid composition are associated with drug resistance in human ovarian carcinoma cells. *Biochem J* **395**: 311-318.

81. Lee, J. T., J. Xu, J. M. Lee, G. Ku, X. Han, D. I. Yang, S. Chen, and C. Y. Hsu. 2004. Amyloid-beta peptide induces oligodendrocyte death by activating the neutral sphingomyelinase-ceramide pathway. *J Cell Biol* **164**: 123-131.

82. Smith, E. R., and A. H. Merrill, Jr. 1995. Differential roles of de novo sphingolipid biosynthesis and turnover in the "burst" of free sphingosine and sphinganine, and their 1-phosphates and N-acyl-derivatives, that occurs upon changing the medium of cells in culture. *J Biol Chem* **270**: 18749-18758.

83. Merrill, A. H., Jr., S. Lingrell, E. Wang, M. Nikolova-Karakashian, T. R. Vales, and D. E. Vance. 1995. Sphingolipid biosynthesis de novo by rat hepatocytes in culture. Ceramide and sphingomyelin are associated with, but not required for, very low density lipoprotein secretion. *J Biol Chem* **270**: 13834-13841.

84. Kelleher, J. K. 2004. Probing metabolic pathways with isotopic tracers: insights from mammalian metabolic physiology. *Metab Eng* **6**: 1-5.

85. Lligona-Trulla, L., A. Arduini, T. A. Aldaghlas, M. Calvani, and J. K. Kelleher. 1997. Acetyl-L-carnitine flux to lipids in cells estimated using isotopomer spectral analysis. *J Lipid Res* **38**: 1454-1462.

86. Kelleher, J. K., A. T. Kharroubi, T. A. Aldaghlas, I. B. Shambat, K. A. Kennedy, A. L. Holleran, and T. M. Masterson. 1994. Isotopomer spectral analysis of cholesterol synthesis: applications in human hepatoma cells. *Am J Physiol* **266**: E384-395.

87. Kharroubi, A. T., T. M. Masterson, T. A. Aldaghlas, K. A. Kennedy, and J. K. Kelleher. 1992. Isotopomer spectral analysis of triglyceride fatty acid synthesis in 3T3-L1 cells. *Am J Physiol* **263**: E667-675.

88. R. Wolfe, R., and D. L. Chinkes. 2004. Isotope tracers in metabolic research: principles and practice of kinetic analysis.

89. Antoniewicz, M. R., J. K. Kelleher, and G. Stephanopoulos. 2006. Determination of confidence intervals of metabolic fluxes estimated from stable isotope measurements. *Metab Eng* **8**: 324-337.

90. Siler, S. Q., R. A. Neese, E. J. Parks, and M. K. Hellerstein. 1998. VLDL-triglyceride production after alcohol ingestion, studied using [2-13C1] glycerol. *J Lipid Res* **39**: 2319-2328.

91. Macallan, D. C., C. A. Fullerton, R. A. Neese, K. Haddock, S. S. Park, and M. K. Hellerstein. 1998. Measurement of cell proliferation by labeling of DNA with stable isotope-labeled glucose: studies in vitro, in animals, and in humans. *Proc Natl Acad Sci U S A* **95**: 708-713.

92. Hellerstein, M. K. 2004. New stable isotope-mass spectrometric techniques for measuring fluxes through intact metabolic pathways in mammalian systems: introduction of moving pictures into functional genomics and biochemical phenotyping. *Metab Eng* **6**: 85-100.

93. Sun, D., M. G. Cree, and R. R. Wolfe. 2006. Quantification of the concentration and 13C tracer enrichment of long-chain fatty acyl-coenzyme A in muscle by liquid chromatography/mass spectrometry. *Anal Biochem* **349**: 87-95.

94. Tserng, K. Y., and R. Griffin. 2003. Quantitation and molecular species determination of diacylglycerols, phosphatidylcholines, ceramides, and sphingomyelins with gas chromatography. *Anal Biochem* **323**: 84-93.

95. Sun, D., M. G. Cree, X. J. Zhang, E. Boersheim, and R. R. Wolfe. 2006. Measurement of stable isotopic enrichment and concentration of long-chain fatty acyl-carnitines in tissue by HPLC-MS. *J Lipid Res* **47**: 431-439.

96. Siler, S. Q., R. A. Neese, and M. K. Hellerstein. 1999. De novo lipogenesis, lipid kinetics, and whole-body lipid balances in humans after acute alcohol consumption. *Am J Clin Nutr* **70**: 928-936.

97. Hellerstein, M. K., and R. A. Neese. 1999. Mass isotopomer distribution analysis at eight years: theoretical, analytic, and experimental considerations. *Am J Physiol* **276**: E1146-1170.

98. Hu, W., J. Bielawski, F. Samad, A. H. Merrill, Jr., and L. A. Cowart. 2009. Palmitate increases sphingosine-1-phosphate in C2C12 myotubes via upregulation of sphingosine kinase message and activity. *J Lipid Res*.

99. Weigert, C., K. Brodbeck, H. Staiger, C. Kausch, F. Machicao, H. U. Haring, and E. D. Schleicher. 2004. Palmitate, but not unsaturated fatty acids, induces the expression of interleukin-6 in human myotubes through proteasome-dependent activation of nuclear factor-kappaB. *J Biol Chem* **279**: 23942-23952.

100. Abdel-Halim, M. N., and S. I. Farah. 1985. Short-term regulation of acetyl CoA carboxylase: is the key enzyme in long-chain fatty acid synthesis regulated by an existing physiological mechanism? *Comp Biochem Physiol B* **81**: 9-19.

101. Barber, M. C., A. J. Vallance, H. T. Kennedy, and M. T. Travers. 2003. Induction of transcripts derived from promoter III of the acetyl-CoA carboxylase-alpha gene in mammary gland is associated with recruitment of SREBP-1 to a region of the proximal promoter defined by a DNase I hypersensitive site. *Biochem J* **375**: 489-501.

102. Lopez, J. M., M. K. Bennett, H. B. Sanchez, J. M. Rosenfeld, and T. E. Osborne. 1996. Sterol regulation of acetyl coenzyme A carboxylase: a mechanism for coordinate control of cellular lipid. *Proc Natl Acad Sci U S A* **93**: 1049-1053.

103. Wakil, S. J. 1986. The relationship between structure and function for and the regulation of the enzymes of fatty acid synthesis. *Ann N Y Acad Sci* **478**: 203-219.

104. Jayakumar, A., S. S. Chirala, and S. J. Wakil. 1997. Human fatty acid synthase: assembling recombinant halves of the fatty acid synthase subunit protein reconstitutes enzyme activity. *Proc Natl Acad Sci U S A* **94**: 12326-12330.

105. Chirala, S. S., W. Y. Huang, A. Jayakumar, K. Sakai, and S. J. Wakil. 1997. Animal fatty acid synthase: functional mapping and cloning and expression of the domain I constituent activities. *Proc Natl Acad Sci U S A* **94**: 5588-5593.

106. Jayakumar, A., W. Y. Huang, B. Raetz, S. S. Chirala, and S. J. Wakil. 1996. Cloning and expression of the multifunctional human fatty acid synthase and its subdomains in Escherichia coli. *Proc Natl Acad Sci U S A* **93**: 14509-14514.

107. Faergeman, N. J., and J. Knudsen. 1997. Role of long-chain fatty acyl-CoA esters in the regulation of metabolism and in cell signalling. *Biochem J* **323 (Pt 1)**: 1-12.

108. Schulz, H. 2008. Oxidation of fatty acids in eukaryotes. *in Biochemistry of Lipids, Lipoproteins & Membranes (D. E. Vance and J. E. Vance, eds.), Elsevier (Amsterdam)*: Chapter 5.

109. Miyazaki, M., and J. M. Ntambi. 2008. Fatty acid desaturation and chain elongation in mammals. *in Biochemistry of Lipids, Lipoproteins & Membranes (D. E. Vance and J. E. Vance, eds.), Elsevier (Amsterdam)*: Chapter 7.

110. Magnes, C., F. M. Sinner, W. Regittnig, and T. R. Pieber. 2005. LC/MS/MS method for quantitative determination of long-chain fatty acyl-CoAs. *Anal Chem* **77**: 2889-2894.

111. Mauriala, T., K. H. Herzig, M. Heinonen, J. Idziak, and S. Auriola. 2004. Determination of long-chain fatty acid acyl-coenzyme A compounds using liquid chromatography-electrospray ionization tandem mass spectrometry. *J Chromatogr B Analyt Technol Biomed Life Sci* **808**: 263-268.

112. Kalderon, B., V. Sheena, S. Shachrur, R. Hertz, and J. Bar-Tana. 2002. Modulation by nutrients and drugs of liver acyl-CoAs analyzed by mass spectrometry. *J Lipid Res* **43**: 1125-1132.

113. Hankin, J. A., Murphy, Robert C. 1997. MALDI-TOF and electrospray tandem mass spectrometric analysis of fatty acyl-CoA esters. *International Journal of Mass Spectrometry and Ion Processes* **165/166**: 467-474.

114. Millington, D. S., D. L. Norwood, N. Kodo, R. Moore, M. D. Green, and J. Berman. 1991. Biomedical applications of high-performance liquid chromatography-mass spectrometry with continuous-flow fast atom bombardment. *J Chromatogr* **562**: 47-58.

115. Norwood, D. L., C. A. Bus, and D. S. Millington. 1990. Combined high-performance liquid chromatographic-continuous-flow fast atom bombardment mass spectrometric analysis of acylcoenzyme A compounds. *J Chromatogr* **527**: 289-301.

116. Welsh, C. J., M. Robinson, T. R. Warne, J. H. Pierce, G. C. Yeh, and J. M. Phang. 1994. Accumulation of fatty alcohol in MCF-7 breast cancer cells. *Arch Biochem Biophys* **315**: 41-47.

117. Merrill, A. H., Jr., T. H. Stokes, A. Momin, H. Park, B. J. Portz, S. Kelly, E. Wang, M. C. Sullards, and M. D. Wang. 2009. Sphingolipidomics: a valuable tool for understanding the roles of sphingolipids in biology and disease. *J Lipid Res* **50 Suppl**: S97-102.

118. Bandyopadhyay, S., R. Zhan, Y. Wang, S. K. Pai, S. Hirota, S. Hosobe, Y. Takano, K. Saito, E. Furuta, M. Iiizumi, S. Mohinta, M. Watabe, C. Chalfant, and K. Watabe. 2006. Mechanism of apoptosis induced by the inhibition of fatty acid synthase in breast cancer cells. *Cancer Res* **66**: 5934-5940.

119. Menendez, J. A., and R. Lupu. 2007. Fatty acid synthase and the lipogenic phenotype in cancer pathogenesis. *Nat Rev Cancer* **7**: 763-777.

120. Ellis, B. A., A. Poynten, A. J. Lowy, S. M. Furler, D. J. Chisholm, E. W. Kraegen, and G. J. Cooney. 2000. Long-chain acyl-CoA esters as indicators of lipid metabolism

and insulin sensitivity in rat and human muscle. *Am J Physiol Endocrinol Metab* **279**: E554-560.

121. Rosendal, J., and J. Knudsen. 1992. A fast and versatile method for extraction and quantitation of long-chain acyl-CoA esters from tissue: content of individual long-chain acyl-CoA esters in various tissues from fed rat. *Anal Biochem* **207**: 63-67.

122. Deutsch, J., S. I. Rapoport, and A. D. Purdon. 1997. Relation between free fatty acid and acyl-CoA concentrations in rat brain following decapitation. *Neurochem Res* **22**: 759-765.

123. Sohlenius-Sternbeck, A. K. 2006. Determination of the hepatocellularity number for human, dog, rabbit, rat and mouse livers from protein concentration measurements. *Toxicol In Vitro* **20**: 1582-1586.

124. Zia, A., E. H. Kolodny, and G. M. Pastores. 2007. Very long chain acyl-CoA dehydrogenase deficiency in a pair of mildly affected monozygotic twin sister in their late fifties. *J Inherit Metab Dis* **30**: 817.

125. Bell, T. A., 3rd, M. D. Wilson, K. Kelley, J. K. Sawyer, and L. L. Rudel. 2007. Monounsaturated fatty acyl-coenzyme A is predictive of atherosclerosis in human apoB-100 transgenic, LDLr-/- mice. *J Lipid Res* **48**: 1122-1131.

126. Heimerl, S., C. Moehle, A. Zahn, A. Boettcher, W. Stremmel, T. Langmann, and G. Schmitz. 2006. Alterations in intestinal fatty acid metabolism in inflammatory bowel disease. *Biochim Biophys Acta* **1762**: 341-350.

127. Gregersen, N., P. Bross, and B. S. Andresen. 2004. Genetic defects in fatty acid beta-oxidation and acyl-CoA dehydrogenases. Molecular pathogenesis and genotype-phenotype relationships. *Eur J Biochem* **271**: 470-482.

128. Gomez, F. E., D. E. Bauman, J. M. Ntambi, and B. G. Fox. 2003. Effects of sterculic acid on stearoyl-CoA desaturase in differentiating 3T3-L1 adipocytes. *Biochem Biophys Res Commun* **300**: 316-326.

129. Kridel, S. J., F. Axelrod, N. Rozenkrantz, and J. W. Smith. 2004. Orlistat is a novel inhibitor of fatty acid synthase with antitumor activity. *Cancer Res* **64**: 2070-2075.

130. Pemble, C. W. t., L. C. Johnson, S. J. Kridel, and W. T. Lowther. 2007. Crystal structure of the thioesterase domain of human fatty acid synthase inhibited by Orlistat. *Nat Struct Mol Biol* **14**: 704-709.

131. Kuhajda, F. P., E. S. Pizer, J. N. Li, N. S. Mani, G. L. Frehywot, and C. A. Townsend. 2000. Synthesis and antitumor activity of an inhibitor of fatty acid synthase. *Proc Natl Acad Sci U S A* **97**: 3450-3454.

132. Goldberg, I., J. R. Walker, and K. Bloch. 1973. Inhibition of lipid synthesis in Escherichia coli cells by the antibiotic cerulenin. *Antimicrob Agents Chemother* **3**: 549-554.

133. Weis, B. C., A. T. Cowan, N. Brown, D. W. Foster, and J. D. McGarry. 1994. Use of a selective inhibitor of liver carnitine palmitoyltransferase I (CPT I) allows quantification of its contribution to total CPT I activity in rat heart. Evidence that the dominant cardiac CPT I isoform is identical to the skeletal muscle enzyme. *J Biol Chem* **269**: 26443-26448.

134. Wenz, A., C. Thorpe, and S. Ghisla. 1981. Inactivation of general acyl-CoA dehydrogenase from pig kidney by a metabolite of hypoglycin A. *J Biol Chem* **256**: 9809-9812.

135. Miyake, Y., Y. Kozutsumi, S. Nakamura, T. Fujita, and T. Kawasaki. 1995. Serine palmitoyltransferase is the primary target of a sphingosine-like immunosuppressant, ISP-1/myriocin. *Biochem Biophys Res Commun* **211**: 396-403.

136. Mano, N., M. Uchida, H. Okuyama, I. Sasaki, S. Ikegawa, and J. Goto. 2001. Simultaneous detection of cholyl adenylate and coenzyme A thioester utilizing liquid chromatography/electrospray ionization mass spectrometry. *Anal Sci* **17**: 1037-1042.

137. Spiegel, S., and S. Milstien. 2000. Sphingosine-1-phosphate: signaling inside and out. *FEBS Lett* **476**: 55-57.

138. Zheng, W., J. Kollmeyer, H. Symolon, A. Momin, E. Munter, E. Wang, S. Kelly, J. C. Allegood, Y. Liu, Q. Peng, H. Ramaraju, M. C. Sullards, M. Cabot, and A. H. Merrill, Jr. 2006. Ceramides and other bioactive sphingolipid backbones in health and disease: lipidomic analysis, metabolism and roles in membrane structure, dynamics, signaling and autophagy. *Biochim Biophys Acta* **1758**: 1864-1884.

139. El Alwani, M., B. X. Wu, L. M. Obeid, and Y. A. Hannun. 2006. Bioactive sphingolipids in the modulation of the inflammatory response. *Pharmacol Ther*.

140. Sandhoff, K., and G. van Echten. 1993. Ganglioside metabolism--topology and regulation. *Adv Lipid Res* **26**: 119-142.

141. Maceyka, M., H. Sankala, N. C. Hait, H. Le Stunff, H. Liu, R. Toman, C. Collier, M. Zhang, L. S. Satin, A. H. Merrill, Jr., S. Milstien, and S. Spiegel. 2005. SphK1 and SphK2, sphingosine kinase isoenzymes with opposing functions in sphingolipid metabolism. *J Biol Chem* **280**: 37118-37129.

142. Tettamanti, G., R. Bassi, P. Viani, and L. Riboni. 2003. Salvage pathways in glycosphingolipid metabolism. *Biochimie* **85**: 423-437.

143. Merrill, A. H., Jr., M. C. Sullards, E. Wang, K. A. Voss, and R. T. Riley. 2001. Sphingolipid metabolism: roles in signal transduction and disruption by fumonisins. *Environ Health Perspect* **109 Suppl 2**: 283-289.

144. Suzuki, K. 1970. Formation and turnover of myelin ganglioside. *J Neurochem* **17**: 209-213.

145. Hannun, Y. A., and L. M. Obeid. 2002. The Ceramide-centric universe of lipid-mediated cell regulation: stress encounters of the lipid kind. *J Biol Chem* **277**: 25847-25850.

146. Tserng, K. Y., and R. Griffin. 2004. Studies of lipid turnover in cells with stable isotope and gas chromatograph-mass spectrometry. *Anal Biochem* **325**: 344-353.

147. Berdyshev, E. V., I. A. Gorshkova, P. Usatyuk, Y. Zhao, B. Saatian, W. Hubbard, and V. Natarajan. 2006. De novo biosynthesis of dihydrosphingosine-1-phosphate by sphingosine kinase 1 in mammalian cells. *Cell Signal*.

148. Wang, H., A. E. Giuliano, and M. C. Cabot. 2002. Enhanced de novo ceramide generation through activation of serine palmitoyltransferase by the P-glycoprotein antagonist SDZ PSC 833 in breast cancer cells. *Mol Cancer Ther* **1**: 719-726.

149. Mikami, T., M. Kashiwagi, K. Tsuchihashi, T. Akino, and S. Gasa. 1998. Substrate specificity and some other enzymatic properties of dihydroceramide desaturase (ceramide synthase) in fetal rat skin. *J Biochem (Tokyo)* **123**: 906-911.

150. Sampath, H., and J. M. Ntambi. 2005. The fate and intermediary metabolism of stearic acid. *Lipids* **40**: 1187-1191.

151. Haynes, C. A., J. C. Allegood, K. Sims, E. W. Wang, M. C. Sullards, and A. H. Merrill, Jr. 2008. Quantitation of fatty acyl-coenzyme A molecular species in mammalian cell extracts by liquid chromatography-electrospray ionization tandem mass spectrometry (LC-ESI MS/MS). *J Lipid Res*.

152. Riley, R. T., D. M. Hinton, W. J. Chamberlain, C. W. Bacon, E. Wang, A. H. Merrill, Jr., and K. A. Voss. 1994. Dietary fumonisin B1 induces disruption of sphingolipid metabolism in Sprague-Dawley rats: a new mechanism of nephrotoxicity. *J Nutr* **124**: 594-603.

153. Merrill, A. H., Jr., G. van Echten, E. Wang, and K. Sandhoff. 1993. Fumonisin B1 inhibits sphingosine (sphinganine) N-acyltransferase and de novo sphingolipid biosynthesis in cultured neurons in situ. *J Biol Chem* **268**: 27299-27306.

154. Norred, W. P., E. Wang, H. Yoo, R. T. Riley, and A. H. Merrill, Jr. 1992. In vitro toxicology of fumonisins and the mechanistic implications. *Mycopathologia* **117**: 73-78.

155. Haschek, W. M., G. Motelin, D. K. Ness, K. S. Harlin, W. F. Hall, R. F. Vesonder, R. E. Peterson, and V. R. Beasley. 1992. Characterization of fumonisin toxicity in orally and intravenously dosed swine. *Mycopathologia* **117**: 83-96.

156. Weibking, T. S., D. R. Ledoux, A. J. Bermudez, J. R. Turk, G. E. Rottinghaus, E. Wang, and A. H. Merrill, Jr. 1993. Effects of feeding Fusarium moniliforme culture material, containing known levels of fumonisin B1, on the young broiler chick. *Poult Sci* **72**: 456-466.

157. van der Westhuizen, L., G. S. Shephard, S. D. Snyman, S. Abel, S. Swanevelder, and W. C. Gelderblom. 1998. Inhibition of sphingolipid biosynthesis in rat primary hepatocyte cultures by fumonisin B1 and other structurally related compounds. *Food Chem Toxicol* **36**: 497-503.

158. Fewou, S. N., H. Bussow, N. Schaeren-Wiemers, M. T. Vanier, W. B. Macklin, V. Gieselmann, and M. Eckhardt. 2005. Reversal of non-hydroxy:alpha-hydroxy galactosylceramide ratio and unstable myelin in transgenic mice overexpressing UDP-galactose:ceramide galactosyltransferase. *J Neurochem* **94**: 469-481.

159. Burger, K. N., P. van der Bijl, and G. van Meer. 1996. Topology of sphingolipid galactosyltransferases in ER and Golgi: transbilayer movement of monohexosyl sphingolipids is required for higher glycosphingolipid biosynthesis. *J Cell Biol* **133**: 15-28.

160. Hannun, Y. A., and L. M. Obeid. 2008. Principles of bioactive lipid signalling: lessons from sphingolipids. *Nat Rev Mol Cell Biol* **9**: 139-150.

161. Spiegel, S., and S. Milstien. 2003. Sphingosine-1-phosphate: an enigmatic signalling lipid. *Nat Rev Mol Cell Biol* **4**: 397-407.

162. Hanada, K., T. Hara, M. Nishijima, O. Kuge, R. C. Dickson, and M. M. Nagiec. 1997. A mammalian homolog of the yeast LCB1 encodes a component of serine palmitoyltransferase, the enzyme catalyzing the first step in sphingolipid synthesis. *J Biol Chem* **272**: 32108-32114.

163. Weiss, B., and W. Stoffel. 1997. Human and murine serine-palmitoyl-CoA transferase--cloning, expression and characterization of the key enzyme in sphingolipid synthesis. *Eur J Biochem* **249**: 239-247.

164. Hornemann, T., S. Richard, M. F. Rutti, Y. Wei, and A. von Eckardstein. 2006. Cloning and initial characterization of a new subunit for mammalian serine-palmitoyltransferase. *J Biol Chem* **281**: 37275-37281.

165. Han, G., K. Gable, L. Yan, M. Natarajan, J. Krishnamurthy, S. D. Gupta, A. Borovitskaya, J. M. Harmon, and T. M. Dunn. 2004. The topology of the Lcb1p subunit of yeast serine palmitoyltransferase. *J Biol Chem* **279**: 53707-53716.

166. Inuzuka, M., M. Hayakawa, and T. Ingi. 2005. Serinc, an activity-regulated protein family, incorporates serine into membrane lipid synthesis. *J Biol Chem* **280**: 35776-35783.

167. Han, G., S. D. Gupta, K. Gable, S. Niranjanakumari, P. Moitra, F. Eichler, R. H. Brown, Jr., J. M. Harmon, and T. M. Dunn. 2009. Identification of small subunits of mammalian serine palmitoyltransferase that confer distinct acyl-CoA substrate specificities. *Proc Natl Acad Sci U S A* **106**: 8186-8191.

168. Braun, P. E., P. Morell, and N. S. Radin. 1970. Synthesis of C18- and C20-dihydrosphingosines, ketodihydrosphingosines, and ceramides by microsomal preparations from mouse brain. *J Biol Chem* **245**: 335-341.

169. Williams, R. D., E. Wang, and A. H. Merrill, Jr. 1984. Enzymology of long-chain base synthesis by liver: characterization of serine palmitoyltransferase in rat liver microsomes. *Arch Biochem Biophys* **228**: 282-291.

170. Memon, R. A., W. M. Holleran, A. H. Moser, T. Seki, Y. Uchida, J. Fuller, J. K. Shigenaga, C. Grunfeld, and K. R. Feingold. 1998. Endotoxin and cytokines increase hepatic sphingolipid biosynthesis and produce lipoproteins enriched in ceramides and sphingomyelin. *Arterioscler Thromb Vasc Biol* **18**: 1257-1265.

171. Herget, T., C. Esdar, S. A. Oehrlein, M. Heinrich, S. Schutze, A. Maelicke, and G. van Echten-Deckert. 2000. Production of ceramides causes apoptosis during early neural differentiation in vitro. *J Biol Chem* **275**: 30344-30354.

172. Wang, H., B. J. Maurer, C. P. Reynolds, and M. C. Cabot. 2001. N-(4-hydroxyphenyl)retinamide elevates ceramide in neuroblastoma cell lines by coordinate activation of serine palmitoyltransferase and ceramide synthase. *Cancer Res* **61**: 5102-5105.

173. Perry, D. K., J. Carton, A. K. Shah, F. Meredith, D. J. Uhlinger, and Y. A. Hannun. 2000. Serine palmitoyltransferase regulates de novo ceramide generation during etoposide-induced apoptosis. *J Biol Chem* **275**: 9078-9084.

174. Holleran, W. M., Y. Uchida, L. Halkier-Sorensen, A. Haratake, M. Hara, J. H. Epstein, and P. M. Elias. 1997. Structural and biochemical basis for the UVB-induced alterations in epidermal barrier function. *Photodermatol Photoimmunol Photomed* **13**: 117-128.

175. Farrell, A. M., Y. Uchida, M. M. Nagiec, I. R. Harris, R. C. Dickson, P. M. Elias, and W. M. Holleran. 1998. UVB irradiation up-regulates serine palmitoyltransferase in cultured human keratinocytes. *J Lipid Res* **39**: 2031-2038.

176. Grether-Beck, S., A. Timmer, I. Felsner, H. Brenden, D. Brammertz, and J. Krutmann. 2005. Ultraviolet a-induced signaling involves a ceramide-mediated autocrine loop leading to ceramide de novo synthesis. *J Invest Dermatol* **125**: 545-553.

177. Taha, T. A., T. D. Mullen, and L. M. Obeid. 2006. A house divided: ceramide, sphingosine, and sphingosine-1-phosphate in programmed cell death. *Biochim Biophys Acta* **1758**: 2027-2036.

178. Williams, R. D., D. W. Nixon, and A. H. Merrill, Jr. 1984. Comparison of serine palmitoyltransferase in Morris hepatoma 7777 and rat liver. *Cancer Res* **44**: 1918-1923.

179. van Echten-Deckert, G. 2000. Sphingolipid extraction and analysis by thin-layer chromatography. *Methods Enzymol* **312**: 64-79.

180. Liu, G., L. Kleine, and R. L. Hebert. 2000. A direct method for the simultaneous measurement of ceramide and phospholipase D activity. *Prostaglandins Leukot Essent Fatty Acids* **63**: 187-194.

181. Mizutani, Y., A. Kihara, and Y. Igarashi. 2006. LASS3 (longevity assurance homologue 3) is a mainly testis-specific (dihydro)ceramide synthase with relatively broad substrate specificity. *Biochem J* **398**: 531-538.

182. Pewzner-Jung, Y., S. Ben-Dor, and A. H. Futerman. 2006. When do Lasses (longevity assurance genes) become CerS (ceramide synthases)?: Insights into the regulation of ceramide synthesis. *J Biol Chem* **281**: 25001-25005.

183. Mandon, E. C., I. Ehses, J. Rother, G. van Echten, and K. Sandhoff. 1992. Subcellular localization and membrane topology of serine palmitoyltransferase, 3-dehydrosphinganine reductase, and sphinganine N-acyltransferase in mouse liver. *J Biol Chem* **267**: 11144-11148.

184. Merrill, A. H., Jr., and E. Wang. 1986. Biosynthesis of long-chain (sphingoid) bases from serine by LM cells. Evidence for introduction of the 4-trans-double bond after de novo biosynthesis of N-acylsphinganine(s). *J Biol Chem* **261**: 3764-3769.

185. Alvarez, S. E., S. Milstien, and S. Spiegel. 2007. Autocrine and paracrine roles of sphingosine-1-phosphate. *Trends Endocrinol Metab* **18**: 300-307.

186. Chalfant, C. E., and S. Spiegel. 2005. Sphingosine 1-phosphate and ceramide 1-phosphate: expanding roles in cell signaling. *J Cell Sci* **118**: 4605-4612.

187. Wang, H., B. J. Maurer, Y. Y. Liu, E. Wang, J. C. Allegood, S. Kelly, H. Symolon, Y. Liu, A. H. Merrill, Jr., V. Gouaze-Andersson, J. Y. Yu, A. E. Giuliano, and M. C. Cabot. 2008. N-(4-Hydroxyphenyl)retinamide increases dihydroceramide and synergizes with dimethylsphingosine to enhance cancer cell killing. *Mol Cancer Ther* **7**: 2967-2976.

188. Coward, J., G. Ambrosini, E. Musi, J. P. Truman, A. Haimovitz-Friedman, J. C. Allegood, E. Wang, A. H. Merrill, Jr., and G. K. Schwartz. 2009. Safingol (L-threo-sphinganine) induces autophagy in solid tumor cells through inhibition of PKC and the PI3-kinase pathway. *Autophagy* **5**: 184-193.

189. Schiffmann, S., J. Sandner, R. Schmidt, K. Birod, I. Wobst, H. Schmidt, C. Angioni, G. Geisslinger, and S. Grosch. 2009. The selective COX-2 inhibitor celecoxib modulates sphingolipid synthesis. *J Lipid Res* **50**: 32-40.

190. Sanchez, A. M., S. Malagarie-Cazenave, N. Olea, D. Vara, C. Cuevas, and I. Diaz-Laviada. 2008. Spisulosine (ES-285) induces prostate tumor PC-3 and LNCaP cell death by de novo synthesis of ceramide and PKCzeta activation. *Eur J Pharmacol* **584**: 237-245.

191. Halter, D., S. Neumann, S. M. van Dijk, J. Wolthoorn, A. M. de Maziere, O. V. Vieira, P. Mattjus, J. Klumperman, G. van Meer, and H. Sprong. 2007. Pre- and post-Golgi translocation of glucosylceramide in glycosphingolipid synthesis. *J Cell Biol* **179**: 101-115.

192. Mashek, D. G., and R. A. Coleman. 2006. Cellular fatty acid uptake: the contribution of metabolism. *Curr Opin Lipidol* **17**: 274-278.

193. Lee, J. S., S. K. Pinnamaneni, S. J. Eo, I. H. Cho, J. H. Pyo, C. K. Kim, A. J. Sinclair, M. A. Febbraio, and M. J. Watt. 2006. Saturated, but not n-6 polyunsaturated, fatty acids induce insulin resistance: role of intramuscular accumulation of lipid metabolites. *J Appl Physiol* **100**: 1467-1474.

194. Kelpe, C. L., P. C. Moore, S. D. Parazzoli, B. Wicksteed, C. J. Rhodes, and V. Poitout. 2003. Palmitate inhibition of insulin gene expression is mediated at the transcriptional level via ceramide synthesis. *J Biol Chem* **278**: 30015-30021.

195. Smith, S., A. Witkowski, and A. K. Joshi. 2003. Structural and functional organization of the animal fatty acid synthase. *Prog Lipid Res* **42**: 289-317.

196. Millar, A. A., and L. Kunst. 1997. Very-long-chain fatty acid biosynthesis is controlled through the expression and specificity of the condensing enzyme. *Plant J* **12**: 121-131.

197. Miyazaki, M., H. J. Kim, W. C. Man, and J. M. Ntambi. 2001. Oleoyl-CoA is the major de novo product of stearoyl-CoA desaturase 1 gene isoform and substrate for the biosynthesis of the Harderian gland 1-alkyl-2,3-diacylglycerol. *J Biol Chem* **276**: 39455-39461.

198. Bederman, I. R., A. E. Reszko, T. Kasumov, F. David, D. H. Wasserman, J. K. Kelleher, and H. Brunengraber. 2004. Zonation of labeling of lipogenic acetyl-CoA across the liver: implications for studies of lipogenesis by mass isotopomer analysis. *J Biol Chem* **279**: 43207-43216.

199. Bandsma, R. H., F. Kuipers, R. J. Vonk, R. Boverhof, P. J. Sauer, G. T. Nagel, H. Elzinga, R. A. Neese, M. K. Hellerstein, and F. Stellaard. 2000. The contribution of newly synthesized cholesterol to bile salt synthesis in rats quantified by mass isotopomer distribution analysis. *Biochim Biophys Acta* **1483**: 343-351.

200. Bandsma, R. H., F. Stellaard, R. J. Vonk, G. T. Nagel, R. A. Neese, M. K. Hellerstein, and F. Kuipers. 1998. Contribution of newly synthesized cholesterol to rat plasma and bile determined by mass isotopomer distribution analysis: bile-salt flux promotes secretion of newly synthesized cholesterol into bile. *Biochem J* **329 (Pt 3)**: 699-703.

201. Faix, D., R. Neese, C. Kletke, S. Wolden, D. Cesar, M. Coutlangus, C. H. Shackleton, and M. K. Hellerstein. 1993. Quantification of menstrual and diurnal

periodicities in rates of cholesterol and fat synthesis in humans. *J Lipid Res* **34**: 2063-2075.

202. Neese, R. A., D. Faix, C. Kletke, K. Wu, A. C. Wang, C. H. Shackleton, and M. K. Hellerstein. 1993. Measurement of endogenous synthesis of plasma cholesterol in rats and humans using MIDA. *Am J Physiol* **264**: E136-147.

203. Clarenbach, J. J., B. Lindenthal, M. T. Dotti, A. Federico, J. K. Kelleher, and K. von Bergmann. 2005. Isotopomer spectral analysis of intermediates of cholesterol synthesis in patients with cerebrotendinous xanthomatosis. *Metabolism* **54**: 335-344.

204. Bederman, I. R., T. Kasumov, A. E. Reszko, F. David, H. Brunengraber, and J. K. Kelleher. 2004. In vitro modeling of fatty acid synthesis under conditions simulating the zonation of lipogenic [13C]acetyl-CoA enrichment in the liver. *J Biol Chem* **279**: 43217-43226.

205. Lindenthal, B., T. A. Aldaghlas, A. L. Holleran, T. Sudhop, H. K. Berthold, K. Von Bergmann, and J. K. Kelleher. 2002. Isotopomer spectral analysis of intermediates of cholesterol synthesis in human subjects and hepatic cells. *Am J Physiol Endocrinol Metab* **282**: E1222-1230.

206. Holleran, A. L., B. Lindenthal, T. A. Aldaghlas, and J. K. Kelleher. 1998. Effect of tamoxifen on cholesterol synthesis in HepG2 cells and cultured rat hepatocytes. *Metabolism* **47**: 1504-1513.

207. Sabri, A., G. Bare, P. Jacques, A. Jabrane, M. Ongena, J. C. Van Heugen, B. Devreese, and P. Thonart. 2001. Influence of moderate temperatures on myristoyl-CoA metabolism and acyl-CoA thioesterase activity in the psychrophilic antarctic yeast Rhodotorula aurantiaca. *J Biol Chem* **276**: 12691-12696.

208. Johnson, D. R., A. D. Cox, P. A. Solski, B. Devadas, S. P. Adams, R. M. Leimgruber, R. O. Heuckeroth, J. E. Buss, and J. I. Gordon. 1990. Functional analysis of protein N-myristoylation: metabolic labeling studies using three oxygen-substituted analogs of myristic acid and cultured mammalian cells provide evidence for protein-sequence-specific incorporation and analog-specific redistribution. *Proc Natl Acad Sci U S A* **87**: 8511-8515.

209. Moreau, C., P. Froment, L. Tosca, V. Moreau, and J. Dupont. 2006. Expression and regulation of the SCD2 desaturase in the rat ovary. *Biol Reprod* **74**: 75-87.

210. Scaglia, N., and R. A. Igal. 2005. Stearoyl-CoA desaturase is involved in the control of proliferation, anchorage-independent growth, and survival in human transformed cells. *J Biol Chem* **280**: 25339-25349.

211. Rahman, S. M., A. Dobrzyn, S. H. Lee, P. Dobrzyn, M. Miyazaki, and J. M. Ntambi. 2005. Stearoyl-CoA desaturase 1 deficiency increases insulin signaling and glycogen accumulation in brown adipose tissue. *Am J Physiol Endocrinol Metab* **288**: E381-387.

212. Miyazaki, M., A. Dobrzyn, P. M. Elias, and J. M. Ntambi. 2005. Stearoyl-CoA desaturase-2 gene expression is required for lipid synthesis during early skin and liver development. *Proc Natl Acad Sci U S A* **102**: 12501-12506.